# Electroweak Radiative Corrections in Super-Allowed Beta Decays from *Ab Initio* Theory

by

Michael Gennari

B.Sc., University of Waterloo, 2019

M.Sc., University of Victoria, 2021

A Dissertation Submitted in Partial Fulfillment of the
Requirements for the Degree of

DOCTOR OF PHILOSOPHY

in the Department of Physics and Astronomy

© Michael Gennari, 2025
University of Victoria

All rights reserved. This dissertation may not be reproduced in whole or in part, by photocopying or other means, without the permission of the author.

We acknowledge and respect the Lək̓ʷəŋən Peoples on whose territory the university stands, and the Lək̓ʷəŋən (Songhees and Esquimalt) and W̱SÁNEĆ Peoples whose historical relationships with the land continue to this day.

# Supervisory Committee

Electroweak Radiative Corrections in Super-Allowed Beta Decays from *Ab Initio* Theory

by

Michael Gennari

B.Sc., University of Waterloo, 2019

M.Sc., University of Victoria, 2021

## Supervisory Committee

Dr. Petr Navratil, Co-Supervisor
Department of Physics and Astronomy

Dr. Robert Kowalewski, Co-Supervisor
Department of Physics and Astronomy

Dr. Pavel Kovtun, Department Member
Department of Physics and Astronomy

Dr. Irina Paci, External Member
Department of Chemistry

# Abstract

A systematically improvable, *ab initio* model is developed to compute nuclear-structure-dependent electroweak radiative corrections in superallowed Fermi $\beta$ decays. With inter-nucleon interactions derived from the low-energy symmetries of quantum chromo-dynamics via a prescription of effective field theory, the nuclear many-body configurations are obtained in the quasi-exact, no-core shell model. This approach rigorously treats all nucleons as active degrees of freedom in solution of the non-relativistic, many-body Schrödinger equation with Hamiltonian constructed from chiral effective field theory.

One of the two key nuclear-structure corrections to superallowed $\beta$ decays, known as $\delta_{\rm NS}$, arises from modifications to the one-nucleon $\gamma W$ box diagram when immersed in the nuclear medium. It is computed for the two lightest superallowed transitions: the $^{10}\mathrm{C} \to {}^{10}\mathrm{B}$ and $^{14}\mathrm{O} \to {}^{14}\mathrm{N}$ transitions. The nuclear $\gamma W$ box amplitude is itself explicitly evaluated as the time-ordered product of the electromagnetic and charge-changing weak current operators, providing a transparent multipole decomposition of the currents. The resulting complicated amplitude structure involves many-body resolvent operators which are treated with the Lanczos strengths method, the key tool of this dissertation. As much as is permitted by the Lanczos algorithm, this method incorporates quasi-exact information about the complete intermediate nuclear spectrum. For $^{10}\mathrm{C} \to {}^{10}\mathrm{B}$, we find the nuclear-structure-dependent radiative correction $\delta_{\rm NS}$ to be

$$\delta_{\rm NS}\big[{}^{10}\mathrm{C} \to {}^{10}\mathrm{B}\big] = -0.422\,(14)_{\rm PME}(4)_{\Omega}(9)_{\chi}(24)_{\rm sh}(12)_{n,\rm el}\,\% \quad ,$$

which represents a 1.6x reduction in the quoted uncertainty compared to prior literature estimates despite the accounting for additional uncertainties. Preliminary results for the $^{14}\mathrm{O} \to {}^{14}\mathrm{N}$ transition indicate a markedly different distribution of the amplitude strengths, reflecting a strong Gamow-Teller suppression and highlighting the need for higher-multipole analysis before a final value is quoted.

These precision gains directly impact the determination of $V_{ud}$ and thus the top-row, Cabibbo-Kobayashi-Maskawa matrix unitarity test, motivating renewed experimental efforts – particularly a more precise measurement of the $^{10}\mathrm{C}$ branching ratio – and opening the way to analogous, precision *ab initio* studies for other electroweak processes in light nuclei.

# Contents

# List of Figures

# List of Tables

# Declaration

This dissertation comprises the original work of the author, M. Gennari, under the superversion of Dr. Petr Navrátil, completed with collaborators M. Drissi, C.-Y. Seng and M. Gorchtein. The content of this dissertation has been dedicated to a singular topic with the intent of presenting a full, cohesive story about calculations of electroweak radiative corrections in a modern nuclear theory setting. The main results presented in this dissertation as related to the $^{10}\mathrm{C} \to {}^{10}\mathrm{B}$ have been published in the following reference. The derivations as performed by myself are presented in full in this thesis. Writing of the manuscript was completed primarily by myself.

M. Gennari, M. Drissi, M. Gorchtein, P. Navrátil, and C.-Y. Seng, "Ab Initio Strategy for Taming the Nuclear-Structure Dependence of $V_{ud}$ Extractions: The $^{10}\mathrm{C} \to {}^{10}\mathrm{B}$ Superallowed Transition," *Physical Review Letters*, vol. 134, p. 012501, Jan 2025

Very much related works on the $^{14}\mathrm{O} \to {}^{14}\mathrm{N}$ Fermi transition, the evaluation of the $\gamma\gamma$ box diagram in light nuclei and total muon capture cross sections have manuscripts currently in preparation or work well underway. The former is the next iteration of the work presented here, and I have a significant hand in the latter two which are led by M. Drissi and D.A. Najera, respectively.

M. Gennari, M. Drissi, M. Gorchtein, P. Navrátil, and C.-Y. Seng, "*On the* $^{14}\mathrm{O} \to {}^{14}\mathrm{N}$ *transition.* In preparation."

M. Drissi, M. Gennari, and P. Navrátil, "*On the* $\gamma\gamma$ *box.* In preparation."

D. A. Najera, M. Gennari, L. Jokiniemi, M. Drissi, and P. Navrátil, "*On muon capture.* In progress."

That is not to say that it is the only work which has been completed throughout the timeline of the degree. Along with M. Vorabbi and collaborators, the following additional work was published. In the below work, I derived and implemented a form of the nonlocal, translation invariant spin density operator in the NCSM codes to facilitate the inclusion of the target spin in a generalized optical potential formalism. We supply the microscopic input for the construction of such potentials by M. Vorabbi. Writing of the manuscript was completed primarily by M. Vorabbi.

M. Vorabbi, M. Gennari, P. Finelli, C. Giusti, P. Navrátil, and R. Machleidt, "Elastic proton scattering off nonzero spin nuclei," *Physical Review C*, vol. 105, p. 014621, Jan 2022

# Chapter 1

# Introduction

Nuclear physics is the study of the atomic nucleus, a quantum system which is the foundation of all macroscopic structures we see in nature, from molecules to cells to stars. Theoretical nuclear physics is concerned with understanding the emergence of these structures from the most fundamental theory of quanta available to us, the Standard Model (SM) of Particle Physics, as well as how these systems interact with their environment and undergo reactions and decays. However, nuclei are non-trivial to describe, requiring competency in Quantum Field Theory (QFT) and quantum many-body theory, as well as advanced mathematical and computational techniques, to describe even the simplest systems with which we are familiar.

Unfortunately for the already fatigued nuclear physicist, nuclear structure is governed by the theory of colour interactions and strongly-interacting phenomena – denoted Quantum Chromo-dynamics (QCD) – which, in the low-energy regime where nuclei exist, is highly non-perturbative. There has been tremendous progress with our understanding of QCD since its formulation during the earliest days of the SM in the 1960s. Yet, as of today, we continue to suffer under the weight of strongly-coupled gauge theories and limited analytic information is known about critical aspects of the physical theory, e.g., colour confinement. We have since turned to numerical models to ascertain properties of the theory at different energy scales via approaches such as Lattice QCD (LQCD) for sub-nuclear physics or models for nuclei based upon effective field theories of QCD and quantum many-body theory. While we may fantasize about the possibility of one day describing nuclei directly from LQCD, the colour-confining aspects of QCD and the consideration of low-energy phenomena make it very much possible to describe the bulk properties of nuclei in terms of effective, composite states of the fundamental quanta of QCD. These states are the proton, neutron and the pions; the former two frequently referred to as nucleons and all of them made from colourless combinations of quarks and gluons, the true degrees of freedom in QCD. Then, in this picture of nuclei, the underlying theory of QCD is responsible for the effective inter-nucleon interactions experienced by protons and neutrons – very much akin to a Van der Waals type interaction – which is ultimately what binds the atomic nucleus. The quantum many-body description of nuclei with realistic inter-nucleon potentials derived via a mathematically well-defined connection to QCD has been a long-standing goal of what is nowadays referred to as *ab initio* nuclear theory.

Now, dear reader, if you are a non-nuclear physicist, perhaps you may be asking yourself the following questions or making the following comments.

> *Why expend the effort? After all, all we know is perturbation theory!*
> *Is nuclear phenomenology not enough? We have been doing it for decades and it works just fine!*
> *Shall we not just leave the quarks and gluons and the protons and neutrons be?*
>
> *– Someone, Somewhere, Sometime*

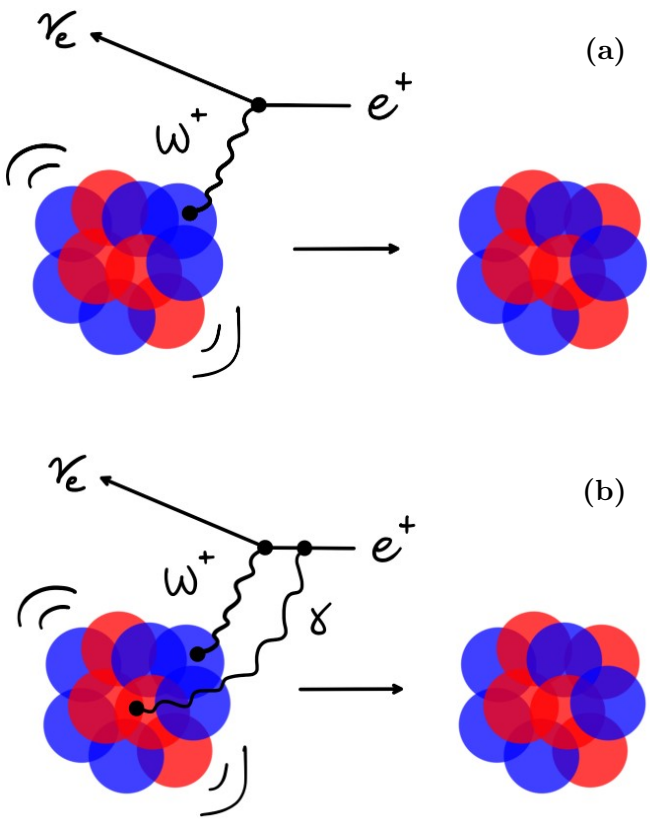


Figure 1.1: Pictured in subfigure **(a)** is the tree-level $\beta$ decay process of $\Psi_i \to \Psi_f + \nu_e + e^+$ for the nuclear Fermi transition $^{10}\mathrm{C} \to {}^{10}\mathrm{B}$. In subfigure **(b)**, we illustrate a higher-order, virtual electroweak process for the same transition, known as the $\gamma W$ box. Protons are shown in blue and neutrons in red.

To answer, let me begin by stating that a fully predictive *ab initio* theory for nuclear structure and reactions is critical for the wider physics community. The regime of nuclear physics is vast and thus overlaps with many sectors of theory and experiment in various fields of physics. The principle narrative of this dissertation will be that our ability to investigate nuclei can significantly impact high-precision, fundamental symmetry tests of the SM and, furthermore, our understanding of the existence of new physics.

For example, in studying special forms of $\beta$ decay observed in nuclei, referred to as nuclear Fermi transitions, it is possible to probe aspects of the weakly-interacting sector of the SM. We refer to subfigure **(a)** of Fig. 1.1, which shows the tree-level Fermi decay of the lightest possible transition in $^{10}\mathrm{C} \to {}^{10}\mathrm{B}$. The amplitude for such a transition between lepton-nucleus, plane-wave QFT states is given by

$$M_{\mathrm{tree}}(p_f, p_i, k_f, k_i) = -\frac{G_F}{\sqrt{2}}\, L_\lambda(k_f, k_i)\, \left\langle\, \Psi_f\,;\, \vec{p}_f \,\middle|\, J_{\mathrm{W}}^{\dagger\lambda}(q) \,\middle|\, \Psi_i\,;\, \vec{p}_i \,\right\rangle \quad , \tag{1.1}$$

where $L_\lambda$ is the leptonic current and the amplitude between external hadronic nuclear states $\Psi_i$ and $\Psi_f$ is of the charge-changing weak current operator $J_{\mathrm{W}}^{\dagger\lambda}$. We will dissect this in more detail in Sec. 4, however, superficially this current arises from the weak charge-changing (WCC) part of the SM Lagrangian

$$\mathcal{L}_{\mathrm{WCC}} = -\frac{G_F}{\sqrt{2}} \begin{pmatrix} \bar{u}_L & \bar{c}_L & \bar{t}_L \end{pmatrix} \gamma^\mu W_\mu^+ V_{\mathrm{CKM}} \begin{pmatrix} d_L \\ s_L \\ b_L \end{pmatrix} + \text{h.c.} \quad , \tag{1.2}$$

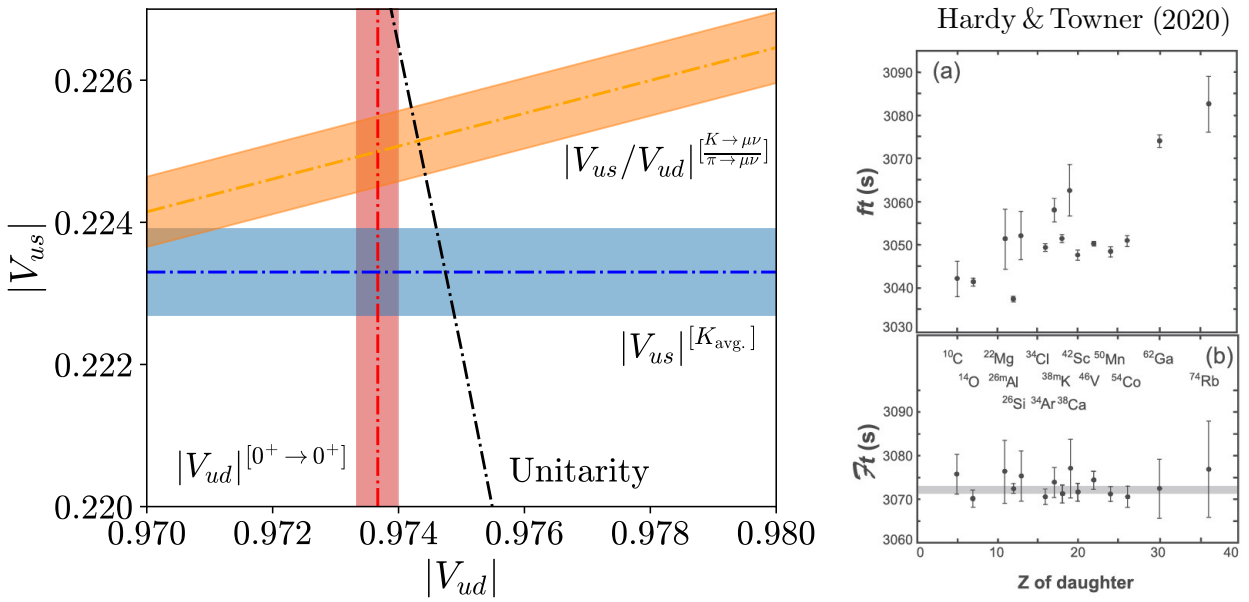


Figure 1.2: **(Left)** The modern CKM unitarity landscape with values for $V_{ud}$, $V_{us}$ and the ratio $V_{ud}/V_{us}$ annotated with their corresponding experimental extractions [6]. The dashdot lines and bands respectively represent the central value and uncertainty in the extraction of a given top-row element of the CKM matrix. The black line indicates the exact unitarity constraint. **(Right)** Figures taken directly from Ref. [7] with evaluations for a range of nuclei from $^{10}$C to $^{74}$Rb of **(a)** $ft$ values as extracted from experiment **(b)** corrected $\mathcal{F}t$ values with higher-order SM processes included.

and, for the moment, what is most important to know is that the SM object responsible for guiding such decays at the quark level – the Cabbibo-Kobayashi-Maskawa (CKM) matrix – appears as a $3 \times 3$ unitary matrix in said Lagrangian [8, 9]. Via processes such as nuclear Fermi decays, it is possible to constrain an entry of the CKM matrix, $V_{ud}$, which describes the probability of an up-down quark transition and is the largest contributor to the top-row unitarity condition

$$|V_{ud}|^2 + |V_{us}|^2 + |V_{ub}|^2 = 1 \quad . \tag{1.3}$$

Due to the properties of the interaction as well as the interacting nuclei, e.g., the conserved-vector-current hypothesis and the $0^+ \to 0^+$ nature of the decay, one may derive that

$$|V_{ud}|^2 = \frac{K}{ft} + \text{higher-order corrections} \quad , \tag{1.4}$$

where the quantity $ft$ is the product of a phase-space factor and the half-life of the decaying nuclear system, and $K$ is a constant [7]. The most remarkable feature of this relation is that, up to higher-order corrections, we should expect *identical* values of $ft$ across the nuclear chart irrespective of the decay we choose to observe.

We refer to Fig. 1.2. Pictured in the subfigure on the left-hand-side is the modern landscape of CKM unitarity constraints, with $V_{ud}$ as extracted from the 15 most precisely measured nuclear Fermi transitions ranging from $^{10}$C to $^{74}$Rb. See Ref. [6] and references therein for details on the evaluations of $V_{ud}$ and $V_{us}$ as shown in this subfigure. We note that the contribution of $V_{ub}$ to the top-row unitarity sum is neglected as its absolute magnitude lies below the current precision of theory and experiment. If we quickly turn our attention to subfigure **(a)** on the right-hand-side, we see the extractions of $ft$ for the set

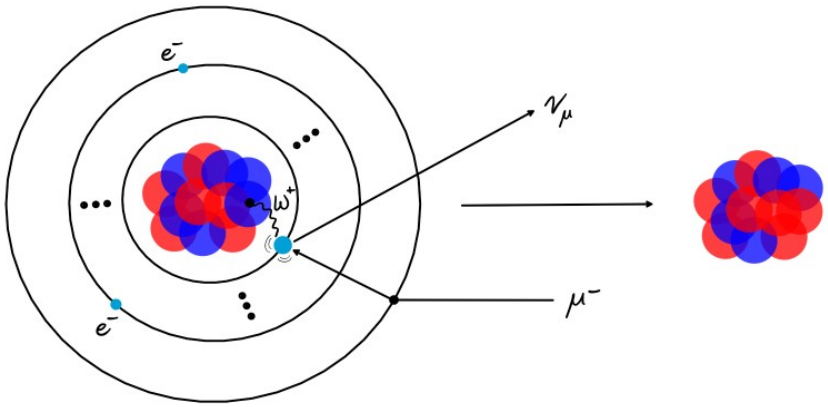


Figure 1.3: Pictured is the muon-capture-driven, tree-level $\beta$ decay process of $\Psi_i + \mu^- \rightarrow \Psi_f + \nu_\mu$ for the known transition $^{12}\mathrm{C} \rightarrow {}^{12}\mathrm{B}$. Protons are shown in blue and neutrons in red.

of transitions are clearly not identical. In reality, at the precision level of $10^{-4}$ that we currently target in the top-row unitarity test, these aforementioned higher-order corrections are of great importance. It is only after inclusion of such corrections that we may arrive at a quasi-transition-independent extraction of $V_{ud}$, e.g., see subfigure **(b)** of Fig. 1.1 for an example of a higher-order electroweak process, with the transition-independent $\mathcal{F}t$ values as pictured in subfigure **(b)** of Fig. 1.2. The major takeaway from this discussion is that we require precision estimates of these higher-order corrections in nuclei if we want to extract $V_{ud}$ from Fermi decays; these cannot be obtained from phenomenology. Thus, if we can apply our state-of-the-art models of nuclei in conjunction with precision electroweak theory, we may indeed say something important about the fundamental character of weak interactions in the SM; see Refs. [10, 11, 12] for examples of discussions on just how much we can do!

Moreover, a series of recent analyses of the CKM unitarity condition [12, 13, 14, 15, 16] provide compelling evidence of a statistical discrepancy with the SM prediction, as can be seen in the subfigure on the left-hand-side of Fig. 1.2 by the non-overlap of the unitarity constraint (the black line) with the current estimates of $V_{ud}$ and $V_{us}$. This condition, if unsatisfied, is a key indicator of missing physics in the weak sector of the SM. Important to note is that the size of the nuclear uncertainties entering the extraction of $V_{ud}$ almost doubled between subsequent evaluations in 2015 [17] and 2020 [7] due to unmanaged nuclear structure effects. This dissertation is then very timely in that the focus is entirely on improving the precision of the dominant nuclear structure uncertainty in the $V_{ud}$ extraction [18], the so-called $\gamma W$ box diagram illustrated in subfigure **(b)** of Fig. 1.1, so that we may make clear the nature of this discrepancy.

### Other Processes of Importance in Nuclei

We have focused on nuclear Fermi decays as they are the core topic of this dissertation, however, with a predictive *ab initio* theory, one could contribute to a variety of fundamental symmetry tests of the SM. We mention several here (but not all) that are currently under pursuit by our community.

*Neutrino-less Double Beta Decay* – While to this day unobserved, a famous process referred to as neutrino-less double $\beta$ decay ($0\nu\beta\beta$) is very frequently touted as the next potential major discovery, confirmation of which would indicate the Majorana plus Dirac nature of the neutrino [19]. Several of our colleagues at TRIUMF and many others in the community have paid numerous hours to improving the precision of nuclear amplitudes entering $0\nu\beta\beta$ and it is a very active area of theory research [20, 21, 22, 23, 24, 25]

with a plethora of nuclear physics experiments under construction with the hope of achieving the first observation. Its cousin, two-neutrino double $\beta$ decay ($2\nu\beta\beta$), is the rarest observed process in nature and significant effort from the community was made to benchmark predictions in nuclei for unphysical variants of such transitions [20]. As a test of the machinery developed in this dissertation, we replicate the original benchmarks performed in Ref. [20] and perform new ones (which remain unpublished) with the valence space, in-medium similarity renormalization group (VS-IMSRG) approach levied by our fellow group at TRIUMF. More details will be presented in Sec. 3.4.

*Muon Capture and Muonic Atoms* – Beyond this, we refer to the muon capture process depicted in Fig. 1.3, theoretical predictions of which serve as an excellent testing ground for the amplitudes which enter $0\nu\beta\beta$ and $2\nu\beta\beta$ calculations, with similar momentum transfer, electroweak currents and nuclei at play [26]. As a follow-up to the work presented in this dissertation, we are pursuing two separate projects, one on muon capture and another on muonic atoms in the same formalism.

*Neutrino-Nucleus Scattering* – The various next-generation accelerator programs dedicated to the study of neutrino-nucleus interactions, e.g., ANNIE [27], COHERENT [28], CONNIE [29] and MINER [30], naturally provide motivation for a parallel theory program on lepton-nucleus interactions. Such experiments will offer comprehensive studies into neutrino physics, e.g., see Refs. [31, 32, 33], including but not limited to (i) electromagnetic properties of the neutrino, (ii) deviations from the Weinberg angle at the MeV scale, and (iii) non-standard neutrino interactions with hadrons. Improvements to the theory of neutrino-nucleus interactions are thus crucial to the success of the up-and-coming experimental programs, particularly in the disentanglement of new physics effects and SM predictions. Preliminary ab initio studies have already been performed in $^{40}$Ar [34] as early as 2019, more recently in heavier systems [35], and more broadly with the shell model for a wide range of systems relevant to experiment [36].

*Anapole Moments and Electric Dipole Moments* – Experimental measurments of electric dipole moments (EDMs) are similarly sought after as any realistic, non-zero observation with today's technology would indicate new physics as the threshold for measurment presently expected from SM physics for electrons, nucleons, and nuclei is beyond the capabilities of modern techniques. With sophisticated nuclear approaches, we may highlight nuclei of interest for future experimental studies, e.g. $^{11}$Be, which has a ground state halo structure with strong electromagnetic transitions to other low-lying bound states, meaning significant enhancements to the nuclear electric dipole moment are anticipated [37]. Closely related to the EDM experimental program are measurments of the so-called "anapole moments", as originally proposed in Ref. [38], which arise from the heavily suppressed, parity non-conserving, neutral-current weak interactions in nuclei. In the SM, these arise as loop-level radiative corrections to electromagnetic interactions which imbue the system with the quoted additional electromagnetic moment. Precision measurments of anapole moments in nuclei seek to act as a gateway to increasingly precise measurments and theoretical predictions of nuclear EDMs [39, 40].

*Reactions for Astrophysics* – Additionally, predictive nuclear theories are intrinsic to a deeper understanding of nuclear astrophysics. Relevant reactions are often not accessible through laboratory experiments, due to the low-energy nature of cosmic processes. The development of an *ab initio* theory for the description of astrophysical processes is paramount [41, 42] as one can then address the experimental obstacles typically encountered in nuclear astrophysics, providing direct connections between macroscopic astrophysics and QCD. Reactions of major theoretical interest include the $^{12}\mathrm{C}(\alpha,\gamma)^{16}\mathrm{O}$ transfer reaction and $^{13}\mathrm{C}(\alpha,n)^{16}\mathrm{O}$ radiative capture reaction, which are needed for complete understanding of the astrophysical processes (such as the $s$-process in stars) responsible for producing heavy elements. Of similar interest is the $^{14}\mathrm{N}(p,\gamma)^{15}\mathrm{O}$ proton capture reaction, which must be well understood for an accurate description of the famous Carbon-Nitrogen-Oxygen (CNO) cycle in stars. Another reaction of interest is the neutron-induced $^{14}\mathrm{N}(n,p)^{14}\mathrm{C}$ charge exchange reaction, which is relevant for stellar nucleosynthesis. While there

exists fair amounts of experimental data, there also exists a discrepancy in the $^{14}\mathrm{N}(n,p)^{14}\mathrm{C}$ cross sections [43]. Lastly, there is great effort in attempting to understand the formation of heavy-elements from the primordial abundance of light nuclei [44]. The complicated reaction processes in the first stars are the gateway to understanding how light-nuclei clustered into their heavier counterparts. A fully predictive *ab initio* theory capable of describing clustering in nuclei could assist in shedding light on the early formation of heavy elements in our universe.

The timely future investment in the development of ab initio theory for the description of precision SM and beyond SM processes – particularly in, for example, light-nuclei where the many-body errors are more rigorously understood – will provide value not just in benchmarking with less-exact, yet scalable many-body methods but in furthering a research program which addresses critical goals of the wider nuclear, particle and astrophysics communities.

### The State-of-the-Art in Nuclear Theory

Broadly speaking, research efforts in modern nuclear theory may be divided into two main categories: the formulation of effective strong and electroweak interactions in nuclei and the development of quantum many-body methods that can employ said interactions in realistic calculation. The former will be *briefly* discussed in the subsequent sections with some early history presented below. For the latter, I will present a birds-eye view of the field here while in Sec. 2.3.3 I will introduce the favourite many-body method of our sub-group at TRIUMF: the no-core shell model.

This division highlights the longstanding and still fundamental challenge of arriving at a unified description of nuclear structure and dynamics from the underlying Standard Model (SM). As bound states of (nucleons, which are bound states of) quarks and gluons, nuclei exist as complex bound states of strongly-interacting quantum matter which form via the theory of Quantum Chromo-Dynamics (QCD). What's more, additional complexity arises in the nuclear environment due to electromagnetic interactions, described via Quantum Electro-Dynamics (QED), as well as the weak sector of the SM. At the time of writing this dissertation, the intractable complexity of describing bound systems in Quantum Field Theory (QFT) coupled with the highly non-perturbative form of the QCD Lagrangian in the strong coupling regime has made effective field theory (EFT) methods truly indispensable tools in the construction of realistic models of nuclei. At the absolutely highest level, EFTs are quantum field theories which are by construction valid within a bounded energy domain, often characterized by an energy cutoff scale. Such a construction naturally permits a systematic, order-by-order expansion of the Lagrangian in powers of ratios of the characteristic momentum of the constituents of the theory and its cutoff scale. To our knowledge, the earliest discussions of an EFT formalism for the treatment of strongly-interacting systems were presented by Schwinger in Ref. [45] and Weinberg in his seminal work on $\pi - \pi$ scattering [46]. Despite the early success of the formalism in reproducing the state-of-the-art results of current algebra with a substantial reduction in effort, it took some time for the ideas to be fully appreciated − even in Weinberg's own work − as discussed in his various addresses on the historical developments of EFT, e.g., see Ref. [47]. First presented in applications to strong interactions in Ref. [48] and later formalized and extended by Gasser and Leutwyler in Refs. [49, 50], Chiral EFT ($\chi$EFT) has become recognized as the "gold standard" for a low-energy, effective description of QCD. While I believe that I could never do true justice to the material here, in the first two preliminary sections I aim to provide a grounded and accessible picture of the foundation of modern $\chi$EFT approaches.

On the other end of the field, more where our group at TRIUMF is situated, we are concerned with the development of solvers for the quantum many-body problem and with the application of many-body theory. Our group's favourite method is the no-core shell model, a direct large-basis discretization and diagonalization approach to constructing solutions to the nuclear Hamiltonian with roots dating as far back as the mid- to late-1990s. We will provide more background on this approach later. Since

that time, a wealth of approaches have emerged in nuclear theory, several with direct inspiration from approaches in quantum chemistry, e.g., Coupled Cluster [51], IM-SRG [52] with related works in quantum chemistry [53], Self-Consistent Green Functions [54] and many others. The field has been characterized by the rapid expansion in methods capable of scaling better with the number of quanta to consider, pushing well beyond the traditional realm of light nuclei. I highly recommend the interested reader in perusing Ref. [55] for a "guided tour" of the recent developments in the last two decades.

This dissertation covers many topics and the dissertation is organized as follows. The first chapter following the introduction, Chapter 2, will cover the low-energy, symmetry properties of QCD and develop the most basic form of $\chi$EFT for the pion sector of the theory. In the remaining two sections, I will introduce the no-core shell model (NCSM), a non-relativistic quantum many-body formalism for the numerical solution of the Schrödinger equation, as well as the supremely important Lanczos algorithm, which provides much more than it claims to at first glance. In Chapter 3, we will re-derive expressions for the non-relativistic reductions of the electroweak current operators as seen in literature, provide a rigorous connection of QFT amplitudes to their non-relativistic counterparts and present the reproduction of prior NCSM results for $2\nu\beta\beta$ amplitudes as a test of the current machinery. In Chapter 4, we will present the main results of this dissertation on calculations of the $\gamma W$ box electroweak radiative correction for the two lightest nuclear Fermi decays possible, the $^{10}\mathrm{C} \to {}^{10}\mathrm{B}$ and $^{14}\mathrm{O} \to {}^{14}\mathrm{N}$. To get there will require deriving a form of the Compton tensor for a time-ordered product of electroweak currents suitable for nuclear theory calculations as well as a thorough analysis of the pole structure of the $\gamma W$ box function. We will then summarize our findings and make a statement about the possible impact on related experimental programs.

# Chapter 2

# Preliminaries

As I have emphasized in the introduction, the *ab initio* nuclear theory community is divided into two parallel efforts, one side tackling the construction of realistic inter-nucleon interactions and the other developing solvers for the quantum many-body problem with theories constructed from said inter-nucleon interactions. The preliminary sections I present here reflect this, with the first two sections focused on the low-energy characteristics of QCD and its realization via chiral effective field theory ($\chi$EFT), while the latter two sections focus on the favourite many-body formalism of our group at TRIUMF, the no-core shell model (NCSM), and important results in the field of many-body theory à la Lanczos.

While not the focus of my personal research program, in the first two sections of this chapter, I will discuss the symmetries of low-energy QCD and I will guide the reader through the derivation of the leading order (LO) contributions to the pion sector of chiral EFT. This was completed in the hopes of improving my own competency in the contemporary language and tools of EFT which have become a part of almost every facet of nuclear theory. The presentation is inspired by several key review articles, e.g., see Refs. [56, 57, 58], which offer more comprehensive treatments of the formalism. As taken directly from an address by Weinberg, a pragmatic implementation of an EFT typically follows the following sequence of well-defined steps.

(i) Identify the relevant low- and high-energy scales as well as the low-energy degrees of freedom.

(ii) Identify the symmetries and the symmetry breaking patterns of the low- and high-energy theories.

(iii) Construct the most general effective Lagrangian possible consistent with the broken (and the unbroken) symmetries.

(iv) Organize an expansion in the low-energy regime using ratios of momenta with powers of the high-energy scale.

(v) Evaluate the set of infinite Feynman diagrams to the desired accuracy.

We note that the formal development of EFT, particularly in the context of strongly coupled theories such as $\chi$EFT [59], is an active area of research with ongoing debates about best practices, potential caveats and lots of unanswered questions about the domains of applicability in many-fermion systems. Where deemed necessary, we will reference ongoing debate in the literature.

In the latter two sections, I will discuss content directly relevant to my core research program. In particular, we will focus on a sole method which has been developed over the last 30 or so years, with the earliest papers emerging in the late 1990s [60, 61, 62]. This approach is known as the no-core shell model and, up to the assumptions of the model regarding nuclei as composite structures of protons and neutrons, in the infinite basis limit the method is exact. Coupled with the Lanczos algorithm for the tri-diagonalization of large, sparse matrices, the no-core shell model is a conceptually simple yet powerful approach well-suited to the rigorous description of light $s$- and $p$-shell nuclei. More on this later.

Let us now begin our walk through of $\chi$EFT.

## 2.1 Quantum Chromo-Dynamics

The Standard Model is our greatest modern theory of quantum interactions. In nuclear theory, we are concerned with every aspect of the SM, though are principally interested in the theory of the strong interaction known as QCD. We refer the reader to Ref. [63] for introductory lectures on QCD intended for students of high-energy phenomenology as well as Ref. [6] for a brief but all-encompassing, modern collection of reviews on the subject. We will keep the discussion at a relatively high-level with the intent of summarizing results relevant to the effective field theory narrative.

The strong interaction is one of four known fundamental interactions in nature and one of the three successfully incorporated into the SM. QCD is a Yang-Mills gauge theory with a local gauge invariance, i.e., an invariance with respect to space-time dependent transformations, described by the $\mathrm{SU}(3)_c$ colour group. The first suggestion of the existence of colour charge came in independent works by Greenberg in 1964 [64] and Han and Nambu in 1965 [65]. Today, we know that in QCD there exist fermionic fields with colour quantum numbers, known as quarks, and colour-changing bosonic fields, known as gluons, which are the basic constituents of the theory. Quark fields exist in the fundamental representation of the colour group **3** and anti-quarks in the corresponding conjugate representation **3***; the dimension of the representation comes solely from the number of colour degrees of freedom observed in nature, that is, $N_c = 3$. Thorough analysis via high-energy spectroscopy inidcates that there are six quark flavours of different mass but identical dynamical properties with respect to the gluon fields. The modern 3-generation QCD Lagrangian with six flavours ($N_f = 6$) of quarks is written as

$$\mathcal{L}_{\mathrm{QCD}} = \sum_{q=1}^{N_f} i\,\bar{\psi}_q^i\,\gamma^\mu \big[D_\mu\big]_{ij}\,\psi_q^j - m_q\,\bar{\psi}_q^i\,\psi_{qi} - \frac{1}{4}\,G^a_{\mu\nu}\,G^{a\mu\nu} \qquad\qquad \psi_q = \begin{pmatrix}\psi_{q,R}\\ \psi_{q,G}\\ \psi_{q,B}\end{pmatrix} \quad , \tag{2.1}$$

in which we have the 3-spinor $\psi_q^i$ quark colour fields with mass $m_q$, flavour $q \in \{u, d, s, c, b, t\}$ and colour index $i \in \{R, G, B\}$. Definitions of the gamma matrices may be found in Appendix A. The gluon field strength tensor is given by

$$G^a_{\mu\nu} = \partial_\mu\,A^a_\nu - \partial_\nu\,A^a_\mu + \alpha_s\,f^a_{bc}\,A^b_\mu\,A^c_\nu \quad , \tag{2.2}$$

where we write the vector field which mediates colour charge as $A_\mu = T^a A^a_\mu$ in the basis of gluon fields $A^a_\mu$, i.e., the basis of QCD bosons. Akin to electromagnetic field of QED, this field is responsible for all interactions between quanta with colour charge. The quantity $\alpha_s$ is the coupling constant of QCD which is perturbatively small at high-energies but $\mathcal{O}(1)$ at low-energy. The covariant derivative $D_\mu$ in the above expression is defined as

$$\big[D_\mu\big]_{ij} = \delta_{ij}\,\partial_\mu - \frac{i\alpha_s}{2}\,T^a_{ij}\,A^a_\mu \quad , \tag{2.3}$$

where the coupling $g_s$ is the strong interaction coupling and the set $\{T^a\}$ are the eight generators of the $\mathrm{SU}(3)_c$ colour group. These generators, referred to as the Gell-Mann matrices [66], act in the fundamental representation of the colour group as linear maps (rotations of the quark colour fields) and satsify the SU(3) Lie bracket algebra

$$\big[\,T^a,\,T^b\,\big] = i\,f_{abc}\,T^c \qquad\qquad a, b, c \in \{\,1, \cdots, 8\,\} \quad , \tag{2.4}$$

where $f_{abc}$ are the real and anti-symmetric algebraic structure constants.

### The Bosons of QCD

The gluon field is composed of the colour-charged QCD gauge bosons and it tells us how colour-charged quanta interact with one another. In order to exhibit the general exchange of colour charge, the gluon

fields must themselves be composed of a superposition of colour and anti-colour configurations; they must be built from at least quark-anti-quark pairs. Thus, in terms of the colour degrees of freedom, the gluons must be represented in the product space $\mathbf{3} \otimes \mathbf{3^*} = \mathbf{8} \oplus \mathbf{1}$ which indicates eight possible gluon states.

*Remark* 2.1.1 (**Colour Singlet Gluon State**). From the Young-Tableaux decomposition $\mathbf{3} \otimes \mathbf{3^*} = \mathbf{8} \oplus \mathbf{1}$, there exists a gluon state which occupies the singlet representation $\mathbf{1}$. This state is incapable of colour changing processes and is given by $\left|G_9\right\rangle = \frac{1}{\sqrt{3}} \left(\left|r\bar{r}\right\rangle + \left|g\bar{g}\right\rangle + \left|b\bar{b}\right\rangle\right)$ .

### Colour Confinement

Today, the property of QCD most perplexing to theorists is referred to as "colour confinement" and its principle implies that quark and gluon fields, as we describe them in QCD, are not directly observable in nature; only colour-less *gauge invariant* objects are observable. This means that any detectable quanta constructed from quarks and gluons must be colourless! The gauge-invariant, many-quark bound states that we observe in nature are referred to as hadrons. Confinement is thought to arise from the uniquely different structure of the QCD Lagrangian compared to other physical theories. We point to the gluon field strength tensor defined in Eq. (2.2) which notably contains terms quadratic in the gluon fields due to the non-abelian structure of SU(3) algebra, then meaning that the QCD Lagrangian in Eq. (2.1) is quartic in the gluon fields. This results in fervid self-interactions between the gluon fields, particularly at low-energy where the QCD coupling $\alpha_s$ is $\mathcal{O}(1)$. Obviously, this is quite different from the QED Lagrangian with the electromagnetic field strength tensor given by

$$F_{\mu\nu} = \partial_\mu A_\nu - \partial_\nu A_\mu \quad ,$$

and no direct coupling between the bosonic fields. The result is that photon self-interactions are weak and only emerge at high-order in perturbation theory, contrary to low-energy QCD where the gluonic self-interactions produce highly non-linear behaviour and result in a theory which is mathematically challenging to understand. As an aside, one of the first major breakthroughs in our understanding of confinement for QCD-like theories came from Wilson, who made great insights with lattice simulations in the early 1970s [67], pioneering our understanding of confinement in quarks. There are several works from Seiberg and Witten, e.g., the famous work on four-dimensional SU(2) supersymmetric Yang-Mills theory [68, 69], which further pushed the frontier of our understanding of confinement. Needless to say, there is much to be done on this front, but there are several novel pursuits which have emerged in recent years attempting to probe theories by deformation from the SUSY limit [70, 71]. Much of the work being done these days is in the form of numerical simulation via LQCD, which has made tremendous progress on describing the fundamental QCD spectrum and, more recently, electroweak processes embedded on the lattice.

### The Flavour Symmetry of QCD with Equal Mass Quarks

In the following, we will typically use indices $(i, j)$ to represent the colour degrees of freedom and we will use indices $(q, r)$ for flavour indices. Let us consider the case of a QCD-like theory with an arbitrary number $N_f$ of quarks with equal mass $m$. Then, in the limit of equal mass quarks, we find that the

Lagrangian for QCD becomes

$$\lim_{m_q \to m \; \forall q} \mathcal{L}_{\text{QCD}} = \sum_{q=1}^{N_f} i\, \bar{\psi}^{qi} \left( \gamma^\mu \big[ D_\mu \big]_{ij} - m \right) \psi_q^j \quad . \tag{2.5}$$

If we apply an infinitesimal global flavour transformation of the form

$$\psi_q^i \to e^{i\delta\alpha^a T_a}\, \psi_q^i \qquad\qquad e^{i\delta\alpha^a T_a} = 1 + i\delta\alpha^a T_a + \mathcal{O}(\alpha_a^2) \quad ,$$

then we may write the variation in the quark fields $\psi_q$ to first order as

$$\delta\psi_q^i = -i\,\delta\alpha^a \left[ T_a \right]_q^{\;r} \psi_r^i \qquad\qquad \delta\bar{\psi}_q^i = i\,\delta\alpha^a\, \bar{\psi}_r^i \left[ T_a \right]_{\;q}^r \qquad\qquad \delta A_{a\mu} = 0 \quad ,$$

where we have of course applied the Euler-Lagrange equations in deriving the above. We now pause to introduce Noether's theorem, one of the most important theorems in modern theoretical physics.

**Theorem 2.1.1** (**Noether's Theorem**)**.** If a Lagrangian has a continuous symmetry of either global or local character, then there exists an associated Noether current that is conserved when the equations of motion are satisfied [72]. Consider a Lagrangian $\mathcal{L}(\phi_1, \ldots, \phi_N)$ which is invariant under a continuous infinitesimal transformation that we parameterize by the set of variations $\delta\alpha_a$ for $a \in \{\, 1, \ldots, N \,\}$, then the variation of $\mathcal{L}$ with respect to $\alpha_a$ is

$$\frac{\delta\mathcal{L}}{\delta\alpha_a} = \sum_{n=1}^{N} \left\{ \left[ \frac{\partial\mathcal{L}}{\partial\phi_n} - \partial_\mu \frac{\partial\mathcal{L}}{\partial\big(\partial_\mu\phi_n\big)} \right] \frac{\delta\phi_n}{\delta\alpha_a} + \partial_\mu \left[ \frac{\partial\mathcal{L}}{\partial\big(\partial_\mu\phi_n\big)} \frac{\delta\phi_n}{\delta\alpha_a} \right] \right\} = 0 \qquad . \tag{2.6}$$

Of course, the first term is the set of Euler-Lagrange equations that define the equations of motion for the theory, and when they are satisfied, this term is zero. The result of Noether's theorem is hence

$$\partial_\mu\, J^{a\mu} = \partial_\mu \left[ \frac{\partial\mathcal{L}}{\partial\big(\partial_\mu\phi_n\big)} \frac{\delta\phi_n}{\delta\alpha_a} \right] = 0 \quad , \tag{2.7}$$

where $J^{a\mu}$ is a conserved Noether current.

Let us now apply the above theorem to the equal-quark-mass version of the QCD Lagrangian in Eq. (2.5). This yields the set of conserved Noether currents in terms of the basis of gluon fields

$$J^{a\mu} = -i \lim_{m_q \to m \; \forall q} \frac{\partial\mathcal{L}_{\text{QCD}}}{\partial\big(\partial_\mu\psi_q^i\big)} \left[ T^a \right]_q^{\;r} \psi_r^i = \bar{\psi}_i^q\, \gamma^\mu \left[ T^a \right]_q^{\;r} \psi_r^i \qquad\qquad \partial_\mu J^{a\mu} = 0 \qquad ,$$

which gives rise to the following conserved charges

$$Q^a(t) = \int d^3x\; J^{a0}(t, \vec{x}\,) = \int d^3x\; \bar{\psi}_i^q(t, \vec{x}\,)\, \gamma^0 \left[ T^a \right]_q^{\;r} \psi_r^i(t, \vec{x}\,) \quad .$$

We say that these are conserved charges as the current conservation condition implies

$$\partial_0\, Q^a(t) = \int d^3x\; \partial_0\, J^{a0}(t, \vec{x}\,) = -\int d^3x\; \vec{\nabla} \cdot \vec{J}^{\,a}(t, \vec{x}\,) \qquad \Longrightarrow \qquad Q^a(t) \equiv Q \qquad ,$$

that is to say, the charges $Q^a$ are time-independent and thus commute with the Hamiltonian of the theory. The charges then satisfy the $\text{SU}(N_f)$ algebra

$$\big[\, Q^a,\, Q^b \,\big] = i\, f_{abc}\, Q^c \qquad\qquad a, b, c \in \big\{\, 1, \ldots, N_f^2 - 1 \,\big\} \quad ,$$

and we identify the basis of charges $Q^a$ as the generators of flavour transformations. We have thus identified explicit flavour symmetry in the Lagrangian. We further see that the one-particle QFT states (which have yet to be defined clearly but I promise it will come) transform under flavour rotations as

$$\big|\,\vec{p};\,\psi\,\big\rangle = Q^a\big|\,\vec{p};\,r\,\big\rangle = -T^a\big|\,\vec{p};\,r\,\big\rangle \quad .$$

The realization of a global symmetry in this way, i.e., with the appearance of a multiplet of identical mass particles, is known as the Wigner-Weyl realization. While we know from experiment that, unfortunately, there does not exist a multiplet of equal-mass quarks, we will soon find that the Wigner-Weyl mode is not the only possible way to realize a global symmetry of the Lagrangian. In fact, it is not the way in which nature prefers to realize the $\mathrm{SU}(3)_c$ colour group. Nevertheless, in the true theory, the three lightest quark states $(u, d, s)$ exhibit an approximate flavour symmetry due to their light masses with respect to the heavy $(c, b, t)$ quark states. This is an important point to note for the following discussions.

**The Approximate Flavour Symmetry of QCD**

Let us now consider a modification of Eq. (2.5) in which we perturb the theory around the equal mass limit. We may take the quark masses to be $m_q = m + \delta m_q$ which, if we work out the variation of the Lagrangian with respect to the same global flavour transformations, leads to the following approximately conserved Noether current

$$J^{a\mu} = -i \lim_{m_q \to m\ \forall q} \frac{\partial \mathcal{L}_{\mathrm{QCD}}}{\partial\big(\partial_\mu \psi^i_q\big)} \left[T^a\right]^{\,r}_q \psi^i_r = \bar{\psi}^q_i \gamma^\mu \left[T^a\right]^{\,r}_q \psi^i_r$$

$$\partial_\mu J^{a\mu} \neq 0 \sim \mathcal{O}(\delta m_a - \delta m_b) \qquad ,$$

which is non-zero and directly proportional to the differences in the quark masses. The flavour symmetry of the QCD Lagrangian is explicitly broken by the non-equal quark masses. However, physically speaking, there are a subset of quarks for which the mass differences are small enough to be considered perturbative effects and so the symmetry is approximately preserved. The approximate flavour symmetry of the light-quark QCD Lagrangian manifests itself in the observed properties of the lightest hadrons. In the idealized case where quark masses are identical, hadrons would self-organize into degenerate multiplets of the flavour group $\mathrm{SU}(N_f)$. While this exact symmetry is generally broken in nature due to the non-zero quark mass differences, it is physically observable that a subset of quarks − most notably the up $(u)$ and down $(d)$ quarks − exhibit an approximate preservation of the symmetry. Compelling empirical evidence for this comes from the near-equality of the proton and neutron masses, as well as the approximate mass degeneracy of the charged and neutral pions. Mechanically speaking, the approximate flavour symmetry of the $u$ and $d$ quarks is described by invariance of the light-quark QCD Lagrangian under the SU(2) nuclear isospin group. In this way, nucleons are conveniently represented as isospin-1/2 doublets which transform under the fundamental representation $(\mathbf{2})$ of SU(2) and anti-nucleons belonging to the conjugate representation $(\mathbf{2^*})$. On the other hand, as pairs of quarks and anti-quarks, pions are then assigned to the isospin-1 adjoint representation $(\mathbf{3})$ of the decomposition $\mathbf{2} \otimes \mathbf{2^*} = \mathbf{3} \oplus \mathbf{1}$.

With these features of QCD in mind, we now turn our attention to the construction of a low-energy effective field theory for QCD, known as $\chi$EFT.

## 2.2 Chiral Effective Field Theory

The starting point for the construction of any EFT is to recognize the relevant symmetries and symmetry breaking patterns of the underlying theory as these provide the constraints needed to build a general effective Lagrangian consistent with the symmetries of the underlying theory. As we have taken the time in the previous section to understand the low-energy, approximate flavour symmetry of the quark fields in QCD, we may extend that discussion to chiral symmetry.

Recall the QCD Lagrangian in Eq. (2.1) and let us now restrict ourselves to a consideration of only the lightest two quark states, the up ($u$) and down ($d$) quarks. In this case, the flavour group reduces from the full SU(6) flavour group down to an SU(2) flavour group with the $\{T^a\}$ taking the form of the Pauli matrices. If we define the chiral projectors as

$$P_L = \frac{1}{2}\left(1-\gamma_5\right) \qquad\qquad P_R = \frac{1}{2}\left(1+\gamma_5\right) \qquad , \tag{2.8}$$

which project the quark fields onto their left- and right-handed components, respectively, we may rewrite the light-quark QCD Lagrangian $\mathcal{L}_<$ with suppressed colour indices in the chirally projected basis as

$$\mathcal{L}_< = i\,\bar{\psi}_{qL}\,\gamma^\mu D_\mu\,\psi_{qL} + i\,\bar{\psi}_{qR}\,\gamma^\mu D_\mu\,\psi_{qR} - i\,\bar{\psi}_{qL}\,M\,\psi_{qR} - i\,\bar{\psi}_{qR}\,M\,\psi_{qL} - \frac{1}{4}\,G^a_{\mu\nu}\,G^{a\mu\nu} \quad , \tag{2.9}$$

where $M = \mathrm{diag}\big(m_u, m_d\big)$ is the quark mass matrix. In this way, we can explicitly see the two terms which mix chirality, i.e., the chiral representations are mixed via the mass matrix. We can thus approach chiral transformations in a similar manner to our discussion on flavour transformations in the prior sections. Such transformations are near identical to flavour transformations, albeit with the inclusion of the $\gamma_5$ matrix.

As before, in the following we will typically use indices $(i,j)$ to represent the colour degrees of freedom and we will use indices $(q,r)$ for flavour indices. Consider an infinitesimal chiral rotation parameterized by $\{\delta\alpha_a\}$, then

$$\delta\psi^i_q = -i\,\delta\alpha^a\left[T_a\right]^{\ r}_q\,\gamma_5\,\psi^i_r \qquad\qquad \delta\bar{\psi}^i_q = i\,\delta\alpha^a\,\bar{\psi}^i_r\,\gamma_5\left[T_b\right]^{\ r}_q \qquad\qquad \delta A_{a\mu} = 0 \qquad .$$

If we again consider the special case of $m_u = m_d = m$, the variation of the Lagrangian $\mathcal{L}_<$ with respect to $\delta\alpha_a$ is non-zero and may be written as

$$\lim_{m_q\to m\ \forall q}\delta\mathcal{L}_< = 2im\,\delta\alpha^a\,\bar{\psi}^q_i\left[T_a\right]^{\ r}_q\,\gamma_5\,\psi^i_r \quad .$$

Contrary to the emergent SU($N_f$) flavour symmetry in the equal-mass QCD Lagrangian, we immediately see from this expression that *any non-zero quark mass* would explicitly break chiral symmetry. If we slightly modify the above result to consider the case of inequal quark masses, we instead have

$$\delta\mathcal{L}_< = i\,\delta\alpha^a\,\bar{\psi}^q_i\left[\left\{M,T_a\right\}\right]^{\ r}_q\,\gamma_5\,\psi^i_r \quad , \tag{2.10}$$

with $\{\cdot\}$ denoting the usual anti-commutator operation and $M$ denoting the quark mass matrix. As the variation is only non-zero for massless QCD, it is instructive for us to first consider this case.

### Chiral Symmetry in Massless, Light-Quark QCD

We have established that, in consideration of two-quark massless QCD, the Lagrangian of the theory is invariant under flavour and chiral (recognizable as axial-flavour) transformations. An application of Noether's theorem then yields the conserved currents

$$J^{a\mu} = \bar{\psi}^q_i\,\gamma^\mu\left[T^a\right]^{\ r}_q\,\psi^i_r \qquad\qquad \partial_\mu J^{a\mu} = 0 \qquad ,$$

$$J^{a\mu}_5 = \bar{\psi}^q_i\,\gamma^\mu\,\gamma_5\left[T^a\right]^{\ r}_q\,\psi^i_r \qquad\qquad \partial_\mu J^{a\mu}_5 = 0 \qquad ,$$

where we use the subscript "5" to indicate an axial structure. As before, we obtain the corresponding Noether charges

$$Q^a = \int d^3x \; J^{a0} \qquad\qquad Q_5^a = \int d^3x \; J_5^{a0} \tag{2.11}$$

which define the complete set of chiral rotations and satisfy the following product algebra

$$\big[\, Q^a,\, Q^b \,\big] = i\, f_{abc}\, Q^c \qquad \big[\, Q^a,\, Q_5^b \,\big] = i\, f_{abc}\, Q_5^c \qquad \big[\, Q_5^a,\, Q_5^b \,\big] = i\, f_{abc}\, Q^c \qquad a,b,c \in \{1,2,3\} \quad .$$

It is worth commenting that, as can be seen from the third relation above, the axial charges alone do not form a complete algebra as they are not closed under the commutator operation. It is much more intuitive to express the charges via the aforementioned left- and right-handed projectors as

$$Q_L^a = \frac{1}{2}\left(Q^a - Q_5^a\right) \qquad\qquad Q_R^a = \frac{1}{2}\left(Q^a + Q_5^a\right) \quad ,$$

for which the algebra satisfies

$$\big[\, Q_L^a,\, Q_L^b \,\big] = i\, f_{abc}\, Q_L^c \qquad \big[\, Q_R^a,\, Q_R^b \,\big] = i\, f_{abc}\, Q_R^c \qquad \big[\, Q_L^a,\, Q_R^b \,\big] = 0 \qquad a,b,c \in \{1,2,3\} \quad ,$$

clearly indicating that the left- and right-handed charges are now completely decoupled. Each set of charges defines a set of SU(2) transformations and so the full chiral group is given by

$$G_{\text{chiral}} = \text{SU}(2)_L \times \text{SU}(2)_R \quad . \tag{2.12}$$

where the flavour transformations discussed in the previous sections form a diagonal subgroup of the chiral group, $\text{SU}(2)_V \subset \text{SU}(2)_L \times \text{SU}(2)_R$. This is often denoted the isospin (flavour) group.

### Chiral Symmetry in Light-Quark QCD

Non-zero quark masses explicitly break chiral symmetry in $\mathcal{L}_<$ and, suprise surprise, in nature quarks have non-zero masses! The effects of chiral symmetry breaking may be treated perturbatively if the light-quark masses are substantially smaller than the characteristic confinement scale of QCD, that is, if

$$m_u,\, m_d \ll \Lambda_{\text{QCD}} \quad .$$

Given the empirically small quark masses, we are then left with a (very well-preserved) approximate $\text{SU}(2)_L \times \text{SU}(2)_R$ chiral symmerty. The question now becomes how to realize such a symmetry. As discussed in the context of flavour transformations, the inequal quark masses do not permit a realization via the Wigner-Weyl mode, particularly in the case of chiral (axial-flavour) transformations which would be characterized by

$$\big|\, \vec{p};\, \psi \,\big\rangle = Q_5^a \,\big|\, \vec{p};\, r+ \,\big\rangle = -T^a \,\big|\, \vec{p};\, r- \,\big\rangle \quad ,$$

where the $\pm$ in the kets indicates the parity of the state. Then, the above expression states that we should experimentally observe parity doublets for all states in the QCD spectrum of which we observe none. Without delving too deep into the details, we note that a critical assumption of the linear realization of a gauge symmetry via the Wigner-Weyl is that the vacuum of the theory is invariant under the same symmetry group as the Lagrangian, i.e., the charges can only annhilate the vacuum as

$$Q^a \,\big|0\big\rangle = 0 \qquad\qquad Q_5^a \,\big|0\big\rangle = 0 \quad .$$

It is now that we pause to introduce Goldstone's theorem.

**Theorem 2.2.1** (**Goldstone's Theorem**). Consider a Lagrangian $\mathcal{L}(\phi) \propto V(\phi)$ invariant under the action of a continuous symmetry group $G$, where $V$ is some well-behaved field potential. Let $Q$ be an associated generator of the continuous symmetry transformation of $\mathcal{L}$. Taking the variation of $\mathcal{L}$ under the symmetry transformation parameterized by the generator $Q$ and evaluating the field $\phi$ at the extrema of the potential $V$ gives

$$\left(\frac{\partial^2 V}{\partial\phi_a\,\partial\phi_b}\right)\Bigg|_{\phi=\bar{\phi}} Q^i_{bc}\bar{\phi}^c = 0 \quad . \tag{2.13}$$

In the above theorem, the second order partial derivative of the potential is regarded as the mass matrix for fluctuations of the fields about the minimum of the potential. The condition may be met in two possible ways: (i) the aforementioned Wigner-Weyl linear realization (ii) the so-called Nambu-Goldstone realization, to be described now. If we imagine that the assumption made in the Wigner-Weyl realization is not upheld, that is, if

$$Q^a\left|0\right\rangle \neq 0 \qquad\qquad Q^a_5\left|0\right\rangle \neq 0 \qquad ,$$

then the generators $\{\, Q^a,\, Q^a_5 \,\}$ are said to be spontaneously broken by the vacuum. In order to uphold the symmetry relation in Eq. (2.13), the "mass matrix" must have at least one zero eigenvalue. Thus, for each broken generator of the symmetry group, a massless fluctuation known as a Nambu-Goldstone boson is produced upon quantization of the theory. The number of Nambu-Goldstone bosons produced is $N = \dim(G) - \dim(\tilde{G})$, where $\tilde{G}$ is the residual symmetry group unbroken by the vacuum of the theory. This phenomenon is known as *spontaneous symmetry breaking* and this is known as the Nambu-Goldstone realization of a symmetry breaking pattern.

Let us bring this back into the context of chiral symmetry. We can immediately say that the axial generators $\{Q^a_5\}$ must be spontaneously broken since, as we have already seen, the ordinary flavour symmetry is more or less still intact. This symmetry breaking pattern is represented by the reduction of the symmetry group from the chiral $\mathrm{SU}(2)_L \times \mathrm{SU}(2)_R \to \mathrm{SU}(2)_V$ down to the residual isospin (flavour) subgroup. The direct consequence of this theorem is the "prediction" of three Nambu-Goldstone bosons for $\chi$EFT which are readily identified as the charged and neutral pions. Though Goldstone's theorem predicts massless fluctuations, the mass of the pions can be understood as a result of the additional, explicit chiral symmetry breaking that appears in $\mathcal{L}_<$ due to the non-zero quark masses which causes the Nambu-Goldstone bosons (the pions) to acquire a mass.

This completes our understanding of the low-energy, properties of QCD and provides us with the foundation for constructing an effective field theory based on the chiral symmetry breaking pattern.

### 2.2.1 Effective Lagrangians for the Pion from Chiral Symmetry

The next step in formulating an EFT for low-energy QCD involves writing down the most general Lagrangian that respects both the explicit and spontaneously broken symmetries of the underlying theory [73, 74]. However, in order to tractably use the diagramatic approach in QFT, we require a valid perturbative scheme in which to implement the expansion. Yet, as we have emphasized, the strong coupling regime of QCD makes the interaction highly non-perturbative and without fancy (to this day, non-existent) resummation techniques, the diagramtic approach is doomed to fail for any finite sum of terms.

### Cutoff Scale and Perturbativity

Then, first and foremost, we must specify the characteristic energy scales of the low- and high-energy regimes such that we may organize an expansion in the desired energy regime. To capture the bulk properties of nuclei and their dynamics, it is reasonable (if not appropriate) to adopt a hadronic description in which the relevant degrees of freedom are nucleons and pions. Although nucleons are composite objects, within the framework of $\chi$EFT they are treated as fundamental quantum fields as we are not interested in probing the internal structure of such quanta. The pions, which emerge as the pseudo-Nambu-Goldstone bosons due to the spontaneous breaking of chiral symmetry in light-quark QCD, are central to reproducing the correct dynamics of the low-energy theory. It is however possible to integrate out the pions completely from the theory and arrive at a theory purely in terms of nucleon degrees of freedom, called pion-less effective field theory, which enjoys substantial usage throughout the *ab initio* nuclear theory community [75, 76, 77] due to its more elegant, analytic structure in comparison to straight $\chi$EFT. Nevertheless, there remain similar concerns about the breakdown of the EFT expansion in the many-body sector [78, 79].

The breakdown scale $\Lambda_\chi$ of the effective field theory beyond which the perturbative expansion is no longer valid may be qualitatively motivated in several ways. Firstly, as we focus only on the up ($u$) and down ($d$) quarks, we have an immediate separation of scales between said quarks − and to some extent the strange ($s$) quark − and the heavy quark states ($c$, $b$, $t$), which are on the order of $\sim 1$ GeV. Even within the ($u$, $d$, $s$) triplet, the strange quark mass lies significantly higher in energy with a gap of roughly 100 MeV to the lightest quark states. Furthermore, the mass gap to the pseudo-Nambu-Goldstone bosons of $\chi$EFT, the pions, is roughly $135 - 140$ MeV while the mass gap to the lowest-lying vector $\rho$ meson is $\sim 775$ MeV. Loosely speaking, this hierarchy establishes that the choice of a cutoff scale for $\chi$EFT should be such that "perturbativity" in ratios of nucleon momenta $|\vec{p}| \sim m_\pi$ to the cutoff scale is maintained, while simultaneously straying reasonably far from the chiral symmetry breakdown scale at which point explicit quark-gluon degrees of freedom would play a substantial role. As a purely qualitative guide to the choice of cutoff scale, this is by no means an expert analysis and there are sufficient reviews on the topic, such as those quoted at the beginning of this chapter. I further refer the reader to Refs. [80, 81, 82] which discuss renomalizability and the efforts in producing renormalization group invariant formulations of $\chi$EFT.

*Remark* 2.2.1 (**What About the High-Energy Physics?**). One might wonder about the neglected physics above the cutoff scale $\Lambda_c$ and its role in nuclear dynamics. Such physics is absorbed into the definition of the low-energy coupling constants which emerge at, in principle, each order of the EFT expansion. They are fundamentally parameters of the theory and must be treated with phenomenology or, if sophisticated calculations exist, they may be determined from Lattice QCD (LQCD) simulations.

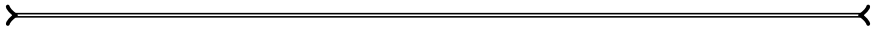

To summarize, we have qualitatively identified the low- and high-energy scales of $\chi$EFT and identified that we may organize a systematic expansion in powers of $|\vec{p}|/\Lambda_c$, where the nucleon momentum $|\vec{p}|$ is on the order of the pion mass $m_\pi$.

### Pions

Let us build up the EFT from the chiral vacuum, beginning with the massless version of light-quark QCD so that chiral symmetry is exact. The lowest energy states which can exist in $\chi$EFT are the pions and we thus go about constructing the Lagrangian for $\pi\pi$ interactions. Construction of $\mathcal{L}_{\pi\pi}$ proceeds by

examining the chiral transformation properties of the pion fields. We state the following:

1. The pions form as quark-anti-quark pairs which leads to three species of pions; the $\big|\pi^+\big\rangle = \big|u\bar{d}\big\rangle$, the $\big|\pi^-\big\rangle = \big|d\bar{u}\big\rangle$ and the $\big|\pi^0\big\rangle = \frac{1}{\sqrt{2}}\Big(\big|u\bar{u}\big\rangle - \big|d\bar{d}\big\rangle\Big)$.

2. The pion fields form an triplet in the isospin space and will transform linearly under $\mathrm{SU}(2)_V \subset \mathrm{SU}(2)_L \times \mathrm{SU}(2)_R$ global isospin transformations.

3. The chiral group must be realized non-linearly as we only have three pion fields, yet $\mathrm{SU}(2)_L \times \mathrm{SU}(2)_R \sim \mathrm{SO}(4)$ requires four coordinates to construct the fundamental representation.

Let us then consider the transformation properties of the pion fields under linear SO(4) rotations. Such rotations may be completely parameterized by the six conserved Noether charges derived in Eq. (2.12), that is, the set $\{Q^a, Q_5^a\}$ for $a \in \{\,1,\,2,\,3\,\}$. A general linear rotation in this representation is then

$$\begin{pmatrix} \vec{\pi} \\ \sigma \end{pmatrix} \to \begin{pmatrix} \vec{\pi}\,' \\ \sigma' \end{pmatrix} = \Big[\, \mathbb{1} + q^a\, V_a + q_5^a\, A_a \,\Big] \begin{pmatrix} \vec{\pi} \\ \sigma \end{pmatrix} \quad ,$$

where the 4-vector is relativistically constrained as $|\vec{\pi}\,|^2 + \sigma^2 = F^2$ with $F$ a normalization constant of dimension mass and the $\{\, V_a,\, A_a \,\}$ defined such that

$$q^a\, V_a = \begin{pmatrix} 0 & -q^3 & q^2 & 0 \\ q^3 & 0 & -q^1 & 0 \\ -q^2 & q^1 & 0 & 0 \\ 0 & 0 & 0 & 0 \end{pmatrix} \qquad q_5^a\, A_a = \begin{pmatrix} 0 & 0 & 0 & q_5^1 \\ 0 & 0 & 0 & q_5^2 \\ 0 & 0 & 0 & q_5^3 \\ -q_5^1 & -q_5^2 & -q_5^3 & 0 \end{pmatrix} \quad .$$

The particular form of the $\{V_a\}$ matrices is important as they are in a one-to-one correspondance with the generators of the fundamental representation of $\mathrm{SO}(3) \sim \mathrm{SU}(2) \subset \mathrm{SO}(4)$, as in, the $\{V_a\}$ generate all possible SO(3) rotations in the subgroup of the larger SO(4) group. Utilizing the relativistic constraint to replace all instances of $\sigma$ with the pion fields, we have

$$\vec{\pi} \xrightarrow{\vec{q}} \vec{\pi}\,' = \vec{\pi} + \vec{q} \times \vec{\pi} \quad ,$$

$$\vec{\pi} \xrightarrow{\vec{q}_5} \vec{\pi}\,' = \vec{\pi} + \vec{q}_5 \sqrt{F^2 - |\vec{\pi}\,|^2} \quad ,$$

which is precisely the non-linear realization of the chiral group with the triplet of pion fields that we need. Note that we have maintined the requirement that the pion fields transform linearly under the $\mathrm{SU}(2)_V \simeq \mathrm{SO}(3)$ isospin (flavour) transformations. As noted in Ref. [57], we may conveniently write linear transformations in SO(4) as

$$\begin{aligned} U &= \frac{1}{F}\left(\, \sigma\, \mathbb{1}_{2\times 2} + i\, \vec{\pi} \cdot \vec{\tau}\, \right) \\ &= \frac{1}{F}\Big(\, \sqrt{F^2 - |\vec{\pi}\,|^2}\, \mathbb{1}_{2\times 2} + i\, \vec{\pi} \cdot \vec{\tau}\, \Big) \quad , \end{aligned}$$

where $\vec{\tau}$ is the usual vector of Pauli matrices. We note that the condition $|\vec{\pi}\,|^2 + \sigma^2 = F^2$ enforces that the matrix $U$ is indeed unitary. We lastly demand that such a unitary transforms according to

$$U \to U' = L\, U\, R^\dagger = R\, U\, L^\dagger \quad ,$$

$$L \in \mathrm{SU}(2)_L \qquad R \in \mathrm{SU}(2)_R \quad ,$$

where $L$ and $R$ are global flavour rotations acting in the left- and right-handed chiral spaces, respectively. As we only consider global flavour rotations in this presentation of $\chi$EFT, we note that derivatives of the unitary $\partial_\mu U$ will hence transform in the same manner as $U$.

*Remark* 2.2.2 (**The Choice of Non-linear Realization**). A subtle but important feature of this framework lies in the non-uniqueness of the representation chosen for the chiral symmetry group. There exists an infinite number of valid realizations of the chiral group, leading to ambiguity in the definition of the unitary transformation $U$ of the pion fields. This naturally raises the question of whether or not the choice of representation leads to meaningful physical predictions. As discussed in Refs. [73, 74], all such representations are related by non-linear field redefinitions and share the same group-theoretic structure. Consequently, they are physically equivalent. This equivalence is similarly established by Haag's theorem [83], which tells us that non-linear field redefinitions leave the $S$-matrix invariant.

### The Leading Order Pion Lagrangian

With our understanding of the pion field transformations complete, we proceed as in Ref. [57] and construct the terms of the effective Lagrangian using trace operations in the flavour space of products of the unitaries and products of derivatives of the unitaries. Via Lorentz covariance, we may restrict the number of derivatives in such terms to always be even. This leads to the leading order pion Lagrangian

$$\begin{aligned}\mathcal{L}_\pi^{(2)} &= \frac{F^2}{4}\left\langle\, \partial_\mu U\, \partial^\mu U^\dagger \,\right\rangle_{\mathrm{f}} \\ &= \frac{1}{2}\,\partial_\mu\vec{\pi}\cdot\partial^\mu\vec{\pi} + \frac{1}{2F^2}\left(\,\partial_\mu\vec{\pi}\cdot\vec{\pi}\,\right)^2 + \mathcal{O}\big(|\vec{\pi}\,|^6\big) \quad ,\end{aligned}$$

as the $\mathcal{L}_{\pi\pi}^{(0)} = U\,U^\dagger$ may be discarded. The constant $F$ is naturally chosen to match the usual Lagrangian for a massless scalar field, leading to identification of $F$ with the pion decay constant $F_\pi$.

Notably, we are still working in the massless regime where we have no explicit chiral symmetry breaking in the QCD Lagrangian. The natural method to extend this to the massive form of the theory is to introduce an external field $H$ which interacts with the quark fields as

$$\mathcal{L}_{\text{ext.}} = -\sum_q \bar{\psi}_q\, H\, \psi_q \quad ,$$

which then enters at $\mathcal{L}_{\pi\pi}^{(0)}$. If we restrict $H$ to transform in precisely the same manner as $U$, then we do not break the chiral invariance of the massless QCD Lagrangian. As above, we then need to include all chiral invariant terms constructed from the products and derivatives of $H$, $U$ and $U^\dagger$. In the end, we will take the external field to be the quark mass matrix $M = \mathrm{diag}(\,m_u,\, m_d\,)$.

Since we treat the quark masses as perturbative effects in QCD, the LO terms which contribute to the Lagrangian should only contain a single insertion of the external field $H$ and no derivatives of the pion fields. Thus, making the substitution $H \to M$, only a single symmetry breaking term is possible at LO, and it is given by:

$$\begin{aligned}\mathcal{L}_{\text{ext.}} &= \frac{F^2 B}{2}\big\langle\, M\,U + M\,U^\dagger \,\big\rangle_{\text{f}} \\ &= F^2\,B\,\big(m_u + m_d\big) - \frac{B}{2}\,\big(m_u + m_d\big)|\vec{\pi}\,|^2 + \mathcal{O}\big(|\vec{\pi}\,|^4\big) \\ &= M^2\,F^2 - \frac{1}{2}\,M^2\,|\vec{\pi}\,|^2 + \mathcal{O}\big(|\vec{\pi}\,|^4\big) \quad .\end{aligned}$$

The first term is constant and may be discarded. On the other hand, the second term remarkably shows us how the pion mass arises from the explicit chiral symmetry breaking due to the non-zero quark masses. Notably, the theory predicts that all pions $\{|\pi^{\pm}\rangle, |\pi^0\rangle\}$ have equal masses set by $m_\pi^2 = B\,\big(m_u + m_d\big)$.

We have thus constructed the leading-order pion Lagrangian consistent with the chiral symmetry breaking pattern, both explicit and spontaneous, of low-energy QCD. The final form is then

$$\mathcal{L}_\pi^{(2)} = \frac{F^2}{4}\,\big\langle\, \partial_\mu U\,\partial^\mu U^\dagger \,\big\rangle_{\text{f}} + 2B\,\big\langle\, M\,U + M\,U^\dagger \,\big\rangle_{\text{f}} \quad . \tag{2.14}$$

The pion-nucleon ($\pi$N), nucleon-nucleon (NN) and three-nucleon (3N) interactions are all derived in a similar spirit and are comprehensively described in the reviews at the very beginning of this section. In particular, we have not presented any content related to power counting and systematically organizing the diagramatic expansion such that pions and nucleons are treated on (relatively) equal footing. Developing consistent (depending on one's chosen definition) power counting schemes, particularly in applications of $\chi$EFT to the many-body sector, are open problems.

## 2.3 The No-Core Shell Model

With a basic understanding of the modern developments for nuclear interactions complete, we will now introduce the non-relativistic, quantum many-body problem and a quasi-exact approach to its solution with solely the nuclear interaction as input, known as the *ab initio* no-core shell model (NCSM). See Ref. [41] for the most recent review on the approach and Refs. [84, 85, 86] for a historical perspective on developments in the NCSM framework.

### 2.3.1 The Quantum Many-Body Problem for Fermions

The general form of the non-relativistic, quantum many-body problem for $n$ interacting fermions of mass $m$ existing with the support of some potential $V$ is represented using the Schrödinger equation. The potential is usually taken to be two-body, however, for non-local theories, e.g., $\chi$EFT, there may exist many-body interactions. For such a configuration of fermions we may write the Schrödinger equation as

$$H\,|\Psi\rangle = \Big[\, H^{(0)} + W \,\Big]\,|\Psi\rangle = \left[\, \sum_{i=1}^{n} \frac{\vec{P}_i^{\,2}}{2m} + \sum_{i<j}^{n} V_{ij} \,\right] |\psi\rangle = E_\psi\,|\Psi\rangle \ , \tag{2.15}$$

where $T_i = \vec{P}_i^{\,2}/2m$ is the one-particle kinetic term and $V_{ij}$ is the (here assumed to be) two-body interaction term. In terms of a coordinate representation, we will assume that the potential $V$ is to have the property that $V(\vec{x}_i,\, \vec{x}_j) \equiv V\big(\vec{x}_i - \vec{x}_j\big)$, where we have suppressed possible spin and isospin character of the potential. We make note that the above Hamiltonian has been written utilizing one-particle coordinates, i.e., a cartesian coordinate assigned to each fermion $\{\, \vec{x}_1,\, \ldots,\, \vec{x}_n \,\}$ with an arbitrary, direct tensor product $n$-particle state given by

$$\big\langle\, \vec{x}_1 \cdots \vec{x}_n \,\big|\, \psi_\alpha \,\big\rangle = \big\langle\, \vec{x}_1 \cdots \vec{x}_n \,\big|\, \phi_{\alpha_1} \,\cdots\, \phi_{\alpha_n} \,\big\rangle = \phi_{\alpha_1}(\vec{x}_1) \cdots \phi_{\alpha_n}(\vec{x}_n) \quad ,$$

where $\alpha = \{\, \alpha_1,\, \ldots,\, \alpha_n \,\}$ denotes the set of one-particle quantum numbers for each fermion in the many-body configuration $\psi_\alpha$. A comment on the required anti-symmetrization of such configurations in the case of fermions will be made shortly. This is chosen over the the more natural, relative coordinate formulation typical of non-relativistic formalisms with Jacobi coordinates $\{\, \vec{\xi}_1,\, \ldots,\, \vec{\xi}_{n-1} \,\}$. The importance of employing relative coordinate formulations in calculations of observables has been explored in several works by our group at TRIUMF and collaborators [87, 88, 89], however, we will see that a more natural connection to the relativistic formalism of QFT can be made when thinking in terms of one-particle coordinates.

Let us begin by formulating solutions to the Schrödinger equation for $H$ in terms of an expansion over a complete set of known, analytic and orthonormal one-particle functions $\{\phi_i\}$. Then, we may write the eigensolution $\Psi$ in terms of this basis as

$$|\Psi\rangle = \sum_\alpha c_\alpha |\psi_\alpha\rangle = \sum_{\alpha_1,\,\ldots,\,\alpha_n} c_{\alpha_1\,\cdots\,\alpha_n}\,\big|\,\phi_{\alpha_1}\,\cdots\,\phi_{\alpha_n}\,\big\rangle_{\mathcal{A}} \quad , \tag{2.16}$$

$$E_\Psi = \langle\Psi|\,H\,|\Psi\rangle = \sum_{\alpha\beta} c_\beta^*\, c_\alpha\, \langle\psi_\beta|\,H\,|\psi_\alpha\rangle \quad . \tag{2.17}$$

where the $\mathcal{A}$ denotes the anti-symmetric nature of the configuration $\psi_\alpha$. As we are studying a system of indistinguishable fermions, we must ensure that the many-body configurations $\psi_\alpha$ respect the correct fermionic statistics as established in the *spin-statistics theorem*. This theorem was first derived by Pauli from the remarkably simple postulates of (i) positive energy and (ii) commutation of observables with no causal connection [90]. We quote the theorem here for completion.

**Theorem 2.3.1** (**Spin-Statistics Theorem**)**.** The spin-statistics theorem of Pauli states the following:

(i) Particles with half-integer spin are restricted by the exclusion principle, that is, only one Fermion may occupy a given quantum state in an arbitrarily small, space-time localized, many-particle configuration.

(ii) Particles with integer spin are not unrestricted in this sense, i.e., an arbitrary number of bosons may occupy the same quantum state in arbitrarily small regions of space-time.

Utilization of this beautiful theorem obliges us to, when working with bound collections of indistinguishable fermions, ensure that our states are completely anti-symmetric under action of the permutation operator $P_\sigma$ where $\sigma : \mathbb{N} \to \mathbb{N}$. This operator acts on sets as

$$P_{ij} \circ \{ 1, \ldots, i, \ldots, j, \ldots, n \} = \{ 1, \ldots, j, \ldots, i, \ldots, n \} \quad ,$$

and is implemented on the many-body configurations as

$$\begin{aligned} &\left\langle \vec{x}_1 \cdots \vec{x}_n \right| P_{ij} \left| \, \phi_{\alpha_1} \, \ldots \, \phi_{\alpha_i}, \, \ldots, \, \phi_{\alpha_j}, \, \ldots, \, \phi_{\alpha_n} \right\rangle_{\mathcal{A}} \\ &\qquad = (-1) \left\langle \, \vec{x}_1 \cdots \vec{x}_n \, \right| \, \phi_{\alpha_1} \, \ldots \, \phi_{\alpha_j}, \, \ldots, \, \phi_{\alpha_i}, \, \ldots, \, \phi_{\alpha_n} \, \right\rangle_{\mathcal{A}} \quad . \end{aligned}$$

Mechanically speaking, it is straightforward to implement antisymmetrization with a basis of orthonormal functions $\{\phi_i\}$ in the one-particle, cartesian coordinate representation with the use of Slater determinants [91]. For an arbitrary, anti-symmetric many-body configuration $\psi_\alpha$ written in terms of a one-particle basis of functions $\{\phi_i\}$, we have

$$\left\langle \, \vec{x}_1 \cdots \vec{x}_n \, \right| \left. \psi_\alpha \, \right\rangle_{\mathcal{A}} = \left\langle \, \vec{x}_1 \cdots \vec{x}_n \, \right| \left. \phi_{\alpha_1} \, \cdots \, \phi_{\alpha_n} \, \right\rangle_{\mathcal{A}} = \frac{1}{\sqrt{n!}} \begin{vmatrix} \phi_{\alpha_1}(\vec{x}_1) & \cdots & \phi_{\alpha_1}(\vec{x}_n) \\ \vdots & \ddots & \vdots \\ \phi_{\alpha_n}(\vec{x}_n) & \cdots & \phi_{\alpha_n}(\vec{x}_n) \end{vmatrix} \quad . \tag{2.18}$$

The operation $|\cdot|$ is referred to as a symbolic determinant and we operate on a matrix composed of all possible permutations of the ordered set of one-particle functions and coordinates. Merely by the properties of determinants, if we have $\alpha_i = \alpha_j$ for arbitrary indices $i, j \in \{ 1, \ldots, n \}$, the result of the determinant operation will be null. Hence, Pauli exclusion is explicitly enforced by Slater determinant anti-symmetrization, as desired.

At a basic level, this discussion characterizes the conceptually simplest approach to constructing solutions to the many-body Schrödinger equation for the many-body fermion problem. We thus see that the main ingredients are the one- and two-body amplitudes of the Hamiltonian, with higher-body contributions to the potential possible in non-local theories. Nevertheless, we may say more about the problem given details about the structure of the Hamiltonian.

### Symmetries of the Hamiltonian

To further characterize features of our many-body eigensolutions $\Psi$, we must identify the symmetries of the Hamiltonian operator introduced in Eq. (2.15). Rather than working with the Lagrangian an identifying the conserved charges via Noether's theorem, we may directly work with the Hamiltonian and identify the set of operators which commute with said Hamiltonian. If we have a set of operators which simultaneously commute with the Hamiltonian, there will exist a representation in which the operators are simultaneously diagonalizable.

*Total Spin Momentum* – The total spin momentum operator (angular momentum) is naturally defined as the vectorial combination of the orbital spin operator (orbital angular momentum) and intrinsic spin operator as

$$\vec{J} = \vec{L} + \vec{S} \quad . \tag{2.19}$$

As we have made the assumption in Eq. (2.15) that the potential satisifies $V(\vec{x}_i, \vec{x}_j) \equiv V\big(\vec{x}_i - \vec{x}_j\big)$, then the entire Hamiltonian may be cast into a form dependent upon the relative coordinates $\vec{x}_i - \vec{x}_j$ and a centre-of-mass coordinate $\vec{R}$, decoupling the intrinsic many-body system from its centre-of-mass (c.m.) motion. Details on the definition of relative coordinates as applied in the NCSM and on the decoupling of intrinsic and c.m. motion may be found in Appendix A.5 and A.4. It can then be proven that the Hamiltonian is invariant to the orientation of the system, more clearly stated as

$$\big[\, H,\, \vec{J}^{\,2} \,\big] = 0 \qquad\qquad \big[\, H,\, J_z \,\big] = 0 \quad , \tag{2.20}$$

where we have chosen the spin-projection axis as the $x_3$-axis. Thus, we may choose our many-body configurations $\Psi$ such that they have definite values of spin $J$ and spin projection $J_z$.

*Total Parity* – The total parity operator for an even or odd configuration $\Psi$ is defined as

$$P\,\big|\Psi\,;\,\pi = \pm 1\big\rangle = \pi\,\big|\Psi\,;\,\pi = \pm 1\big\rangle \quad , \tag{2.21}$$

where the parity of an $n$-particle configuration is given by

$$\pi = \prod_{i=1}^{n}\, \pi^{(i)}_{\text{intrinsic}} \cdot \pi^{(i)}_{\text{orbital}} = \prod_{i=1}^{n}\, (-1)^{l_i} \quad , \tag{2.22}$$

with $\pi_{\text{intrinsic}} = 1$ the intrinsic parity of the nucleon and $\pi_{\text{orbital}}$ the orbital spin contribution to the parity. Under the chosen conditions for the potential $V(\vec{x}_i, \vec{x}_j) \equiv V\big(\vec{x}_i - \vec{x}_j\big)$, it can be proven that the parity operator commutes with the nuclear Hamiltonian

$$\big[\, H,\, P \,\big] = 0 \quad . \tag{2.23}$$

and so the eigensolutions of the Hamiltonian may be separated into two equivalence classes according to their transformation under parity. Thus, we may choose our many-body configurations $\Psi$ such that they have definite values of parity $\pi$.

*Remark* 2.3.1 (**Parity Conserving and Non-Conserving Interactions**). We make note that, to this day, we have seen that the strong and electromagnetic interactions conserve parity. Famously proposed by Lee and Yang [92] and shown by Wu and collaborators [93], the weak interaction Hamiltonian does not conserve parity. As we have noted in the introduction, searches for larger-than-anticipated charge-parity violation in electromagnetic interactions in nuclei are underway [37] and we further note the more recent efforts in heavy-ion collisions which investigate the possibility of parity violation in the strong interaction via the so-called "chiral magnetic effect" [94].

*Nuclear Isospin* – The nuclear isospin operator obeys the same algebraic rules as the Pauli spin operators, though with no connection to spin momentum, and is identically defined for isospin-1/2 particles; protons

are labelled with isospin projection $t_z = +1/2$ and neutrons with projection $t_z = -1/2$. The proton and neutron are then seen as two projections of the same object, i.e., the nucleon, which, as discussed in the prior sections on QCD and $\chi$EFT, is made transparent by the connection between the approximate flavour symmetry of light-quark QCD and nuclear isospin. It is similarly trivial to show that for the nuclear isospin operator $\vec{\mathcal{T}}$, one has that

$$\left[ H, \vec{\mathcal{T}}^{\,2} \right] \approx 0 \quad , \tag{2.24}$$

and so the eigensolutions of the Hamiltonian may be approximately separated into equivalence classes according to their nuclear isospin representations. Note that for an arbitrary nucleus with $N_p$ protons and $N_n$ neutrons, we have that $T_z = (N_p - N_n)/2$.

*Remark* 2.3.2 (**Approximate Nuclear Isospin Symmetry**). A particular consequence of exact isospin symmetry would be the existence of mirror symmetry in nuclei, that is to say, systems with opposite numbers of protons and neutrons would have identical spectra. However, we know that the strong interaction naturally breaks isospin symmetry due to the unequal quark masses. Yet any major deviation from mirror symmetry is largely due to electromagnetic effects, i.e., the Coulomb interaction, which strongly breaks isospin symmetry. Measurments of mirror nuclei have become instrumental in probing electroweak physics, even having an impact on $V_{ud}$ determinations and CKM unitarity [10].

### 2.3.2 The Fock Space, Creation and Annhilation Operators

Here we provide a rudimentary introduction to the creation-annihilation operator formalism as applied in the context of non-relativistic, many-body theory. These techniques are disucssed in absolutely every introductory book on nuclear theory, e.g., see Refs. [95, 96, 97], and the formalism is frequently referred to as "second quantization", language which we will try to avoid in this dissertation. Mostly familiar to the practicing particle physicist, this formalism is the most natural way to think about nuclear configurations in a language very similar to that of QFT. We begin with the definition of the anti-symmetrized sector of the complete $n$-particle Fock space

$$\Big[\mathcal{F}_n\big(\mathcal{H}\big)\Big]_{\mathcal{A}} = \bigoplus_n \left[\mathcal{H}^{\otimes n}\right]_{\mathcal{A}} = \mathbb{1} \oplus \mathcal{H} \oplus \left[\mathcal{H} \otimes \mathcal{H}\right]_{\mathcal{A}} \oplus \left[\mathcal{H} \otimes \mathcal{H} \otimes \mathcal{H}\right]_{\mathcal{A}} \oplus \cdots \quad , \tag{2.25}$$

where $\mathcal{H}$ is the one-particle Hilbert space from which the many-particle Fock space is constructed and the ellipses denote contributions to the Fock space with more than three particles. States in the Fock space by definition have well-defined, integer particle number. For the case of $n$ indistinguishable fermions, the anti-symmetric subspace of $\mathcal{F}_n$ is spanned by a basis of anti-symmetric many-body configurations constructed from the standard direct product representation of the one-particle Hilbert spaces for each particle. The different-particle-number subspaces of the Fock space are mapped between via the creation $c^\dagger$ and annihilation operators $c$, which respectively create and destroy quanta of type $\phi$, defined via the action on the vacuum and one-particle states as

$$c_\alpha^\dagger \left|0\right\rangle = \left|\phi_\alpha\right\rangle \qquad c_\alpha^\dagger \left|\phi_\alpha\right\rangle = 0 \quad , \tag{2.26}$$

$$c_\alpha \left|0\right\rangle = 0 \qquad c_\alpha \left|\phi_\alpha\right\rangle = \left|0\right\rangle \quad , \tag{2.27}$$

with $c_\alpha$ defined as destroying the vacuum. These operators further obey the usual anti-commutation algebra

$$\left\{ c_\alpha, c_\beta \right\} = 0 \qquad \left\{ c_\alpha^\dagger, c_\beta^\dagger \right\} = 0 \qquad \left\{ c_\alpha, c_\beta^\dagger \right\} = \delta_{\alpha\beta} \quad , \tag{2.28}$$

which precisely captures the Fermi-Dirac statistics for fermions. Thus, $n$-particle states of the Fock space are then created from the Fock vacuum state $\big|0\big\rangle$ through the action of creation operators as

$$c^\dagger_{\alpha_n} \cdots c^\dagger_{\alpha_1} \big|0\big\rangle = \big|\, \phi_{\alpha_1} \cdots \phi_{\alpha_n} \,\big\rangle \tag{2.29}$$

which is inherently anti-symmetric due to the properties of the creation and annihilation operators in Eq. (2.28). This may explicitly shown as equivalent to the Slater determinant anti-symmetrization given in Eq. (2.18).

This formalism is remarkably convenient and is the standard approach to discretizing operators over a basis of one-particle configurations $\{\phi_i\}$ in calculation of nuclear amplitudes. Though, one must pay special attention to the annihilation operator $c$. While the creation operator $c^\dagger$ spherical tensor with well-defined rank, the same cannot be said of $c$, e.g., see the appendix of Ref. [98]. However, it is straightforward to construct an operator which does obey the correct spherical tensor transformation properties as

$$\tilde{c}_\alpha = (-1)^{j-m}\big(c^\dagger\big)^\dagger_{\tilde{\alpha}} = (-1)^{j-m} c_{\tilde{\alpha}} \quad , \tag{2.30}$$

where $\tilde{\alpha}$ has spin projection $m \to -m$. See Chapter 3 of Ref. [99] for a complete discussion on the transformation properties of irreducible tensor operators.

### 2.3.3 The Model

In this section we introduce the model-specific details of the *ab initio* NCSM [41], the computational many-body approach utilized by our group at TRIUMF. The NCSM describes the nucleus as a system of $A$ non-relativistic, point-like quanta interacting via inter-nucleonic forces with all nucleons active degrees of freedom. *Ab initio* refers to the fact that the NCSM is a first-principles approach to constructing solutions of the $A$-nucleon, many-body Schrödinger equation with no approximations outside of the non-relativistic, EFT treatment of nucleons and pions as the fundamental constituents of the theory. It takes solely the two- and three-nucleon interactions as input, nowadays usually derived from $\chi$EFT, and so we may write the Hamiltonian as

$$H = T_{\rm rel} + V = \frac{1}{A}\sum_{i<j}^{A} \frac{\big(\vec{p}_i - \vec{p}_j\big)^2}{2m} + \sum_{i<j}^{A} V_{ij}^{(\rm NN)} + \sum_{i<j<k}^{A} V_{ijk}^{(\rm 3N)} + \cdots \quad , \tag{2.31}$$

where $m$ denotes the nucleon mass. Notably, this Hamiltonian differs from Eq. (2.15) in the manner of explicitly preserving translation invariance. More attention will be paid to this fact shortly. In principle, in the EFT picture one generates up to $A$-body interaction terms at higher orders in the perturbative expansion, however, in $\chi$EFT there emerges a natural heirarchy which orders the importance of higher-body interaction terms such that NN $>$ 3N $> \cdots$, as one would expect. At present it is only possible to include the full two- and three-nucleon interactions due to the dramatic computational overhead and storage requirements in generating higher-body interaction terms. Nevertheless, interest in testing the impact of four-nucleon interactions remains [100, 101]. In many cases, *ab initio* calculations of intermediate mass nuclei have shown that the few-body physics captured by the two- and three-nucleon interactions is often sufficient for describing bulk properties of nuclei [102, 103].

Pragmatically speaking, the NCSM makes use of a large but finite expansion in a set of anti-symmetric, $A$-body harmonic oscillator (HO) basis states represented with either relative coordinates or with the cartesian one-particle coordinates. See Appendix A.5 for the definitions of relative coordinates employed in the NCSM. The expansions for the eigensolutions to the Hamiltonian operator are then respectively

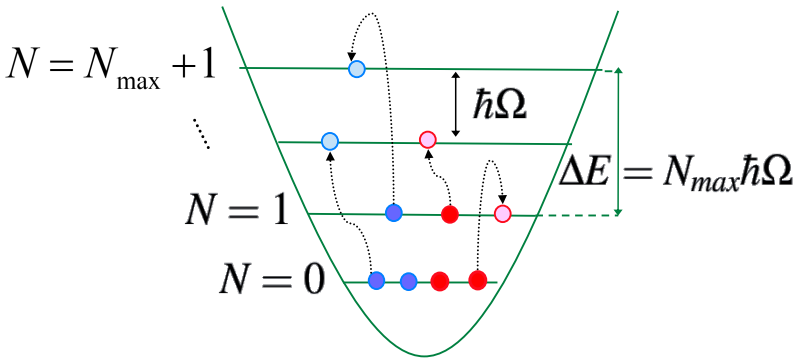


Figure 2.1: The $N_{\max}$ truncation scheme for the many-body harmonic oscillator basis expansion with fixed oscillator frequency $\hbar\Omega$, as employed in the NCSM. For a given value of the truncation parameter $N_{max}$, all possible nucleonic excitations from the lowest Pauli configuration (LPC) such that the sum of oscillator quanta $N$ is less than $N_{\rm LPC} + N_{\max}$ are considered.

given by

$$\left\langle\, \vec{\xi}_1 \cdots \vec{\xi}_{A-1} \,\middle|\, \Psi^A \,\right\rangle = \sum_{N=0}^{N_{\max}} \sum_{\alpha} \; c_{N\alpha} \left\langle\, \vec{\xi}_1 \cdots \vec{\xi}_{A-1} \,\middle|\, \psi^A_{N\alpha} \,\right\rangle_{\mathcal{A}} \quad , \tag{2.32}$$

$$\left\langle\, \vec{x}_1 \cdots \vec{x}_n \,\middle|\, \Psi^A \,\right\rangle = \sum_{N=0}^{N_{\max}} \sum_{\alpha} \; c^{(\rm SD)}_{N\alpha} \left\langle\, \vec{x}_1 \cdots \vec{x}_n \,\middle|\, \psi^A_{N\alpha} \,\right\rangle_{\rm SD} = \left\langle\, \vec{\xi}_1 \cdots \vec{\xi}_{A-1} \,\middle|\, \Psi^A \,\right\rangle \, \phi_{000}\big(\vec{R}_{c.m.}\big) \quad , \tag{2.33}$$

where $\alpha = \{\, \alpha_1, \ldots, \alpha_A \,\}$ labels the set of quantum numbers for the constituents of the many-body configuration and the abbreviation SD refers to the process of anti-symmetrization via the Slater determinant approach detailed in Eq. (2.18). We emphasize that, as is written in Eq. (2.33) above, the HO basis allows for exact factorization of the c.m. and intrinsic degrees of freedom when utilizing the $N_{\max}$ truncation scheme to be described below [104]. Note that we have suppressed spin and isospin indices for brevity. This is critical as, when working with relative coordinates, the process of anti-symmetrization is factorially complex with $A$-particle systems. This is in contrast to the Slater determinant anti-symmetrization which is automatic when building the $A$-particle configurations. Practical calculations typically employ the cartesian one-particle coordinates due to this great simplification, though, one must now contend with the induced spurious c.m. motion. This is well-understood and may be analytically removed in the NCSM when calculating amplitudes of arbitrary operators [105]. See Refs. [87, 88, 89, 106] for realistic calculations exploiting this factorization and an analysis of the effects of c.m. removal on observables. The nuclear many-body state $\Psi^A$ satisfies the symmetry properties described in the prior section, that is to say, they are chosen to be simultaneous eigensolutions of the total spin momentum and projection, parity, and approximately isospin.

We refer to Fig. 2.1. The NCSM expansion is characterized by two parameters, namely, the oscillator frequency $\hbar\Omega$ and the truncation on the number of oscillator excitation quanta $N_{\max}$. The nucleons begin as distributed according to the lowest Pauli configuration (LPC) of the system, i.e., minimal oscillator excitations, and we count the number of oscillator quanta to be $N_{\rm LPC}$. Then, for a given value of $N_{\max}$, we consider all possible nucleonic excitations of the system bounded by a condition on the number of oscillator quanta:

$$N = \sum_{i=1}^{A} N_i = \sum_{i=1}^{A} 2n_i + l_i \;\; \leq N_{\rm LPC} + N_{\max} \quad . \tag{2.34}$$

The set of quantum numbers $\{\, n,\, l \,\}$ are the typical radial and orbital spin numbers used in labelling the oscillator basis, which we will now discuss below.

### The Harmonic Oscillator Basis

The one-particle HO wavefunctions are the eigensolutions to the problem of a central oscillator potential, with more or less the same form for a Hamiltonian as presented in Eq. (2.15), and are given by

$$\phi_{nlm}\big(\, r\,;\,\hbar\Omega\,\big) = \frac{1}{r}\; R_{nl}\big(\, r\,;\,\hbar\Omega\,\big)\; Y_{lm}\big(\hat{r}\big) \qquad\qquad E_{nl} = \left(N + \frac{3}{2}\right)\hbar\Omega \quad , \tag{2.35}$$

where $R_{nl}$ is the radial function built from the Hermite polynomials and $Y_{lm}$ are the usual spherical harmonics for which we adopt the conventions in Ref. [99]. The oscillator length

$$b = \sqrt{\frac{(\hbar c)^2}{(mc^2)\hbar\Omega}} \tag{2.36}$$

is completely determined by the frequency $\hbar\Omega$ and constants. The eigenenergies for a given oscillator configuration are specified by the total number of oscillator quanta $N = 2n + l$. Greater details on the use of the one-particle HO basis in many-body theory may be found in Refs. [107, 108, 97]. To summarize the cited works, the main advantages of expansion over a complete set of anti-symmetrized, many-body HO states are

1. The cartesian coordinate representation of the many-body wavevector factorizes as a product of the intrinsic wavevector in relative coordinates and a spurious c.m. motion; this is analytic in the NCSM formalism and may be removed exactly. Use of any basis other than the oscillator basis results in the mixing of c.m. and internal motion making its exact removal more challenging.

2. The Talmi-Moshinksy transformation greatly simplifies the calculation of operator amplitudes dependent on relative coordinates by relation to those in the one-particle, cartesian coordinate representation.

### A Final Comment on the Removal of Spurious C.M. Motion

The majority of the contamination in the spectrum of $H$ resulting from the c.m. motion may be discarded by a modification of the intrinsic Hamiltonian in Eq. (2.15). One may further add the so-called Lawson-Palumbo term to the nuclear Hamiltonian, defined as

$$H_\beta = \beta\,\left(H_{\text{c.m.}} - \frac{3}{2}\,\hbar\Omega\right) \quad , \tag{2.37}$$

and

$$H_{\text{c.m.}} = T_{\text{c.m.}} + U_{\text{c.m.}} = \frac{\vec{P}^{\,2}}{2M} + \frac{1}{2}Am\Omega^2\,\vec{R}^{\,2} \quad , \tag{2.38}$$

with the c.m. vector $\vec{R}$ is defined as in Appendix A.5 and $M$ twice the reduced mass of the partitioned system. The addition of the Lawson term to the Hamiltonian raises excitations of the spurious c.m. motion by a factor of $\beta$, effectively projecting them out of practically visible subset of the spectrum [109]. While we rely on this procedure, we typically do not refer to $\beta$ as a parameter of the NCSM as the eigenenergies of the physical states are completely independent of it, i.e., they have no parametric dependence on $\beta$. While this removes excitations of the c.m. motion, the 0 $\hbar\Omega$ ground state c.m. motion remains as contamination in the NCSM eigensolutions. As mentioned prior, this may be analytically removed in the NCSM [105] via the Talmi-Moshinsky transformation, as described in Appendix A.4.

## 2.4 Lanczos Methods

In this section, we will pay brief homage to the Lanczos algorithm and a related technique, referred to as the Lanczos Strengths Method (LSM) or Lanczos Method of Moments, which are absolutely fundamental to the research articulated in this dissertation. As a result of the representation of our eigensolutions with the creation-anhilation operator formalism and the (in the exact limit, infinite) expansion in many-body HO configurations, we have the definition of the Hamiltonian in the NCSM representation given by

$$H \doteq \begin{pmatrix} \langle \psi_1 | H | \psi_1 \rangle & \cdots & \langle \psi_1 | H | \psi_d \rangle \\ \vdots & \ddots & \vdots \\ \langle \psi_d | H | \psi_1 \rangle & \cdots & \langle \psi_d | H | \psi_d \rangle \end{pmatrix} \quad , \tag{2.39}$$

where $d$ is the dimension of the many-body HO basis $\{ \psi_1, \ldots, \psi_d \}$ and the elements $H_{ij} = \langle \psi_i | H | \psi_j \rangle$ are the amplitudes of the Hamiltonian between elements of said basis. We then see that the heavy-lifting required in constructing the solutions to the quantum many-body problem is cast into the standard matrix algebra problem of diagonalization, which gives the nuclear eigensolutions in terms of the many-body HO basis. However, the diagonalization procedure is non-trivial given that $H$ is a large, sparse matrix, with our group's largest-to-date calculations pushing a basis dimension of 1 – 1.5 billion.

Once we construct the Hamiltonian in this high-dimensional basis, the iterative Lanczos algorithm is applied [110, 111] with the number of iterations determined based on certain characteristics of the system in question, e.g., (i) the number of desired states and the density of states, (ii) the number of particles in the nucleus, (iii) the $N_{\max}$ configuration space size, and so on. More details on the Lanczos remarkable algorithm are to be given below. While, in general, completion of the algorithm would completely tri-diagonalize the $d \times d$ matrix representation of the Hamiltonian, in practical scenarios, a finite number of iterations $m$ much less than the dimension of the matrix $d$ are applied. This brings an $m \times m$ sub-block of the Hamiltonian into tri-diagonal form and, based on the subsequent diagonalization of this small matrix, gives a *very* reasonable approximation of the first $m$ extremal eigenvalues and eigenvectors of the original matrix, most notably reproducing bulk properties of the spectrum.

The many-body code utilized to compute the nuclear eigensolutions discussed in this work is known as the `ncsd.f`, the no-core Slater determinant code, of P. Navrátil and collaborators. As we have noted above, the size of these calculations is quite significant and requires large-scale parallelization techniques and access to massive supercomputers.

### 2.4.1 Lanczos Algorithm

At its most basic level, the Lanczos algorithm [110] works on the principle that we may construct a special basis in which the Hamiltonian has a tri-diagonal representation. At a deeper level, the algorithm itself falls under the class of Krylov subspace methods which iteratively generate orthonormal bases from recursive applications of an operator, e.g., a Hamiltonian, on an initial pivot vector and the subsequently generated set of orthogonal vectors. Schematically, we may view the construction of the Lanczos basis for a linear operator $H$ as proceeding in the following way:

$$\begin{aligned} H|\eta_0\rangle &= \alpha_0|\eta_0\rangle + \beta_0|\eta_1\rangle \\ H|\eta_1\rangle &= \beta_0|\eta_0\rangle + \alpha_1|\eta_1\rangle + \beta_1|\eta_2\rangle \\ H|\eta_2\rangle &= \beta_1|\eta_1\rangle + \alpha_2|\eta_2\rangle + \beta_2|\eta_3\rangle \\ H|\eta_3\rangle &= \beta_2|\eta_2\rangle + \alpha_3|\eta_3\rangle + \beta_3|\eta_4\rangle \\ &\vdots \end{aligned}$$

where each new element of the basis is explicitly constructed as orthonormal to its left and right neighbours according to

$$\beta_i \left|\eta_{i+1}\right\rangle = H \left|\eta_i\right\rangle - \alpha_i \left|\eta_i\right\rangle - \beta_{i-1} \left|\eta_{i-1}\right\rangle \quad , \tag{2.40}$$

$$\alpha_i = \left\langle \eta_i \right| H \left|\eta_i\right\rangle \qquad\qquad \beta_i^2 = \left|\left|\ \left(H - \alpha_i \mathbb{1}\right)\left|\eta_i\right\rangle - \beta_{i-1}\left|\eta_{i-1}\right\rangle\ \right|\right|_{L^2}^2 \quad , \tag{2.41}$$

which is straightforward to show satisfies the purported orthonormality condition. In theory, the vector $\eta_0$ which initializes the algorithm is chosen to be a random vector; there are requirements of non-zero overlap between $\eta_0$ and the desired eigensolution $\Psi$, but in the high-dimensional spaces in which we normally operate this is trivial to fulfill via random selection of the coordinates. In more pragmatic cases, we typically perform a sequence of Lanczos calculations in increasing configuration space dimensions. One may then utilize the approximate eigensolution from the lower-dimensional configuration space as a pivot for the higher-dimensional configuration space calculation by embedding the approximate eigensolution within the higher-dimensional space. This proves to accelerate the convergence of the ground state eigenvalue with respect to the number of Lanczos iterations used in the higher-dimensional space.

As we have stated in the introduction to this section, the application of the algorithm then leaves us with a remarkably small $m \times m$ dimensional matrix which is subsequently diagonalized with a more standard algorithm as

$$E = P^{-1} H_{\text{Lanczos}}\, P \quad . \tag{2.42}$$

The approximate eigenvalues and eigenvectors are extracted from the diagonal $m \times m$ matrix $E$ and by use of the coordinates of the eigenvectors in the Lanczos basis stored in $P$ to reconstruct the $n$-dimensional eigenvectors from the Lanczos basis vectors. The convergence properties of this algorithm were already well-understood in the context in which they were studied by Lanczos [110], but more recent studies have illucidated additional details about the convergence and bounds on the Lanczos-type methods, see Ref. [112] and references therein as well as the seemingly unpublished Ref. [113].

### 2.4.2 Lanczos Strengths Method

Let us now consider a different kind of problem which, in the end, will turn out to be not so different after all. These results have been pointed out in numerous works over the decades, e.g., see the early ideas developed for the "recursion method" as applied in electronic structure in the individual and combined works of Haydock, Heine and Kelly [114, 115, 116, 117, 118], as well as the 1987 conference proceedings in Ref. [119] which highlight several related developments in line with these original works. As well, several papers within the *ab initio* nuclear theory community have emerged over the decades exploiting this technique [37, 120, 121, 122].

Let us consider some bounded linear operator $H$ and say that we would like to evaluate amplitudes of the following form

$$\mathcal{A}_{fi} = \left\langle \Psi_f \right| O_2 \left(z - H\right)^{-1} O_1 \left|\Psi_i\right\rangle = \left\langle \Psi_f \right| O_2 \left|\Psi_{\text{R}}\right\rangle \quad , \tag{2.43}$$

where $z \in \mathbb{C}$ is such that the resolvent $R(z) = (z - H)^{-1}$ exists and is bounded. We will further assume in this discussion that $O_1$ and $O_2$ are irreducible spherical tensor operators which carry good parity number, though the discussion can be trivially extended to general operators by projection onto good spin with an expansion akin to the multipole decomposition, e.g., see Sec. 3.1. It is then clear that, by definition, we have

$$\left(z - H\right)\left|\Psi_{\text{R}}\right\rangle = O_1 \left|\Psi_i\right\rangle \quad , \tag{2.44}$$

which looks an awful lot like the Schrödinger equation we have just discussed the formalism for solving, albeit with an inhomogeneity. As it turns out, there is functionally no difference between solving a homogeneous or inhomogeneous differential equation via the Lanczos algorithm, one must only set the "pivot" point of the algorithm. So, rather than initializing the Krylov subspace randomly we may instead choose the pivot for the algorithm to be the normalized form of the constraint on $\Psi_R$ as either

$$\left|\eta_0\right\rangle = \frac{1}{\sqrt{\left\langle\Psi_i\right| O_1^\dagger O_1 \left|\Psi_i\right\rangle}} O_1 \left|\Psi_i\right\rangle \qquad \text{or} \qquad \left|\zeta_0\right\rangle = \frac{1}{\sqrt{\left\langle\Psi_f\right| O_2^\dagger O_2 \left|\Psi_f\right\rangle}} O_2 \left|\Psi_f\right\rangle \quad . \tag{2.45}$$

We may then perform the Lanczos tri-diagonalization as before. For the following discussion, let us assume that we are working with the Lanczos basis generated from $\eta_0$, though we emphasize that the derivation beginning with the pivot $\zeta_0$ is identical. Importantly, in the case where $O_1$ has good rank $J_1$ and parity $\pi_1$, as we have assumed here, commutation of the Hamiltonian with the spin momentum and parity operators in combination with the normalized pivot constrains us to spin and parity subspaces of the Hamiltonian. This set of $J^\pi$ subspaces are characterized by the spin and parity numbers arising from satisfication of the triangle inequaltiy and parity composition as

$$\pi = \pi_i \cdot \pi_1 \qquad\qquad \left|J_i - J_1\right| \leq J \leq J_i + J_1 \qquad . \tag{2.46}$$

Otherwise put, the Lanczos algorithm will now only converge eigensolutions within the valid subspace of the Hamiltonian mapped to by the action of $O_1$.

Now, from the tri-diagonalization itself it is possible to extract a continued fraction representation for the resolvent, as has been shown in the important work by Haydock [114] – though notably this was not the first discovery of the connection between the spectrum of a linear operator and a continued fraction representation of the corresponding Green function. Formally speaking, we can think of this approximate inversion as representing the resolvent as a power series in the Hamiltonian and the parameter $z$ as

$$(z - H)^{-1} = \frac{1}{z}\left(\mathbb{1} + \frac{1}{z}H + \frac{1}{z^2}H^2 \cdots\right) \quad ,$$

which is well-defined and convergent for certain conditions on the norm of $||H/z||$. However, for the applications which we will consider in the coming chapters, we will be required to dynamically evaluate the resolvent on complicated grids of energy and 3-momenta and so, due to the on-the-fly computation of the standard continued fraction approach, the required continual access to the Lanczos vectors will instead hamper our efforts. Rather, we may follow the procedure outlined in Dagotto [123] to construct the transition amplitudes which arise in the numerator of the resolvent when represented in a chosen basis, e.g., the basis of the intermediate nuclear spectrum, with a minor generalization of the approach to off-diagonal transitions. Let us represent the resolvent of Eq. (2.43) in the basis of the intermediate spectrum such that

$$\mathcal{A}_{fi} = \sum\!\!\!\!\!\!\int_n \frac{\left\langle\Psi_f\right| O_2 \left|\Psi_n\right\rangle\left\langle\Psi_n\right| O_1 \left|\Psi_i\right\rangle}{z - \omega_n} \quad , \tag{2.47}$$

where the species of the intermediate nuclear spectrum is set by the action of the transition operator $O_1$ on the initial configuration and this notation formally represents the fact that the nuclear spectrum contains both discrete and continuous configurations. Then, all we need to construct such an object are the transition amplitudes in the numerator and the eigenvalues of the intermediate spectrum $\omega_n$, the latter which we obviously obtain from the Lanczos algorithm. If we explicitly consider the expansion of the intermediate eigensolutions $\Psi_n$ in the basis of the Lanczos vectors as generated from the pivot, by definition given by

$$\left|\Psi_n\right\rangle = \sum_n c_{nm} \left|\eta_m\right\rangle \quad , \tag{2.48}$$

then it turns out that we may immediately extract the transition amplitudes as

$$\begin{aligned}\left\langle \Psi_n \right| O_1 \left| \Psi_i \right\rangle &= \left| \left\langle \Psi_i \right| O_1^\dagger O_1 \left| \Psi_i \right\rangle \right| \left\langle \Psi_n \,|\, \eta_0 \right\rangle = \left| \left\langle \Psi_i \right| O_1^\dagger O_1 \left| \Psi_i \right\rangle \right| \sum_m c^*_{nm} \left\langle \eta_m \,|\, \eta_0 \right\rangle \\ &= \left| \left\langle \Psi_i \right| O_1^\dagger O_1 \left| \Psi_i \right\rangle \right| \sum_m \left\langle \eta_m \right| P \left| \eta_n \right\rangle^* \left\langle \eta_m \,|\, \eta_0 \right\rangle \\ &= \left| \left\langle \Psi_i \right| O_1^\dagger O_1 \left| \Psi_i \right\rangle \right| \left\langle \eta_n \right| P^\dagger \left| \eta_0 \right\rangle \quad , \end{aligned} \tag{2.49}$$

and

$$\begin{aligned}\left\langle \Psi_f \right| O_2 \left| \Psi_n \right\rangle &= \left| \left\langle \Psi_f \right| O_2^\dagger O_2 \left| \Psi_f \right\rangle \right| \left\langle \zeta_0 \,|\, \Psi_n \right\rangle = \left| \left\langle \Psi_f \right| O_2^\dagger O_2 \left| \Psi_f \right\rangle \right| \sum_m c_{nm} \left\langle \zeta_0 \,|\, \eta_m \right\rangle \\ &= \left| \left\langle \Psi_f \right| O_2^\dagger O_2 \left| \Psi_f \right\rangle \right| \sum_m \left\langle \eta_m \right| P \left| \eta_n \right\rangle \left\langle \zeta_0 \,|\, \eta_m \right\rangle \quad . \end{aligned} \tag{2.50}$$

For clarity, we note that the matrix $P$ is the unitary matrix (orthogonal in the NCSM formalism) defined in Eq. (2.42) of the prior section which diagonlizes the $m \times m$ tri-diagonal representation of the Hamiltonian in the Lanczos basis. Thus, for a given process, one only needs to compute the overlaps of the final eigensolution with the Lanczos basis and store the unitary matrix $P$ which contains the coordinates of the intermediate nuclear eigensolutions in terms of the Lanczos basis. In this way, one can then very simply evaluate arbitrary integrals of the above amplitudes

$$I = \int dz \sum\!\!\!\!\!\!\int_n f(z, \omega_n) \left\langle \Psi_f \right| O_2 \left| \Psi_n \right\rangle \left\langle \Psi_n \right| O_1 \left| \Psi_i \right\rangle \quad , \tag{2.51}$$

without any further operations on the Lanczos vectors required. The amplitudes $A_{fi}$ are merely a simple case with the choice of function $f(z, \omega_n) = 1/(z - \omega_n)$. The integrals are of course subject to the convergence properties of the amplitudes and the function $f$. Convergence theorems exist for the diagonal forms of such amplitudes [118, 123, 124] and can be approximately derived for the off-diagonal forms.

The results of this last section summarize the machinery for what is needed in our calculational program.

# Chapter 3

# Amplitudes of Current Operators

To start, we begin by stating the expressions for the electromagnetic and charged-weak current operators as defined in the Standard Model. Since we are interested in accessing electroweak physics at the scale of nuclei with a non-relativistic many-body theory of nucleons and pions, these *more fundamental* currents at the level of quarks will ultimately be used to construct effective currents at the level of the nucleon. These currents are respectively defined as

$$J^{\mu}_{\text{em}} = \frac{2}{3}\bar{u}\gamma^{\mu}u - \frac{1}{3}\bar{d}\gamma^{\mu}d \qquad\qquad J^{\dagger\,\mu}_{\text{W}} = \bar{d}\gamma^{\mu}\big(1-\gamma_5\big)u \quad . \tag{3.1}$$

While most of what we will derive in this section is in fact applicable at the quark level, it will still be with the end goal of describing electroweak interactions in nuclei in an EFT picture where protons and neutrons act as the fundamental degrees of freedom. Let us then write down some familiar objects.

In the SM, if we consider the interaction of a free photon field with a nuclear configuration, we may write down the following Hamiltonian which, in the language of QED, completely characterizes at leading order the interaction between the nucleus and electromagnetic radiation:

$$\begin{aligned} H = H_{\text{nuc}} + \sum_{\lambda}\int d^3k\ \omega_k\, a^{\dagger}_{\lambda}\big(\vec{p}\,\big)\, a_{\lambda}\big(\vec{p}\,\big) - e\int d^3x\ \mathcal{J}_{\text{nuc}}\big(\vec{x}\,\big)\cdot\vec{A}\big(\vec{x}\,\big) \\ + \frac{e^2}{8\pi}\int d^3x' d^3x\ \frac{\rho_{\text{nuc}}\big(\vec{x}\,\big)\,\rho_{\text{nuc}}\big(\vec{x}\,'\big)}{\big|\vec{x}-\vec{x}\,'\big|} \quad , \end{aligned} \tag{3.2}$$

where the vector potential for the photon field in terms of the creation and annihilation operators, and in the Coulomb gauge, is given by

$$\vec{A}\big(\vec{x}\,\big) = \sum_{\lambda}\int \frac{d^3p}{(2\pi)^3}\ \frac{1}{\sqrt{2\omega_p}}\ \Big(\ \hat{e}^{*}_{\lambda}(\hat{p})\, a^{\dagger}_{\lambda}\big(\vec{p}\,\big)\, e^{-i\vec{p}\cdot\vec{x}} + \hat{e}_{\lambda}(\hat{p})\, a_{\lambda}\big(\vec{p}\,\big)\, e^{i\vec{p}\cdot\vec{x}}\ \Big) \quad . \tag{3.3}$$

The above expressions are general in that they make no assumption on the character of the nucleus, i.e., there must only exist some local current operator $\mathcal{J}(x)$ and it need not be described in terms of nucleons. As we care principally about the interactions between these fields and not about the free behaviour, we need only consider amplitudes of the term involving the product of the nuclear current operator and electromagnetic vector potential as

$$\big\langle\ \Psi_f\lambda_f\,;\,\vec{p}_f\ \vec{q}\ \big|\ H_{\text{int.}}\ \big|\ \Psi_i\,;\,\vec{p}_i\ \big\rangle = -e\ \big\langle\ \Psi_f\,;\,\vec{p}_f\ \big|\int d^3x\ e^{i\vec{p}\cdot\vec{x}}\ \hat{e}^{*}_{\lambda}(\hat{p})\cdot\vec{J}\big(\vec{x}\,\big)\ \big|\ \Psi_i\,;\,\vec{p}_i\ \big\rangle \quad . \tag{3.4}$$

The structure of these amplitudes is very much universal in that they involve the Fourier transform of the current operator; it will permit us to decompose these amplitudes into multipoles of the nuclear current operator, regardless of the underlying character of the current at hand.

Similarly, the semi-leptonic weak Hamiltonian describing lepton-nucleus interactions may be written at lowest order in the weak coupling constant $G_F$ as a current-current product,

$$H_{\rm W} = -\frac{G_F}{\sqrt{2}} \int d^3x \; j_\mu^{\rm lep.}(\vec{x}\,)\, \mathcal{J}^\mu(\vec{x}\,) \quad , \tag{3.5}$$

which upon expanding the lepton tensor directly will give us an identical form to the expression shown above for QED.

Understanding how to compute amplitudes of these complicated current operators in terms of a simple multipole structure – very much akin to the multipole decomposition of a classical electromagnetic field – will in turn allow us to compute complex lepton-nucleus scattering processes in both the electromagnetic and weak sectors of the SM. We refer the reader to Ref. [96] for a sublime, historical introduction to weak interaction phenomenology, electromagnetic theory and everything to do with nuclear processes in the SM. For further comprehensive derivations, discussion and pedagogical reviews in literature which may extend beyond the discussion of the methods presented in this section, see Refs. [95, 125, 126, 127], and for examples of state-of-the-art calculations exploiting the formalism to be presented here, see Refs. [128, 129, 130]. Now, we turn our attention towards the multipole decomposition.

## 3.1 Multipoles of Current Operators

We begin by denoting an arbitrary current operator as $O$. Where necessary, we will specify the inherent structure of the current, e.g., scalar $S$, pseudoscalar $P$, vector $V$, axial-vector $A$ or tensor $T$, with the respective current operators defined as

$$S(x) = \bar{q}(x)\,\Gamma\,q(x) \qquad P(x) = \bar{q}(x)\,\Gamma\,\gamma_5\,q(x)$$

$$V^\mu(x) = \bar{q}(x)\,\Gamma\,\gamma^\mu\,q(x) \qquad A^\mu(x) = \bar{q}(x)\,\Gamma\,\gamma^\mu\gamma_5\,q(x)$$

$$T^{\mu\nu}(x) = \bar{q}(x)\,\Gamma\,\gamma^\mu\gamma^\nu\,q(x) \qquad .$$

Here, $q(x) = (u,d)^T$ is the SU(2) isospin doublet representation of the light quark fields introduced in the prior section and $\Gamma \in \mathrm{SU}(2)$ an isospin rotation matrix which may mix the two quark flavours. We intend to use a unified notation in deriving the properties of the above objects which, for a given operator rank, admit near identical multipole decompositions up to the action of the $\gamma_5$ operator. Except where necessary to resolve structural differences in the multipoles, we will use the general notation of $\mathcal{R}$ for scalar and pseudoscalar currents, $\mathcal{J}^\mu$ for vector and axial-vector currents, and $\mathcal{T}^{\mu\nu}$ for tensor currents. We are primarily interested in the multipole decomposition of a momentum space operator, i.e., the Fourier transform of a position space operator, onto a basis of radial and angular functions which will be defined below. Consider a current operator $O(x)$ of arbitrary type represented in coordinate space. We may write the purely spatial Fourier transform of the operator as

$$O\big(q_0,\vec{q}\,\big) = \int d^3x\; e^{-i\vec{q}\cdot\vec{x}}\; O\big(q_0,\vec{x}\,\big) \tag{3.6}$$

where the $t = x_0$ coordinate is left untouched by the Fourier transform. Convenient for calculations in non-relativistic formalisms, we may decompose the plane-wave exponential factor into a basis of spherical tensor operators as

$$\begin{aligned} e^{-i\vec{q}\cdot\vec{x}} &= e^{-iz\hat{q}\cdot\hat{x}} \\ &= 4\pi\sum_{J=0}^{\infty}\sum_{M=-J}^{J}(-i)^J j_J(z)\,Y^*_{JM}\big(\hat{q}\big)Y_{JM}\big(\hat{x}\big) \\ &= 4\pi\sum_{J=0}^{\infty}\sum_{M=-J}^{J}(-i)^J\;Y^*_{JM}\big(\hat{q}\big)\,M_{JM}\big(z,\hat{x}\big) \quad , \end{aligned} \tag{3.7}$$

where $z = |\vec{q}\,||\vec{x}\,|$ and we make the following definition

$$M_{JM}\big(z,\hat{x}\big) = j_J(z)\,Y_{JM}\big(\hat{x}\big) \quad . \tag{3.8}$$

Notice that we may further choose to write the expansion of the exponential as

$$\begin{aligned} e^{-i\vec{q}\cdot\vec{x}} &= \frac{i}{|\vec{q}\,|}\;\hat{q}\cdot\Big[\,\vec{\nabla}_x\,e^{-i\vec{q}\cdot\vec{x}}\,\Big] \\ &= 4\pi\sum_{J=0}^{\infty}\sum_{M=-J}^{J}(-i)^J\;Y^*_{JM}\big(\hat{q}\big)\,\frac{i}{|\vec{q}\,|}\Big(\hat{q}\cdot\Big[\,\vec{\nabla}_x\,M_{JM}\big(z,\hat{x}\big)\,\Big]\Big) \quad , \end{aligned} \tag{3.9}$$

where $z = |\vec{q}\,||\vec{x}\,|$ as above. This will expose more convenient (and intuitive) properties when we consider the expansion of vector-like currents. This basis of projection functions $\big\{\,M_{JM},\;\vec{\nabla}_x\,M_{JM}\,\big\}$ built from

the spherical bessel and spherical harmonic functions is, at the most basic level, all that is needed to decompose a given current operator into its corresponding multipoles.

Moreover, when dealing with current operators of rank greater than zero it is convenient to define additional bases of projection functions. In the case of vector-like current operators, it is useful to decompose the 3-vector part of the current into a spherical basis whose definition is set by the 4-momentum argument of the current. Consider a vector-like current operator

$$\mathcal{J}(q_0,\vec{q}) = \Big(\mathcal{J}_0(q_0,\vec{q}),\ \vec{\mathcal{J}}(q_0,\vec{q})\Big) \quad ,$$

and let us define an orthonormal basis of spherical unit vectors $\{\hat{e}_\lambda(\hat{q})\}$ with $i \in \{-1,0,1\}$ by the following properties:

$$\hat{e}_\lambda(\hat{q}) \cdot \hat{e}_j^*(\hat{q}) = \delta_{ij} \qquad \hat{q} \cdot \hat{e}_{\pm1}(\hat{q}) = 0 \qquad \hat{q} \cdot \hat{e}_0(\hat{q}) \neq 0 \quad . \tag{3.10}$$

Note that we have defined the basis with an explicit dependence on the direction of the 3-momentum argument of the current; all that we have introduced thus far is general for arbitrary 3-momenta. We may then trivially decompose the 3-vector part of the current operator as

$$\vec{\mathcal{J}}(q_0,\vec{q}) = \sum_{\lambda=-1}^{1} \vec{\mathcal{J}}_\lambda(q_0,\vec{q})\, \hat{e}_\lambda^*(\hat{q}) \qquad \vec{\mathcal{J}}_\lambda(q_0,\vec{q}) = \hat{e}_\lambda \cdot \vec{\mathcal{J}}(q_0,\vec{q}) \quad . \tag{3.11}$$

We see from the above expression and the plane-wave expansion in Eq. (3.7) that we are required to couple the representations of the spherical basis and the remaining spherical harmonic $Y^*_{JM}$ in order to ensure the correct spherical tensor structure of the eventual multipoles. We are then motivated by convenience to define the vector spherical harmonics as

$$\vec{Y}_{J1}^{Lm}(\hat{q},\hat{x}) = \sum_{M=-J}^{J} \sum_{\lambda=-1}^{1} C^{J1\,;\,Lm}_{JM\,;\,1\lambda}\, Y_{JM}(\hat{x})\, \vec{e}_\lambda(\hat{q}) \quad , \tag{3.12}$$

and furthermore the basis of vector projection functions $\{\vec{M}_{J1}^{Lm}\}$ as

$$\vec{M}_{J1}^{Lm}(z,\hat{q},\hat{x}) = j_J(z)\ \vec{Y}_{J1}^{Lm}(\hat{q},\hat{x}) \quad . \tag{3.13}$$

The above definitions are completely general, that is to say, there is no restriction on the choice of coordinate system in which the current is to be represented. We may exploit this freedom and choose a convenient form of the spherical basis $\{\hat{e}_\lambda(\hat{q})\}$ which ultimately defines a quantization axis for the current operator of interest. In particular, we select a set of coordinates such that the 3-momentum of the current operator is aligned with the quantization axis of the system,

$$\hat{e}_0(\hat{q}) = \hat{q} = \hat{x}_3 \quad , \tag{3.14}$$

which is enough to greatly simplify the following derivations via simplification of the spherical harmonic that is a function of the $\hat{q}$-domain as

$$Y_{JM}(\hat{x}_3) = \sqrt{\frac{2J+1}{4\pi}}\ \delta_{M0} \quad . \tag{3.15}$$

While perfectly valid in the context of purely the current operator, this choice is not suitable for arbitrary interactions of currents and QFT states which, in general, may be prepared with a quantization axis different from the axis defined by the 3-momentum of the current. We illustrate this in Fig. 3.1 and note that the remedy is straightforward, involving SO(3) rotations of the current operator or QFT state onto a common quantization axis for the entire system; we direct the reader to Chapter 4 on "Wigner

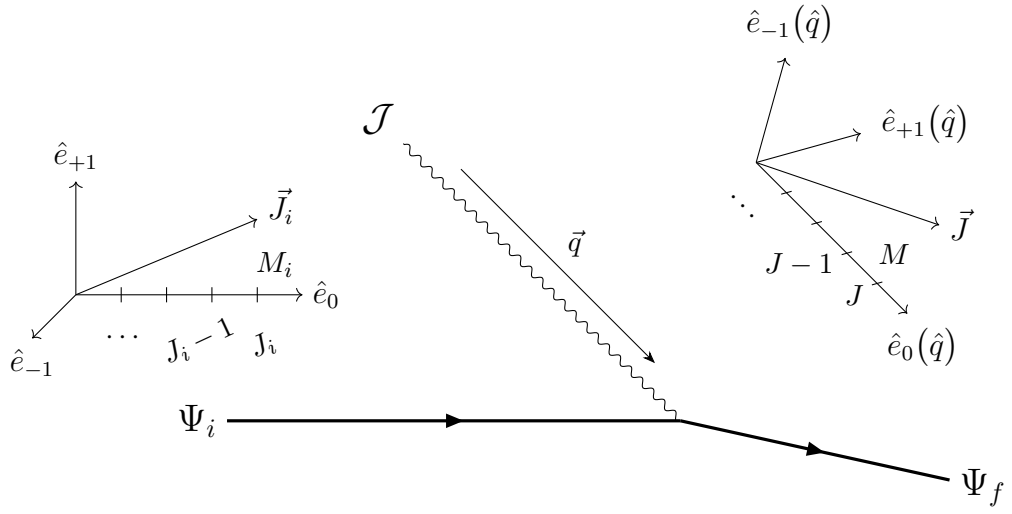


Figure 3.1: Illustration of the chosen coordinate system and quantization axis for a vector-like current operator $\mathcal{J}$ with the 3-momentum transfer $\vec{q}$ defining the $\hat{e}_0(\hat{q})$ axis, as well as the possibly different coordinate system for the prepared initial QFT state.

$D$-Functions" from the bible-esque Ref. [99] for a comprehensive review of this (and frankly any material in the theory of spin algebra that one could possibly dream up!) and further to Ref. [131] for a relevant example in state-of-the-art nuclear reaction calculations.

These expressions presented at the beginning of this section are the foundation of the multipole expansion formalism. The remaining work to be done is purely that of calculus and spin algebra. Indeed, it is almost as simple as that!

**Multipoles of Vector and Axial-Vector Current Operators**

Consider a generic vector-like current operator $\mathcal{J} = (\mathcal{J}_0, \vec{\mathcal{J}})$. In the following section, we will separate our treatment of $\mathcal{J}_0$ and $\vec{\mathcal{J}}$ for convenience. Let us begin with the momentum space representation of the so-called *charge density operator* $\mathcal{J}_0$ which, in terms of the Fourier transform of the spatial current operator, may be expressed as

$$\begin{aligned}
\mathcal{J}_0(q_0, \vec{q}) &= \int d^3x \; e^{-i\vec{q}\cdot\vec{x}} \; \mathcal{J}_0(q_0, \vec{x}) \\
&= 4\pi \sum_{J=0}^{\infty} \sum_{M=-J}^{J} (-i)^J \; Y^*_{JM}(\hat{q}) \int d^3x \; M_{JM}(z, \hat{x}) \, \mathcal{J}_0(q_0, \vec{x}) \\
&= 4\pi \sum_{J=0}^{\infty} \sum_{M=-J}^{J} (-i)^J \; Y^*_{JM}(\hat{q}) \; \bar{M}_{JM}(q_0, |\vec{q}|) \quad ,
\end{aligned}$$

where $z = |\vec{q}||\vec{x}|$ and we define the first multipole of the current operator $\mathcal{J}$ to be

$$\bar{M}_{JM}(q_0, |\vec{q}|) = \int d^3x \; M_{JM}(z, \hat{x}) \, \mathcal{J}_0(q_0, \vec{x}) \quad . \tag{3.16}$$

This expression may be further reduced by our choice of coordinates $\hat{q} = \hat{x}_3$ since we have by definition of the spherical harmonics that which yields our final expression for the charge density operator:

$$\mathcal{J}_0(q_0, \vec{q}) = \sqrt{4\pi} \sum_{J=0}^{\infty} (-i)^J \sqrt{2J+1}\ \bar{M}_{J0}(q_0, |\vec{q}|) \quad . \tag{3.17}$$

The remaining part of the current $\mathcal{J}$, the so-called vector current operator $\vec{\mathcal{J}}$, is to be treated by an expansion over a set of spherical basis vectors as outlined in the introduction to this section. These expressions may be better treated by inspecting the components of the expansion in the spherical basis, i.e., the $\lambda = 0$ and $\lambda = \pm 1$ contributions, separately. We will begin with the $\lambda = 0$ component as this has a particularly special treatment; we use the alternative expansion for the exponential given in Eq. (3.9) which, upon substitution into the definition for the components of the vector-like current operator in terms of the spherical basis, gives

$$\begin{aligned}
\vec{\mathcal{J}}_0(q_0, \vec{q}) &= 4\pi \sum_{J=0}^{\infty} \sum_{M=-J}^{J} (-i)^J\ Y^*_{JM}(\hat{q})\ \frac{i}{|\vec{q}|} \int d^3x\ \Big[\ \vec{\nabla}_x\, M_{JM}(z, \hat{x})\ \Big] \cdot \vec{\mathcal{J}}(q_0, \vec{x}) \\
&= \sqrt{4\pi} \sum_{J=0}^{\infty} (-i)^J \sqrt{2J+1}\ \frac{i}{|\vec{q}|} \int d^3x\ \Big[\ \vec{\nabla}_x\, M_{J0}(z, \hat{x})\ \Big] \cdot \vec{\mathcal{J}}(q_0, \vec{x}) \quad ,
\end{aligned}$$

where we have simplified the spherical harmonic that is a function of the $\hat{q}$-domain in the second line. It is straightforward to read off the corresponding multipole from this $\hat{q}$-projected part of the vector current,

$$\vec{\mathcal{J}}_0(q_0, \vec{q}) = \sqrt{4\pi} \sum_{J=0}^{\infty} (-i)^J \sqrt{2J+1}\ \mathcal{L}_{J0}(q_0, \vec{q}) \quad .$$

with the *longitudinal* multipole defined as

$$\mathcal{L}_{JM}(q_0, \vec{q}) = \frac{i}{|\vec{q}|} \int d^3x\ \Big[\ \vec{\nabla}_x\, M_{JM}(z, \hat{x})\ \Big] \cdot \vec{\mathcal{J}}(q_0, \vec{x}) \quad . \tag{3.18}$$

This form is specific to the choice $\hat{e}_0(\hat{q}) = \hat{q}$.

We may now turn our attention to the $\lambda = \pm 1$ components of the vector current operator which require a bit more work to ease out. Beginning with Eq. (3.11), we have

$$\begin{aligned}
\vec{\mathcal{J}}(q_0, \vec{q}) &= \sum_{\lambda=-1}^{1} \vec{\mathcal{J}}_\lambda(q_0, \vec{q})\, \hat{e}^*_\lambda(\hat{q}) \\
&= \sum_{\lambda=-1}^{1} \hat{e}^*_\lambda(\hat{q}) \int d^3x\ e^{-i\vec{q}\cdot\vec{x}}\, \hat{e}_\lambda(\hat{q}) \cdot \vec{\mathcal{J}}(q_0, \vec{x}) \\
&= 4\pi \sum_{\lambda=-1}^{1} \hat{e}^*_\lambda(\hat{q}) \sum_{J=0}^{\infty} \sum_{M=-J}^{J} (-i)^J\ Y^*_{JM}(\hat{q}) \int d^3x\ \Big[ j_J(z)\, Y_{JM}(\hat{x})\, \hat{e}_\lambda(\hat{q}) \Big] \cdot \vec{\mathcal{J}}(q_0, \vec{x}) \\
&= 4\pi \sum_{\lambda=-1}^{1} \hat{e}^*_\lambda(\hat{q}) \sum_{J=0}^{\infty} \sum_{M=-J}^{J} (-i)^J\ Y^*_{JM}(\hat{q}) \sum_{L=|J-1|}^{J+1} \sum_{m=-L}^{L} C^{J1\,;\,Lm}_{JM\,;\,1\lambda} \\
&\qquad \times \int d^3x\ \Big[\ j_J(z)\, \vec{Y}^{Lm}_{J1}(\hat{q}, \hat{x})\ \Big] \cdot \vec{\mathcal{J}}(q_0, \vec{x}) \\
&= 4\pi \sum_{\lambda=-1}^{1} \hat{e}^*_\lambda(\hat{q}) \sum_{J=0}^{\infty} \sum_{M=-J}^{J} (-i)^J\ Y^*_{JM}(\hat{q}) \sum_{L=|J-1|}^{J+1} C^{J1\,;\,Lm}_{JM\,;\,1\lambda}\, \bar{\bar{M}}^{Lm}_{J1}(q_0, \vec{q}) \quad .
\end{aligned}$$

where again $z = |\vec{q}||\vec{x}\,|$, the sum over the projection number $m$ is trivially reduced by the requirement that $\lambda = M - m$, and we define the object

$$\bar{\bar{M}}^{Lm}_{J1}(q_0,\vec{q}\,) = \int d^3x\ \vec{M}^{Lm}_{J1}(z,\hat{q},\hat{x})\cdot\vec{\mathcal{J}}(q_0,\vec{x}\,) = \int d^3x\ \Big[\ j_J(z)\,\vec{Y}^{Lm}_{J1}(\hat{q},\hat{x})\ \Big]\cdot\vec{\mathcal{J}}(q_0,\vec{x}\,) \quad . \tag{3.19}$$

As before, we reduce the spherical harmonic that is a function of the $\hat{q}$-domain which gives

$$\vec{\mathcal{J}}_\lambda(q_0,\vec{q}\,) = \sqrt{4\pi}\sum_{J=1}^{\infty}(-i)^J\sqrt{2J+1}\sum_{L=|J-1|}^{J+1} C^{J1\,;\,L\lambda}_{J0\,;\,1\lambda}\ \bar{\bar{M}}^{L\lambda}_{J1}(q_0,\vec{q}\,) \quad .$$

In order to obtain the two remaining transverse multipoles, we must explicitly perform the summation over the $L$ number. We note that the sum is attached only to the vector basis functions $\{\vec{M}^{Lm}_{J1}\}$ that we have defined in the introduction to this section, and as such we may consider

$$\begin{aligned}
&\sum_{L=|J-1|}^{J+1} C^{J1\,;\,L\lambda}_{J0\,;\,1\lambda}\ \vec{M}^{L\lambda}_{J1}(z,\hat{q},\hat{x}) \\
&\qquad = C^{J1\,;\,J-1\lambda}_{J0\,;\,1\lambda}\ \vec{M}^{J-1\lambda}_{J1}(z,\hat{q},\hat{x}) + C^{J1\,;\,J+1\lambda}_{J0\,;\,1\lambda}\ \vec{M}^{J+1\lambda}_{J1}(z,\hat{q},\hat{x}) + C^{J1\,;\,J\lambda}_{J0\,;\,1\lambda}\ \vec{M}^{J\lambda}_{J1}(z,\hat{q},\hat{x}) \\
&\qquad = \sqrt{\frac{J-1}{2(2J+1)}}\ \vec{M}^{J-1\lambda}_{J1}(z,\hat{q},\hat{x}) + \sqrt{\frac{J+2}{2(2J+1)}}\ \vec{M}^{J+1\lambda}_{J1}(z,\hat{q},\hat{x}) - \frac{\lambda}{\sqrt{2}}\ \vec{M}^{J\lambda}_{J1}(z,\hat{q},\hat{x}) \quad .
\end{aligned}$$

Importantly, from the definition of the vector projection functions, for the case of $\lambda = \pm 1$ we must always have that the first index is greater than or equal to one. This then allows us to reorder the infinite sum over multipoles as $J \to J+1$ in the first term, as $J \to J-1$ in the second term and with the total summation (expressly for these terms) restricted as $J \geq 1$. With some manipulation, we find

$$\begin{aligned}
&\sum_{J=1}^{\infty}(-i)^J\sqrt{2J+1}\sum_{L=|J-1|}^{J+1} C^{J1\,;\,L\lambda}_{J0\,;\,1\lambda}\ \vec{M}^{L\lambda}_{J1}(z,\hat{q},\hat{x}) \\
&\quad = \frac{1}{\sqrt{2}}\sum_{J=1}^{\infty}(-i)^J\sqrt{2J+1}\ \left[\ i\sqrt{\frac{J+1}{2J+1}}\,\vec{M}^{J\lambda}_{J-11}(z,\hat{q},\hat{x}) - i\sqrt{\frac{J}{2J+1}}\,\vec{M}^{J\lambda}_{J+11}(z,\hat{q},\hat{x}) - \lambda\,\vec{M}^{J\lambda}_{J1}(z,\hat{q},\hat{x})\ \right] \\
&\quad = \frac{1}{\sqrt{2}}\sum_{J=1}^{\infty}(-i)^J\sqrt{2J+1}\ \left[\ \frac{1}{|\vec{q}|}\vec{\nabla}_x\times\vec{M}^{J\lambda}_{J1}(z,\hat{q},\hat{x}) - \lambda\,\vec{M}^{J\lambda}_{J1}(z,\hat{q},\hat{x})\ \right] \quad ,
\end{aligned}$$

where we have utilized a most convenient vector identity for such basis functions,

$$\frac{1}{|\vec{q}|}\vec{\nabla}_x\times\vec{M}^{J\lambda}_{J1}(z,\hat{q},\hat{x}) = i\sqrt{\frac{J+1}{2J+1}}\vec{M}^{J\lambda}_{J-11}(z,\hat{q},\hat{x}) - i\sqrt{\frac{J}{2J+1}}\vec{M}^{J\lambda}_{J+11}(z,\hat{q},\hat{x}) \quad , \tag{3.20}$$

taken as seen in Eq. (60) of Chapter 7 on "Tensor Spherical Harmonics" from Ref. [99]. Folding this expression back into the decomposition of the vector current operator, we arrive at the final form for the $\lambda = \pm 1$ contributions:

$$\vec{\mathcal{J}}_\lambda(q_0,\vec{q}\,) = \sqrt{2\pi}\sum_{J=1}^{\infty}(-i)^J\sqrt{2J+1}\ \left[\ T^{\rm el}_{JM}(q_0,\vec{q}\,) - \lambda\,T^{\rm mag}_{JM}(q_0,\vec{q}\,)\ \right] \quad ,$$

with the so-called *transverse electric* and *transverse magnetic* multipoles respectively defined as

$$T^{\rm el}_{JM}(q_0,\vec{q}) = \frac{1}{|\vec{q}|}\int d^3x\ \Big[\ \vec{\nabla}_x \times \vec{M}^{J\lambda}_{J1}(z,\hat{q},\hat{x})\ \Big]\cdot\vec{\mathcal{J}}(q_0,\vec{x}) \quad , \tag{3.21}$$

$$T^{\rm mag}_{JM}(q_0,\vec{q}) = \int d^3x\ \vec{M}^{J\lambda}_{J1}(z,\hat{q},\hat{x})\cdot\vec{\mathcal{J}}(q_0,\vec{x}) \quad , \tag{3.22}$$

where $z = |\vec{q}||\vec{x}\,|$ as before.

We summarize this section by stating that one may find the Coulomb multipole in Eq. (3.16), the longitudinal multipole in Eq. (3.18), and the transverse electric and magnetic multipoles in the above Eq. (3.21) and Eq. (3.22), respectively. The multipoles are defined entirely in terms of the fundamental vector-like current operator and the scalar and vector basis functions given in Eq. (3.8) and Eq. (3.13), respectively. These multipoles completely characterize the operator $\mathcal{J}$ and, up to the one-nucleon form factors (see the later section) and the potential action of the $\gamma_5$ matrix in the fundamental current, are identical for any vector and axial-vector currents which may appear in the Standard Model. Thus, the charge density operator is given by

$$\mathcal{J}_0(q_0,\vec{q}) = \sqrt{4\pi}\sum_{J=0}^{\infty}(-i)^J\sqrt{2J+1}\ \bar{M}_{J0}(q_0,|\vec{q}|) \quad , \tag{3.23}$$

and the vector current operator by

$$\begin{aligned}\vec{\mathcal{J}}(q_0,\vec{q}) &= \sqrt{4\pi}\sum_{J=0}^{\infty}(-i)^J\sqrt{2J+1}\ \mathcal{L}_{J0}(q_0,\vec{q})\ \hat{e}_0^*(\hat{q}) \\ &+ \sqrt{2\pi}\sum_{\lambda=\pm1}\sum_{J=1}^{\infty}(-i)^J\sqrt{2J+1}\ \Big[\ T^{\rm el}_{JM}(q_0,\vec{q}) - \lambda\, T^{\rm mag}_{JM}(q_0,\vec{q})\ \Big]\ \hat{e}_\lambda^*(\hat{q}) \quad .\end{aligned} \tag{3.24}$$

Additional properties of the multipoles related to parity and time-reversal symmetry may be found in Ref. [125].

### Multipoles of Scalar and Pseudoscalar Current Operators

The decomposition of a general scalar-like current operator is in fact trivial after having worked out the multipole expansion for a vector-like current operator. One can match the relevant operator structures directly onto the multipoles generated from the *charge density operator* $\mathcal{J}_0$ as derived in the prior section.

### Multipoles of Tensor Current Operators

The decomposition of a general tensor current operator is unfortunately beyond the current scope of this text but may be added in the future given an adequate amount of time. Let's see how the summer goes!

## 3.2 Non-Relativistic Quantum Field Theory

This section is a general aside on the discussion of QFT amplitudes of current operators, the goal of which is to establish a rigorous (enough-for-this-dissertation) connection between QFT states and their non-relativistic counterparts. While this will be a weak treatment of the true formalism for Non-Relativistic QFT (NRQFT) in the mathematical sense, the presentation will allow us to correctly interpret the non-relativistic amplitudes of current operators that we will encounter later in this dissertation in terms of the true, relativistic QFT states. I hope that this will provide an intuitive picture to the reader about the language connection between the particle theory and nuclear theory communities. The contents of this section are worked out based on the personal notes of David Morrissey [132] and brief discussion in David Tong's "Lectures on Quantum Field Theory" [133], with further inspiration taken from Ref. [134] and discussions with Chien-Yeah Seng.

Let us begin this discussion by writing down a clear definition of the QFT states.

**Definition 3.2.1** (**Relativistic Plane-Wave Eigensolutions**)**.** We define the relativistic plane-wave basis to be the set of eigensolutions to the free-space, relativistic four-momentum operator $P_\mu = \big(P_0, \vec{P}\,\big)$ where $P_0 = H$ is the free-space, relativistic Hamiltonian operator and $\vec{P}$ is the relativistic 3-momentum operator. More rigorously, for a given quantum particle of arbitrary character ($m$, $\varphi$, $\pi$) labelled solely by its mass $m$, the set of eigensolutions to the four-momentum operator $P^\mu$ define the relativistic plane-wave basis as

$$\big(p^\mu - P^\mu\big)\big|\,\varphi\,;\,\vec{p}\,\big\rangle = 0 \qquad\qquad \Big\{\ \big|\,\varphi\,;\,\vec{p}\,\big\rangle\ :\ \vec{p}\in\mathbb{R}^3\ \Big\} \quad , \tag{3.25}$$

with eigenvalues $p_\mu = \big(\omega_p, \vec{p}\,\big)$ where $\omega_p = \sqrt{m^2 + |\vec{p}\,|^2}$ is the relativistic energy of the quantum particle $\varphi$. In these notes, we adopt the most frequent convention for the normalization of the plane-wave eigensolutions

$$\big\langle\,\varphi\,;\,\vec{p}\,'\,\big|\,\varphi\,;\,\vec{p}\,\big\rangle = 2\omega_p\,(2\pi)^3\,\delta^{(3)}\big(\vec{p}\,' - \vec{p}\,\big) \qquad\qquad \mathbb{1} = \int \frac{d^3p}{(2\pi)^3}\ \frac{1}{2\omega_p}\ \big|\,\varphi\,;\,\vec{p}\,\big\rangle\big\langle\,\varphi\,;\,\vec{p}\,\big| \quad . \tag{3.26}$$

For a truly rigorous definition and exploration of the relativistic plane-wave eigensolutions, including a purely algebraic derivation of their properties, we refer the reader to Section 2.5 of Ref. [135].

Consider the Lagrangian density for a massive, spin-1/2 Dirac fermion ($m$, $\psi$, $\pi$) for which the free quantum particle is described by

$$\mathcal{L} = \bar{\psi}\,\big(i\gamma^\mu\partial_\mu - m\big)\,\psi \qquad\qquad \psi = \begin{pmatrix}\psi_+\\ \psi_-\end{pmatrix} \quad , \tag{3.27}$$

with $\psi$ the spinor of particle ($+$) and anti-particle ($-$) solutions for the field; the components $\psi_\pm$ are themselves bi-spinors representing the spin-1/2 nature of the quantum particle. The definition of the gamma matrices may be found in Appendix A, along with the definitions for any related objects. If we consider a field re-definition of the form $\psi \to e^{-imt}\psi$ then, in terms of the components of $\psi$, the Lagrangian density becomes

$$\begin{aligned}
\mathcal{L} &= \big(e^{imt}\,\bar{\psi}\,\big)\,\big(i\gamma^\mu\partial_\mu - m\big)\,\big(e^{-imt}\,\psi\big) \\
&= m\psi_+^2 + m\psi_-^2 + i\psi_+^\dagger\,\partial_0\,\psi_+ + i\psi_-^\dagger\,\partial_0\,\psi_- + i\psi_-^\dagger\,\sigma^i\partial_i\,\psi_+ + i\psi_+^\dagger\,\sigma^i\partial_i\,\psi_- - m\psi_+^2 + m\psi_-^2 \\
&= i\psi_+^\dagger\,\partial_0\,\psi_+ + \psi_-^\dagger\big(2m + i\partial_0\big)\psi_- + i\psi_-^\dagger\,\sigma^i\partial_i\,\psi_+ + i\psi_+^\dagger\,\sigma^i\partial_i\,\psi_- \quad ,
\end{aligned}$$

in which we see that we have removed the mass term which mixes the two components in favour of a mass term dependent on only the lower component. Formally speaking, we may solve for the equations of motion of the lower component $\psi_-$ via the Euler-Lagrange equations and eliminate it from the above Lagrangian density. We find that

$$\frac{\partial \mathcal{L}}{\partial \psi_-} - \partial_\mu \frac{\partial \mathcal{L}}{\partial(\partial_\mu \psi_-)} = 2m\psi_-^\dagger - i\partial_0\, \psi_-^\dagger - i\partial_i\big(\psi_+^\dagger\, \sigma^i\big) = 0 \quad ,$$

which gives the formal solutions for the conjugate and normal lower component fields in terms of the upper component fields as

$$\psi_-^\dagger = \big(2m - i\partial_0\big)^{-1}\big(i\partial_i\, \psi_+^\dagger\, \sigma^i\big) = \big(2m - i\partial_0\big)^{-1}\big(i\sigma^i\partial_i\, \psi_+^\dagger\big) \quad , \tag{3.28}$$

$$\psi_- = \big(2m + i\partial_0\big)^{-1}\big(\partial_i\, \big[i\psi_+^\dagger\, \sigma^i\big]^\dagger\big) = \big(2m + i\partial_0\big)^{-1}\big(-i\sigma^i\partial_i\, \psi_+\big) \quad , \tag{3.29}$$

Making use of these formal solutions for $\psi_-$ in the Lagrangian density then gives

$$\begin{aligned}\mathcal{L} &= i\psi_+^\dagger\, \partial_0\, \psi_+ + \psi_-^\dagger\big(-i\sigma^i\partial_i\psi_+\big) + i\psi_-^\dagger\, \sigma^i\partial_i\, \psi_+ + i\psi_+^\dagger\, \sigma^i\partial_i\, \big(2m + i\partial_0\big)^{-1}\big(-i\sigma^i\partial_i\, \psi_+\big) \\ &= i\psi_+^\dagger\, \partial_0\, \psi_+ + i\psi_+^\dagger\, \sigma^i\partial_i\, \big(2m + i\partial_0\big)^{-1}\big(-i\sigma^i\partial_i\, \psi_+\big) \quad .\end{aligned}$$

As we will always be integrating the Lagrangian density over space-time, we may integrate by parts in the second term to rewrite it in a more convenient form. This leads to

$$\begin{aligned}&\int d^4x\; i\psi_+^\dagger\, \sigma^i\partial_i\, \big(2m + i\partial_0\big)^{-1}\big(-i\sigma^i\partial_i\, \psi_+\big) \\ &\quad = \Big[i\psi_+^\dagger\, \sigma^i\, \big(2m + i\partial_0\big)^{-1}\big(-i\sigma^i\partial_i\, \psi_+\big)\Big]_\infty - \int d^4x\; \big(-i\sigma^i\partial_i\psi_+\big)^\dagger\big(2m + i\partial_0\big)^{-1}\big(-i\sigma^i\partial_i\, \psi_+\big) \quad ,\end{aligned}$$

where we will assume vanishing field configurations at infinity. We thus arrive at the final form of our Lagrangian density prior to a non-relativistic reduction

$$\mathcal{L} = i\psi_+^\dagger\, \partial_0\, \psi_+ - \frac{1}{2m}\, \big(\sigma^i\partial_i\psi_+\big)^\dagger \left(1 + \frac{i\partial_0}{2m}\right)^{-1} \big(\sigma^i\partial_i\, \psi_+\big) \quad . \tag{3.30}$$

In order to make sense of the above Lagrangian density in a non-relativistic setting, we will write it as a formal power series in powers of $1/m$ by expanding the intermediate resolvent for the time-derivative operator, i.e.,

$$\mathcal{L} = i\psi_+^\dagger\, \partial_0\, \psi_+ - \frac{1}{2m}\, \big(\sigma^i\partial_i\psi_+\big)^\dagger \left[1 + \frac{i\partial_0}{2m} + \mathcal{O}\Big(\big[i\partial_0/2m\big]^2\Big)\right] \big(\sigma^i\partial_i\, \psi_+\big) \quad . \tag{3.31}$$

If we only take the lowest-order contribution to the Lagrangian density and explicitly write it out in terms of the components of the field $\psi_+ = (\psi_1,\, \psi_2)^T$ then we have

$$\mathcal{L}_0 = i\psi_1^*\, \partial_0\, \psi_1 + i\psi_2^*\, \partial_0\, \psi_2 - \frac{1}{2m}\, \big|\vec{\nabla}\psi_1\big|^2 - \frac{1}{2m}\, \big|\vec{\nabla}\psi_2\big|^2 \quad , \tag{3.32}$$

which we recognize as two copies of the Lagrangian density for a non-relativistic, spin-1/2 quantum particle of mass $m$; this is the Lagrangian density which will give rise to (two copies of) the time-dependent Schrödinger equation. Let us consider only one of the two components in Eq. (3.32) for the following discussion since (i) the other component is simply a copy of the same theory with slight modifications to the dynamics and (ii) a single component of the original four-component Dirac field $\psi$ behaves as a scalar field. We will henceforth denote the single-component, non-relativistic field and conjugate field operators for a quantum particle of mass $m$ as

$$\big(m,\, \varphi^{\scriptscriptstyle\vee},\, \pi^{\scriptscriptstyle\vee}\big) \qquad\qquad \pi^{\scriptscriptstyle\vee} = i(\varphi^{\scriptscriptstyle\vee})^* \quad , \tag{3.33}$$

where the caron symbol is utilized to emphasize their non-relativistic nature. We thus find the Hamiltonian for such a system to be

$$H_0(\varphi^{\scriptscriptstyle\vee}) = \int d^3x\; \pi^{\scriptscriptstyle\vee}\, \partial_0\, \varphi^{\scriptscriptstyle\vee} - \mathcal{L}_0(\varphi^{\scriptscriptstyle\vee}) = \int d^3x\; \frac{1}{2m}\big|\vec{\nabla}\varphi^{\scriptscriptstyle\vee}\big|^2 \quad ,$$

as anticipated. Notably, in the non-relativistic setting the Hamiltonian is a positive-definite operator and thus the negative energy solutions typical of the relativistic theory are not present in its spectrum; there is no *natural* occurence of anti-particles in the non-relativistic setting. The further lack of need for a Lorentz invariant theory (only Galileo may be found here!) hence motivates the expansion of the field operator $\varphi^{\check{}}$ to be written as

$$\varphi^{\check{}}(t,x) = \int \frac{d^3p}{(2\pi)^3}\; a\big(\vec{p}\big)\; e^{-i\omega_p t}\; e^{i\vec{p}\cdot\vec{x}} \qquad\qquad \omega_p = m + \frac{|\vec{p}|^2}{2m} + \mathcal{O}(1/m^2) \qquad , \tag{3.34}$$

where $\omega_p$ is the non-relativistic energy of the quantum particle. If we impose the canonical equal-time commutation relations on the fields $\varphi^{\check{}}$ and $\pi^{\check{}} = i(\varphi^{\check{}})^\dagger$ we then arrive at the Hamiltonian operator in terms of the basis of creation and annihilation operators as

$$H_0 = \int \frac{d^3p}{(2\pi)^3}\; \frac{\vec{p}\cdot\vec{p}}{2m}\; a^\dagger\big(\vec{p}\big)\, a\big(\vec{p}\big) \quad . \tag{3.35}$$

We thus interpret the one-particle Hilbert space of the non-relativistic quantum field theory as the Fock space with vacuum $\big|0\big\rangle$ and one-particle momentum states

$$\big(p^\mu - P^\mu\big)\big|\,\varphi^{\check{}}\,;\,\vec{p}\,\big\rangle = 0 \qquad\qquad p^\mu = \Big(m + \frac{|\vec{p}|^2}{2m},\; \vec{p}\Big)$$

$$\Big\{\;\big|\,\varphi^{\check{}}\,;\,\vec{p}\,\big\rangle \;:\; \vec{p}\in\mathbb{R}^3,\;\; |\vec{p}|^2/m \ll 1\;\Big\} \quad . \tag{3.36}$$

With the Hamiltonian operator reminiscent of traditional free-particle quantum theory and a clear one-particle Hilbert space in mind, we may extend the discussion to clearly define the notion of a wavefunction.

### The Notion of a Wavefunction

In the non-relativistic setting described above, we may recover the exact quantum theoretic formalism centered around the dynamics of "wavefunctions" by the following steps. Consider the action of the non-relativistic field operator $\varphi^{\check{}}$ on the vacuum state

$$\big|\,\varphi^{\check{}}\,;\,t,\vec{x}\,\big\rangle = \varphi^{\check{}}(t,\vec{x}\,)\big|0\big\rangle \quad ,$$

which we interpret as creating a one-particle state at time $t$ and position $\vec{x}$. One can show that this satisfies

$$\begin{aligned}
\big\langle\,\varphi^{\check{}}\;;\;t',\vec{x}\,'\,\big|\,\varphi^{\check{}}\;;\;t,\vec{x}\,\big\rangle &= \big\langle 0\big|\,\varphi^{\check{}}(t',\vec{x}\,')\,\varphi^{\check{}\,\dagger}(t,\vec{x}\,)\,\big|0\big\rangle \\
&= \int \frac{d^3p'}{(2\pi)^3}\frac{d^3p}{(2\pi)^3}\; e^{-it'\omega_{p'}+it\omega_p}\; e^{i\vec{p}\,'\cdot\vec{x}\,'-i\vec{p}\cdot\vec{x}}\;\big\langle 0\big|\,a\big(\vec{p}\,'\big)\,a^\dagger\big(\vec{p}\big)\,\big|0\big\rangle \\
&= \delta(t'-t)\,\delta^{(3)}\big(\vec{x}\,'-\vec{x}\,\big) \quad ,
\end{aligned}$$

and

$$\big\langle\,\varphi^{\check{}}\;;\;t,\vec{x}\,\big|\,\varphi^{\check{}}\;;\;\vec{p}\,\big\rangle = \big\langle 0\big|\,\varphi^{\check{}}(t,\vec{x}\,)\,\big|\,\varphi^{\check{}}\;;\;\vec{p}\,\big\rangle = \int \frac{d^3p'}{(2\pi)^3}\; e^{-it\omega_{p'}}\; e^{i\vec{p}\,'\cdot\vec{x}}\;\big\langle 0\big|\,a\big(\vec{p}\,'\big)\,\big|\,\varphi^{\check{}}\;;\;\vec{p}\,\big\rangle = e^{i(\vec{p}\cdot\vec{x}-\omega_p t)} \quad ,$$

as expected. Then we may construct the following quantity

$$\vec{X} = \int d^3x\;\vec{x}\;\varphi^{\check{}\,\dagger}(t,\vec{x}\,)\,\varphi^{\check{}}(t,\vec{x}\,) \qquad\qquad \vec{X}\,\big|\,\varphi^{\check{}}\;;\;t,\vec{x}\,\big\rangle = \vec{x}\,\big|\,\varphi^{\check{}}\;;\;t,\vec{x}\,\big\rangle \quad , \tag{3.37}$$

which one can see by eye satisfies the quoted relation and, similarly to the relativistic 3-momentum operator and basis, we may define

$$\vec{P} = \int \frac{d^3p}{(2\pi)^3}\;\vec{p}\;a^\dagger\big(\vec{p}\big)\,a\big(\vec{p}\big) \qquad\qquad \big\langle\,\varphi^{\check{}}\;;\;\vec{p}\,\big|\,\vec{P}\,\big|\,\varphi^{\check{}}\;;\;\vec{p}\,\big\rangle = \vec{p} \quad . \tag{3.38}$$

These sets of states $\{\,|\,\varphi^{\backsim}\,;\,\vec{x}\,\rangle\}$ and $\{|\,\varphi^{\backsim}\,;\,\vec{p}\,\rangle\,\}$ are, in complete analog to the original QFT states $\{|\,\varphi\,;\,\vec{p}\,\rangle\}$, a complete and orthonormal basis within the one-particle Hilbert space of the non-relativistic theory. We make a critical note that resolution of identity with the respective bases yields

$$\mathbb{1} = \int d^3x\ |\,\varphi^{\backsim}\,;\,\vec{x}\,\rangle\langle\,\varphi^{\backsim}\,;\,\vec{x}\,| \qquad\qquad \mathbb{1} = \int \frac{d^3p}{(2\pi)^3}\ |\,\varphi^{\backsim}\,;\,\vec{p}\,\rangle\langle\,\varphi^{\backsim}\,;\,\vec{p}\,| \quad ,$$

where we emphasize the difference between the normalization of the momentum states in the relativistic and non-relativistic formalisms. We are now poised to make the following definition of a Schrödinger state.

**Definition 3.2.2** (**The Schrödinger State**)**.** We define the Schrödinger state for a classical field configuration $\Psi \in L^2(\mathbb{R}\times\mathbb{R}^3)$ of the non-relativistic field operator $\varphi^{\backsim}$ as

$$|\Psi(t)\rangle = \int d^3x\ \Psi(t,\vec{x})|\,\varphi^{\backsim}\,;\,\vec{x}\,\rangle \quad , \tag{3.39}$$

for which we immediately observe the following properties

$$\langle\,\varphi^{\backsim}\,;\,\vec{x}\,|\Psi(t)\rangle = \Psi(t,\vec{x}) \qquad\qquad \langle\,\varphi^{\backsim}\,;\,\vec{x}\,|\,\vec{X}\,|\Psi(t)\rangle = \vec{x}\,\Psi(t,\vec{x}) \quad . \tag{3.40}$$

One may further show the anticipated result for the 3-momentum operator

$$\begin{aligned}
\langle\,\varphi^{\backsim}\,;\,t',\vec{x}\,'\,|\,\vec{P}\,|\Psi(t)\rangle &= \int d^3x\ \langle 0|\,\varphi^{\backsim}(t',\vec{x}\,')\,\vec{P}\,\Psi(t,\vec{x})\,\varphi^{\backsim\,\dagger}(t,\vec{x})\,|0\rangle \\
&= \int d^3x \frac{d^3p\,'}{(2\pi)^3}\frac{d^3p}{(2\pi)^3}\frac{d^3k}{(2\pi)^3}\ \vec{k}\ e^{i(\vec{p}\,'\cdot\vec{x}\,'-\omega_{p'}t')}\ e^{-i(\vec{p}\cdot\vec{x}-\omega_p t)}\ \Psi(t,\vec{x})\ \langle 0|\,a(\vec{p}\,')\,a^\dagger(\vec{k})\,a(\vec{k})\,a^\dagger(\vec{p})\,|0\rangle \\
&= \int d^3x \frac{d^3p}{(2\pi)^3}\ \vec{p}\ e^{i\vec{p}\cdot(\vec{x}\,'-\vec{x})}\ \Psi(t,\vec{x}) \\
&= -i\vec{\nabla}\,\Psi(t,\vec{x}) \quad ,
\end{aligned}$$

as expected.

This definition establishes the connection of the QFT formalism to the more old-school picture of non-relativistic quantum theory which we all know and love. To finish the discussion, if we apply this definition in the case of the free-particle Hamiltonian in Eq. (3.35) as we have done for the 3-momentum operator above, we immediately find the expected result

$$\langle\,\varphi^{\backsim}\,;\,\vec{x}\,|\,H_0\,|\Psi(t)\rangle = -\frac{1}{2m}\vec{\nabla}^2\,\Psi(t,\vec{x}) \quad , \tag{3.41}$$

which indeed has the correct form of the Schrödinger equation for a free-particle of mass $m$. Remarkable! However, we note that we have not made any comment on the normalization of the Schrödinger state $\Psi(t)$ and so the above expression, while in the right shape, does not admit the Born probability interpretation of standard quantum theory. Not to worry, this is readily corrected by noting that the non-relativistic Lagrangian $\mathcal{L}_0$ that we have derived (and in fact the original QFT Lagrangian for good reason) is invariant under global symmetry transformations as

$$\psi \to e^{-i\alpha}\,\psi \quad ,$$

which leads to the following conserved current

$$j^\mu = \left(\,\varphi^{\backsim\,\dagger}\varphi^{\backsim},\,-\frac{i}{2m}\varphi^{\backsim\,\dagger}\,\vec{\nabla}\,\varphi^{\backsim}\,\right) \quad . \tag{3.42}$$

We can then readily show that the conserved Noether charge satisfies

$$\begin{aligned}\big\langle \Psi(t)\big|\, \varphi^{\check{}\,\dagger}(\vec{x}\,)\,\varphi^{\check{}}(\vec{x}\,)\,\big|\Psi(t)\big\rangle &= \int d^3x''d^3x'\ \big\langle \Psi(t)\big|\, \varphi^{\check{}}\,;\,\vec{x}\,''\big\rangle\big\langle\, \varphi^{\check{}}\,;\,\vec{x}\,'\,\big|\,\Psi(t)\big\rangle\ \big\langle \vec{x}\,''\big|\, \varphi^{\check{}\,\dagger}(\vec{x}\,)\,\varphi^{\check{}}(\vec{x}\,)\,\big|\vec{x}\,'\big\rangle \\ &= \int d^3x\ \big|\Psi(t,\vec{x}\,)\big|^2 \quad , \end{aligned} \tag{3.43}$$

which is simply interpretable as the conservation of particle number, or, in the case where we choose the normalization of the classical field configuration $\Psi$ to be unity, conservation of probability. Now that we have shown how to arrive at the traditional picture of non-relativistic quantum theory from a reduction of QFT, we state the following remark which is the most important result of this work for what is to come.

*Remark* 3.2.1 (**The Relation Between States in QFT and NRQFT**). The relationship between a state in a non-relativistic reduction of QFT which obeys the traditional quantum theoretic description may be related, in the valid momentum domain of applicability, to a relativistic QFT state via the simple relationship

$$\sqrt{m}\,\big|\,\varphi^{\check{}}\,;\,\vec{p}\,\big\rangle = \big|\,\varphi\,;\,\vec{p}\,\big\rangle + \mathcal{O}\big([1/m]^{3/2}\big) \quad , \tag{3.44}$$

when the domain of 3-momentum is restricted such that

$$\Big\{\ \big|\,\varphi^{\check{}}\,;\,\vec{p}\,\big\rangle\ :\ \ \vec{p}\in\mathbb{R}^3,\ \ |\vec{p}\,|^2/m \ll 1\ \Big\} \quad .$$

Ultimately, it comes purely from the definition of the measure of the theory which is Lorentz invariant for QFT and merely Galilean invariant for NRQFT.

The above derivations and final remark collectively provide everything we need to connect a relativistic QFT state to the traditional quantum theoretic formalism exploited in quantum many-body methods. I note that while this may appear a simple result, with little to no references in literature making clear this relationship, it took a longer to figure out than I would care to admit!

## 3.3 Electroweak Amplitudes for the Nucleon

None of what has been derived thus far relies on a low-energy effective field theory for strongly-interacting nuclear systems in terms of protons, neutrons and pions. The multipole expansion formalism presented in the previous section is entirely at the quark level and is blind to external QFT states which appear in the amplitudes; it is ignorant to the doublet of light quarks which we will now be forced to consider to arrive at a meaningful connection to state-of-the-art many-body methods in low-energy, *ab initio* nuclear theory.

As nicely presented in Chapters 42 and 43 of Ref. [96], the charge-changing weak current, the neutral weak current and the electromagnetic current operators may be summarily expressed in terms of an SU(2) doublet in the isospin space of the quarks, i.e.,

$$V_\mu\big(x,\Gamma\big) = \bar{\psi}(x)\,\gamma_\mu\big(1-\gamma_5\big)\,\Gamma\,\psi(x) \tag{3.45}$$

$$A_\mu\big(x,\Gamma\big) = \bar{\psi}(x)\,\gamma_\mu\big(1+\gamma_5\big)\,\Gamma\,\psi(x) \tag{3.46}$$

where $\psi(x) = (u,d)^T$ and $\Gamma \in \{1, \tau_3, \tau_\pm\}$ for the vector current and $\Gamma \in \{\tau_\pm\}$ for the axial-vector current. The most convenient way for us to go about determining the hadronic amplitudes of these currents for nuclei is to begin with the amplitudes for free-nucleon QFT states and perform a non-relativistic reduction. Utilizing Lorentz invariance, the properties of parity and strong isospin invariance and current conservation allows us to write down the most general possible forms of such amplitudes [96]. For a vector or axial current operator, one has that the on-shell one-nucleon amplitudes are given by

$$\big\langle\, \psi_f\,;\,\vec{p}_f\,\big|V^\mu\big(0,\Gamma\big)\big|\,\psi_i\,;\,\vec{p}_i\,\big\rangle = \bar{u}\big(\vec{p}_f,s_f\big)\,\Big[\,F_1\gamma_\mu + \frac{iF_2}{2m}\sigma^{\mu\nu}(p_f-p_i)_\nu - F_s q_\mu\,\Big]\,u\big(\vec{p}_i,s_i\big)\,\big\langle\psi_f\big|\,\Gamma\,\big|\psi_i\big\rangle \quad , \tag{3.47}$$

$$\big\langle\, \psi_f\,;\,\vec{p}_f\,\big|A^\mu\big(0,\Gamma\big)\big|\,\psi_i\,;\,\vec{p}_i\,\big\rangle = \bar{u}\big(\vec{p}_f,s_f\big)\,\Big[\,F_A\gamma_\mu\gamma_5 - \frac{F_P}{2m}\gamma_5(p_f-p_i)^\mu + F_T\sigma^{\mu\nu}q_\nu\gamma_5\,\Big]\,u\big(\vec{p}_i,s_i\big)\,\big\langle\psi_f\big|\,\Gamma\,\big|\psi_i\big\rangle \quad , \tag{3.48}$$

where $\psi_a$ characterizes the type of one-particle QFT state of the nucleon with quantum numbers $a = \{\, s,\, m_s,\, t,\, m_t \,\}$. As we are interested in application of pure SM processes, we have ignored the possibility of the so-called "second-class currents" which, as pointed out in a theorem of Ref. [136], should not exist in the SM due to violation of various symmetry properties. Of course, the nucleons themselves are composite objects and thus do not exactly admit totally localized interactions; the above are only expressly valid in the limit of point-like fermions. In the context of an effective field theory of low-energy QCD in terms of nucleons, we may partially prescribe the non-point-like nature of the nucleon by an implicit dependence of the $\{F_1, F_2, F_A, F_P\}$ couplings on the 4-momentum transfer, that is to say,

$$F_i \to F_i\big(q^2\big) \quad . \tag{3.49}$$

These are the "one-nucleon form factors" and they must be determined from fits to experiment or from LQCD simulations. In such calculations of electroweak processes in nuclei, the need for the one-nucleon form factors represents a source of phenomenology (at a deeper level, an uncontrolled theoretical uncertainty) which we would one day like to eliminate!

With the one-nucleon amplitudes in hand, we may now proceed to the next step of our program which is to rigorously evaluate the amplitudes of the vector and axial-vector currents between many-nucleon (nuclear) hadronic states. Of particular relevance here is the discussion in the prior Sec. 3.2 on the connection between QFT states and the corresponding NRQFT states in the non-relativistic limit; the main result in Remark 3.2.1 will be utilized in the following. We will now present a fully-worked-out example of the non-relativistic reduction for the Coulomb multipole of an underlying vector current operator. This will illustrate the procedure of how to arrive at one-nucleon amplitudes for an arbitrary current operator which may be directly utilized in nuclear many-body methods. The remaining multipoles may be typed up in a future version of these notes but for the time being will be left as an exercise to the motivated reader.

### The Coulomb Multipole of a Vector Current

We begin by taking the one-nucleon amplitude of the Coulomb multipole as it appears in Eq. (3.16) between non-relativistic external hadronic (NRQFT) states $\Psi_i$ and $\Psi_f$ which obey the properties discussed in the prior section.

The amplitude with the Coulomb multiople of a vector current operator is then

$$\begin{aligned}\left\langle \Psi_f \right| \bar{M}_{JM}\big(q_0,\vec{q}\big) \left|\Psi_i\right\rangle &= \left\langle \Psi_f \right| \int d^3x\ M_{JM}\big(z,\hat{x}\big)\ V_0\big(q_0,\vec{x}\,\big) \left|\Psi_i\right\rangle \\ &= \int d^3x_f d^3x_i \frac{d^3p_f}{(2\pi)^3}\frac{d^3p_i}{(2\pi)^3}\ \Big[e^{i\vec{p}_f\cdot\vec{x}_f}\ \Psi_f(x_f)\Big]\Big[e^{-i\vec{p}_i\cdot\vec{x}_i}\ \Psi_i(x_i)\Big] \\ &\quad \times m\ \big\langle\ \varphi_f\,;\,\vec{p}_f\ \big|\int d^3x\ M_{JM}\big(z,\hat{x}\big)\ V_0\big(q_0,\vec{x}\,\big)\,\big|\,\varphi_i\,;\,\vec{p}_i\ \big\rangle \quad ,\end{aligned} \tag{3.50}$$

where, in arriving at the last line, we have used the result of Remark 3.2.1. Note that in the above we have suppressed spin indices for brevity, however, the external hadronic states must carry spin-isospin indices. For the nucleonic states we have taken $m_i = m_f = m$. It is then straightforward to show, after shifting the current operator in the hadronic amplitude to the origin, that the non-relativistic reduction to $\mathcal{O}(|\vec{p}|/m)$ with external QFT plane-wave states gives

$$\big\langle\ \varphi_f\,;\,\vec{p}_f\ \big|\,V_0\big(q_0,\vec{0}\,\big)\,\big|\,\varphi_i\,;\,\vec{p}_i\ \big\rangle \approx 2mF_1\chi_{s_i} + \mathcal{O}(1/m) \quad . \tag{3.51}$$

This leads us to the following, literal expression which we utilize in our codes

$$\left\langle \Psi_f \right| \bar{M}_{JM}\big(q_0,\vec{q}\big) \left|\Psi_i\right\rangle = \int d^3x\ \Psi_f^*(\vec{x})\,\chi_{s_f}^\dagger \Big[\,M_{JM}\big(z,\hat{x}\big)F_1(q^2)\Big]\,\Psi_i(\vec{x})\,\chi_{s_i} \quad ,$$

We have provided the above, very simple example merely to show procedurally how one arrives from the very beginnings of the multiople expansion to a current operator amplitude suitable for use in non-relativistic, nuclear many-body theory. Derivation of the other multipoles is quite a bit more involved and, eventually, a basis of form factor independent electroweak operators may be formed; the decomposition and maneuvering of these multipoles into suitable amplitudes for use in nuclear theory has been accomplished in literature quite some time ago [125, 126].

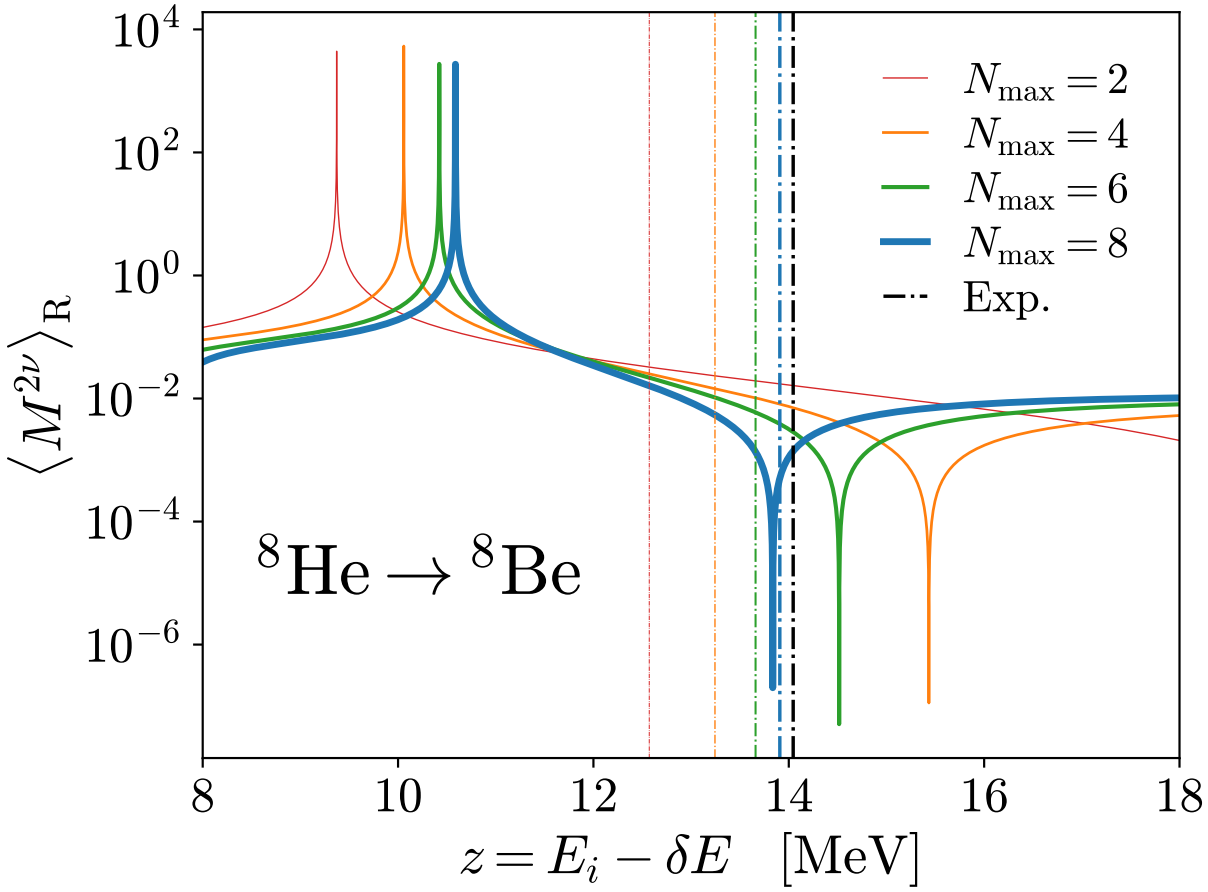


Figure 3.2: A series of NCSM calculations from $N_{\max} = 2 - 8$ of the $|M^{2\nu}|$ amplitudes as a function of the energy displacement $\delta E$ for the $^8$He $\rightarrow$ $^8$Be transition. The dashdot vertical lines correspond to the NCSM prediction of the $Q$ value (in colour) and the experimental $Q$ value (black) of the transition. Spikes in the distribution correspond to the poles in the Green function from bound states in the NCSM.

## 3.4 Benchmark Amplitudes for Two-Neutrino Double Beta Decay

As briefly discussed in the introduction, neutrinoless double-beta decay, usually dentoed $0\nu\beta\beta$ is a hypothesized lepton-number violating process in which a nucleus emits two electrons without accompanying neutrinos. Observation of this decay would confirm that neutrinos are Majorana plus Dirac particles identical to their own anti-particles and offer critical insight into the origin of neutrino mass and the matter-antimatter asymmetry of the universe. Global efforts have set increasingly stringent lower bounds on the $0\nu\beta\beta$ half-life, currently around $10^{26}$ years. However, interpreting these bounds in terms of fundamental neutrino properties requires precise knowledge of the nuclear structure amplitudes which relate the decay lifetime to the effective Majorana neutrino mass. Unfortunately, such amplitudes are not directly observable and theoretical predictions vary significantly, often by factors of three to five, depending on the many-body framework employed. Recent developments in $\chi$EFT have further complicated the picture by showing that the standard long-range $0\nu\beta\beta$ decay operator must be supplemented by a zero-range (contact) operator of unknown strength. Active research is underway to determine this contact term from quantum chromodynamics (QCD) and to quantify its impact.

In an effort to address these uncertainties, in Ref. [20], the authors employ coupled-cluster (CC) theory and $\chi$EFT interactions to perform *ab initio* calculations of the $0\nu\beta\beta$ decay matrix element in $^{48}$Ca. Among all $0\nu\beta\beta$-decay candidate isotopes, $^{48}$Ca is attractive due to its (relatively) simple structure, which helps to facilitate precision calculations of electroweak properties. While the primary goal of the study is to deliver amplitudes for $0\nu\beta\beta$, a

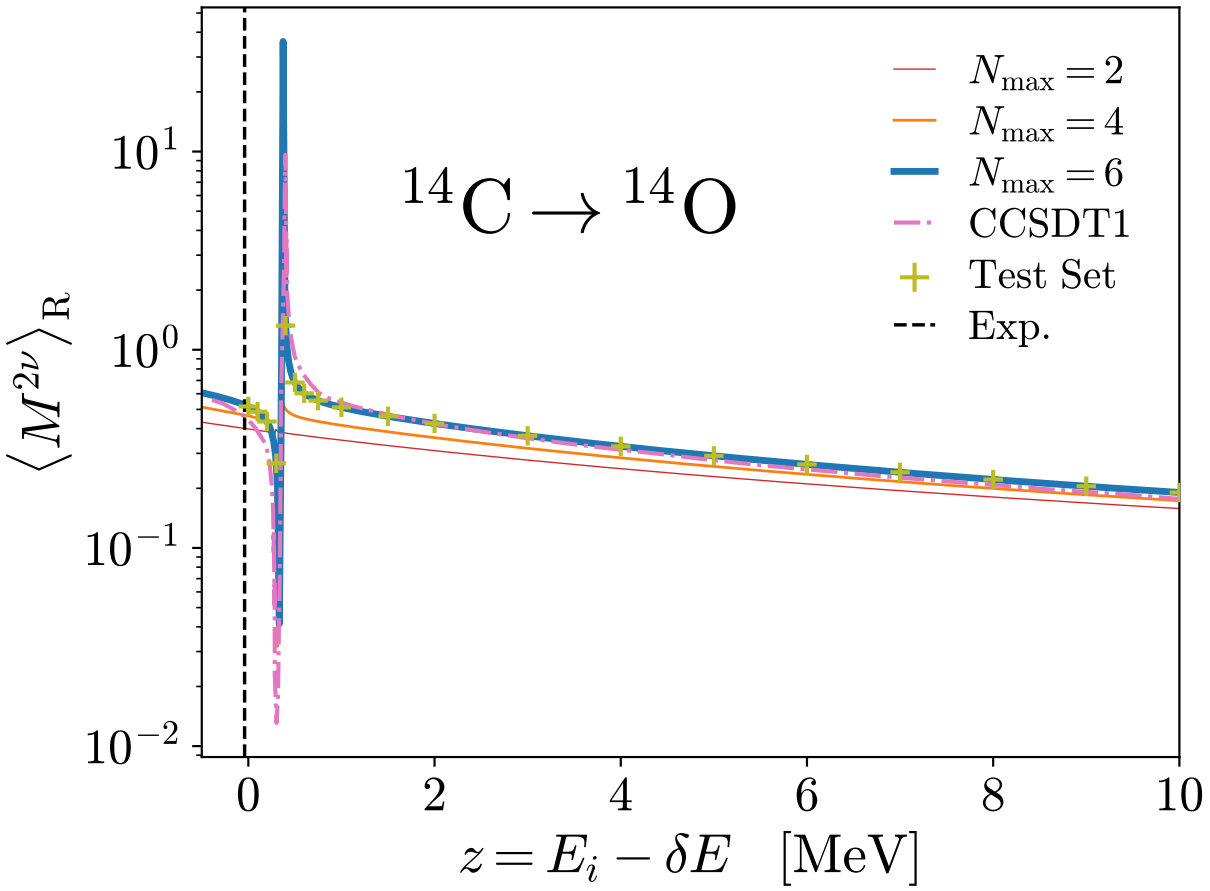


Figure 3.3: A series of NCSM calculations from $N_{\max} = 2 - 6$ of the $|M^{2\nu}|$ amplitudes as a function of the energy displacement $\delta E$ for the $^{14}\mathrm{C} \rightarrow {}^{14}\mathrm{O}$ transition. The dashdot vertical lines correspond to the NCSM prediction of the $Q$ value (in colour) and the experimental $Q$ value (black) of the transition. Spikes in the distribution correspond to the poles in the Green function from bound states in the NCSM. CC results for this transition are as taken from Ref. [20] and are shown in magenta, while a test set of prior NCSM results are shown in gold cross-hairs.

substantial effort was made to analyze two-neutrino double-beta decay ($2\nu\beta\beta$) in unphysical systems accessible to a several many-body methods – though importantly the quasi-exact NCSM – to validate the quality of the CC calculations.

We replicate the benchmarking performed in the original study here as a test of the new framework that has been implemented, and perform some novel benchmarks with the VS-IMSRG approach in the interest of further benchmarking; these results to this day remain unpublished. The relevant amplitude is given by

$$M^{2\nu} = \sum\!\!\!\!\!\!\int_n \frac{\langle \Psi_f | \, \sigma\tau^- \, | \Psi_n \rangle \langle \Psi_n | \, \sigma\tau^- \, | \Psi_i \rangle}{[E_i - E_n] - \delta E} \tag{3.52}$$

where $\sigma\tau^-$ is the Gamow-Teller operator and the denominator of the Green function is parameterized in terms of $\delta E$. We note that the Gamow-Teller operator is the long-wavelength approximation of the axial transverse electric multipole which we have derived the general form for in the prior sections. The relation between the two in the

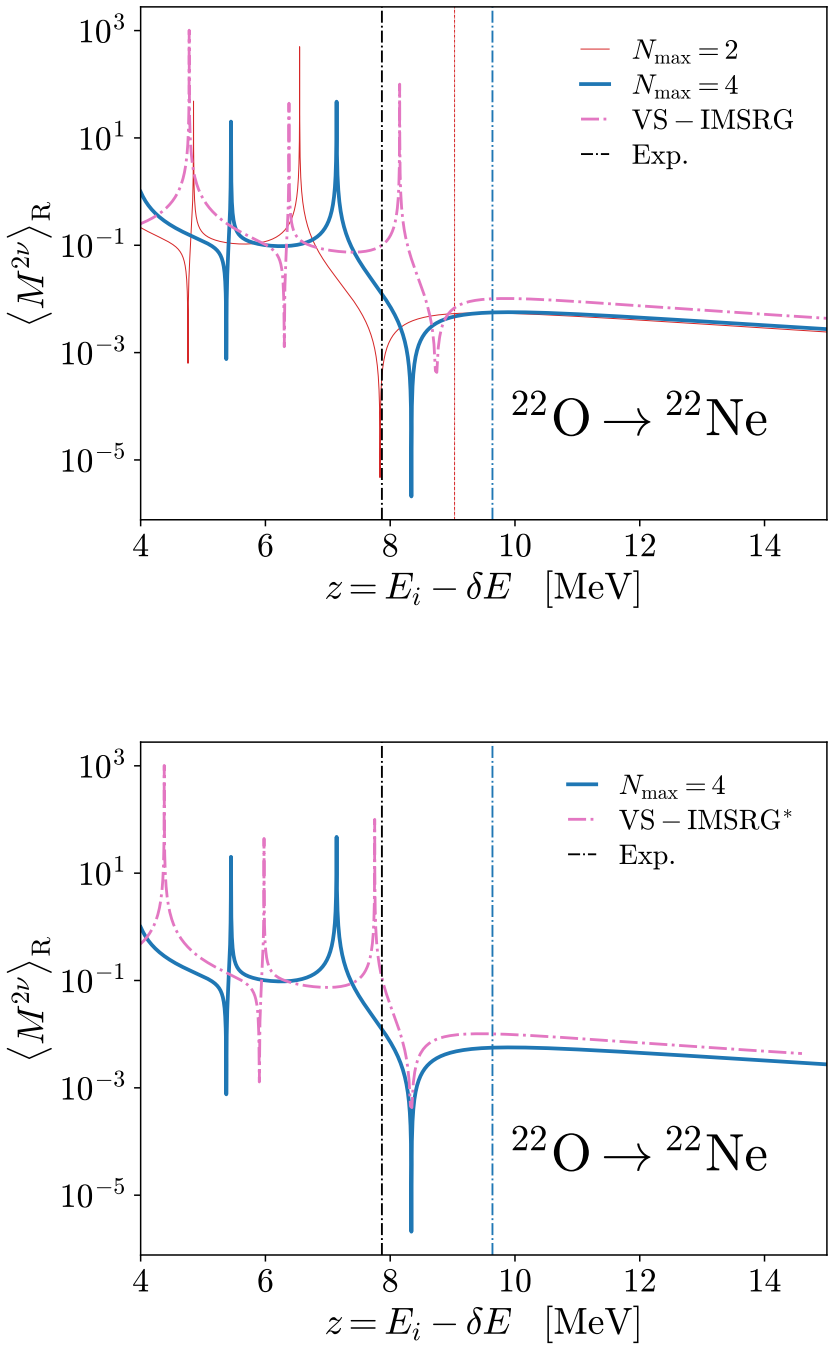


Figure 3.4: A series of NCSM calculations from $N_{\max} = 2 - 4$ of the $|M^{2\nu}|$ amplitudes as a function of the energy displacement $\delta E$ for the $^{22}\mathrm{O} \rightarrow {}^{22}\mathrm{Ne}$ transition. The dashdot vertical lines correspond to the NCSM prediction of the $Q$ value (in colour) and the experimental $Q$ value (black) of the transition. Spikes in the distribution correspond to the poles in the Green function from bound states in the NCSM. In the upper figure, the raw comparison between the NCSM and VS-IMSRG results is shown while in the lower figure the VS-IMSRG results have been shifted by 0.5 MeV to better illustrate the structural similarity of the two results.

limit of $|\vec{q}| \to 0$ gives, in terms of the multipole moment,

$$M^{2\nu} = \frac{6\pi}{g_A^2} \sum\!\!\!\!\!\!\int_n \frac{\langle \Psi_f | T^{5,el}(|\vec{q}|) | \Psi_n \rangle \langle \Psi_n | T^{5,el}(|\vec{q}|) | \Psi_i \rangle}{[E_i - E_n] - \delta E} \quad , \tag{3.53}$$

which is precisely the amplitude we compute to test this new framework in comparison with the old benchmarks. We mention here that all calculations have been performed using the "so-called" magic interaction for a chiral Hamiltonian. As we are not discussing the physical implications of these results, I will not say more regarding the interaction – also because I am not much of a fan.

In the following figures, the appearance of a black dashed line indicates the experimental $Q$ value of the transition. We first refer to Fig. 3.2 in which a series of $N_{\max}$ calculations of the resolvent amplitudes for the $^8$He $\to$ $^8$Be unphysical $2\nu\beta\beta$ transition have been performed. While we cannot say much of physical interest here, we note the consistency of the calculations of the spectrum even from relatively small $N_{\max}$ configuration space sizes. Unfortunately we did not have time to make a comparison to the CC results for this system. We then refer to Fig. 3.3 which contains the $M^{2\nu}$ results from the original benchmarking performed between the CC and NCSM groups in the $^{14}$C $\to$ $^{14}$O transition. In the gold cross-hairs are the original NCSM results, which we see that the new method reproduces exactly for the same-size configuration space calculation at $N_{\max} = 6$. As was seen in the original CC work, the agreement between the two approaches is excellent in across the entire energy range studied. It further seems that the $N_{\max}$ convergence is well under control in the NCSM. We lastly refer to the two subfigures in Fig. 3.4. The top figure shows a raw comparison between the NCSM and VS-IMSRG results with the VS-IMSRG taken in a much larger configuration space than is possible for the NCSM at this particle number. Nevertheless, we observe a very reasonable agreement between the two approaches which is even more telling in the lower subfigure. In this figure, we have shifted the VS-IMSRG result by approximately 0.5 MeV, which gives a much better picture of the structural similarity of the predictions. We naturally expect not to reproduce the exact same energies, particularly with the small NCSM calculation in such a large system, however the observed similarity in the results is certainly comforting.

These comparisons are by no means comprehensive, however, I wanted to include them in my dissertation as they were part of the earliest work on this project and involved the first few major modifications to the relevant code which has now been completely overhauled. More comprehensive benchmarking has been performed of this framework, with a variety of different tests, and I will discuss several later in evaluation of the radiative corrections in nuclear systems.

# Chapter 4

# Electroweak Radiative Corrections in Nuclear Beta Decay

Before discussing the nuclear structure correction of interest, labelled by the $\gamma W$ box and $\delta_{\rm NS}$ quantities, we first introduce some very basic formalism for the theory of beta decay and the corresponding one-loop radiative corrections. We will assume isospin symmetry in the following relativistic derivation, but it should be made clear that the physical isospin breaking effects are included on the nuclear structure side of the calculation. This is generally well-justified as Fermi transitions occur between nearly degenerate isospin analog states. While the discussion below is tailored towards nuclear beta decays, the same discussion is more or less identical for free neutron decay, and can be readily generalized to a discussion on arbitrary electroweak radiative corrections in nuclei.

### A Comment on the Hamiltonians Utilized in Calculation

Before beginning our discussion on electroweak radiative corrections, we emphasize to the reader that all numerical results for nuclei presented in this section are obtained with $\chi$EFT interactions. We employ two different interactions which are consistent at the two-body level but differ at the three-body level. At the two-body level, we use the Entem-Machleidt-Nosyk next-to-next-to-next-to-next-to-leading order ($\mathrm{N^4LO}$) interaction [137], labelled as $\mathrm{NN{-}N^4LO(500)}$. At the three-body level we apply (a) the $\mathrm{3N_{lnl}}$ interaction [138], and (b) the $\mathrm{3N^*_{lnl}}$ interaction [139, 131, 26]. The latter contains an additional sub-leading contact interaction (the so-called $E_7$ term) which enhances the strength of the spin-orbit coupling in three-body systems [140].

Beyond the use of the raw interactions as derived in $\chi$EFT, to accelerate the convergence of many-body properties with respect to the size of the many-body configuration space, the chiral interactions are further softened at short-distance scales via Similarity Renormalization Group (SRG) [141]. Presently, we use the evolution parameters of $\lambda_{\rm SRG} = 1.8$ fm$^{-1}$ and $\lambda_{\rm SRG} = 2.0$ fm$^{-1}$ for the $\mathrm{NN{-}N^4LO(500){+}3N_{lnl}}$ and $\mathrm{NN{-}N^4LO(500){+}3N^*_{lnl}}$ interactions, respectively. To gauge convergence of the numerical calculations, model spaces of up to $N_{\rm max} = 7$ with oscillator frequencies in the range of $\hbar\Omega = 16{-}20$ MeV have been applied. In addition, all integration results are presented with any infinitesimal-like parameters of the calculation, e.g., complex offsets in the denominator of propagator amplitudes, taken to the minimum possible value while ensuring numerical stability. This is usually of order $\sim 10^{-12}$.

## 4.1 A High-Level Introduction

For clarity, we begin by re-stating the definition of the electromagnetic and charged-weak currents as utilized in the following work. Respectively, these are

$$J^{\mu}_{\rm em} = \frac{2}{3}\bar{u}\gamma^{\mu}u - \frac{1}{3}\bar{d}\gamma^{\mu}d \qquad\qquad J^{\dagger\,\mu}_{\rm W} = \bar{d}\gamma^{\mu}\big(1-\gamma_5\big)u \quad . \tag{4.1}$$

In the EFT picture of the nucleus as composite of protons and neutrons, the nuclear beta decays we are interested in may be simply written as

$$\Phi_i(p_i) + e^+(p_e) \longrightarrow \Phi_f(p_f) + \nu_e(p_\nu) \quad ,$$

which has a corresponding tree-level amplitude

$$M_{\rm tree}\big(p_f,p_i,k_f,k_i\big) = -\frac{G_F}{\sqrt{2}}\; L_\lambda(k_f,k_i)\; \big\langle\, \Psi_f\,;\,\vec{p}_f \,\big|\, J^{\dagger\,\lambda}_{\rm W}(q) \,\big|\, \Psi_i\,;\,\vec{p}_i\,\big\rangle \quad , \tag{4.2}$$

where $L_\lambda$ is the leptonic current

$$L^{\lambda} = \bar{u}_e\,\gamma^{\lambda}\,(1-\gamma_5)\,v_\nu \quad . \tag{4.3}$$

In the special case of exact isospin symmetry and spinless external states (quasi-exact for Fermi transitions in nuclei), the hadronic matrix element can be decomposed into two form factors

$$F^{\lambda}(p_f,p_i) = \big\langle \Psi_f(p_f)\big|\, J^{\lambda}_{\rm W}(0)\,\big|\Psi_i(p_i)\big\rangle = f_+\Big(\,[p-p']^2\,\Big)\,(p+p')^{\lambda} + f_-\Big(\,[p-p']^2\,\Big)\,(p-p')^{\lambda} \quad , \tag{4.4}$$

which are normalized such that $f_+(0) = \sqrt{2}$ and $f_-(0) = 0$ in isospin $T = 1$ systems. As we have heavily emphasized in the introduction, at the level of $10^{-4}$ precision sought after in modern tests of CKM unitarity, the tree-level amplitude is not sufficient and electroweak radiative corrections from the SM must be explicitly included in extraction of $V_{ud}$. A general framework for the analysis of radiative corrections from electroweak theories was developed some time ago by Sirlin [142] which forms the basis for the analysis performed in the current study. Applying Sirlin's representation to study the one-loop radiative corrections to hadronic decays yields a number of additional diagrammatic processes which must be considered, almost all of which which go beyond the scope of this document. The analysis of radiative corrections in the context of superallowed Fermi decays is most clearly presented in the more recent review of Ref. [143].

Ultimately, the master formulae for obtaining $V_{ud}$ from a given transition is

$$|V_{ud}|^2 = \frac{\hbar^7}{G_F^2 m_e^5 c^4}\;\frac{\pi^3 \ln(2)}{\mathcal{F}t(1+\Delta^V_R)} \qquad\qquad \mathcal{F}t = ft(1+\delta'_R)(1-\delta_C+\delta_{NS}) \quad , \tag{4.5}$$

where $G_F$ is the Fermi constant and the $\mathcal{F}t$ value contains all (corrected) nuclear structure information related to a given transition; $f$ is a statistical phase-space factor and $t$ corresponds to the half-life of the transition. There are four theoretical corrections entering in the above expressions, mostly electroweak radiative corrections, which we now outline.

*(I) The Inner Radiative Correction* – The first correction $\Delta^V_R$ is the "inner radiative correction" and is universal to all Fermi transitions. It comprises many radiative effects, the most challenging of which to compute is hadronic-structure-dependent $\gamma W$ box contribution; all other corrections at loop level can be factorized to be independent of the structure of the hadron. The $\gamma W$ box dominates the uncertainty of $\Delta^V_R$ and is the piece for which theoretical errors were greatly improved in the last seven years [13, 14, 144, 145, 146].

*(II) The Outer Radiative Correction* – The second correction $\delta'_R$ is the "outer radiative correction", the long-range counterpart to $\Delta^V_R$, which accounts for QED effects in the infrared limit, e.g., bremmsstrahlung photon emission, as well as Coulomb distortion of the electron wave function. It is understood quite well relative to the other corrections and calculable to order $Z\alpha^3$ in QED [147, 148, 149, 150, 151], though recent analyses call partially into question results some results from these historial works [152, 153, 154].

*(III) The Electroweak Radiative Nuclear Structure Correction* – The third correction $\delta_{\rm NS}$ corresponds to the modification of the one-nucleon axial $\gamma W$ box diagram, as described above for the "inner radiative correction", due to

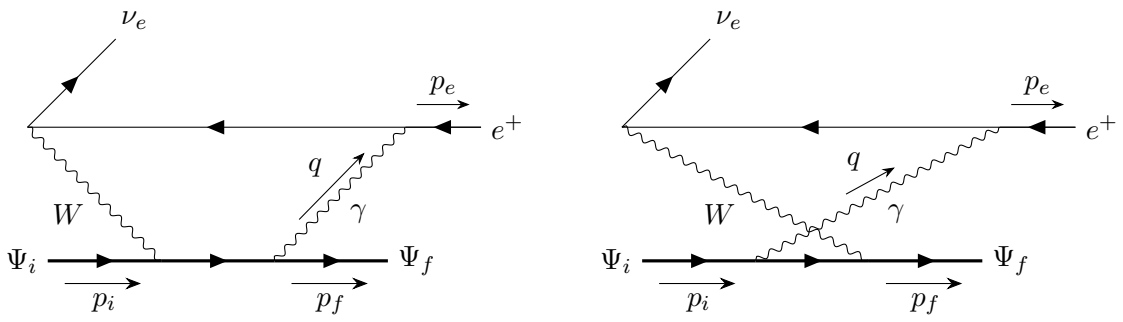


Figure 4.1: The nuclear $\gamma W$ box diagrams.

effects from the nuclear medium. It parameterizes the difference between the $\gamma W$ box evaluated on a free nucleon and on a nucleus and is thus not independent of $\Delta_R^V$. This correction is the focus of our work and will be given a brief introduction below.

*(IV) The Isospin Symmetry Breaking Correction* – The fourth correction $\delta_{\rm C}$ is known as the isospin symmetry breaking correction which parameterizes the renormalization of the Fermi matrix element due to isospin non-conserving interactions, i.e., the strong and Coulomb interactions.

For our discussion, the most important correction is the $\gamma W$ box contribution, shown in Fig. 4.1, which gives rise to both $\Delta_R^V$ and $\delta_{\rm NS}$. This correction is the only one at the one-loop level which truly probes the structure of the external hadronic states in a non-perturbative way and, naturally, it dominates the radiative correction uncertainty to Fermi decays [155]. Despite both $\delta_{\rm NS}$ (being the most ill-determined) and $\delta_{\rm C}$ having been approached with nuclear models in the past, by applying the current state-of-the-art approaches in *ab initio* nuclear theory there is much room for improvement. Historically speaking, the only model successfully producing a quasi-alignment of the nucleus-independent $\mathcal{F}t$ values across the chart involved shell-model type calculations with Woods-Saxon potentials, see Ref. [7] for the latest review and references therein. Other varied approaches in literature have not been able to produce the same agreement obtained by the Hardy and Towner works, for example, Refs. [156, 157]. Notwithstanding early efforts on the front of $\delta_{\rm C}$ [158, 159], in the last two decades the *ab initio* nuclear theory community has not pushed to reduce the theoretical uncertainties [10] despite extensive criticism of the current estimates [160, 161, 162], though it is not clear how well-founded are such criticisms. This is the perfect working ground for an *ab initio* nuclear theory!

While there are many terms contributing to the $\gamma W$ box in Section 3 of Ref. [155], the discussion concludes by identifying the following piece as the dominant contribution,

$$\delta\mathcal{M}^b_{\gamma W} = -i\frac{e^2}{\sqrt{2}}G_F\,L_\lambda \int \frac{d^4q}{(2\pi)^4}\,\frac{M_W^2}{M_W^2-q^2}\,\frac{1}{q^2+i\epsilon_1}\,\frac{\epsilon^{\mu\nu\alpha\lambda}\,q_\alpha}{(p_e-q)^2-m_e^2+i\epsilon}\,T_{\mu\nu}(p_f,p_i,q) \quad , \tag{4.6}$$

where the generalized Compton scattering amplitude reads

$$T^{\mu\nu}\big(p_i,p_f,q\big) = \frac{1}{2}\int d^4x\; e^{iq\cdot x}\,\big\langle\,\Psi_f\,;\,\vec{p}_f\,\big|\,T\big[J^\mu_{\rm em}\big(t,\vec{x}\big)\,J^{\dagger\,\nu}_{\rm W}\big(0,\vec{0}_x\big)\big]\,\big|\,\Psi_i\,;\,\vec{p}_i\,\big\rangle \quad . \tag{4.7}$$

This contains all the hadronic structure information and is hence our central object of interest. The following section will be dedicated to the decomposition of this object into quantities we may work readily with in *ab initio* nuclear theory.

As discussed in Ref. [155], the general decomposition for the $\gamma W$ box radiative correction is given by

$$\mathcal{M}_{\gamma W} = \mathcal{M}^a_{\gamma W} + \mathcal{M}^b_{\gamma W} \quad , \tag{4.8}$$

however, in the forward limit and for exact isospin symmetry, the $\mathcal{M}^a_{\gamma W}$ contribution may be partially cancelled with other radiative corrections, which results in a negligible contribution to the Fermi amplitude. We can then focus solely on $\delta\mathcal{M}^b_{\gamma W}$, which by linearity may further be decomposed into vector and axial pieces as

$$\mathcal{M}^b_{\gamma W} = \mathcal{M}^{b,V}_{\gamma W} + \mathcal{M}^{b,A}_{\gamma W} \quad , \tag{4.9}$$

for which the velocity-dependent vector piece again vanishes in the forward limit and for exact isospin symmetry since the tensor $T^{\mu\nu}$ is symmetric in the Lorentz indices. Under this set of approximations,

$$\mathcal{M}_{\gamma W}^{b,A} \approx \Box_{\gamma W}^{b}\, \mathcal{M}_0 \quad , \tag{4.10}$$

where $\mathcal{M}_0$ is the tree-level amplitude and $\Box_{\gamma W}^{b}$ is the $\gamma W$ box function. The precision determination of this function in nuclei is the ultimate goal of our efforts.

To reiterate, it is the improved determination of the $\gamma W$ box diagram for free-neutron decays which reduced the uncertainty in $\Delta_R^V$ by a factor of 2, leading to the current CKM unitarity puzzle. Of course, we are interested in the nuclear-structure-dependent correction $\delta_{\rm NS}$, which may or may not augment this tension with the SM prediction of CKM unitarity. This correction is defined in the literature as the pure difference between the $\gamma W$ box when evaluated on a free nucleon and on a nucleus, i.e.,

$$\delta_{NS} = 2\big[\,\Box_{\gamma W}^{b,\rm nuc.} - \Box_{\gamma W}^{b,\rm n}\,\big] \quad , \tag{4.11}$$

where the subtraction is performed to not double count the $\gamma W$ box contribution already included in the $\mathcal{F}t$ value corrections via $\Delta_R^V$. Thus, we have a clear path forward. First, the determination of the Compton amplitude in *ab initio* nuclear theory followed by evaluation of the $\gamma W$ box function, which will be explicitly written down later. When properly combined with the result for free neutron decay [13], this will give us the nuclear-structure-dependent electroweak radiative correction to Fermi decays, $\delta_{\rm NS}$.

## 4.2 Decomposition of the Compton Tensor

Let us begin our analysis of the radiative corrections for beta decay with the hadronic object which makes its appearance in the axial box diagram, the Compton tensor of Eq. (4.7). Built from the time-ordered product of the electromagnetic and the weak current operators, it reads

$$T^{\mu\nu}(p_i,p_f,q) = \frac{1}{2}\int d^4x\; e^{iq\cdot x}\,\langle\,\Psi_f\,;\,\vec{p}_f\,|\,T\big[J^{\mu}_{\rm em}(t,\vec{x})\,J^{\dagger\,\nu}_{\rm W}(0,\vec{0}_x)\big]\,|\,\Psi_i\,;\,\vec{p}_i\,\rangle \quad ,$$

and we aim to find a non-relativistic limit for the amplitudes in terms of the momentum-space current operators. This is necessary in order to apply the well-known multipole expansion formalism for current operators derived in the previous chapter and utilzied for decades in nuclear theory. For internal consistency in these notes, in what follows all states and operators are taken to be in the Heisenberg picture.

We begin by making explicit the time-ordered product of the current operators and by resolution of identity with a complete set of plane-wave eigensolutions. We have

$$\begin{aligned}
&T^{\mu\nu}(p_i,p_f,q)\\
&\quad=\frac{1}{2}\int d^4x\; e^{iq\cdot x}\,\langle\,\Psi_f\,;\,\vec{p}_f\,|\,T\big[J^{\mu}_{\rm em}(t,\vec{x})\,J^{\dagger\,\nu}_{\rm W}(0,\vec{0}_x)\big]\,|\,\Psi_i\,;\,\vec{p}_i\,\rangle\\
&\quad=\frac{1}{2}\int d^3x\; e^{-i\vec{q}\cdot\vec{x}}\,\langle\,\Psi_f\,;\,\vec{p}_f\,|\left(\int_0^\infty dt\; e^{iq_0t}\,J^{\mu}_{\rm em}(t,\vec{x})\,J^{\dagger\,\nu}_{\rm W}(0,\vec{0}_x)+\int_{-\infty}^0 dt\; e^{iq_0t}J^{\dagger\,\nu}_{\rm W}(0,\vec{0}_x)\,J^{\mu}_{\rm em}(t,\vec{x})\right)|\,\Psi_i\,;\,\vec{p}_i\,\rangle\\
&\quad=\frac{1}{2}\int d^3x\; e^{-i\vec{q}\cdot\vec{x}}\left(\int_0^\infty dt\; e^{iq_0t}\,\langle\,\Psi_f\,;\,\vec{p}_f\,|J^{\mu}_{\rm em}(t,\vec{x})\Big[\sum_a|\,\psi_a\,;\,\vec{p}_a\,\rangle\langle\,\psi_a\,;\,\vec{p}_a\,|\Big]\,J^{\dagger\,\nu}_{\rm W}(0,\vec{0}_x)\,|\,\Psi_i\,;\,\vec{p}_i\,\rangle\right.\\
&\qquad\left.+\int_{-\infty}^0 dt\; e^{iq_0t}\langle\,\Psi_f\,;\,\vec{p}_f\,|\,J^{\dagger\,\nu}_{\rm W}(0,\vec{0}_x)\Big[\sum_b|\,\psi_b\,;\,\vec{p}_b\,\rangle\langle\,\psi_b\,;\,\vec{p}_b\,|\Big]J^{\mu}_{\rm em}(t,\vec{x})\,|\,\Psi_i\,;\,\vec{p}_i\,\rangle\right) \quad .
\end{aligned}$$

As we are working with Heisenberg picture operators, we may remove all space-time translations via action of the four-momentum operator. Explicitly, for a general current operator $O(x)$ we may write

$$O(t,\vec{x}) = e^{ix_\nu P^\nu}\,O(0,\vec{0}_x)\,e^{-ix_\sigma P^\sigma} = e^{itH}e^{i\vec{x}\cdot\vec{P}}\,O(0,\vec{0}_x)\,e^{-itH}e^{-i\vec{x}\cdot\vec{P}} \quad . \tag{4.12}$$

By construction, the plane-wave functions are eigensolutions of the four-momentum operator and, thus, simultaneous eigensolutions of the relativistic Hamiltonian operator $H = P_0$ and of the 3-momentum operator $\vec{P}$. Returning to our problem in particular, this decomposition of the current operators then allows us to isolate the time dependence of the currents and perform the $t = x_0$ integral analytically. Moreover, rearranging the order of the sums and integrals and maintaining the spatial dependence of the current operators for the time being, we have

$$\begin{aligned}
&T^{\mu\nu}(p_i,p_f,q)\\
&\quad=\frac{1}{2}\sum_a\int d^3x\; e^{-i\vec{q}\cdot\vec{x}}\int_0^\infty dt\; e^{iq_0t}\langle\,\Psi_f\,;\,\vec{p}_f\,|\,e^{itH}\,J^{\mu}_{\rm em}(0,\vec{x})\,e^{-itH}\,|\,\psi_a\,;\,\vec{p}_a\,\rangle\langle\,\psi_a\,;\,\vec{p}_a\,|\,J^{\dagger\,\nu}_{\rm W}(0,\vec{0}_x)\,|\,\Psi_i\,;\,\vec{p}_i\,\rangle\\
&\qquad+\frac{1}{2}\sum_b\int d^3x\; e^{-i\vec{q}\cdot\vec{x}}\int_{-\infty}^0 dt\; e^{iq_0t}\langle\,\Psi_f\,;\,\vec{p}_f\,|\,J^{\dagger\,\nu}_{\rm W}(0,\vec{0}_x)\,|\,\psi_b\,;\,\vec{p}_b\,\rangle\langle\,\psi_b\,;\,\vec{p}_b\,|\,e^{itH}\,J^{\mu}_{\rm em}(0,\vec{x})\,e^{-itH}\,|\,\Psi_i\,;\,\vec{p}_i\,\rangle\\
&\quad=\frac{1}{2}\sum_a\int d^3x\; e^{-i\vec{q}\cdot\vec{x}}\int_0^\infty dt\; e^{it(q_0+\omega_f-\omega_a)}\langle\,\Psi_f\,;\,\vec{p}_f\,|\,J^{\mu}_{\rm em}(0,\vec{x})\,|\,\psi_a\,;\,\vec{p}_a\,\rangle\langle\,\psi_a\,;\,\vec{p}_a\,|\,J^{\dagger\,\nu}_{\rm W}(0,\vec{0}_x)\,|\,\Psi_i\,;\,\vec{p}_i\,\rangle\\
&\qquad+\frac{1}{2}\sum_b\int d^3x\; e^{-i\vec{q}\cdot\vec{x}}\int_{-\infty}^0 dt\; e^{it(q_0-\omega_i+\omega_b)}\langle\,\Psi_f\,;\,\vec{p}_f\,|\,J^{\dagger\,\nu}_{\rm W}(0,\vec{0}_x)\,|\,\psi_b\,;\,\vec{p}_b\,\rangle\langle\,\psi_b\,;\,\vec{p}_b\,|\,J^{\mu}_{\rm em}(0,\vec{x})\,|\,\Psi_i\,;\,\vec{p}_i\,\rangle \quad .
\end{aligned}$$

Now, by inserting the appropriate Heaviside functions $\Theta(t)$ and $\Theta(-t)$ in their respective integrals, we can immediately associate each of the integrals to the Fourier transform of the corresponding Heaviside function. This has

an analytic form given by

$$\breve{\Theta}(s) = \mathcal{F}\big[\Theta\big](s) = \int_{-\infty}^{\infty} dt\; e^{-2\pi i t s}\,\Theta(t) = \frac{1}{2}\left(\delta(s) - \frac{i}{\pi}\text{p.v.}\left[\frac{1}{s}\right]\right) \quad , \tag{4.13}$$

where the definition of the principal value integral p.v. may be found in the appendix and the equality is to be understood in the sense of distributions. Following this defintion, for the first integral and second integrals we take

$$s_a = -\frac{1}{2\pi}(q_0 + \omega_f - \omega_a) \qquad\qquad s_b = \frac{1}{2\pi}(q_0 - \omega_i + \omega_b) \quad , \tag{4.14}$$

respectively, and we further substitute $t' = -t$ in the second integral. Turning the metaphorical crank with the above machinery yields

$$\begin{aligned}
&T^{\mu\nu}(p_i, p_f, q) \\
&= \frac{1}{2}\sum\!\!\!\!\!\!\int_a d^3x\; e^{-i\vec{q}\cdot\vec{x}} \big\langle\, \Psi_f\,;\,\vec{p}_f \,\big|\, J^{\mu}_{\text{em}}\big(0,\vec{x}\,\big) \,\big|\, \psi_a\,;\,\vec{p}_a\,\big\rangle\big\langle\, \psi_a\,;\,\vec{p}_a \,\big|\, J^{\dagger\,\nu}_{\text{W}}\big(0,\vec{0}_x\big)\big|\, \Psi_i\,;\,\vec{p}_i\,\big\rangle \int_{-\infty}^{\infty} dt\; e^{-2\pi i t s_a}\,\Theta(t) \\
&\quad + \frac{1}{2}\sum\!\!\!\!\!\!\int_b d^3x\; e^{-i\vec{q}\cdot\vec{x}} \big\langle\, \Psi_f\,;\,\vec{p}_f \,\big|\, J^{\dagger\,\nu}_{\text{W}}\big(0,\vec{0}_x\big) \,\big|\, \psi_b\,;\,\vec{p}_b\,\big\rangle\big\langle\, \psi_b\,;\,\vec{p}_b \,\big|\, J^{\mu}_{\text{em}}\big(0,\vec{x}\,\big)\,\big|\, \Psi_i\,;\,\vec{p}_i\,\big\rangle \int_{-\infty}^{\infty} dt'\; e^{-2\pi i t' s_b}\,\Theta(t') \\
&= \frac{1}{4}\sum\!\!\!\!\!\!\int_a d^3x\; e^{-i\vec{q}\cdot\vec{x}} \big\langle\, \Psi_f\,;\,\vec{p}_f \,\big|\, J^{\mu}_{\text{em}}\big(0,\vec{x}\,\big) \,\big|\, \psi_a\,;\,\vec{p}_a\,\big\rangle\big\langle\, \psi_a\,;\,\vec{p}_a \,\big|\, J^{\dagger\,\nu}_{\text{W}}\big(0,\vec{0}_x\big)\big|\, \Psi_i\,;\,\vec{p}_i\,\big\rangle \left(\delta(s_a) - \frac{i}{\pi}\text{p.v.}\left[\frac{1}{s_a}\right]\right) \\
&\quad + \frac{1}{4}\sum\!\!\!\!\!\!\int_b d^3x\; e^{-i\vec{q}\cdot\vec{x}} \big\langle\, \Psi_f\,;\,\vec{p}_f \,\big|\, J^{\dagger\,\nu}_{\text{W}}\big(0,\vec{0}_x\big) \,\big|\, \psi_b\,;\,\vec{p}_b\,\big\rangle\big\langle\, \psi_b\,;\,\vec{p}_b \,\big|\, J^{\mu}_{\text{em}}\big(0,\vec{x}\,\big)\,\big|\, \Psi_i\,;\,\vec{p}_i\,\big\rangle \left(\delta(s_b) - \frac{i}{\pi}\text{p.v.}\left[\frac{1}{s_b}\right]\right) \quad ,
\end{aligned}$$

where again the equality is to be understood in the distributional sense, i.e., it depends on the function against which $T^{\mu\nu}$ is integrated. So long as we are integrating against a *good test function* of the four-momentum transfer $q$, we can treat the delta function and principal value integrals as well-defined(-enough-for-this-dissertation) objects. We may then make use of the Sokhotski-Plemelj theorem for continuous complex valued functions. Here, we quote the important result of the theorem on the real line for the convenience of the reader,

$$\frac{i}{\pi}\text{p.v.}\left[\frac{1}{x}\right] = \frac{i}{\pi}\lim_{\epsilon\to 0^+}\frac{1}{x \pm i\epsilon} \mp \delta(x) \quad . \tag{4.15}$$

Under the conditions that our integrals are well-enough behaved, we may then write the previous expression for the Compton tensor as

$$\begin{aligned}
&T^{\mu\nu}(p_i, p_f, q) \\
&= \frac{1}{4}\sum\!\!\!\!\!\!\int_a d^3x\; e^{-i\vec{q}\cdot\vec{x}} \,\big\langle\, \Psi_f\,;\,\vec{p}_f \,\big|\, J^{\mu}_{\text{em}}\big(0,\vec{x}\,\big) \,\big|\, \psi_a\,;\,\vec{p}_a\,\big\rangle\big\langle\, \psi_a\,;\,\vec{p}_a \,\big|\, J^{\dagger\,\nu}_{\text{W}}\big(0,\vec{0}_x\big)\big|\, \Psi_i\,;\,\vec{p}_i\,\big\rangle \left(-\frac{i}{\pi}\lim_{\epsilon\to 0^+}\frac{1}{s_a - i\epsilon}\right) \\
&\quad + \frac{1}{4}\sum\!\!\!\!\!\!\int_b d^3x\; e^{-i\vec{q}\cdot\vec{x}} \,\big\langle\, \Psi_f\,;\,\vec{p}_f \,\big|\, J^{\dagger\,\nu}_{\text{W}}\big(0,\vec{0}_x\big) \,\big|\, \psi_b\,;\,\vec{p}_b\,\big\rangle\big\langle\, \psi_b\,;\,\vec{p}_b \,\big|\, J^{\mu}_{\text{em}}\big(0,\vec{x}\,\big)\,\big|\, \Psi_i\,;\,\vec{p}_i\,\big\rangle \left(-\frac{i}{\pi}\lim_{\epsilon\to 0^+}\frac{1}{s_b - i\epsilon}\right) \\
&= \frac{1}{2}\sum\!\!\!\!\!\!\int_a d^3x\; e^{-i\vec{q}\cdot\vec{x}} \lim_{\epsilon\to 0^+} \frac{\big\langle\, \Psi_f\,;\,\vec{p}_f \,\big|\, J^{\mu}_{\text{em}}\big(0,\vec{x}\,\big) \,\big|\, \psi_a\,;\,\vec{p}_a\,\big\rangle\big\langle\, \psi_a\,;\,\vec{p}_a \,\big|\, J^{\dagger\,\nu}_{\text{W}}\big(0,\vec{0}_x\big)\big|\, \Psi_i\,;\,\vec{p}_i\,\big\rangle}{\big[q_0 + \omega_f + i\epsilon\big] - \omega_a} \\
&\quad + \frac{1}{2}\sum\!\!\!\!\!\!\int_b d^3x\; e^{-i\vec{q}\cdot\vec{x}} \lim_{\epsilon\to 0^+} \frac{\big\langle\, \Psi_f\,;\,\vec{p}_f \,\big|\, J^{\dagger\,\nu}_{\text{W}}\big(0,\vec{0}_x\big) \,\big|\, \psi_b\,;\,\vec{p}_b\,\big\rangle\big\langle\, \psi_b\,;\,\vec{p}_b \,\big|\, J^{\mu}_{\text{em}}\big(0,\vec{x}\,\big)\,\big|\, \Psi_i\,;\,\vec{p}_i\,\big\rangle}{\big[-q_0 + \omega_i + i\epsilon\big] - \omega_b} \quad .
\end{aligned}$$

The expression for the Compton tensor is now written entirely in terms of the nuclear propagator, i.e., in this setting the Green function of the many-body system, expanded in the plane-wave basis of the intermediate nuclear configuration. For clarity, we note that, in the remainder of this section, we will neglect to use the limit notation and emphasize to the reader that it is implicit wherever an $i\varepsilon$ appears in a given expression.

The above expression for the Compton tensor amplitudes most certainly has poles in the propagator amplitudes which arise from singularities in the Green function. In particular, these poles exist in the integration domain of the $q_0$ component of the four-momentum transfer and are dependent on the spectrum of the intermediate nuclear configuration. We may decompose the set of poles for the Compton tensor into two sets of poles, each corresponding to one set of amplitudes in the Compton tensor expression. We may write these sets as

$$\mathcal{P}_- = \Big\{ q_0 \in \mathbb{C} \ : \ q_0 = \omega_a - \omega_f - i\epsilon \Big\} \qquad \mathcal{P}_+ = \Big\{ q_0 \in \mathbb{C} \ : \ q_0 = \omega_i - \omega_b + i\epsilon \Big\} \quad , \tag{4.16}$$

where the sign subscript indicates the sign of the imaginary part of the pole. At first glance this may seem troublesome as these sets are infinite, however, with a simple contour deformation it is possible to show that the Compton tensor amplitudes are perfectly well-enough-behaved functions of the four-momentum energy transfer $q_0$ up to the production of residue contributions. This will be discussed in finer detail in Sec. 4.3.3. For now, we return to casting the expression into a more amenable form.

Now that we have neatly tucked away the 4-momentum energy transfer dependence into the nuclear propagator, we may now turn our attention to the remaining spatial dependence of the current operators. We would like to introduce the same type of spatial dependence that we have in $J^\mu_{\text{em}}(0,\vec{x}\,)$ into $J^{\dagger\,\nu}_{\text{W}}(0,\vec{0})$. The purpose of this is to eventually allow for a consistent Fourier transformation of the nuclear current operators into momentum space, which then allows us to exploit the multipole expansion formalism. Moreover, we can immediately Fourier transform the spatial part of $J^\mu_{\text{em}}(0,\vec{x}\,)$. Yet, in order to get $J^{\dagger\,\nu}_{\text{W}}(0,\vec{0})$ into momentum space requires a bit more work. We first remind the reader of the definition of the Fourier and inverse Fourier transforms given in Eq. (3.6),

$$J^\mu(0,\vec{q}\,) = \int d^3x \ e^{-i\vec{q}\cdot\vec{x}} J^\mu(0,\vec{x}\,) \qquad J^\mu(0,\vec{x}\,) = \int \frac{d^3q}{(2\pi)^3} \ e^{i\vec{q}\cdot\vec{x}} J^\mu(0,\vec{q}\,) \quad .$$

As before, we know that we may write the spatial dependence of the current operator as the action of unitary transformations with the *interacting* momentum operator $\vec{P}$. Since all nuclear states are plane wave states, they are eigenstates of the momentum operator at all times. Hence, we may write for an arbitrary current $J$ that

$$J^\mu(0,\vec{0}) = e^{-i\vec{y}\cdot\vec{P}} e^{i\vec{y}\cdot\vec{P}} J^\mu(0,\vec{0})\, e^{-i\vec{y}\cdot\vec{P}} e^{i\vec{y}\cdot\vec{P}} = e^{-i\vec{y}\cdot\vec{P}} J^\mu(0,\vec{y}\,)\, e^{i\vec{y}\cdot\vec{P}} \quad .$$

Expressing $J^{\dagger\,\nu}_{\text{W}}(0,\vec{0})$ using the above result, we then have

$$\begin{aligned} T^{\mu\nu}(p,q) = \frac{i}{2} \sum\!\!\!\!\!\!\int_a & \frac{\big\langle \Psi_f\,;\,\vec{p}_f\,\big|J^\mu_{\text{em}}(0,\vec{q}\,)\big|\,\psi_a\,;\,\vec{p}_a\,\big\rangle\big\langle\,\psi_a\,;\,\vec{p}_a\,\big|e^{-i\vec{y}\cdot\vec{P}} J^{\dagger\,\nu}_{\text{W}}(0,\vec{y}\,)\, e^{i\vec{y}\cdot\vec{P}}\big|\,\Psi_i\,;\,\vec{p}_i\,\big\rangle}{[q_0+\omega_f+i\epsilon]-\omega_a} \\ & + \frac{i}{2} \sum\!\!\!\!\!\!\int_b \frac{\big\langle \Psi_f\,;\,\vec{p}_f\,\big|e^{-i\vec{y}\cdot\vec{P}} J^{\dagger\,\nu}_{\text{W}}(0,\vec{y}\,)\, e^{i\vec{y}\cdot\vec{P}}\big|\,\psi_b\,;\,\vec{p}_b\,\big\rangle\big\langle\,\psi_b\,;\,\vec{p}_b\,\big|J^\mu_{\text{em}}(0,\vec{q}\,)\big|\,\Psi_i\,;\,\vec{p}_i\,\big\rangle}{[-q_0+\omega_i+i\epsilon]-\omega_b} \end{aligned} \tag{4.17}$$

$$= \frac{i}{2} \sum\!\!\!\!\!\!\int_a \ e^{i(\vec{p}_i-\vec{p}_a)\cdot\vec{y}} \ \frac{\big\langle \Psi_f\,;\,\vec{p}_f\,\big|J^\mu_{\text{em}}(0,\vec{q}\,)\big|\,\psi_a\,;\,\vec{p}_a\,\big\rangle\big\langle\,\psi_a\,;\,\vec{p}_a\,\big|J^{\dagger\,\nu}_{\text{W}}(0,\vec{y}\,)\big|\,\Psi_i\,;\,\vec{p}_i\,\big\rangle}{[q_0+\omega_f+i\epsilon]-\omega_a} \tag{4.18}$$

$$+ \frac{i}{2} \sum\!\!\!\!\!\!\int_b \ e^{i(\vec{p}_b-\vec{p}_f)\cdot\vec{y}} \ \frac{\big\langle \Psi_f\,;\,\vec{p}_f\,\big|J^{\dagger\,\nu}_{\text{W}}(0,\vec{y}\,)\big|\,\psi_b\,;\,\vec{p}_b\,\big\rangle\big\langle\,\psi_b\,;\,\vec{p}_b\,\big|J^\mu_{\text{em}}(0,\vec{q}\,)\big|\,\Psi_i\,;\,\vec{p}_i\,\big\rangle}{[-q_0+\omega_i+i\epsilon]-\omega_b} \quad . \tag{4.19}$$

Now, to imbue the weak current operator with a momentum dependence, we may perform the inverse Fourier transform and collect all complex exponential behaviour as

$$\begin{aligned} T^{\mu\nu}(p_i,p_f,q) = \frac{i}{2} \sum\!\!\!\!\!\!\int_a \int \frac{d^3k}{(2\pi)^3} \ e^{i(\vec{p}_i-\vec{p}_a-\vec{k})\cdot\vec{y}} \ & \frac{\big\langle \Psi_f\,;\,\vec{p}_f\,\big|J^\mu_{\text{em}}(0,\vec{q}\,)\big|\,\psi_a\,;\,\vec{p}_a\,\big\rangle\big\langle\,\psi_a\,;\,\vec{p}_a\,\big|J^{\dagger\,\nu}_{\text{W}}(0,\vec{k})\big|\,\Psi_i\,;\,\vec{p}_i\,\big\rangle}{[q_0+\omega_f+i\epsilon]-\omega_a} \\ + \frac{i}{2} \sum\!\!\!\!\!\!\int_b \int \frac{d^3k}{(2\pi)^3} \ e^{i(\vec{p}_b-\vec{p}_f-\vec{k})\cdot\vec{y}} \ & \frac{\big\langle \Psi_f\,;\,\vec{p}_f\,\big|J^{\dagger\,\nu}_{\text{W}}(0,\vec{k})\big|\,\psi_b\,;\,\vec{p}_b\,\big\rangle\big\langle\,\psi_b\,;\,\vec{p}_b\,\big|J^\mu_{\text{em}}(0,\vec{q}\,)\big|\,\Psi_i\,;\,\vec{p}_i\,\big\rangle}{[-q_0+\omega_i+i\epsilon]-\omega_b} \quad . \end{aligned}$$

We may now exploit the fact that, by definition, the right hand side is independent of $\vec{y}$ since we have used it to introduce a fictitious rotation of the current operator. Then, we may integrate over $d^3y$ in some fixed volume $V$ as

$$1 = \frac{1}{V} \int_V d^3y \quad ,$$

and change nothing. Doing so, we have

$$T^{\mu\nu}(p_i,p_f,q) = \frac{i}{2V}\sum\!\!\!\!\!\!\int_a d^3k\ \delta_V^{(3)}\big(\vec{p}_i-\vec{p}_a-\vec{k}\,\big)\ \frac{\big\langle\,\Psi_f\,;\,\vec{p}_f\,\big|J^{\mu}_{\rm em}(0,\vec{q})\big|\,\psi_a\,;\,\vec{p}_a\,\big\rangle\big\langle\,\psi_a\,;\,\vec{p}_a\,\big|J^{\dagger\,\nu}_{\rm W}(0,\vec{k})\big|\,\Psi_i\,;\,\vec{p}_i\,\big\rangle}{[q_0+\omega_f+i\epsilon]-\omega_a}$$
$$+\frac{i}{2V}\sum\!\!\!\!\!\!\int_b d^3k\ \delta_V^{(3)}\big(\vec{p}_b-\vec{p}_f-\vec{k}\,\big)\ \frac{\big\langle\,\Psi_f\,;\,\vec{p}_f\,\big|J^{\dagger\,\nu}_{\rm W}(0,\vec{k})\big|\,\psi_b\,;\,\vec{p}_b\,\big\rangle\big\langle\,\psi_b\,;\,\vec{p}_b\,\big|J^{\mu}_{\rm em}(0,\vec{q})\big|\,\Psi_i\,;\,\vec{p}_i\,\big\rangle}{[-q_0+\omega_i+i\epsilon]-\omega_b}\quad .$$

Importantly, by translation invariance, the current amplitudes automatically must satisfy the 3-momentum conservation and so the Dirac delta is moot in these integrals, e.g., $\delta_V^{(3)}\big(\vec{p}_i-\vec{p}_a-\vec{k}\,\big)=\delta_V^{(3)}\big(\vec{0}_p\big)=V$ in the first integrand (and identically in the second integrand). This leaves us with integrals over $d^3k$ which automatically select out the combination of momenta which satisfies the conservation condition, and leaves us with a cancellation of the just-introduced volume factors. We thus arrive at

$$T^{\mu\nu}(p_i,p_f,q) = \frac{i}{2}\,\big\langle\,\Psi_f\,;\,\vec{p}_f\,\big|\,J^{\mu}_{\rm em}(0,\vec{q})\,(z_i-H)^{-1}\,J^{\dagger\,\nu}_{\rm W}(0,-\vec{q})\,\big|\,\Psi_i\,;\,\vec{p}_i\,\big\rangle$$
$$+\frac{i}{2}\,\big\langle\,\Psi_f\,;\,\vec{p}_f\,\big|\,J^{\dagger\,\nu}_{\rm W}(0,-\vec{q})\,(z_f-H)^{-1}\,J^{\mu}_{\rm em}(0,\vec{q})\big|\,\Psi_i\,;\,\vec{p}_i\,\big\rangle\quad , \tag{4.20}$$

which is our final expression for the Compton tensor $T^{\mu\nu}$ in terms of relativistic, plane-wave nuclear states. Note that $z_i = q_0-\omega_f+i\epsilon$ and $z_f=-q_0+\omega_i+i\epsilon$. We have thus achieved a representation of $T^{\mu\nu}(p_i,p_f,q)$ with current operators in terms of only the boson 3-momentum transfer, while the boson energy dependence is neatly tucked away in the nuclear propagators. As we have mentioned at the beginning of this lengthy derivation, this will facilitate the use of the multipole expansion formalism derived in Sec. 3.1 for which widely available one-nucleon amplitudes exist for many-body nuclear theory calculations.

### Compton Tensor with Non-Relativistic Hadronic States

We make a last comment on the form of these amplitudes based on the main result provided in Remark 3.2.1 of Sec. 3.2, that is, that in substitution of a relativistic QFT plane-wave amplitude for a non-relativistic QFT plane-wave amplitude, we simply incur factors of the square root of the mass. Thus, we have

$$T^{\mu\nu}(p_i,p_f,q) = \frac{i}{2}\,\sqrt{M_iM_f}\,\big\langle\,\Psi_f\,;\,\vec{p}_f\,\big|\,J^{\mu}_{\rm em}(0,\vec{q})\,(z_i-H)^{-1}\,J^{\dagger\,\nu}_{\rm W}(0,-\vec{q})\,\big|\,\Psi_i\,;\,\vec{p}_i\,\big\rangle$$
$$+\frac{i}{2}\,\sqrt{M_iM_f}\,\big\langle\,\Psi_f\,;\,\vec{p}_f\,\big|\,J^{\dagger\,\nu}_{\rm W}(0,-\vec{q})\,(z_f-H)^{-1}\,J^{\mu}_{\rm em}(0,\vec{q})\big|\,\Psi_i\,;\,\vec{p}_i\,\big\rangle\quad , \tag{4.21}$$

which matches precisely the result for the Compton amplitude in Ref. [155], with all quantities in the expression as defined above.

### $T^{\mu\nu}$ in Terms of Structure Functions

The result in Eq. (4.20) is completely general, that is, for arbitrary current operators and external hadronic states. As we are particularly interested in the case of superallowed Fermi transitions in nuclei, which involve spin-less external states, i.e.,

$$\big|J^{\pi}=0^{+};T=1\big\rangle\to\big|0^{+};1\big\rangle\quad , \tag{4.22}$$

we may greatly simplify what needs to be computed. A standard approach to analyzing electroweak hadronic scattering processes is to construct the most general tensor structures consistent with Lorentz and time-reversal invariance (see Section 18 of Ref. [6]). This form of the hadronic tensor consists of spin-momentum-dependent factors attached to scalar amplitudes, themselves determined via hadronic structure modelling. While the details of this decomposition are beyond the scope of this document, the result is important. Particularly in the case of having spin-less external states and the product of a vector and axial-vector current, only one such structure function survives in the hadronic tensor. Without diving too much into the details, the Compton tensor reduces to a dependence on the spin-invariant, parity-odd amplitude $T_3$ as

$$T^{\mu\nu}(p_f,p_i,q) = \frac{i\epsilon^{\mu\nu\alpha\beta}p_\alpha q_\beta}{2p\cdot q}\ T_3(p_f,p_i,q)\quad . \tag{4.23}$$

Then, we are only required to compute the spin-invaraint, parity-odd function $T_3(p,q)$.

## 4.3 Evaluation of the $\gamma W$ Box

Let us begin with Eq. (24) of Ref. [155], that is, the expression for the $\gamma W$ box in the forward limit,

$$\begin{aligned}\Box^{b}_{\gamma W}\big(E_e\big) &= -e^2 \int \frac{d^4q}{(2\pi)^4}\, \frac{M_W^2}{M_W^2-q^2}\, \frac{1}{q^2+i\varepsilon_1}\, \frac{1}{(p_e-q)^2-m_e^2+i\varepsilon_2} \\ &\qquad \times \frac{1}{p\cdot q}\left[q^2 - p\cdot q\, \frac{(p\cdot q)\, m_e^2 - (p_e\cdot q)(p\cdot p_e)}{M^2 m_e^2 - (p\cdot p_e)^2}\right] \frac{T_3\big(q_0,|\vec{q}\,|\big)}{f_+} \\ &= e^2 \int \frac{d^4q}{(2\pi)^4}\, \frac{M_W^2}{M_W^2-q^2}\, \frac{1}{q^2+i\varepsilon_1}\, \frac{1}{(p_e-q)^2-m_e^2+i\varepsilon_2}\, \frac{|\vec{q}\,|\big(|\vec{q}\,|-\nu\beta^{-1}x\big)}{\nu M}\, \frac{T_3\big(\nu,|\vec{q}\,|\big)}{f_+} \quad . \end{aligned} \tag{4.24}$$

First, a few book-keeping items. In arriving at the reduced expression in the second line, we have taken ourselves to be in the isospin limit $M_i = M_f$, in the forward scattering limit $p_i = p_f = p$ and in the rest frame of the initial nucleus, i.e., $p = (M, 0)$. This means that our evaluation of the $\gamma W$ box will be good up to $\mathcal{O}\big([m_u - m_d]^2\big)$ isospin breaking corrections and recoil corrections in the final nuclear configuration. We then have that the electron 4-momentum, the loop 4-momentum and the loop 4-vector norm are, respectively,

$$p_e = \big(E_e, \vec{p}_e\big) \qquad q = \big(q_0, \vec{q}\,\big) \qquad \nu = \frac{p\cdot q}{M} = q_0$$

$$Q^2 = -q^2 = -q_0^2 + |\vec{q}\,|^2 \quad ,$$

where we have replaced $q_0$ in the integrand with the usual invariant quantity $\nu$. The nuclear mass is defined as $M = Zm_p + Nm_n - B(Z,N)$, that is, the nucleonic mass minus the binding energy of the nuclear configuration. We further define the additional quantities

$$x = \cos\theta_{eq} = \hat{p}_e \cdot \hat{q} \qquad\qquad \beta = \frac{|\vec{p}_e|}{E_e} \quad ,$$

which parameterize the angle between the emitted boson and electron and the speed of the electron, respectively. As discussed in Sec. 4.1, all hadronic physics enters the $\gamma W$ box does so via the spin-invariant, parity-odd structure function $T_3$, itself derived from the generalized Compton scattering amplitude involving electromagnetic and weak current operators. We quote the expression for $T_3$ here, as derived in the prior section and appearing in Eq. (76) of Ref. [155], for the convenience of the reader. It reads

$$\begin{aligned} T_3\big(\nu,|\vec{q}\,|\big) = 4\pi i \frac{\nu}{|\vec{q}\,|}\sqrt{M_i M_f}\sum_{J=1}^{\infty}(2J+1)\big\langle\Psi_f\big|\, \Big\{ &- iT^{\text{mag.}}_{J0}\,(z_f-H)^{-1}\, iT^{5,\text{el.}}_{J0} + T^{\text{el.}}_{J0}\,(z_f-H)^{-1}\, T^{5,\text{mag.}}_{J0} \\ &+ T^{5,\text{mag.}}_{J0}\,(z_i-H)^{-1}\, T^{\text{el.}}_{J0} - iT^{5,\text{el.}}_{J0}\,(z_i-H)^{-1}\, iT^{\text{mag.}}_{J0}\Big\}\, \big(|\vec{q}\,|\big)\big|\Psi_i\big\rangle \quad , \end{aligned}$$

where the expressions for the multipoles $T_{JM}$ for the vector electromagnetic and axial charged weak currents are as defined in Sec. 3.1. We recall $f_+$ as the tree-level Fermi amplitude stated in Eq. (4.2). We further characterize the external hadronic (nuclear) states by $\Psi_i$ and $\Psi_f$ and find the $z_i$ and $z_f$ quantities to reduce to

$$z_i = M_i - \nu + i\varepsilon_3 \qquad\qquad z_f = M_f + \nu + i\varepsilon_3 \quad . \tag{4.25}$$

Evidently, the expression for the $\gamma W$ box is complete with a complex pole structure that requires an in-depth analysis prior to any meaningful numerical calculation. Pragmatic evaluation of $T_3$ implores us to deal with the poles appearing in (i) the electron propagator (ii) the photon propagator and (iii) the nuclear propagators, all of which require care. We emphasize that integration over the loop 4-momentum will traverse an infinite number of poles in the discrete and continuum spectra of the involved quanta. It is entirely possible to circumnavigate the vast majority of these poles via a contour deformation à la Wick, yet, we will see that tremendous care is required in application of Cauchy's residue theorem. We then identify that the goal of this chapter is to suitably evaluate

$$\Box^{b}_{\gamma W}(E_e) = \lim_{\varepsilon_1\to 0^+}\lim_{\varepsilon_2\to 0^+}\lim_{\varepsilon_3\to 0^+} \Box^{b}_{\gamma W}(E_e,\varepsilon_1,\varepsilon_2,\varepsilon_3) \quad , \tag{4.26}$$

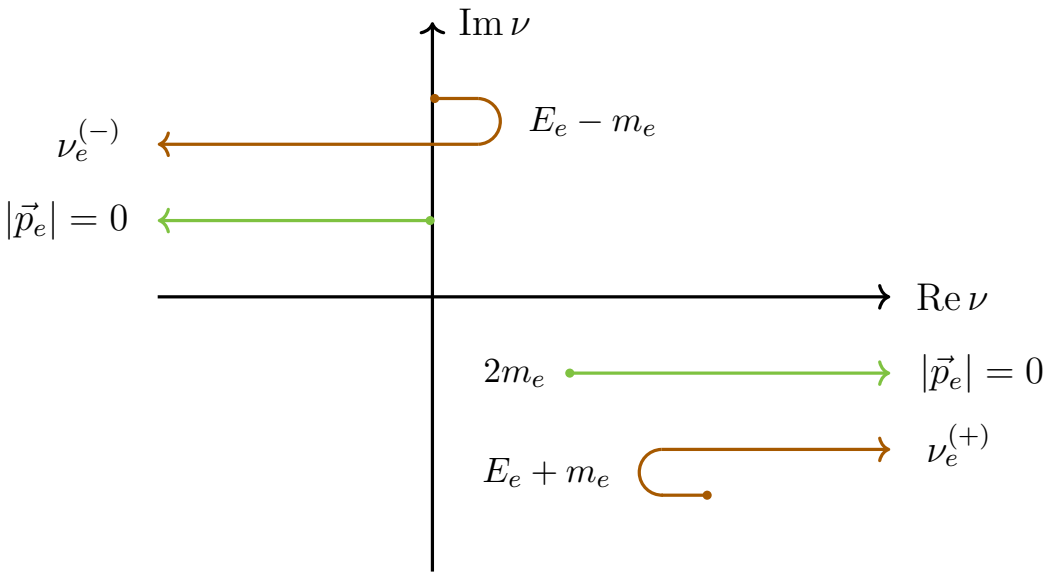


Figure 4.2: Sample trajectories of the $\nu_e^{(\pm)}$ poles in Eq. (4.27) arising from the dynamics of the electron propagator. The lines in green and orange correspond to (i) the $|\vec{p}_e| = 0$ limit and to (ii) $|\vec{p}_e| > 0$ and $|x| > 0$, respectively. Note that the $\nu_e^{(-)}$ pole spends part of its trajectory in the first quadrant of the complex plane.

where the infinitesimals $\varepsilon_i \in \mathbb{R}^+ \setminus \{0\}$ are kept as truly finite parameters in the numerical evaluation of the $\gamma W$ box. In principle, it is possible to completely replace the complicated pole structure of the above integrand with simple poles, e.g., by methods such as Feynman's trick combined with the well-known Sokhotski-Plemelj theorem for complex-valued functions on the real line. However, for the time being, it has not been a priority given the relatively small scale of the integral calculation and observed numerical stanbility. Ideally, this will be explored in a future work.

Lastly, we note to the reader that we will neglect the pole that arises from the $W$-boson propagator in Eq. (4.24) as, while we see that this would may indeed produce a residue contribution after contour deformation of the real line integration, the pole would be located at such high scales, i.e., $|\vec{q}| \sim 80\,\text{GeV}$, which we assume to be outside of the support of the nuclear amplitudes. Whether it makes sense to think of the radiative corrections at such an energy scale in the terms of nuclear physics is a matter on which the author is open to discussion. With this last comment, we now begin our discussion on the pole structure of the $\Box^b_{\gamma W}$ integrand.

### 4.3.1 Poles of the Electron Propagator

Let us begin with the poles of the electron propagator. As the discussion here will be mostly repeated in the subsequent sections on the photon and nuclear propagators, we will keep the details in full and neglect to repeat all but the most important points in the following sections. The poles of the electron propagator occur as solutions to $D_e = 0$ where

$$\begin{aligned} D_e &= (p_e - q)^2 - m_e^2 + i\varepsilon_2 \\ &= \nu^2 - |\vec{q}|^2 - 2\nu E_e + 2|\vec{p}_e||\vec{q}|x + i\varepsilon_2 \quad . \end{aligned}$$

In the spirit of the numerical calculations, if we truly consider $\varepsilon_2$ as finite we obtain the solutions to this equation explicitly in terms of $\varepsilon_2$ by application of De Moivre's formula for complex roots. This yields the following $\nu_e$ roots

$$\nu_e = E_e \pm \left( \left[ \left| \vec{p}_e - \vec{q} \right|^2 + m_e^2 \right]^2 + \varepsilon_2^2 \right)^{\frac{1}{4}} e^{i(\theta + 2\pi n)/2} \qquad \tan\frac{\theta}{2} = -\frac{\varepsilon_2}{\left| \vec{p}_e - \vec{q} \right|^2 + m_e^2} \quad ,$$

where $n \in \{0, 1\}$. Selecting the principal branch of the tangent, i.e., $\theta \in (-\pi, \pi]$ in the limit that $\varepsilon_2 \to 0^+$ requires that $\theta \to 0$. One may then directly Taylor expand the above expressions around the $\epsilon_2 = 0$ point and recover the

expected result (note the sign) for an infinitesimal imaginary shift,

$$\nu_e^{(\pm)} = E_e \pm \sqrt{\left|\vec{p}_e - \vec{q}\right|^2 + m_e^2} \mp i\varepsilon_2 + \mathcal{O}(\varepsilon_2^2) \quad . \tag{4.27}$$

When $\mathrm{Re}\,\nu_e = 0$, the poles by definition sit on the $\mathrm{Im}\,\nu$ axis and are in transition between the quadrants of the complex plane. In picturing said poles, it is helpful to find this transition point in terms of the 3-momentum transfer. From Eq. (4.27), we find that only the $\nu_e^{(-)}$ has the oppurtunity to cross the $\mathrm{Im}\,\nu$ axis and will in fact do so if

$$\mathrm{Re}\,\nu_e^{(-)} = 0 \quad \Longrightarrow \quad |\vec{q}| = |\vec{p}_e| = 0 \qquad \text{or} \qquad |\vec{q}| = 2|\vec{p}_e|x \quad , \tag{4.28}$$

which provides additional restrictions on the angular variable $x$ as well as the upper bound on the 3-momentum modulus domain when the pole is located in the first quadrant:

$$x > x_{\min} = \frac{|\vec{q}|}{2|\vec{p}_e|} \qquad\qquad |\vec{q}| < 2|\vec{p}_e| \quad . \tag{4.29}$$

These above relations will find a use in the coming sections.

It is similarly helpful to find the extremal points of these poles along the $\mathrm{Re}\,\nu$ axis which one may extract straightforwardly by optimizing the argument of the root in terms of the loop 3-momentum, that is,

$$\inf_{\mathbb{R}} \left|\vec{p}_e - \vec{q}\right|^2 = |\vec{p}_e|^2(1 - x^2) \quad , \tag{4.30}$$

where the minimum occurs at $|\vec{q}| = 2|\vec{p}_e|x$. Formally speaking, we must exclude these points from the loop 3-momentum integration domain, which leaves the valid domain for $D_e$ to be

$$\mathrm{Dom}\big(D_e\big) = \left\{ \ |\vec{q}| \in \mathbb{R}^+ \setminus \big\{0,\, 2|\vec{p}_e|x\big\} \ \right\} \quad . \tag{4.31}$$

We pause here to make an important comment regarding the domain exclusions mentioned above and in the following sections on the photon and nuclear propagators.

*Remark* 4.3.1 (**Domain Exclusions**). Importantly, in numerical evaluations of these objects we consider truly finite $\{\varepsilon\}$ parameters which allows us to abuse the integrability of these "pole-less" functions. As we only exclude a finite set of points from the domain, the domain exclusions have no effect on the numerical evaluation of the integral, at least up to the precision of the integration techniques for increasingly sharp distributions as the limits are taken. Formally speaking, all of this is well defined. However, in pursuit of the truly infinitesimal case, which would be analytic in the sense of having no parametric dependence on the $\{\varepsilon_i\}$ limits, these expressions would have to be further masssaged into a suitable principal value integral through the Poincaré-Bertrand theorem, the generalized form of the well-known Sokhotski-Plemelj theorem. This is due to the complicated pole structures that we must contend with in the propagators which may not be readily separated from one another and, hence, not safely integrated via solely the Sokhotski-Plemelj theorem.

In Fig. 4.2, we plot two example trajectories of the $\nu_e^{(\pm)}$ poles found in Eq. (4.27). We show pole trajectories for the $|\vec{p}_e| = 0$ case, plotted in green and labelled accordingly, as well as the more general case of $|\vec{p}_e| > 0$ and $|x| > 0$ case, plotted in orange. While the poles are mostly confined to the second and fourth quadrants of the complex plane, we note to the reader that the $\nu_e^{(-)}$ pole spends a portion of its trajectory in the first quadrant; behaviour which will make our life more difficult later.

### 4.3.2 Poles of the Photon Propagator

The poles of the photon propagator occur as solutions to $D_\gamma = 0$ where

$$D_\gamma = q^2 + i\epsilon_1 = \nu^2 - |\vec{q}|^2 + i\varepsilon_1 \quad .$$

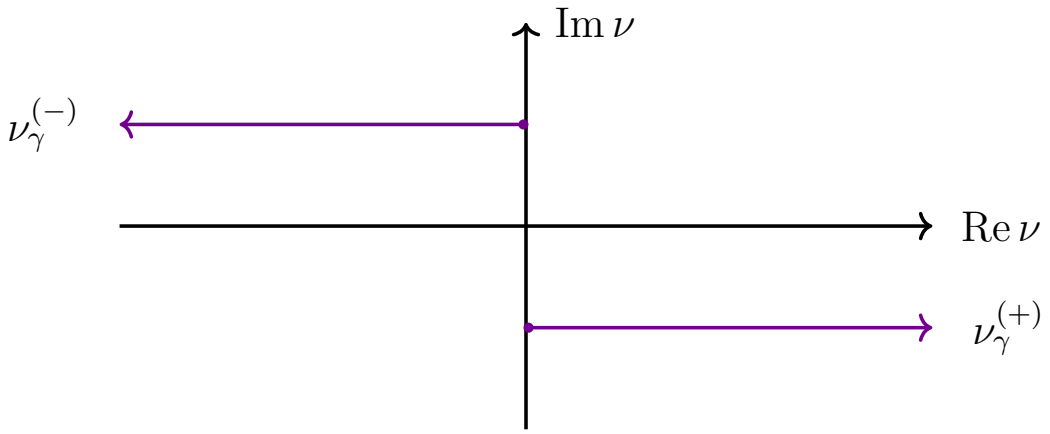


Figure 4.3: Trajectories of the $\nu_\gamma^{(\pm)}$ poles in Eq. (4.33) arising from the dynamics of the photon propagator. Note that neither of the $\nu_\gamma^{(\pm)}$ pole spend time outside of the second or fourth quadrants of the complex plane.

Proceeding with $\varepsilon_1$ as truly finite, we obtain the solutions to this equation explicitly in terms of $\varepsilon_1$ as

$$\nu_\gamma^{(\pm)} = \pm\Big(|\vec{q}|^4 + \varepsilon_1^2\Big)^{\frac{1}{4}}\, e^{i(\theta+2\pi n)/2} \qquad\qquad \tan\frac{\theta}{2} = -\frac{\varepsilon_1}{|\vec{q}|^2} \quad , \tag{4.32}$$

where $n \in \{0, 1\}$. Selecting the principal branch of the tangent, i.e., $\theta \in (-\pi, \pi]$ in the limit that $\varepsilon_1 \to 0^+$ requires that $\theta \to 0$. One may then directly Taylor expand the above expressions around the $\varepsilon_1 = 0$ point and recover the expected result (note the sign) for an infinitesimal imaginary shift,

$$\nu_\gamma^{(\pm)} = \pm|\vec{q}| \mp i\varepsilon_1 + \mathcal{O}(\varepsilon_1^2) \quad . \tag{4.33}$$

When $|\vec{q}| = 0$, the poles will sit on the $\mathrm{Im}\,\nu$ axis and hence we must formerly exclude this point from the loop 3-momentum integration domain. This leaves the valid domain for $D_\gamma$ to be

$$\mathrm{Dom}\big(D_\gamma\big) = \Big\{\ |\vec{q}| \in \mathbb{R}^+ \setminus \{0\}\ \Big\} \quad . \tag{4.34}$$

Refer to Remark 4.3.1 for comments on the domain exclusions.

In Fig. 4.3, we plot the trajectories of the $\nu_e^{(\pm)}$ poles found in Eq. (4.33). We note to the reader that the poles are entirely confined to the second and fourth quadrants of the complex plane.

### 4.3.3 Poles of the Nuclear Propagators

As we have established in Sec. 4.2 and emphasize in the expression for $T_3$ in Eq. (4.21), the $\Box_{\gamma W}^b$ box has implicit dependence on the many-body resolvent for the intermediate spectrum. As a result of the time-ordered product of current operators, we encounter two (mildly) different sets of resolvent amplitudes which must be evaluated. They are

$$\text{(a)} \quad \big(z_i - H_a\big)^{-1} = \sum\!\!\!\!\!\!\int_a \frac{\big|\,\Psi_a\,;\,\vec{p}_a\,\big\rangle\big\langle\,\Psi_a\,;\,\vec{p}_a\,\big|}{z_i - \omega_a} \qquad\qquad \text{(b)} \quad \big(z_f - H_b\big)^{-1} = \sum\!\!\!\!\!\!\int_b \frac{\big|\,\Psi_b\,;\,\vec{p}_b\,\big\rangle\big\langle\,\Psi_b\,;\,\vec{p}_b\,\big|}{z_f - \omega_b} \quad .$$

where $z_i = E_i - \nu + i\varepsilon_3$ and $z_f = E_f + \nu + i\varepsilon_3$. Of noteworthy importance is that the Hamiltonian in these expressions is not only the intrinsic Hamiltonian but the full Hamiltonian, that is, $H = H_{\text{intrinsic}} + H_{\text{c.m.}}$. Furthermore, these expressions are characterized by the species of the intermediate nuclear spectrum $a$ or $b$ over which they are expanded, which respectively correspond to the final or initial nuclear species. It is at this point we choose to remark the following.

*Remark* 4.3.2 (**The Compton Tensor and the Nuclear Model**). The many-body resolvent amplitudes constitute objects which should, under probe by quanta ranging from low- to high-energy scales, encapsulate a wealth of diverse physics. To achieve an exact description of such objects at all scales requires that the amplitudes are informed on (i) the discrete and continuum spectra, e.g., resonance structures, breakup processes and clustering effects, and (ii) the intra-nucleonic physics at the QCD scale and beyond, e.g., hadron resonances and deep inelastic scattering.
It is thus pertinent to note that, at this stage, the nuclear model restricts the type of physics we may access in the Compton amplitudes. The remaining discussion in this section (and beyond) will assume that we are working within the framework of the NCSM, i.e., that we only have access to a discretized nuclear spectrum. In this way, we need only concern ourselves with an infinite tower (in the exact NCSM limit) of discrete poles; one per element of the intermediate spectrum. This infinite tower will be truncated by the number of Lanczos iterations used in extracting the transition amplitudes to the intermediate spectrum, in accordance with the Lanczos Strengths Method described in Sec. 2.4.

As per the above remark, we will only concern ourselves with discrete poles and hence tackle said poles in both flavours of the resolvent amplitudes simultaenously. The poles of the nuclear propagators occur as solutions to $D_{\mathcal{N}}$ where

$$D_{\mathcal{N}} = E + \eta\nu + i\varepsilon_3 - E_n = 0 \qquad E_n = M_n + \frac{|\vec{q}|^2}{2M_n} \quad ,$$

where $\eta = \pm 1$ depending on the electroweak structure under consideration in $T_3$. We define $M_n$ to refer to the rest mass of a given nuclear state in the intermediate spectrum and, in writing the above, we have assumed that the 3-momentum has been transfered to the nucleus entirely in the form of a non-relativistic "kick" to its c.m. motion. In the case that the system under probe is at rest (as we are assuming here) and that the total configuration of the probe and target are indeed non-relativistic, we may replace the energy of the external state with its rest mass as $E = M$ for simplicity. It is straightforward to identify the $\nu_n$ poles as

$$\nu_n = \eta\Big(E_n - M - i\varepsilon_3\Big) = \eta\Big(\Delta_n + \frac{|\vec{q}|^2}{2M_n} - i\varepsilon_3\Big) \tag{4.35}$$

where $\Delta_n = M_n - M$ is the difference in nuclear masses. Then, there will exist poles which sit on the $\mathrm{Im}\,\nu$ axis if

$$\mathrm{Re}\,\nu_n = 0 \quad \Longrightarrow \quad |\vec{q}| = \sqrt{-2\Delta_n M} \qquad \Delta_n < 0 \quad , \tag{4.36}$$

otherwise no solutions exist for $|\vec{q}| \in \mathbb{R}^+$. This leaves the valid domain for $D_{\mathcal{N}}$ to be

$$\mathrm{Dom}\big(D_{\mathcal{N}}\big) = \left\{ \ |\vec{q}| \in \mathbb{R}^+ \setminus \left\{ \nu_n, \sqrt{-2\Delta_n M} \right\} \right\} \quad ,$$

for all $n \in \big\{\, 1, \ldots, N_{\mathrm{Lanczos}} \,\big\}$. Refer to Remark 4.3.1 for comments on the domain exclusions.

### Physically Relevant Cases

Let us study such poles in the systems of physical relevance to us, e.g., the Fermi decays $^{10}\mathrm{C} \to {}^{10}\mathrm{B}$ and $^{14}\mathrm{O} \to {}^{14}\mathrm{N}$. Such transitions begin in the ground state of the initial spectrum and the pole structure depends on the operator which connects said configuration to the intermediate spectrum.

We begin by addressing the set of poles $P_+$. These poles arise from states in the intermediate spectrum which are connected to the ground state of the initial spectrum by the electromagnetic current operator. Then, the initial state can only be mapped to excited states of the same species, e.g., $^{10}\mathrm{C} \to {}^{10}\mathrm{C}$ or $^{14}\mathrm{O} \to {}^{14}\mathrm{O}$, with energy eigenvalues greater than the ground state of the initial spectrum. Put otherwise,

$$\Delta_n > 0 \quad \Longrightarrow \quad \mathrm{Re}\,\nu_n = -\Delta_n - \frac{|\vec{q}|^2}{2M_n} < 0 \qquad \forall\ n \in \{\, 1, \ldots, N_{\mathrm{Lanczos}} \,\} \quad .$$

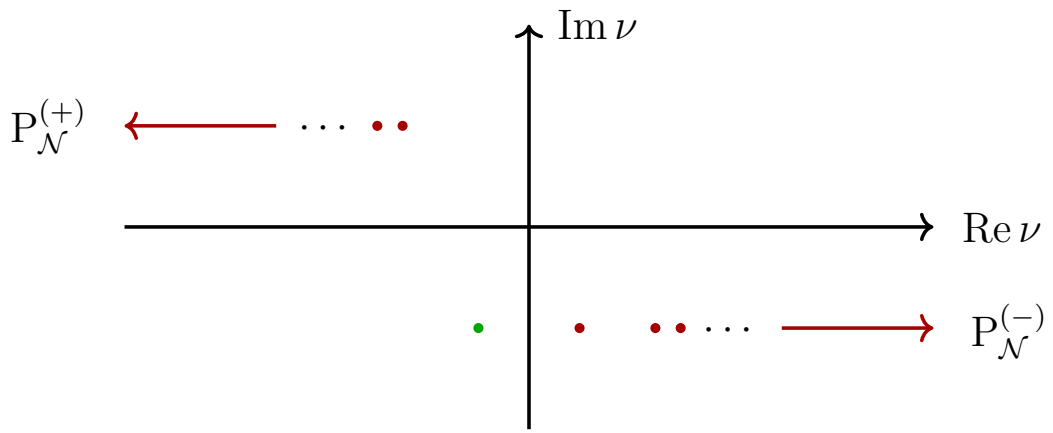


Figure 4.4: Trajectories of the $\nu_k$ poles in Eq. (4.35) arising from the dynamics of the nuclear propagators for the case of $\eta = 1$ for the physically relevant cases discussed in Sec. 4.3.3. These admit two types of poles, those with (i) $\Delta_n > 0$, shown as red dots in the second and fourth quadrants, and (ii) $\Delta_n < 0$, shown as a sole green dot in the third quadrant. We make note of this second case.

which, referring to Fig. 4.4, safely places all poles from the set $P_+$ in the second quadrant of the complex plane.

We now address the set of poles of $P_-$. These poles arise from states in the intermediate spectrum which are connected to the ground state of the initial spectrum by an by the weak charged current operator. Then, the initial state can only be mapped to excited states of the final species, e.g., $^{10}\mathrm{C} \to {}^{10}\mathrm{B}$ or $^{14}\mathrm{O} \to {}^{14}\mathrm{N}$, with energy eigenvalues of arbitrary magnitude. Since, in many cases, the transition ends in an excited state $0^+$ of the final spectrum, this admits two possibilities for the poles:

$$\mathrm{Re}\,\nu_n = \Delta_n + \frac{|\vec{q}|^2}{2M_n} \quad \begin{cases} \Delta_n > 0 & \forall\ n > n_{0^+} \\ \Delta_n < 0 & \forall\ n < n_{0^+} \end{cases} \quad . \tag{4.37}$$

Referring to Fig. 4.4, for all states in the intermediate spectrum with energy eigenvalues above the final state $0^+$ the poles are safely located in the fourth quadrant of the complex plane. However, for any lower-lying states with energy eigenvalues below the final state $0^+$, part of the trajectory of these poles will be spent in the third quadrant of the complex plane; such poles are represented by the sole green pole located in the third quadrant in Fig. 4.4. For example, we may have transitions in $^{10}\mathrm{B}$ between the lower-lying $3^+$ or $1^+$ states and the final state $0^+$, or similarly in $^{14}\mathrm{N}$ between the lower-lying $1^+$ and the final state $0^+$.

In summary, we emphasize to the reader that in this formalism, for each such pole describing a transition which connects a lower-lying state in the final spectrum to the final state $0^+$, we are obliged to evaluate the corresponding residue of the $\gamma W$ box. In particular, the poles are enclosed by the contour for a portion of their trajectory when

$$|\vec{q}| < \sqrt{2\Delta_n M} \quad . \tag{4.38}$$

A summary plot of the pole structure of the $\gamma W$ box integrand is provided in Fig. 4.5 with schematic trajectories along with the chosen contour deformation. From the analysis done here, it is clear that the application of a Wick-style rotation on the 4-momentum integration to avoid the many poles in the nuclear spectrum obliges us to compute residue contributions emerging from the Compton amplitude and electron propagator. We now proceed with and analyze the various terms arising from the Wick rotation.

### 4.3.4 Wick rotation of the $\gamma W$ box

As a result of the complicated pole structure observed in the $\gamma W$ box integrand, particularly that seen in the many-body resolvent amplitudes, a direct numerical evaluation of the $\Box_{\gamma W}(E_e)$ is non-trivial. To mitigate this, we may instead analytically continue the loop integral from a Minkowski formulation into a Riemmanian one via a deformation of the loop integral contour, referred to as a Wick rotation. In essence, we wish to map the intermediate boson 4-momentum such that

$$\nu \to i\nu_E \tag{4.39}$$

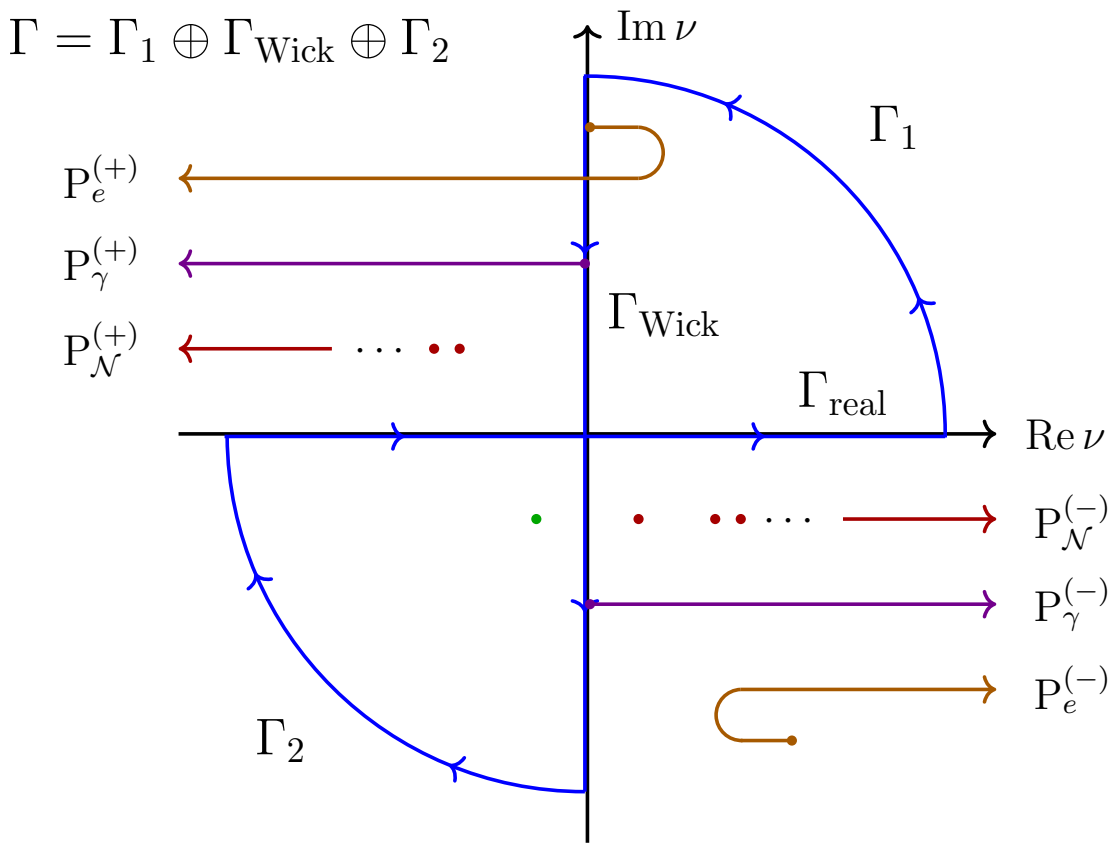


Figure 4.5: Example trajectories of the $\nu$-integral poles in Eq. (4.24) arising from the dynamics of: (i) the nuclear propagators in $T_3$, plotted in red for $\Delta_n > 0$ and green for $\Delta_n < 0$; (ii) the photon propagator, plotted in purple; and (iii) the electron propagator, plotted in orange. The corresponding sets are labelled by $\mathcal{N}$, $\gamma$ and $e$, respectively. The chosen contour deformation $\Gamma$ is the oriented contour defined by $\Gamma = \Gamma_1 \oplus \Gamma_{\text{Wick}} \oplus \Gamma_2$, shown in blue.

where $E$ denotes the Euclidean nature. Doing so would allow us to get a handle on the numerics of the resolvent amplitudes which are, in the case of the Hamiltonian, provably bounded for any non-zero complex offset. While the promise of simpler numerics is alluring, deforming the integration contour must be done with care should there be enclosed poles (residue contributions) produced in the process. It is important to note that, as acknowledged in Refs. [155, 18], prior to the consideration by our group at TRIUMF such residues arising from the low-lying nuclear spectrum and electron dynamics had never before been recognized in radiative corrections of this kind. Since the pole structure of the $\gamma W$ box integrand is now transparent, we begin by citing the famous Cauchy residue theorem.

**Theorem 4.3.1** (**Residue Theorem**). Let $\mathcal{D}$ be a simply connected domain and $\mathcal{C}$ a simple closed contour living entirely in $\mathcal{D}$. If $f : \mathcal{D} \to \mathbb{C}$ is analytic on and within $\mathcal{C}$ except at a finite number of isolated singularities $\{z_1, \ldots, z_N\}$ enclosed by $\mathcal{C}$ (that is to say, meremorphic on $\mathcal{D}$) then

$$\oint_{\mathcal{C}} dz\ f(z) = 2\pi i \sum_{k=1}^{N} W_k\, \mathrm{Res}\big(f(z), z_k\big) \quad ,$$

where the residue for an analytic function with pole of order $n$ is given by

$$\mathrm{Res}\big(f(z), z_0\big) = \frac{1}{(n-1)!} \lim_{z\to z_0} \frac{d^{n-1}}{dz^{n-1}} \big[f(z)(z-z_0)^n\big] \quad ,$$

and the winding number $W_k \in \{\pm w\}$ is positive for positively oriented curves and negative otherwise, and the magnitude $w \in \mathbb{N}$ counts the number of complete enclosures of the pole $z_k$ by the contour $\mathcal{C}$.

Based on the residue theorem and our analysis of the pole structure in the integrand of the $\Box^b_{\gamma W}\big(E_e\big)$, the result of applying the contour deformation presented in Fig. 4.5 is

$$\Box^b_{\gamma W} = \Big(\Box^b_{\gamma W}\Big)_{\mathrm{def.}} + \Big(\Box^b_{\gamma W}\Big)_{\mathrm{Res},e} + \Big(\Box^b_{\gamma W}\Big)_{\mathrm{Res},T_3} \quad . \tag{4.40}$$

We will now discuss each of these terms in detail.

### The Wick Term

Let us begin with Eq. (4.24) and perform the contour deformation as illustrated in Fig. 4.5, focusing solely on the terms which arise directly from the deformation and not from the encirclement of poles. We decompose the contour deformation as

$$\Big(\Box^b_{\gamma W}\Big)_{\mathrm{def.}} = \Big(\Box^b_{\gamma W}\Big)_{\mathrm{Wick}} + \Big(\Box^b_{\gamma W}\Big)_{\Gamma_1} + \Big(\Box^b_{\gamma W}\Big)_{\Gamma_2} \quad . \tag{4.41}$$

As is standard, we will first show that the contributions along the $\Gamma_1$ and $\Gamma_2$ contours vanish. We parameterize the path along $\Gamma_1$ as

$$\Gamma_1 = \left\{ \nu \in \mathbb{C} \ :\ \nu = \lim_{r\to\infty} re^{i\zeta}\ ,\ r \in \mathbb{R}^+ \setminus \{0\}\ ,\ \zeta \in [\,0,\, \pi/2\,] \right\} \quad , \tag{4.42}$$

and by substituting this parameterization and using the properties of limits we may write

$$\Big(\Box^b_{\gamma W}\Big)_{\Gamma_1}\big(E_e\big) = e^2 \int_0^\infty \frac{d|\vec{q}\,|}{(2\pi)^2} |\vec{q}\,|^2 \int_{-1}^{1} dx \int_0^{\frac{\pi}{2}} \frac{d\zeta}{2\pi} \lim_{r\to\infty} \frac{M_W^2}{M_W^2 - (re^{i\zeta})^2 + |\vec{q}\,|^2} \frac{1}{(re^{i\zeta})^2 - |\vec{q}\,|^2 + i\varepsilon_1}$$
$$\times \frac{1}{(re^{i\zeta})^2 - 2E_e(re^{i\zeta}) + 2|\vec{p}_e||\vec{q}\,|x - |\vec{q}\,|^2 + i\varepsilon_2} \frac{|\vec{q}\,|\big(|\vec{q}\,| - (re^{i\zeta})\beta^{-1}x\big)}{(re^{i\zeta})M} \lim_{r\to\infty} \frac{T_3\big(re^{i\zeta}, |\vec{q}\,|\big)}{f_+} \quad .$$

We have intentionally left a limit appended to the $T_3$ amplitude as this warrants a brief but separate discussion. Substituting in our parameterization for $\nu$ into Eq. (4.21), we have

$$\lim_{r\to\infty} T_3\big(re^{i\zeta}, |\vec{q}\,|\big) = 4\pi i \sqrt{M_f M_i} \sum_{J=1}^{\infty} (2J+1) \sum_{u=1}^{4} \lim_{r\to\infty} \frac{re^{i\zeta}}{|\vec{q}\,|} \frac{\mathcal{N}^{(u)}_{J0}\big(|\vec{q}\,|\big)}{\Delta_n + \eta_u(re^{i\zeta}) - \frac{|\vec{q}\,|^2}{2M_n} + i\varepsilon_3} \quad ,$$

where $\Delta_n = M_n - M$ as before and $\mathcal{N}^{(u)}_{J0}$ represents an arbitrary electroweak amplitude in $T_3$. On any part of the contour where $\zeta \in (\,0,\, \pi/2\,]$ there are absolutely no pole-related problems and the limits may be applied as above. Furthermore, for $\zeta = 0$ the photon and electron propagators are similarly not problematic since, in this scheme, we

take $r \to \infty$ well before $|\vec{q}| \to \infty$ in the subsequent integration. That is, we may always find a value for $r$ such that $|\vec{q}|/r \ll 1$.

As pointed out in Remark 4.3.2, the choice of nuclear model limits the physics which enters into the $T_3$ amplitudes, e.g., the discretization of the continuum spectrum. The result of this is, in the exact limit of the NCSM, an infinite tower of discrete poles. However, in any realistic calculation

$$\exists\, r > \sup_{\mathbb{R}} \left\{\nu_1, \ldots, \nu_N\right\} \quad ,$$

where $N < \infty$ is the number of Lanczos iterations performed in extraction of the transition amplitudes to the intermediate spectrum. Moreover, with all of this stated for the purpose of absolute clarity and making the sole assumption on the asymptotic form of the nuclear amplitudes that they have compact support on $\mathbb{R}$, we may write

$$\tilde{T}_3\big(|\vec{q}|\big) = \lim_{r\to\infty}\; T_3\big(re^{i\zeta}, |\vec{q}|\big) = 4\pi i \sum_{J=1}^{\infty}(2J+1)\sum_{u=1}^{4}\frac{\eta_u \mathcal{N}_{J0}^{(u)}\big(|\vec{q}|\big)}{|\vec{q}|} \quad ,$$

which is completely independent of the details of $\zeta$. Thus, for the $\Gamma_1$ contour we have

$$\left|\left|\left(\Box^b_{\gamma W}\right)_{\Gamma_1}\big(E_e\big)\right|\right| = \frac{e^2 M_W^2 \beta^{-1}}{9\pi M f_+}\;\left|\left|\, |\vec{q}|\;\tilde{T}_3\big(|\vec{q}|\big)\;\right|\right|\;\lim_{r\to\infty}\;\frac{1}{r^6} = 0 \quad ,$$

where this norm should be interpreted as a norm on the residual distribution over the domain of the loop 3-momentum. Regardless of the overall factor, the $r$-suppression from the various propagators kills the integral rapidly. As the above argument can be repeated identically for $\Gamma_2$, we have hence shown the anticipated result

$$\left(\Box^b_{\gamma W}\right)_{\Gamma_1} = \left(\Box^b_{\gamma W}\right)_{\Gamma_2} = 0 \qquad \Longrightarrow \qquad \left(\Box^b_{\gamma W}\right)_{\text{def.}} = \left(\Box^b_{\gamma W}\right)_{\text{Wick}} \quad .$$

Then, the meaningful term we need to compute is

$$\left(\Box^b_{\gamma W}\right)_{\text{Wick}}\big(E_e\big) = e^2\int_0^{\infty}\frac{d|\vec{q}|}{(2\pi)^2}\int_{-1}^{-1}dx\int_{-\infty}^{\infty}\frac{d\nu_E}{2\pi}\;\frac{M_W^2}{M_W^2 - q_E^2}\;\frac{1}{q_E^2}\;\frac{1}{(p_e - q_E)^2 - m_e^2} \tag{4.43}$$

$$\times\;\frac{|\vec{q}|\big(|\vec{q}| - \nu_E\beta^{-1}x\big)}{i\nu_E M}\;\frac{T_3\big(i\nu_E, |\vec{q}|\big)}{f_+} \quad . \tag{4.44}$$

where $\nu = i\nu_E$ and $q_E^2 = -\nu_E^2 - |\vec{q}|^2$. As stated previously, for any non-zero imaginary offset the resolvent amplitudes in $T_3$ are guaranteed to be everywhere-bounded and so the only concerns arise at $\nu = i\nu_E = 0$ when the loop 3-momentum is similarly zero; it will be formally excluded from the 3-momentum integration domain, that is,

$$\text{Dom}\big(D_{\mathcal{N}}\big) = \left\{\;|\vec{q}| \in \mathbb{R}^+ \setminus \{0\}\;\right\} \quad .$$

As this expression is completely well-defined on its domain, we may now further simplify the integrand by analytic integration over the angular domain. Consider the following simple integrals,

$$I_1 = \int_{-1}^{1} dx\;\frac{1}{A + Bx} = \frac{1}{B}\ln\left|\frac{A+B}{A-B}\right| \quad , \tag{4.45}$$

$$I_2 = \int_{-1}^{1} dx\;\frac{x}{A + Bx} = \frac{1}{B}\left(2 - \frac{A}{B}\;\ln\left|\frac{A+B}{A-B}\right|\right) \quad . \tag{4.46}$$

If we then take

$$A \equiv A_{\varepsilon_2}\big(E_e, |\vec{q}|, i\nu_E\big) = -\nu_E^2 - |\vec{q}|^2 - 2i\nu_E E_e + i\varepsilon_2 \quad , \tag{4.47}$$

$$B \equiv B\big(|\vec{p}_e|, |\vec{q}|\big) = 2|\vec{p}_e||\vec{q}| \quad , \tag{4.48}$$

and exchange the order of the angular integration and the $(q_E)_0 = i\nu_E$ integration − which is allowed as we are now working with a quantity well-defined and bounded on its entire domain − we may write the relevant part of the $\gamma W$ box integrand as

$$I_{\text{Wick}} = \frac{|\vec{q}|}{i\nu_E}\int_{-1}^{1} dx\ \frac{|\vec{q}| - \nu\beta^{-1}x}{A_{\varepsilon_2} + Bx} = \frac{B^2 + 2i\nu_E E_e A_{\varepsilon_2}}{4i\nu_E|\vec{p}_e|^2 B}\ \ln\left|\frac{A_{\varepsilon_2}+B}{A_{\varepsilon_2}-B}\right| - \frac{E_e}{|\vec{p}_e|^2} \quad .$$

We thus arrive at the final expression for the Wick term in the $\gamma W$ box evaluation

$$\left(\Box^b_{\gamma W}\right)_{\text{Wick}}(E_e) = e^2\int\frac{d|\vec{q}|}{(2\pi)^2}\int_{-\infty}^{\infty}\frac{d\nu_E}{2\pi}\ |\vec{q}|^2\ \frac{M_W^2}{M_W^2 - q_E^2}\ \frac{1}{q_E^2}$$
$$\times\frac{1}{M}\left\{\frac{B^2 + 2i\nu_E E_e A_{\varepsilon_2}}{4i\nu_E|\vec{p}_e|^2 B}\ \ln\left|\frac{A_{\varepsilon_2}+B}{A_{\varepsilon_2}-B}\right| - \frac{E_e}{|\vec{p}_e|^2}\right\}\frac{iT_3\big(i\nu_E, |\vec{q}|\big)}{f_+} \quad . \tag{4.49}$$

This concludes our discussion on the Wick term and so what remains is to deal with the various residue contributions induced by the contour deformation.

### The Electron Residue

From the pole analysis in Sec. 4.3.1 we can immediately see that the $\nu_e^{(-)}$ pole will spend part of its trajectory enclosed by the deformed contour. Recalling the result in Eq. (4.29), for the subset

$$\Big\{\ |\vec{q}| \in \mathbb{R}^+\ :\ |\vec{q}| \le 2|\vec{p}_e|x\ \Big\} \qquad \Longrightarrow \qquad x \ge x_{\min} = \frac{|\vec{q}|}{2|\vec{p}_e|} \quad ,$$

we will have a residue contribution from the electron propagator. As shown above, note that a consequence of this constraint is the additional restriction on the angular integration domain of the electron residue. This is conditional on the order of integration and so the expression for the electron residue term should either be kept as written below or modified accordingly,

$$\left(\Box^b_{\gamma W}\right)_{\text{Res},e}(E_e) = e^2\int_0^{2|\vec{p}_e|}\frac{d|\vec{q}|}{(2\pi)^2}\int_{x_{\min}}^{1} dx\ |\vec{q}|^2\ \frac{M_W^2}{M_W^2 - q^2}\ \frac{1}{q^2 + i\varepsilon_1}\ \frac{1}{\nu_e^{(-)} - \nu_e^{(+)}}$$
$$\times\frac{|\vec{q}|\big(|\vec{q}| - \nu_e^{(-)}\beta^{-1}x\big)}{\nu_e^{(-)}M}\ \frac{iT_3\big(\nu_e^{(-)}, |\vec{q}|\big)}{f_+} \quad , \tag{4.50}$$

where in this term $q = \big(\nu_e^{(-)}, \vec{q}\big)$ and we recall the form of the $\nu_e^{(\pm)}$ poles from Eq. 4.27,

$$\nu_e^{(\pm)} = E_e \pm \sqrt{\big|\vec{p}_e - \vec{q}\big|^2 + m_e^2} \mp i\varepsilon_2 + \mathcal{O}(\varepsilon_2^2) \quad .$$

Naturally, we are not done here! The propagators in the electron residue expression must be analyzed for additional poles along the real line which may appear in the 3-momentum or angular integration domains. We will now classify these poles and, as usual, we will ignore the $W$-boson propagator.

*(a) the photon propagator*

Let us consider the possible poles of the photon propagator as it appears in the electron residue. We must then solve

$$(\nu_e^{(-)})^2 - |\vec{q}|^2 + i\epsilon_1 = 2E_e^2 - 2E_e\sqrt{E_e^2 - 2|\vec{p}_e||\vec{q}|x + |\vec{q}|^2} - 2|\vec{p}_e||\vec{q}|x + i\varepsilon_1 = 0 \quad .$$

Upon quite a bit of simplification, we arrive at a rather clean result which is shockingly independent of the modulus of the loop 3-momentum,

$$x = \pm\frac{1}{\beta} \qquad\qquad \beta = \frac{|\vec{p}_e|}{E_e} < 1 \quad .$$

Recalling the definition for $\beta$, the magnitudes of these poles on the real line are constrained as $|x| > 1$ which is clearly outside of the domain of integration for the angular variable $x \in [\, x_{\min}, 1\,]$. We have thus shown that there are no poles in the photon propagator as it appears in the electron residue.

*(b) the nuclear propagators*

Let us consider the possible poles of the nuclear propagators nested in the Compton amplitude $T_3$ as it appears in the electron residue. Each term in $T_3$ may contribute a pole so, applying the same notation used in Sec. 4.3.3, we incur poles in the integration domains if

$$\Delta_n + \eta\nu_e^{(-)} - \frac{|\vec{q}|^2}{2M_n} = \Delta_n + \eta\Big(E_e - \sqrt{\big|\vec{p}_e - \vec{q}\,\big|^2 + m_e^2} + i\varepsilon_2\Big) - \frac{|\vec{q}|^2}{2M_n} = 0 \quad .$$

After quite some algebra, we arrive at the following depressed quartic in the modulus of the loop 3-momentum,

$$|\vec{q}|^4 + \Big(4M_n\big[\Delta_n - 4M_n - \eta\, E_e\big]\Big)|\vec{q}|^2 + \Big(8M_n^2|\vec{p}_e|x\Big)|\vec{q}| + 4M_n^2\Delta_n\big[\Delta_n - 2\eta E_e\big] = 0 \quad .$$

While an analytic form for these roots may be written down in full, the expressions are much too nasty for the content of this dissertation. Even simpler is to recognize that, ordering the integration such that the angular integration occurs first, it is more sensible to write the solutions to these expressions as poles in the angular integration domain rather than in the 3-momentum modulus integration domain. In this way,

$$x = -\frac{|\vec{q}|^4 + 4M_n\big[\Delta_n - 4M_n - \eta\, E_e\big]|\vec{q}|^2 + 4M_n^2\Delta_n\big[\Delta_n - 2\eta E_e\big]}{8M_n^2|\vec{p}_e||\vec{q}|} \quad , \tag{4.51}$$

defines the pole which may exist in the angular integration domain $x \in [\, x_{\min}, 1\,]$ for a subset of 3-momenta. This completes our understanding of the $\gamma W$ box electron residue and the residual pole structure of the Compton amplitudes as they appears in this term.

### The Compton Residue

From the pole analysis in Sec. 4.3.3 we can immediately see that any nuclear state in the intermediate spectrum of the same species of the final state and with energy less than the energy of the final state will incur a pole which spends part of its trajectory enclosed by the deformed contour. In particular, for the subset

$$\Big\{\, |\vec{q}| \in \mathbb{R}^+ \;:\; |\vec{q}| \leq \sqrt{-2\Delta_n M_n}\,\Big\} \quad ,$$

for all $n$ such that $\Delta_n < 0$, we will have a residue from the Compton amplitude. Application of the residue theorem for the subset of poles $\{\nu_k\} \subset \mathrm{P}_-$ which are enclosed by deformed contour gives

$$\Big(\Box^b_{\gamma W}\Big)_{\mathrm{Res},T_3}(E_e) = -e^2\sum_{\nu_k}\int\frac{d|\vec{q}|}{(2\pi)^2}\int_{-1}^{1}dx\;|\vec{q}|^2\;\frac{M_W^2}{M_W^2 - q_k^2}\;\frac{1}{q_k^2 + i\varepsilon_1}\;\frac{1}{(p_e - q_p)^2 - m_e^2 + i\varepsilon_2}$$

$$\times\;\frac{|\vec{q}|\big(|\vec{q}| - \nu_k\beta^{-1}x\big)}{\nu_k M}\;\frac{i\mathrm{Res}\;T_3\big(\nu_k, |\vec{q}|\big)}{f_+} \quad , \tag{4.52}$$

where $\nu_k = \Delta_p + |\vec{q}|^2/2M_p - i\varepsilon_3$, the 4-momentum $q_k^2 = \nu_k^2 - |\vec{q}|^2$ in this term and the residue of the Compton amplitude is defined as

$$\mathrm{Res}\;T_3\big(\nu_k, |\vec{q}|\big) = \lim_{\nu\to\nu_k}\;T_3\big(\nu, |\vec{q}|\big)\big(\nu - \nu_k\big) \quad . \tag{4.53}$$

We emphasize the sign in Eq. (4.52) which arises due to the orientation of the contour that encircles the poles $\{\nu_k\} \subset \mathrm{P}_-$ in the fourth quadrant of the complex plane, e.g., see Fig. 4.5.

As with the electron residue, we cannot rest easy! The propagators in the Compton residue expression must be analyzed for additional poles along the real line which may appear in the 3-momentum or angular integration domains. We will now classify these poles and, as usual, we will ignore the $W$-boson propagator.

*(a) the photon propagator*

Let us consider the possible poles of the photon propagator as it appears in the Compton residue. We must then solve the depressed quartic

$$0 = \nu_k^2 - |\vec{q}|^2 = \left(\Delta_p + \frac{|\vec{q}|^2}{2M_p}\right)^2 - |\vec{q}|^2 \quad ,$$

which, with a little work, yields the following compact expressions for the poles

$$q_{1,k}^{(\pm)} = -M_p\left(1 \mp \sqrt{1 + 2\Delta_p/M_p}\right) \qquad q_{2,k}^{(\pm)} = M_p\left(1 \pm \sqrt{1 + 2\Delta_p/M_p}\right) \quad . \tag{4.54}$$

With the constraint on the domain of the modulus of the loop 3-momentum given by $0 < |\vec{q}| < \sqrt{-2\Delta_p M_p}$, we can immediately eliminate all but one of the above poles as they lie outside of the valid domain. The sole pole which survives the domain constraints is $q_{2,k}^{(-)}$ which must be appropriately handled during numerical integration.

*(b) the electron propagator*

Let us consider the possible poles of the electron propagator as it appears in the Compton residue. In the interest of performing the angular integration analytically, we define the following angular point

$$x_p = \frac{|\vec{q}|^2 - \nu_k^2 + 2\nu_k E_e - i\varepsilon_2}{2|\vec{p}_e||\vec{q}|} = -\frac{A_{\varepsilon_2}}{B} \quad , \tag{4.55}$$

where, in analogy to what has been done in Sec. 4.3.4, we further define

$$A \equiv A_{\varepsilon_2}\big(E_e, |\vec{q}|, \nu_k\big) = \nu_k^2 - |\vec{q}|^2 - 2\nu_k E_e + i\varepsilon_2$$

$$B \equiv B\big(|\vec{p}_e|, |\vec{q}|\big) = 2|\vec{p}_e||\vec{q}| \quad .$$

Depending on the values of the loop 3-momentum modulus taken on, this may or may not be a pole in the valid angular integration domain. We have defined the above in such a way that, along with the function $f(x)$ defined as

$$f(x) = |\vec{q}| - \nu_k \beta^{-1} x \quad ,$$

we may write the $\gamma W$ box Compton residue as

$$\begin{aligned}\Big(\Box_{\gamma W}^{b}\Big)_{\mathrm{Res},T_3}(E_e) = -e^2 \sum_{\nu_k} \int \frac{d|\vec{q}|}{(2\pi)^2}\ |\vec{q}|^2\ \frac{M_W^2}{M_W^2 - q_k^2}\ \frac{1}{q_k^2 + i\varepsilon_1} \\ \times \left\{\ \frac{1}{2|\vec{p}_e|\nu_k} \int_{-1}^{1} dx\ \frac{f(x)}{x - x_p}\ \right\}\ \frac{1}{M}\ \frac{i\mathrm{Res}\ T_3\big(\nu_k, |\vec{q}|\big)}{f_+} \quad .\end{aligned}$$

The entirety of the angular dependence is captured by the term solely in curly braces and it may be further rewritten using the fact that

$$\int_a^b dx\ \frac{f(x)}{x - x_p} = \int_a^b dx\ \frac{f(x) - f(x_p)}{x - x_p} + f(x_p)\ \ln\left|\frac{b - x_p}{a + x_p}\right| \tag{4.56}$$

which makes the first term regular at the point $x_p$ and casts any potential irregularities into the argument of the logarithmic term (we will deal with these shortly). We then have

$$\begin{aligned}\frac{1}{2|\vec{p}_e|\nu_k} \int_{-1}^{1} dx\ \frac{f(x)}{x - x_p} &= \frac{1}{2|\vec{p}_e|\nu_k} \int_{-1}^{1} dx\ \frac{\big(-\nu_k\beta^{-1}\big)(x - x_p)}{x - x_p} + \Big(|\vec{q}| - \nu_k\beta^{-1}x_p\Big)\ \ln\left|\frac{1 - x_p}{1 + x_p}\right| \\ &= -\frac{E_e}{|\vec{p}_e|^2} + \frac{B^2 + 2\nu_k E_e A_{\varepsilon_2}}{4\nu_k |\vec{p}_e|^2 B}\ \ln\left|\frac{A_{\varepsilon_2} + B}{A_{\varepsilon_2} - B}\right| \quad ,\end{aligned}$$

Substituting this result into our expression for the $\gamma W$ box Compton residue gives

$$\Big(\Box^b_{\gamma W}\Big)_{\mathrm{Res},T_3}\big(E_e\big) = -e^2\sum_{\nu_k}\int\frac{d|\vec{q}\,|}{(2\pi)^2}\;|\vec{q}\,|^2\;\frac{M_W^2}{M_W^2-q_k^2}\;\frac{1}{q_k^2+i\varepsilon_1}$$

$$\times\frac{1}{M}\left\{\;\frac{B^2+2\nu_k E_e A_{\varepsilon_2}}{4\nu_k|\vec{p}_e|^2B}\;\ln\left|\frac{A_{\varepsilon_2}+B}{A_{\varepsilon_2}-B}\right|-\frac{E_e}{|\vec{p}_e|^2}\;\right\}\frac{i\mathrm{Res}\;T_3\big(\nu_k,|\vec{q}\,|\big)}{f_+}\quad , \tag{4.57}$$

which is our final expression for this contribution. Importantly, we have spent the time bringing this contribution into this form so that we may rigoruously analyze the remaining pole structure in the 3-momentum modulus integration domain.

As mentioned prior, any remaining irregularities are cast into the argument of the logarithm and so we are obliged to find possible solutions to $A_{\varepsilon_2}=\pm B$. After much simplification we arrive at the following two depressed quartic equations

$$|\vec{q}\,|^4-4M_k\big(M+E_e\big)|\vec{q}\,|^2\pm8M_k^2|\vec{p}_e||\vec{q}\,|+4M_k^2\Delta_k\big(\Delta_k-2E_e\big)=0\quad , \tag{4.58}$$

for which eight solutions exist; we note that not all will exist in the valid integration domain. The analytic expressions for the poles are utilized directly in the codes. This completes our understanding of the $\gamma W$ box Compton residue and the residual pole structure in the photon and electron propagators as they appear in this term.

**Summary**

For details on the pole structure of the $\gamma W$ box distribution, see: Sec. 4.3.1 for the electron propagator; Sec. 4.3.2 for the photon propagator; and Sec. 4.3.3 for the nuclear propagators. In this section, we have utilized the pole analysis in the quoted sections and the contour deformation in Fig. 4.5 to show that a Wick rotation of the $\gamma W$ box distribution produces two sets of residues, one from the electron propagator and the other from the nuclear propagators, and thus we have identified all of the pieces to the $\Box_{\gamma W}\big(E_e\big)$, i.e.,

$$\Box^b_{\gamma W}\big(E_e\big)=\Big(\Box^b_{\gamma W}\Big)_{\mathrm{Wick}}\big(E_e\big)+\Big(\Box^b_{\gamma W}\Big)_{\mathrm{Res},e}\big(E_e\big)+\Big(\Box^b_{\gamma W}\Big)_{\mathrm{Res},T_3}\big(E_e\big)\quad . \tag{4.59}$$

We have further shown that these remaining contributions, in particular, the two residue terms, have additional poles in the domain of the loop 3-momentum which must be carefully handled in an approach which is numerically "principal value"-esque. We remind the reader however that the infinitesimal parameters $\{\varepsilon_i\}$ remain strictly greater than zero and thus we only evaluate the right-hand-side of Eq. (4.26) for a sequence of infinitesimals. Now, all that is left is to numerically evaluate the above contributions.

### 4.3.5 $\gamma W$ Box to $\mathcal{O}\big(E_e\big)$

Now that we have dealt rigorously with all contributions to the $\gamma W$ box function, we will make some closing comments regarding the Wick term. Since this function has no remaining pole structure, particularly in the electron propagator, we may consider a simplified form in which we take $m_e\to0$ (the ultra-relativistic limit) in the Wick term. This will be done prior to the angular integration and in the end is akin to averaging the expanded term over the electron-boson angular distribution. Taking the ultra-relativistic limit in Eq. (4.43) gives

$$\lim_{m_e\to0}\Big(\Box^b_{\gamma W}\Big)_{\mathrm{Wick}}\big(E_e\big)=e^2\int\frac{d^4q_E}{(2\pi)^4}\;\frac{M_W^2}{M_W^2-q_E^2}\;\frac{1}{q_E^2}\;\frac{1}{(p_e-q_E)^2}\frac{|\vec{q}\,|\big(|\vec{q}\,|-i\nu_E x\big)}{i\nu_E M}\;\frac{T_3\big(i\nu_E,|\vec{q}\,|\big)}{f_+}\quad .$$

In a subsequent limit of $E_e\to0$, it is clear that the function is regular at the origin. With this in mind, as a first estimation of $\delta_{\mathrm{NS}}$ in this approach, we may safely expand the electron propagator in this term and retain the contributions up to $\mathcal{O}\big(E_e\big)$ to simplify the numerics. We make an important note that, based on the form of the electron propagator in the ultra-relativistic limit and the fact that the electron propagator residue will be sub-leading in the expansion, we will neglect it's inclusion here. We then have for the Wick term

$$\frac{1}{(p_e-q)^2+i\epsilon}=\frac{1}{\big(E_e-i\nu_E\big)^2-\big|\vec{p}_e-\vec{q}\,\big|^2}=\frac{1}{q_E^2}\left[1-\frac{2E_e}{q_E^2}\big(i\nu_E-|\vec{q}\,|x\big)\right]^{-1}\quad ,$$

Any terms even in the angular variable $x$ will produce zero contribution to the integral while terms odd in $x$ will simply incur factors of two. Putting this back into our expression for the $\gamma W$ box function and expanding in $E_e$, we find

$$\lim_{m_e\to 0}\left(\Box^b_{\gamma W}\right)_{\rm Wick}(E_e) = e^2\int_0^\infty \frac{d|\vec{q}|}{(2\pi)^2}\int_{-\infty}^{\infty}\frac{d\nu_E}{2\pi}\int_{-1}^{1}dx\;\frac{M_W^2}{M_W^2-q_E^2}\;\frac{1}{q_E^4}\left[1+\frac{2E_e}{q_E^2}\big(i\nu_E-|\vec{q}|x\big)\right]$$
$$\times\frac{|\vec{q}|\big(|\vec{q}|-\nu_E x\big)}{i\nu_E M}\;\frac{T_3\big(i\nu_E,|\vec{q}|\big)}{f_+}+\mathcal{O}\big(E_e^2\big)$$
$$=\boxminus_0+\boxminus_1\,E_e+\mathcal{O}\big(E_e\big)^2\quad , \tag{4.60}$$

where the two simple integrals for the $\mathcal{O}(1)$ and $\mathcal{O}(E_e)$ terms are given by

$$\boxminus_0 = e^2\int\frac{d^4q}{(2\pi)^4}\;\frac{M_W^2}{M_W^2-q^2}\;\frac{1}{q_E^4}\;\frac{|\vec{q}|^2}{\nu_E M}\;\frac{T_3(i\nu_E,|\vec{q}|)}{f_+}\quad , \tag{4.61}$$

$$\boxminus_0 = \frac{8}{3}\,e^2\int\frac{d^4q}{(2\pi)^4}\;\frac{M_W^2}{M_W^2-q^2}\;\frac{1}{q_E^6}\;\frac{|\vec{q}|^2}{M}\;\frac{T_3(i\nu_E,|\vec{q}|)}{f_+}\quad . \tag{4.62}$$

Thus, to make absolutely clear, the results that we intend to present for the $\Box^b_{\gamma W}$ box are evaluated to $\mathcal{O}(E_e)$ in the electron energy expansion for the Wick and electron residue term and include the following contributions:

$$\Box^b_{\gamma W}(E_e)\approx\boxminus_0+\boxminus_1\,E_e+\left(\Box^b_{\gamma W}\right)_{{\rm Res},T_3}(E_e)+\mathcal{O}(E_e^2)\quad . \tag{4.63}$$

Notice that in this decomposition, the electron energy dependence is kept to all orders in the Compton residue term since taking the $m_e\to 0$ limit of this term produces a function which is not regular in the electron energy as $E_e\to 0$.

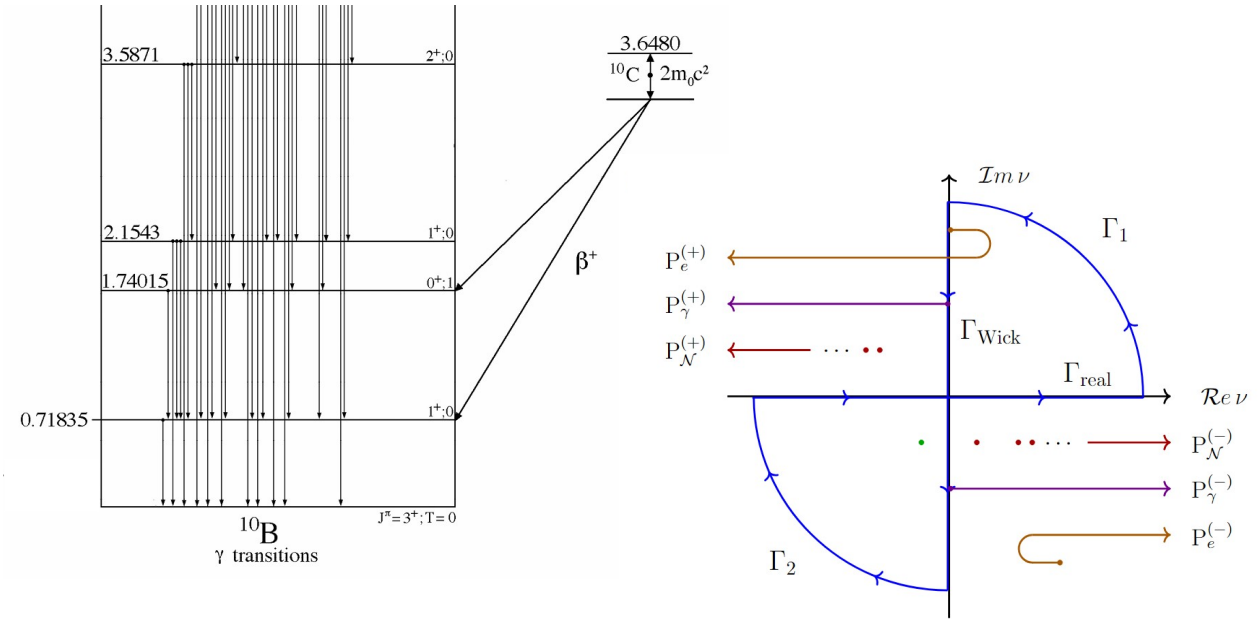


Figure 4.6: Pictured is the experimental spectrum of $^{10}$B taken from the TUNL evaluation [163] alongside the Wick contour deformation with the $^{10}$C decay in mind. Note the lower-lying ground state $3^+$ and first excited state $1^+$ of $^{10}$B which, in this formalism, produce residues (green dots) as described in Sec. 4.3.3.

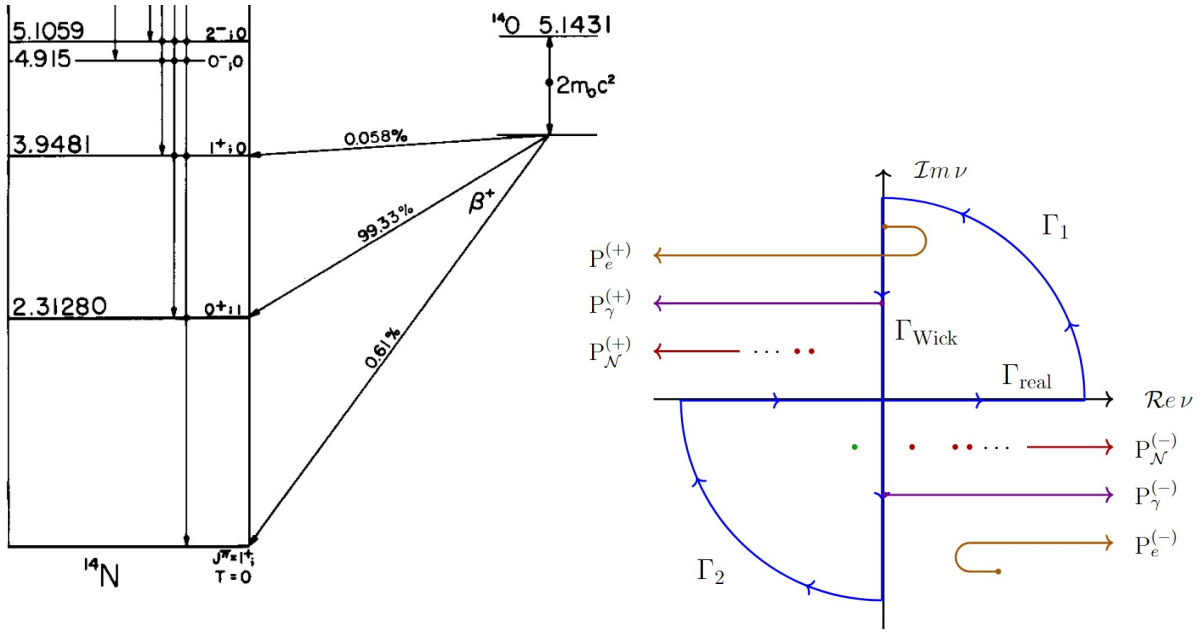


Figure 4.7: Pictured is the experimental spectrum of $^{14}$N taken from the TUNL evaluation [164] alongside the Wick contour deformation with the $^{14}$O decay in mind. Note the lower-lying ground state $1^+$ which, in this formalism, produces a residue (a green dot) as described in Sec. 4.3.3.

## 4.4 The $\gamma W$ Box in $^{10}\mathrm{C} \to {}^{10}\mathrm{B}$ and $^{14}\mathrm{O} \to {}^{14}\mathrm{N}$

Here we present our results for the two lightest transitions of all possible Fermi decays, the $^{10}\mathrm{C} \to {}^{10}\mathrm{B}$ and the $^{14}\mathrm{O} \to {}^{14}\mathrm{N}$ transitions. The results of this section, as pertaining to the $^{10}\mathrm{C} \to {}^{10}\mathrm{B}$ transition, have been published in Ref. [1]. We will more or less reproduce a portion of the discussion from the manuscript and add further details on the available calculations. The results for $^{14}\mathrm{O} \to {}^{14}\mathrm{N}$ are very much *preliminary* and remain unpublished.

First and foremost, we briefly review aspects of the pole structure in the $\gamma W$ box integrand related to the nuclear spectrum. We recall that in this formalism for evaluating the $\gamma W$ box based upon a contour deformation of the virtual gauge boson 4-momentum that, for each nuclear propagator amplitude which describes a direct transition between a lower-lying state in the final spectrum and the final excited state $0^+$, the corresponding pole will be enclosed by the deformed contour for a portion of its trajectory. For reference, we provide Fig. 4.6 and Fig. 4.7 which respectively contain the relevant parts of the $^{10}\mathrm{B}$ and $^{14}\mathrm{N}$ spectra. Such poles which spend a portion of their trajectory in the third quadrant of the complex plane necessarily have

$$\Delta_n = M_n - M < 0 \quad .$$

Thus, for the $^{10}\mathrm{C} \to {}^{10}\mathrm{B}$ transition, we will have residues which arise due to transitions from the ground state $3^+$ and first excited $1^+$ of $^{10}\mathrm{B}$ to the final state $0^+$. Similarly, for the $^{14}\mathrm{O} \to {}^{14}\mathrm{N}$ transition, we will have a residue which arises due to the transition from the ground state $1^+$ of $^{14}\mathrm{N}$ to the final state $0^+$. With this understanding of the residue contributions in mind, we begin with our discussion of the results.

### 4.4.1 Numerical Benchmarks of the Formalism

The first set of results that we present are in fact calculational benchmarks which verify two important properties of the amplitudes we compute, that is: (i) time-reversal symmetry in the scalar isospin components of the $T_3$ amplitudes, as first derived by C.-Y. Seng [165], and (ii) continuity of the $\gamma W$ box function under the chosen contour deformation. Regarding the $\chi$EFT interactions and parameteric dependence of the $\gamma W$ box on the finite $\varepsilon_i$ quantities, we refer the reader to the discussion provided at the beginning of this chapter. Here, we will merely quote what is utilized where.

*(i) Time-Reversal Symmetry of Isocalar $T_3$*

It is possible via a time-reversal symmetry argument to constrain, under isospin symmetry, certain operator structures in the Compton amplitude. This allows us a direct test of our numerical evaluation of $T_3$. With some details provided in Ref. [155], we quote the resultant constraint on the resolvent amplitudes here:

$$\left\langle \Psi_f \middle| T^{5,\mathrm{mag}}_{J0} \left(z_i - H\right)^{-1} T^{\mathrm{el}}_{J0} \middle| \Psi_i \right\rangle = \left\langle \Psi_f \middle| T\big(T^{\mathrm{el}}_{J0}\big)^\dagger T^{-1} \left(z_i - H\right)^{-1} T\big(T^{5,\mathrm{mag}}_{J0}\big) T^{-1} \middle| \Psi_i \right\rangle \quad , \tag{4.64}$$

$$\left\langle \Psi_f \middle| T^{5,\mathrm{el}}_{J0} \left(z_i - H\right)^{-1} T^{\mathrm{mag}}_{J0} \middle| \Psi_i \right\rangle = \left\langle \Psi_i \middle| T\big(T^{\mathrm{mag}}_{J0}\big)^\dagger T^{-1} \left(z_i - H\right)^{-1} T\big(T^{\mathrm{el}}_{J0}\big) T^{-1} \middle| \Psi_f \right\rangle \quad . \tag{4.65}$$

As a numerical test of our ability to compute the resolvent amplitudes, we evaluate the agreement of the above relations for the $^{10}\mathrm{C} \to {}^{10}\mathrm{B}$ transition in a small $N_{\max} = 3$ configuration space with the $\mathrm{NN} - \mathrm{N^4LO}(500) + 3\mathrm{N}_{\mathrm{lnl}}$ and an oscillator frequency of $\hbar\Omega = 18$ MeV. The results for the first and second set of amplitudes are presented in Tables 4.1 and 4.2, respectively. The arrows indicate the direction of application of the resolvent in computing the amplitudes via the Lanczos Strengths Method. We note the excellent agreement of the amplitudes with the numerics being on the order of the typical precision of a NCSM calculation. A simple test such as this provides a modicum of confidence in our capabilities of evaluating $T_3$ and serves as a robust starting point for the more involved numerical calculations.

*(ii) Continuity of the $\gamma W$ Box*

In Figs. 4.8 and 4.9, we show samples of the numerical results for the $\gamma W$ box function, plotted over the modulus of the virtual gauge boson 3-momentum and sliced at a fixed electron energy $E_e \approx m_e$, as defined by its Wick rotated and expanded form given in Eq. (4.63). To be clear, we plot the residual distribution after integration of the distribution over the intermediate boson energy transfer $\nu = q_0$. These plots show the $\gamma W$ box function as determined in the $^{10}\mathrm{C} \to {}^{10}\mathrm{B}$ and the $^{14}\mathrm{O} \to {}^{14}\mathrm{N}$ transitions, respectively. The numerical results are obtained with the $\mathrm{NN^4LO}(500) + 3\mathrm{N}^*_{\mathrm{lnl}}$ interaction, an oscillator frequency of $\hbar\Omega = 18$ MeV, and in their respective $N_{\max} = 7$ configuration spaces, the largest available truncation for both transitions.

| $\|\vec{q}\|$ (MeV) | LHS ($\leftarrow$) | RHS ($\leftarrow$) | LHS ($\rightarrow$) | RHS ($\rightarrow$) |
|---|---|---|---|---|
| 0.0 | $-2.16 \times 10^{-10}$ | $-2.16 \times 10^{-10}$ | $-2.16 \times 10^{-10}$ | $-2.16 \times 10^{-10}$ |
| 0.3 | $5.28818 \times 10^{-7}$ | $5.28854 \times 10^{-7}$ | $5.28811 \times 10^{-7}$ | $5.28858 \times 10^{-7}$ |

Table 4.1: Numerical evaluation of the left-hand-side (LHS) and right-hand-side (RHS) of Eq. (4.64) for the $^{10}\mathrm{C} \rightarrow {}^{10}\mathrm{B}$ transition with a small $N_{\max} = 3$ configuration space, the NN $-$ N$^4$LO(500) $+$ 3N$_{\mathrm{lnl}}$ and an oscillator frequency of $\hbar\Omega = 18$ MeV. The direction of the arrow indicates the direction of application of the resolvent in calculation of the amplitudes.

| $\|\vec{q}\|$ (MeV) | LHS ($\leftarrow$) | RHS ($\leftarrow$) | LHS ($\rightarrow$) | RHS ($\rightarrow$) |
|---|---|---|---|---|
| 0.0 | 0.0 | 0.0 | 0.0 | 0.0 |
| 0.3 | $-7.622419 \times 10^{-6}$ | $-7.622176 \times 10^{-6}$ | $-7.622454 \times 10^{-6}$ | $-7.622619 \times 10^{-6}$ |

Table 4.2: Numerical evaluation of the left-hand-side (LHS) and right-hand-side (RHS) of Eq. (4.65) for the $^{10}\mathrm{C} \rightarrow {}^{10}\mathrm{B}$ transition with a small $N_{\max} = 3$ configuration space, the NN $-$ N$^4$LO(500) $+$ 3N$_{\mathrm{lnl}}$ and an oscillator frequency of $\hbar\Omega = 18$ MeV. The direction of the arrow indicates the direction of application of the resolvent in calculation of the amplitudes.

In Fig. 4.8 on the $^{10}\mathrm{C} \rightarrow {}^{10}\mathrm{B}$ transition, we show the contribution of the $iT^{\mathrm{mag}} \otimes iT^{5,\mathrm{el}}$ operator structure in $T_3$ to the $\Box^b_{\gamma W}(E_e)$ integrand for the $J = 1$ multipole, presented in subfigure **(a)**, and for the $J = 3$ multipole, presented in subfigure **(b)**. Illustrated with the dash-dotted curve is the combination of the electron residue and Wick contributions, i.e., the first two terms of Eq. (4.63), calculated up to $\mathcal{O}(E_e)$ and labelled by *expansion*. With the purely dashed curve we show the Compton residue contribution, the last term of Eq. (4.63), which we simply label as *residue*. We remind the reader that the poles which may induce residue contributions of this kind are associated to an eigenvalue of the low-lying intermediate spectrum with $\omega_n < \omega_f$ when the species is the same the same as the final spectrum. In this case, it refers to the lower-lying ground state $3^+$ and first excited $1^+$ of the $^{10}$B spectrum. As the intermediate spectrum depends on the full Hamiltonian, further recall that $\omega_n = \omega_n(|\vec{q}|)$ depends explicitly on the loop 3-momentum modulus via the c.m. contribution to the kinetic energy, i.e., a "kick" to the entire system. As $|\vec{q}| \rightarrow \infty$, the pole shifts rightward in the complex plane until the c.m. contribution to the kinetic energy is substantial enough to cause the pole to touch the $\mathrm{Im}\,\nu$ axis; the residue contribution ceases to exist. This is precisely what is indicated by the dashed-black vertical line, i.e., the point at which the residue contribution vanishes due to the rightward motion of the pole. Critically, despite the clear discontinuities in the individual *expansion* and *residue* contributions at the residue transition point, the sum of the two contributions is continuous across the entire domain, as expected. Conceptually simple tests such as this ultimately serve as robust tests of the numerical calculations performed in extraction of $\delta_{\mathrm{NS}}$. In Fig. 4.9 on the $^{14}\mathrm{O} \rightarrow {}^{14}\mathrm{N}$ transition, we show an identical analysis of the $iT^{\mathrm{mag}} \otimes iT^{5,\mathrm{el}}$ operator structure contribution in $T_3$ to the $\Box^b_{\gamma W}(E_e)$ integrand, though only for the $J = 1$ multipole. The *expansion* and *residue* pieces are as described above. Notably, the sum of the two curves is continuous over the loop 3-momentum at $|\vec{q}| = \sqrt{-2\Delta_k M_f}$, where the index $k$ represents the index of the ground state $1^+$ in the $^{14}$N spectrum, as expected.

With these numerical tests providing confidence in our evaluation of $T_3$ and in the proper handling of the $\gamma W$ box pole structure, we may fully integrate the distribution and extract the main results for the electroweak radiative corrections to Fermi decays, the values of $\delta_{\mathrm{NS}}$.

### Electron Energy Dependence of the $\gamma W$ Box

For a given operator structure appearing in the Compton amplitude, the residual form of the $\gamma W$ box distribution presented in Figs. 4.8 and 4.9 is then integrated over the domain of the virtual gauge boson 3-momentum, leaving

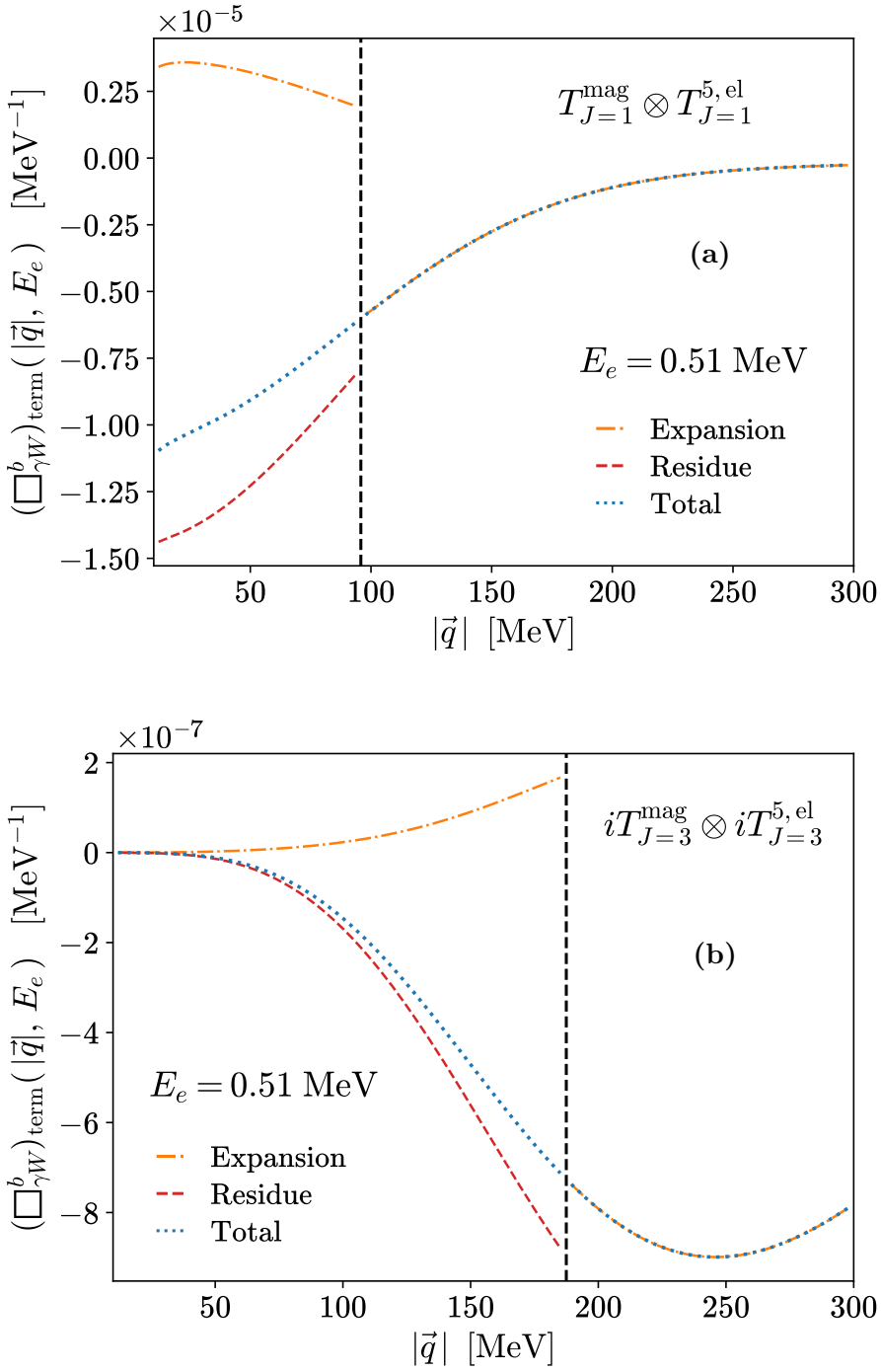


Figure 4.8: A slice of the $iT^{\text{mag}} \otimes iT^{5,\text{el}}$ operator structure in $T_3$ for the $^{10}\text{C} \to {}^{10}\text{B}$ transition. The $J = 1$ and $J = 3$ multipoles are shown in subfigures **(a)** and **(b)**, respectively. The contributions to the $\gamma W$ box integrand are plotted at fixed electron energy $E_e \approx m_e$ and over the modulus of the virtual gauge boson 3-momentum. The Compton residue (dashed), the $\mathcal{O}(E_e)$ expansion (dash-dotted) and the total sum (dotted) are as detailed in Eq. (4.63). The vertical dashed line corresponds to the point at which the residue contribution vanishes, that is, $|\vec{q}| = \sqrt{-2\Delta_k M_f}$, where $M_f$ corresponds to the nuclear mass of the final $0^+$ state and the index $k$ to the lower-lying state of the $^{10}$B spectrum.

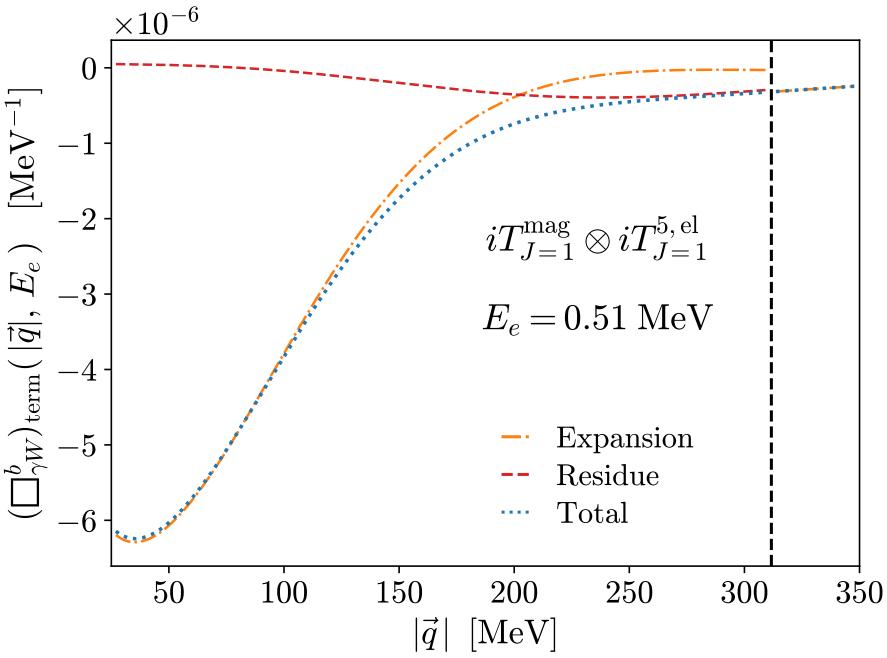


Figure 4.9: A slice of the $iT^{\text{mag}} \otimes iT^{5,\text{el}}$ operator structure in $T_3$ for the $^{14}\text{O} \to {}^{14}\text{N}$ transition. The $J = 1$ multipole contribution to the $\gamma W$ box integrand is plotted at fixed electron energy $E_e \approx m_e$ and over the modulus of the virtual gauge boson 3-momentum. The Compton residue (dashed), the $\mathcal{O}(E_e)$ expansion (dash-dotted) and the total sum (dotted) are as detailed in Eq. (4.63). The vertical dashed line corresponds to the point at which the residue contribution vanishes, that is, $|\vec{q}| = \sqrt{-2\Delta_k M_f}$, where $M_f$ corresponds to the nuclear mass of the final $0^+$ state and the index $k$ to the lower-lying state of the $^{14}$N spectrum.

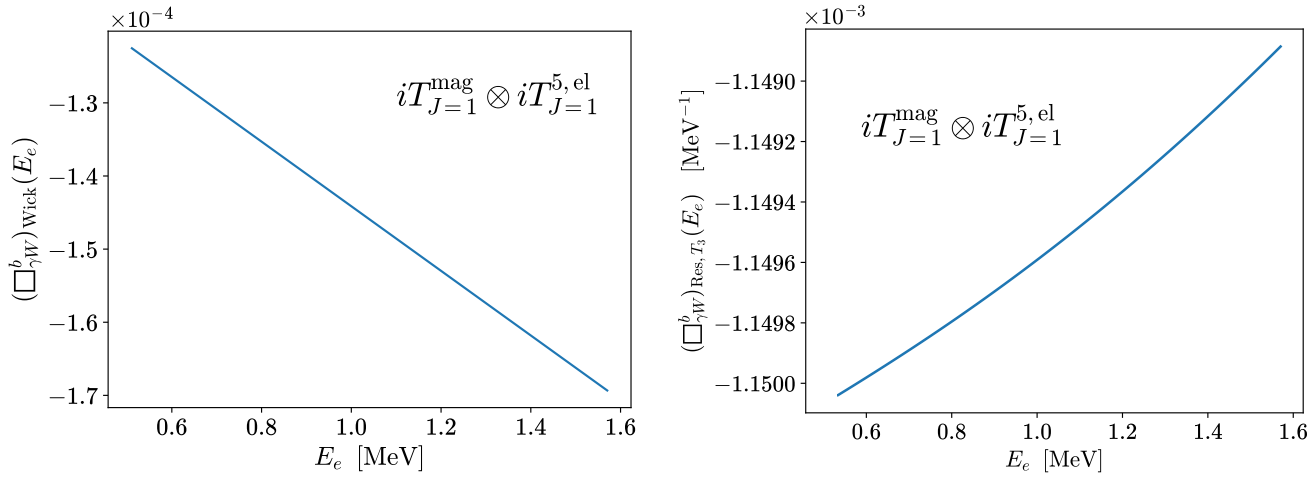


Figure 4.10: The contribution of the $J = 1$ multipole of the $T^{\text{mag}} \otimes T^{5,\text{el}}$ operator structure in $T_3$ to the $\gamma W$ box function for the $^{10}\text{C} \to {}^{10}\text{B}$ transition. We plot the electron energy dependence of the $\gamma W$ box function as in Eq. (4.63), that is, in terms of the $\mathcal{O}(E_e)$ expansion of the electron propagator and Wick terms (left figure) and the *residue* term (right figure).

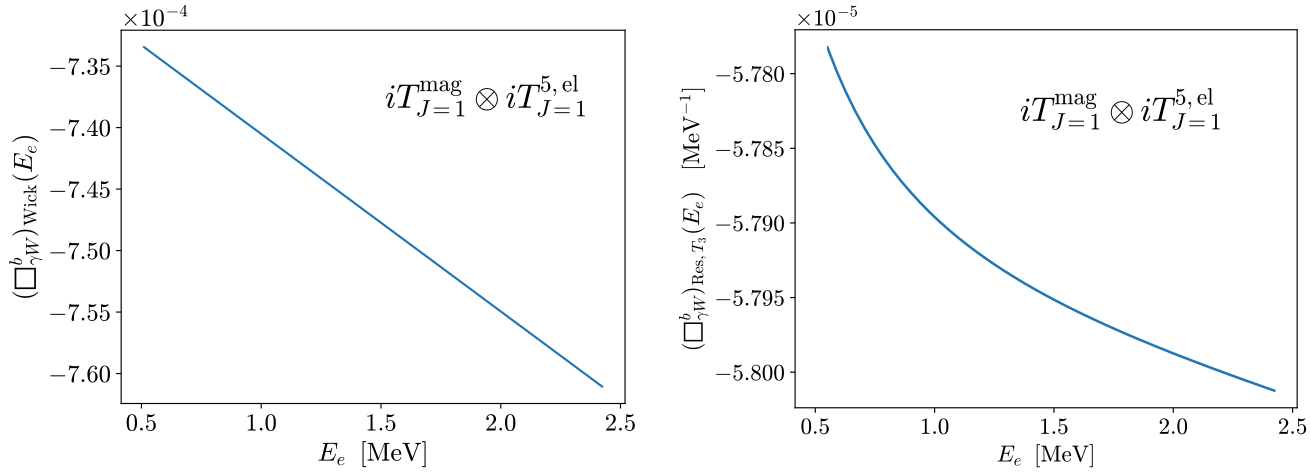


Figure 4.11: The contribution of the $J = 1$ multipole of the $T^{\rm mag} \otimes T^{5,{\rm el}}$ operator structure in $T_3$ to the $\gamma W$ box function for the $^{14}{\rm O} \to {}^{14}{\rm N}$ transition. We plot the electron energy dependence of the $\gamma W$ box function as in Eq. (4.63), that is, in terms of the $\mathcal{O}(E_e)$ expansion of the electron propagator and Wick terms (left figure) and the *residue* term (right figure).

the residual dependence of the distribution to be purely a function of the electron energy. Solely for consistency with the previous discussion, we present results for the $J = 1$ multipole of the $T^{\rm mag} \otimes T^{5,{\rm el}}$ operator structure contribution to $T_3$ for the $^{10}{\rm C} \to {}^{10}{\rm B}$ transition, shown in Fig. 4.10, and for the $^{14}{\rm O} \to {}^{14}{\rm N}$ transition, shown in Fig. 4.11. In these figures, we independently plot the residual electron energy dependence of the expanded electron propagator and Wick terms (left figure), i.e., the $\mathcal{O}(E_e)$ *expansion* terms, and the *residue* term (right figure). Of course, the contribution from the *expansion* terms is at most linear in the electron energy whereas in the *residue* terms we observe a mild curvature. In fact, despite the rather complex dependence on the loop 3-momentum in the $\gamma W$ box distribution, the residual dependence of the residue term is flat with respect to the electron energy. While we only present the $J = 1$ multipole moment for the $T^{\rm mag} \otimes T^{5,{\rm el}}$ operator structure in the main text, the behaviour of all terms with respect to the electron energy dependence is consistent with what we have presented in this discussion.

### 4.4.2 Results for $\delta_{\rm NS}$ in the $^{10}{\rm C} \to {}^{10}{\rm B}$ transition

The various contributions to the total $\gamma W$ box radiative correction are then obtained by integration of the above residual distributions over the electron energy as described in Eq. (4.63) and are, in keeping with our decomposition of $T_3$, presented as a breakdown over (i) the different electroweak operator structures and (ii) the moments of the multipole expansion. In Fig. 4.12, we present our group's the first *ab initio* NCSM calculations of the nuclear structure radiative correction $\delta_{\rm NS}$ for the $^{10}{\rm C} \to {}^{10}{\rm B}$. The numerical results are obtained with the aforementioned ${\rm NN^4LO}(500) + 3{\rm N}^*_{\rm lnl}$ interaction, an oscillator frequency of $\hbar\Omega = 18$ MeV and with an $N_{\rm max} = 7$ configuration space.

Interestingly, looking at the $J = 1$ multipole contribution, we observe a large relative size for the Compton residue (shown as hatched bars) compared to the $\mathcal{O}(E_e)$ contributions (shown as solid bars) in the total evaluation of the nuclear $\gamma W$ box. The residue term involves transition amplitudes to the subset of the intermediate $^{10}{\rm B}$ spectrum lying lower than the final state $0^+$, i.e., they only depend on the low-lying discrete nuclear spectrum. Then, the relative magnitude of the contribution can be attributed to the large $J = 1$ axial-weak transition strength (which at zero momentum transfer corresponds to the Gamow-Teller transition) between the $^{10}{\rm C}$ ground state $0^+$ and the $^{10}{\rm B}$ excited $1^+$. Of course, the strength of the electromagnetic transition between the $^{10}{\rm B}$ excited $0^+$ and $1^+$ states similarly plays a role, though to a lesser extent. Unlike the resolvent amplitudes, these contributions are computationally straightforward to evaluate. The strong dependence of such radiative corrections on the explicitly low-lying nuclear structure, e.g., the natural emergence of the residue term when viewing the corrections in the Wick rotated picture, is a point which was not recongized in this formalism until our most recent pursuit of precision improvements to said corrections. We further note that, historically, the uncertainties arising from approximate treatment of the nuclear spectrum, e.g., see the rather dramatic difference in evaluations between Ref. [17] and

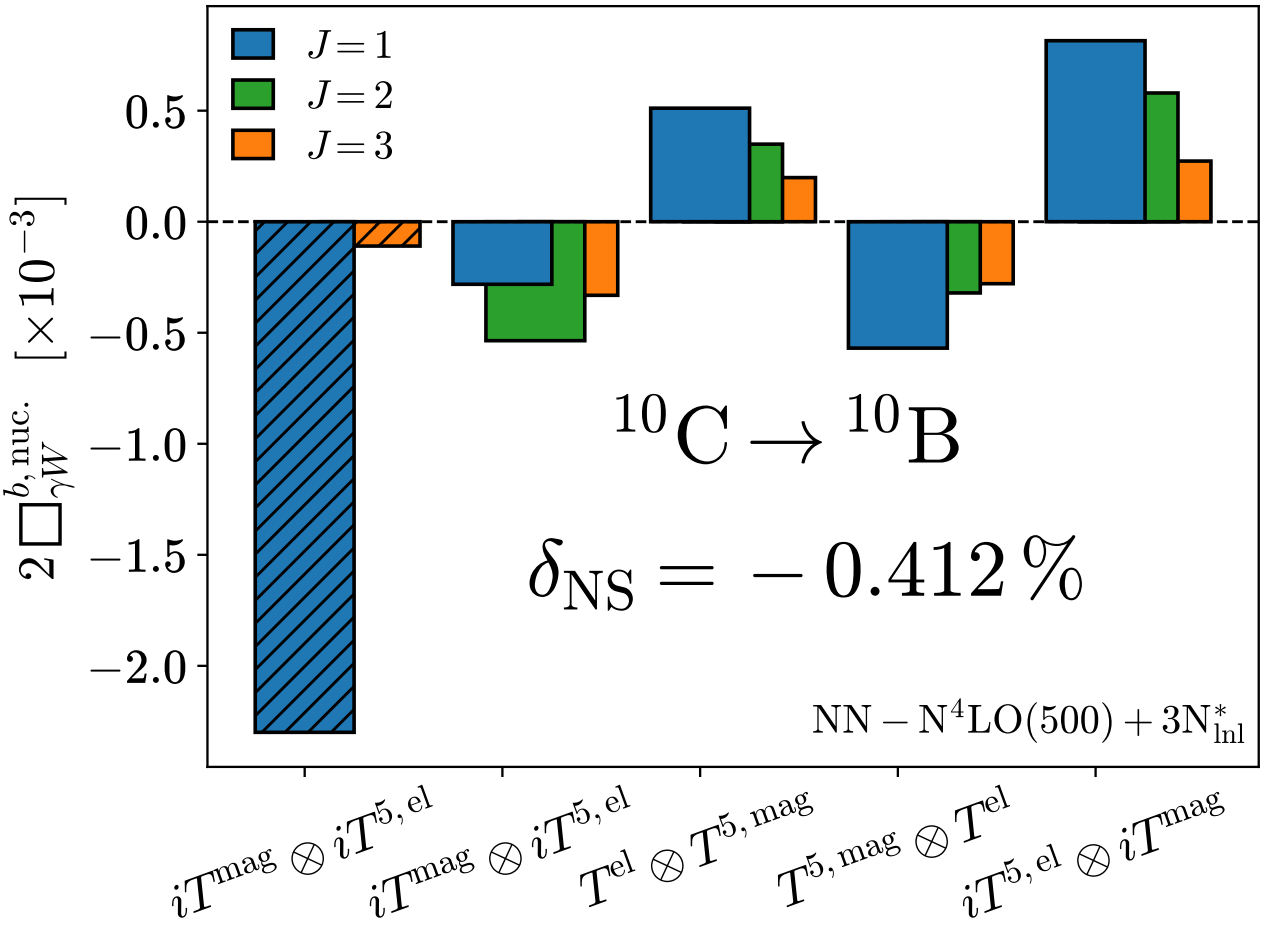


Figure 4.12: Breakdown of the nuclear $\Box^b_{\gamma W}$ for the $^{10}\mathrm{C} \to {}^{10}\mathrm{B}$ into (i) different electroweak operator structures in $T_3$ and (ii) each moment in the multipole expansion. The numerical results are obtained with the chiral $\mathrm{NN^4LO(500)} + 3\mathrm{N^*_{lnl}}$ interaction, an oscillator frequency of $\hbar\Omega = 18$ MeV and with an $N_{\mathrm{max}} = 7$ configuration space. The residue and $\mathcal{O}(E_e)$ contributions are shown as hatched and solid bars, respectively.

Ref. [7], have been underestimated. Recognition and proper evaluation of these contributions in our work in Ref. [1] represents an important step forward in improving the precision of – and providing more realisitc uncertainties for – the nuclear physics entering such evaluations.

In Fig. 4.13, we present evaluations of $\delta_{\mathrm{NS}}$ for the $^{10}\mathrm{C} \to {}^{10}\mathrm{B}$ in the NCSM. In particular, we evaluate the radiative correction over a range of parameters which characterize the many-body basis, that is, with increasing $N_{\mathrm{max}} = 3-7$ configuration space sizes and, for the $\mathrm{NN-N^4LO(500)+3N_{lnl}}$ interaction, a variation of the oscillator frequency $\hbar\Omega = 16-20$ MeV. The frequencies are chosen to lie in and around the empirically obtained variational energy minimum for the $A = 10$ systems. For the $\mathrm{NN^4LO(500)+3N^*_{lnl}}$ interaction, a single frequency of $\hbar\Omega = 18$ MeV is utilized. For brevity in this section, we merely quote the uncertainties entering the $\delta_{\mathrm{NS}}$ extractions and leave the finer details of the uncertainty breakdown to the following subsection (see also Ref. [166] and references therein). At a fixed oscillator frequency, the error assigned to the final point of a sequence of $N_{\mathrm{max}}$ calculations is determined from: (i) the many-body configuration space truncation controlled by the $N_{\mathrm{max}}$ parameter; (ii) the multipole expansion truncation controlled by the $J_{\mathrm{max}}$ parameter; (iii) the one-nucleon form factors, here taken in their approximate dipole form and made consistent with the evaluation in Ref. [167]; and (iv) the subtraction of the elastic part of the free nucleon $\gamma W$ box function [14, 168, 16]. The prediction for $\delta_{\mathrm{NS}}$ quoted in Fig. 4.13 and represented by the black square is obtained by averaging over the results from evaluations with the two interactions at a fixed oscillator frequency of $\hbar\Omega = 18$ MeV. The error which we assign to the nuclear physics is then obtained from the

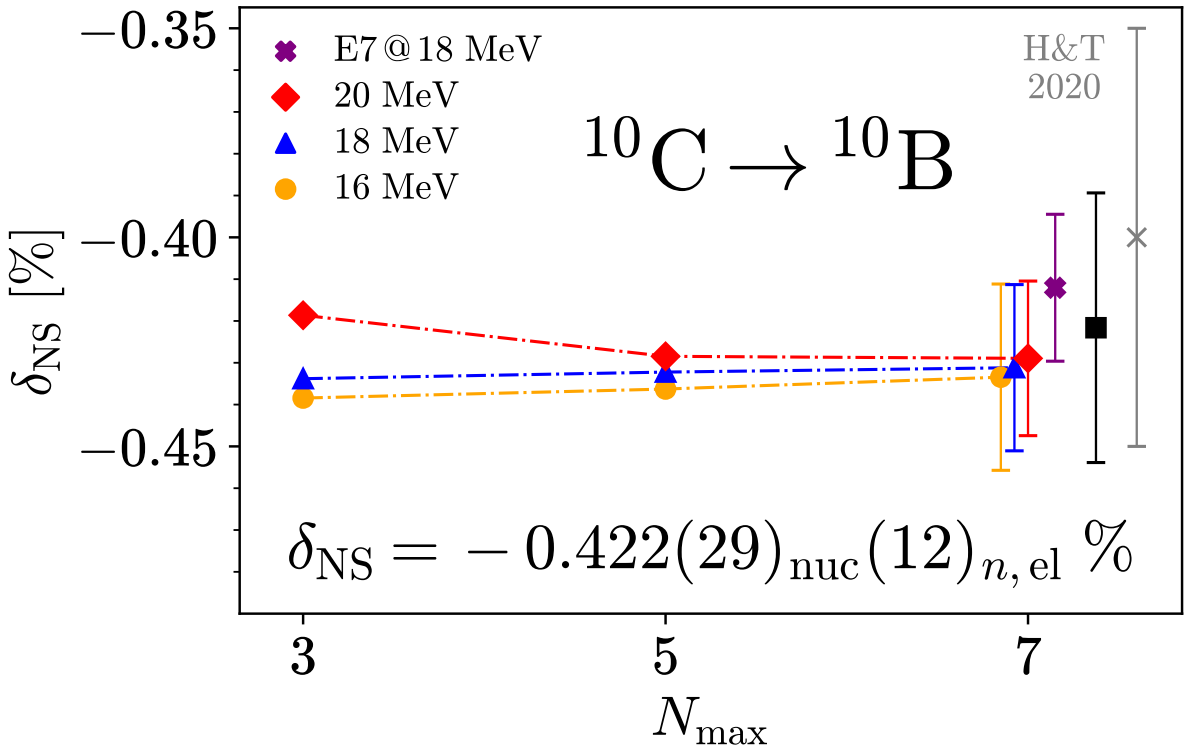


Figure 4.13: Evaluations of $\delta_{\rm NS}$ in the NCSM for the $^{10}\mathrm{C} \rightarrow {}^{10}\mathrm{B}$ with $N_{\rm max} = 3,\, 5,\, 7$ configuration space truncations and, for the NN − N$^4$LO(500)+3N$_{\rm lnl}$, oscillator frequencies in the range of $\hbar\Omega = 16-20$ MeV. For the $E_7$ point generated with the NN$^4$LO(500) + 3N$^*_{\rm lnl}$ interaction, we use a sole frequency of $\hbar\Omega =$ 18 MeV. Error bars are as briefly described in the text below and in detail in the subsequent section. The black square and corresponding error bar indicate the value of $\delta_{\rm NS}$ as extracted from the set of NCSM evaluations described below and in Ref. [1].

quadrature combination of the partial model errors (PMEs), given by (i) − (iv) described above, along with the errors from (v) the chiral expansion truncation, (vi) the choice of the oscillator frequency and (vii) the so-called "nuclear shadowing" effects, labelled by $\chi$, $\Omega$ and "sh", respectively. We note that the purely nuclear structure effect of "shadowing" is a newly introduced contribution to the uncertainty in our evaluation of $\delta_{\rm NS}$. It describes the modified response of the nuclear spectrum – either enhancement or suppression – to high-energy probes. Though, these effects typically lie well above the regime of applicability of the NCSM and, unfortunately, modern experiment and modelling are limited. We refer the reader to Ref. [1] for a very brief discussion of the error associated to the nuclear shadowing effects and emphasize the upcoming work of C.-Y. Seng and M. Gorchtein [165] on a more well-founded quantification of these contributions and their uncertainties.

As is clear by comparison of the black point and error bar to the associated grey point and error bar, our prediction for $\delta_{\rm NS}$ in the $^{10}\mathrm{C} \rightarrow {}^{10}\mathrm{B}$ transition agrees well with the value $\delta_{\rm NS} = -0.400\,(50)$ % quoted in the most recent of the famous reviews of superallowed transitions across the nuclear chart [7]. Notably, our result comes with an overall 1.6x reduction in the total uncertainty. This is achieved despite our accounting for the additional uncertainty arising from nuclear shadowing effects which, to our knowledge, has never been explicitly considered in evaluations of this kind or, more generally, in theoretical predictions of radiative corrections in nuclei. More importantly, our result strongly disagrees with the older value of $\delta_{\rm NS} = -0.347\,(35)$ % which is quoted in the five-year-prior review of Ref. [17]; it lies well outside the error bars of the previous result. The difference between the evaluation in these two reviews is the introduction of an *ad hoc* estimate (based on the Fermi gas picture of nuclei) of contributions to $T_3$ at energies in and around the intermediate nuclear spectrum, e.g., from quasi-elastic

nucleon excitations first pointed out in Refs. [14, 15]. Not only do we confirm the importance of a consideration of the intermediate nuclear spectrum, we further show that there is a substantial enhancement to the radiative corrections when a true consideration of the nuclear spectrum within a many-body formalism is employed.

We thus present the main result of this dissertation. We predict the nuclear-structure-dependent radiative correction to the $^{10}\mathrm{C} \to {}^{10}\mathrm{B}$ superallowed decay rate to be

$$\delta_{\mathrm{NS}} = -0.422\ (14)_{\mathrm{PME}}\ (4)_{\Omega}\ (9)_{\chi}\ (24)_{\mathrm{sh}}\ (12)_{n,\mathrm{el}}\ \% \quad . \tag{4.66}$$

Important to note is that, by construction, the uncertainty from subtraction of the elastic part of the free nucleon $\gamma W$ box function, $\left(\Box^{b,n}_{\gamma W}\right)_{\mathrm{el}}$, is totally anti-correlated to the one which appears in the single-nucleon radiative correction to the Fermi decay rate,

$$\Delta^{V}_{R} = 0.02479\ (12)_{n,\mathrm{el}}\ (14)_{n,\mathrm{inel}}\ (10)_{\mathrm{hi}} \quad . \tag{4.67}$$

This value is taken from Ref. [168], with errors arising from the elastic (el) and inelastic (inel) parts of the single-nucleon box diagram, as well as higher-order QCD+QED corrections (hi). Rather than quoting $\delta_{\mathrm{NS}}$ as we have and hence double-counting the error arising from the single-nucleon radiative correction, it is more natural to quote the combined quantity

$$\Delta^{V}_{R} + \delta_{\mathrm{NS}} = 0.02057\ (29)_{\mathrm{nuc}}\ (14)_{n,\mathrm{inel}}\ (10)_{\mathrm{hi}} \quad , \tag{4.68}$$

as the uncertainty due to the single-nucleon box substraction drops out in the sum.

### 4.4.3 Preliminary Results for $\delta_{\mathrm{NS}}$ in the $^{14}\mathrm{O} \to {}^{14}\mathrm{N}$ transition

In Fig. 4.14, we present our group's very first (and still **preliminary**) *ab initio* NCSM calculations of the nuclear structure radiative correction $\delta_{\mathrm{NS}}$ for the $^{14}\mathrm{O} \to {}^{14}\mathrm{N}$ transition. The numerical results are obtained with the aforementioned $\mathrm{NN}^{4}\mathrm{LO}(500) + 3\mathrm{N}^{*}_{\mathrm{lnl}}$ interaction, an oscillator frequency of $\hbar\Omega = 18$ MeV and with an $N_{\mathrm{max}} = 7$ configuration space.

In stark contrast to the $^{10}\mathrm{C} \to {}^{10}\mathrm{B}$ transition, looking at the $J = 1$ multipole contribution, we observe an almost negligible contribution from the Compton residue (shown as hatched bars) when compared to even the smallest $\mathcal{O}(E_e)$ contributions (shown as solid bars) in the total evaluation of the nuclear $\gamma W$ box. As we recall that the residue involves transition amplitudes between states in the low-lying spectrum, we find a very strongly suppressed axial-weak transition strength between the ground state $0^{+}$ of $^{14}\mathrm{O}$ and the ground state $1^{+}$ in $^{14}\mathrm{N}$, while the electromagnetic transition strength in $^{14}\mathrm{N}$ between the ground state $1^{+}$ and first excited state $0^{+}$ is not particularly suppressed. While we may have had the foresight to empirically infer such behaviour based on the famously long lifetime of $^{14}\mathrm{C}$ – for which an isospin analogue form of this suppressed transition is responsible – confirmation via a microscopic theory lends credibility to the result. As an aside, we note here that while such information may often be taken for granted, our understanding of the anomolously long $^{14}\mathrm{C}$ lifetime has only been rigorously understood at a microscopic level as late as 2011 [169].

In Fig. 4.15, we present evaluations of $\delta_{\mathrm{NS}}$ for the $^{14}\mathrm{O} \to {}^{14}\mathrm{N}$ in the NCSM. At present, we are able to evaluate the radiative correction over a range of $N_{\mathrm{max}} = 3 - 7$ configuration space sizes at a single fixed oscillator frequency $\hbar\Omega = 18$ MeV. The errors are assigned as described briefly in the previous subsection and in detail in the subsequent subsection. The prediction for $\delta_{\mathrm{NS}}$ quoted in Fig. 4.15 is preliminary and taken from the single sequence of calculations which have been performed thus far. We thus find it prudent not to make an explicit claim for $\delta_{\mathrm{NS}}$ in the $^{14}\mathrm{O} \to {}^{14}\mathrm{N}$ transition, though we do state that this early evaluation is in solid agreement with the value $\delta_{\mathrm{NS}} = -0.283\,(64)$ % quoted in Ref. [7]. However, most important to note at this stage is that the error quoted in the figure is fictiously enhanced to ensure a conservative overestimation of the eventual result; a complete calculation will likely provide a reduction in uncertainty with respect to the value from Ref. [7] comparable to what we have seen previously in the $^{10}\mathrm{C} \to {}^{10}\mathrm{B}$ transition. Moreover, to achieve this improved precision, we plan to compute contributions from higher order multipoles since, as can be seen in Fig. 4.14 and was emphasized in its corresponding discussion, the suppression of transition strength through the $J = 1$ multipole disrupts the natural hierarchy of the expansion.

### 4.4.4 Quantification of Uncertainties

In this section we provide the promised finer details on the various nuclear modelling uncertainties which enter the evaluations showcased in Figs. 4.13 and 4.15, as well as Eqs. (4.66) and (4.68), sans the nuclear shadowing

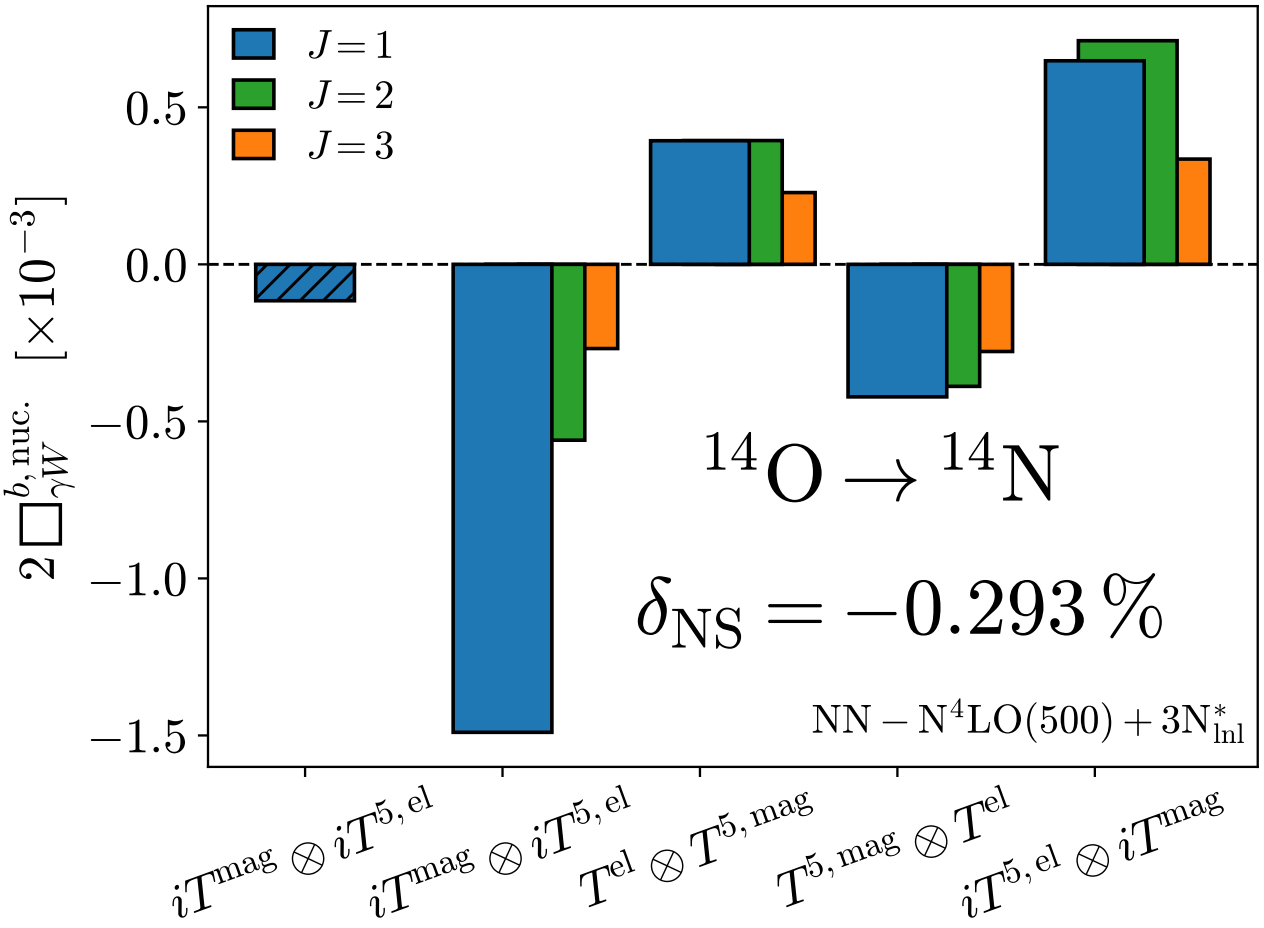


Figure 4.14: Breakdown of the nuclear $\Box_{\gamma W}^{b}$ for the $^{14}\mathrm{O} \to {}^{14}\mathrm{N}$ into (i) different electroweak operator structures in $T_3$ and (ii) each moment in the multipole expansion. The numerical results are obtained with the chiral $\mathrm{NN^4LO(500)} + 3\mathrm{N}^*_{\mathrm{lnl}}$ interaction, an oscillator frequency of $\hbar\Omega = 18$ MeV and with an $N_{\mathrm{max}} = 7$ configuration space. The residue and $\mathcal{O}(E_e)$ contributions are shown as hatched and solid bars, respectively.

effects which have been (as thoroughly as is presently feasible) explored in Ref. [1]. A precise summary of the error breakdown is provided in Table. 4.3 for the $^{10}\mathrm{C} \to {}^{10}\mathrm{B}$ transition. Unfortunately, we are not yet able to provide an equivalent breakdown for the $^{14}\mathrm{O} \to {}^{14}\mathrm{N}$ transition as the analysis is not yet complete.

First and foremost, due to the computational complexity of nuclear many-body calculations we encounter three types of truncation in these calculations: (i) the size of the many-body configuration space in the NCSM, controlled by the truncation parameter $N_{\mathrm{max}}$; (ii) the multipole truncation, controlled by the parameter $J_{\mathrm{max}}$; and (iii) the chiral truncation in our effective nuclear Hamiltonian. Note that truncation of the chiral expansion affects both the modelling of the nuclear Hamiltonian and the SM current operators whose respective chiral orders are not taken into account consistently. Consequently, their associated truncation errors are estimated independently. Furthermore, the nuclear Hamiltonian is SRG evolved while the current operators are not. This approximate treatment of the fully consistent SRG evolution leads to an additional source of uncertainty from neglecting higher-order corrections to the current; their impact must be estimated on top of the chiral truncation. Overall, this amounts to estimating a total uncertainty coming from our modelling of the nuclear Hamiltonian and SM currents. We will now characterize each of these uncertainties one by one.

Beginning with the $N_{\mathrm{max}}$ truncation, which controls the dimension of the many-body configuration space, we recall that in the limit $N_{\mathrm{max}} \to \infty$ we approach the exact NCSM result. Hence, at finite $N_{\mathrm{max}}$, we estimate the truncation error $\epsilon_{N_{\mathrm{max}}}$ by taking the absolute difference between consecutive $N_{\mathrm{max}}$ evaluations of $\delta_{\mathrm{NS}}$ in a given

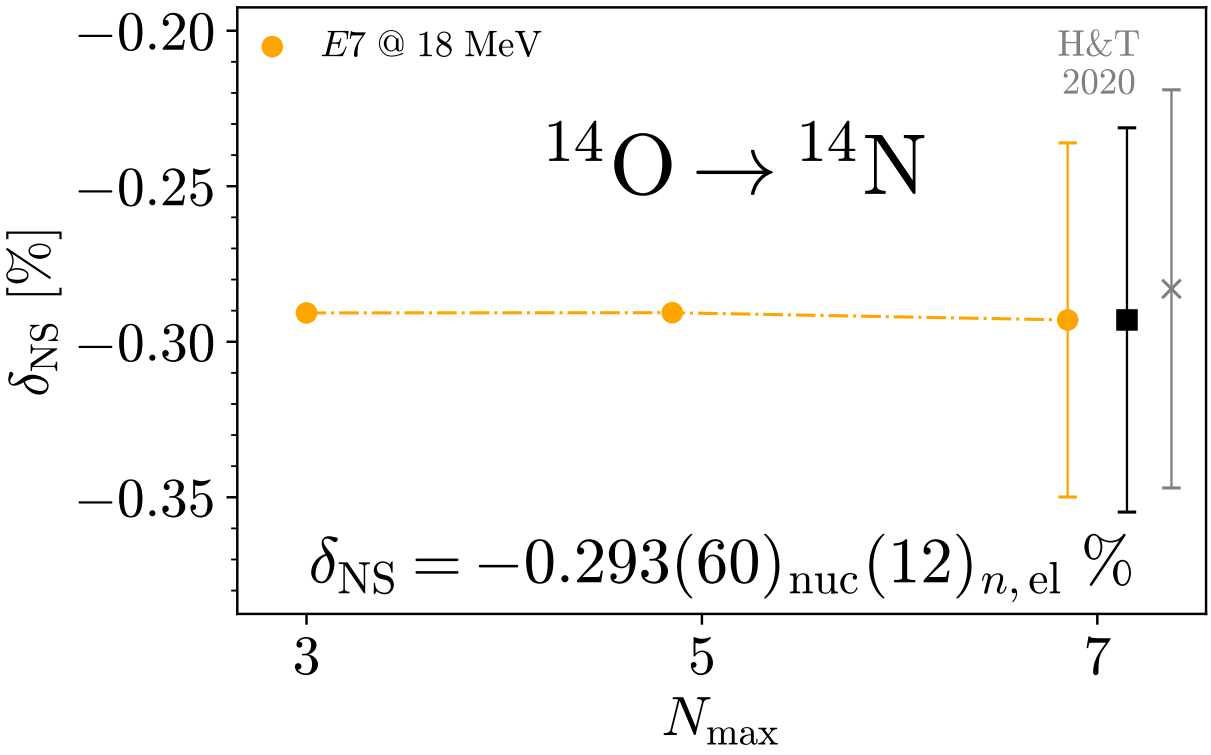


Figure 4.15: Evaluations of $\delta_{\mathrm{NS}}$ in the NCSM for the $^{14}\mathrm{O} \to {}^{14}\mathrm{N}$ with $N_{\mathrm{max}} = 3, 5, 7$ configuration space truncations and, for the NN − N$^4$LO(500)+3N$_{\mathrm{lnl}}$, oscillator frequencies in the range of $\hbar\Omega = 16-20$ MeV. For the $E_7$ point generated with the NN$^4$LO(500) + 3N$^*_{\mathrm{lnl}}$ interaction, we use a sole frequency of $\hbar\Omega =$ 18 MeV. Error bars are as briefly described in the text below and in detail in the subsequent section.

| $^{10}\mathrm{C} \to {}^{10}\mathrm{B}$ | This work | Ref. [7] | $\times 10^{-4}$ |
|---|---|---|---|
| $\epsilon_{J_{\mathrm{max}}}$ | 0.1 | 3.3 | $\epsilon_{\delta_{\mathrm{NS},A}}$ |
| $\epsilon_{M_{\mathrm{scale}}}$ | 0.04 | 3.5 | $\epsilon_{\delta_{\mathrm{NS},B}}$ |
| $\epsilon_{N_{\mathrm{max}}}$ | 0.1 | 1.5 | $\epsilon_{\delta_{\mathrm{NS},E}}$ |
| $\epsilon_{\mathrm{hc}}$ | 1.4 | / | |
| $\epsilon_{\mathrm{PME}}$ | 1.4 | / | |
| $\epsilon_{\Omega}$ | 0.4 | / | |
| $\epsilon_{\chi}$ | 0.9 | / | |
| $\epsilon_{\mathrm{sh}}$ | 2.4 | / | |
| $\epsilon_{\mathrm{nuc}}$ | 2.9 | / | |
| $\epsilon_{n,\mathrm{el}}$ | 1.2 | / | |
| $\epsilon_{\delta_{\mathrm{NS}}}$ | 3.1 | 5.0 | $\epsilon_{\delta_{\mathrm{NS}}}$ |

Table 4.3: List of different uncertainties accounted for in the $\delta_{\mathrm{NS}}$ calculation discussed in this dissertation. For comparison, we also provide the uncertainties as presented in Ref. [7]. Different sub-groups correspond to different degrees of aggregation of the model uncertainties.

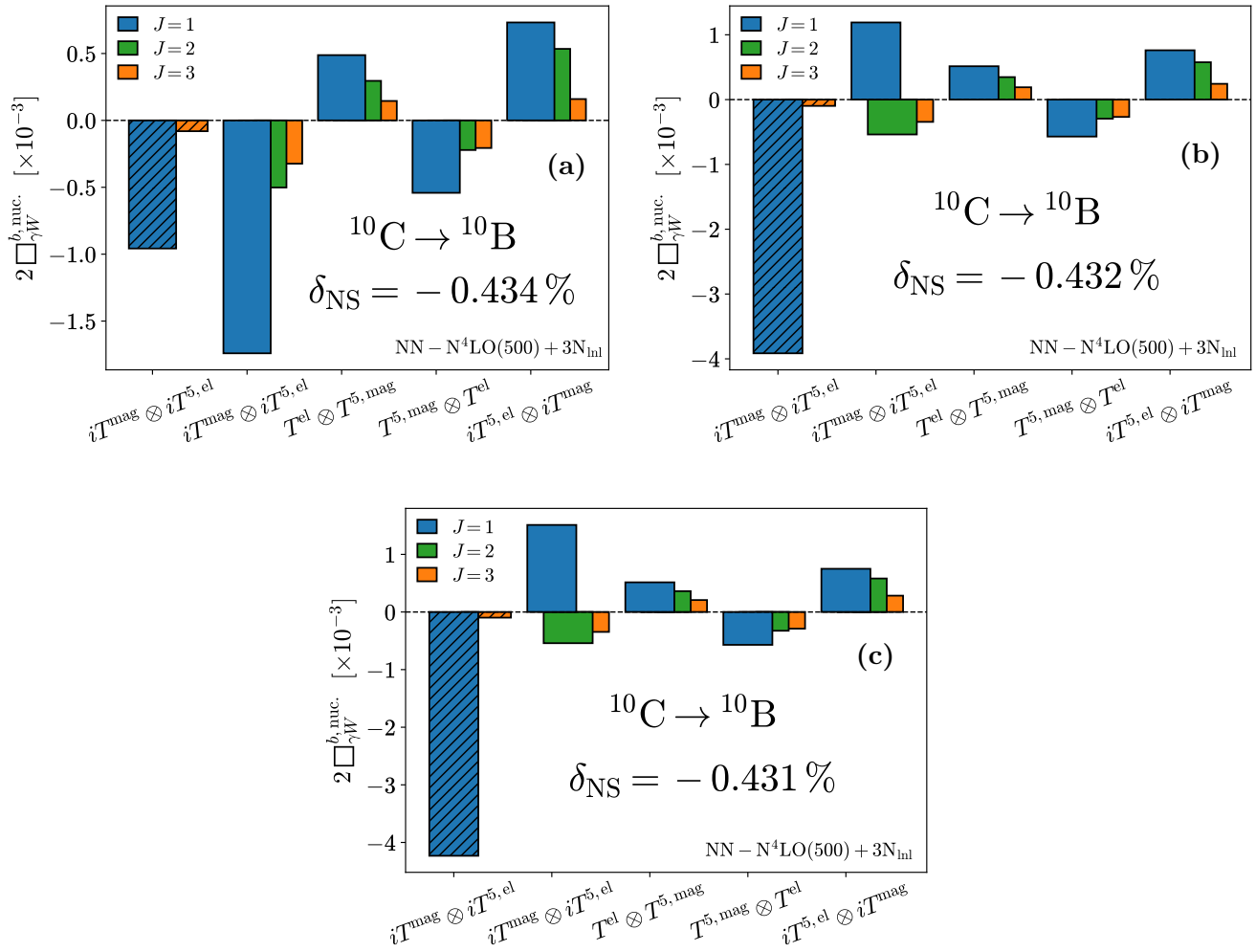


Figure 4.16: Breakdown of the nuclear $\Box_{\gamma W}^{b}$ for the $^{10}\mathrm{C} \to {}^{10}\mathrm{B}$ into (i) different electroweak operator structures in $T_3$ and (ii) each moment in the multipole expansion. The numerical results are obtained with the chiral $\mathrm{NN^4LO(500)} + 3\mathrm{N}^*_{\mathrm{lnl}}$ interaction, an oscillator frequency of $\hbar\Omega = 18$ MeV and with $N_{\mathrm{max}} = 3, 5, 7$ configuration spaces in subfigures **(a)**, **(b)** and **(c)**, respectively. The residue and $\mathcal{O}(E_e)$ contributions are shown as hatched and solid bars, respectively.

sequence. In Fig. 4.16, we present the $\delta_{\mathrm{NS}}$ evaluations for the $^{10}\mathrm{C} \to {}^{10}\mathrm{B}$ for the $\mathrm{NN-N^4LO(500)+3N_{lnl}}$ at fixed $\hbar\Omega = 18$ MeV with configuration space truncations $N_{\mathrm{max}} = 3, 5, 7$ utilized in subfigures **(a)**, **(b)** and **(c)**. While the distribution of transition strength expectedly changes quite a bit from the unphysical $N_{\mathrm{max}} = 3$ model space to the $N_{\mathrm{max}} = 5$ space, the change from $N_{\mathrm{max}} = 5$ to $N_{\mathrm{max}} = 7$ is markedly mild. In addition, we use the residual dependence on the oscillator frequency $\hbar\Omega$ to, in effect, doubly count the remaining dependence on the excluded configuration space when choosing the frequency $\hbar\Omega = 18$ MeV in evaluation of $\delta_{\mathrm{NS}}$. This is assigned in $\epsilon_\Omega$ by taking the maximum absolute difference between varied frequency calculations in the vicinity of $\hbar\Omega = 18$ MeV. In Fig. 4.17, we present the $\delta_{\mathrm{NS}}$ evaluations for the $^{10}\mathrm{C} \to {}^{10}\mathrm{B}$ for the $\mathrm{NN-N^4LO(500)+3N_{lnl}}$ with a fixed $N_{\mathrm{max}} = 7$ configuration space and for oscillator frequencies $\hbar\Omega = 16, 20, 18$ MeV utilized in subfigures **(a)**, **(b)** and **(c)**, respectively. We only comment that the frequency variation is hardly detectable by eye in this figure, except for perhaps in the residue contribution. As this is the only piece truly sensitive to the individual structure of states in the low-lying nuclear spectrum, this is somewhat anticipated in our evaluation.

Turning our attention to the multipole truncation uncertainty, as illustrated in Figs. (3) and (4) of Ref. [170], the integrated amplitudes of odd and even electroweak multipoles present an approximately exponential decay in the magnitude of their contributions with respect to the rank $J$ of the considered operator structure. Moreover, such an observation is reinforced by the well-understood asymptotic behaviour of the Bessel functions which decay

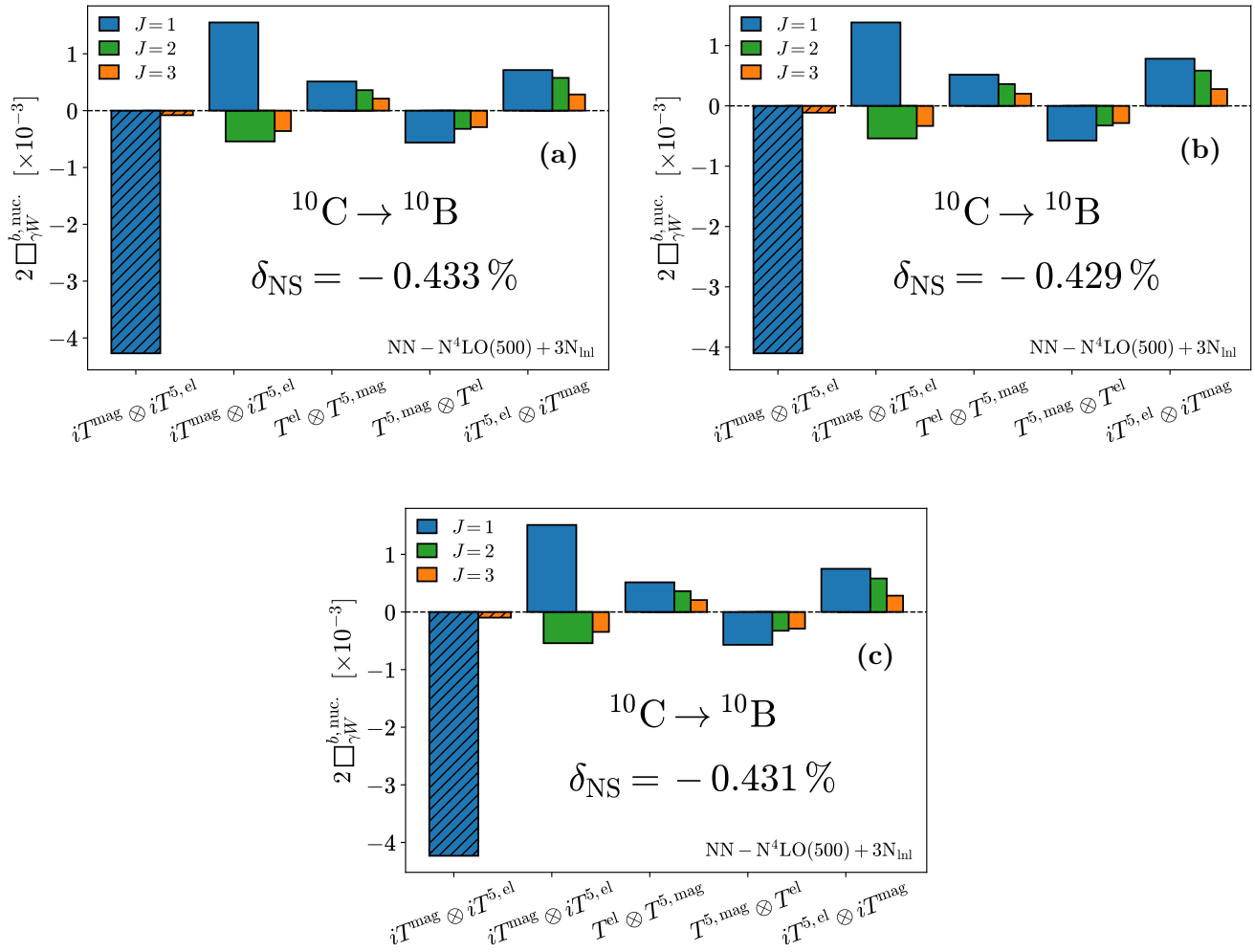


Figure 4.17: Breakdown of the nuclear $\Box^b_{\gamma W}$ for the $^{10}\mathrm{C} \to {}^{10}\mathrm{B}$ into (i) different electroweak operator structures in $T_3$ and (ii) each moment in the multipole expansion. The numerical results are obtained with the chiral $\mathrm{NN^4LO(500)+3N^*_{lnl}}$ interaction, an $N_{\max} = 7$ configuration space and an oscillator frequency of $\hbar\Omega = 16$, 20, 18 MeV in subfigures **(a)**, **(b)** and **(c)**, respectively. The residue and $\mathcal{O}(E_e)$ contributions are shown as hatched and solid bars, respectively.

factorially in $J$. In estimation of $\epsilon_{J_{\max}}$, the error associated to the multipole truncation, we employ a simple two-parameter exponential fit over the multipole index to the amplitudes for a particular operator structure in $T_3$. Extrapolating the fit to $J > J_{\max} = 3$, we sum over all such $J$ until we achieve numerical convergence in the estimate of the "missing strength". As the multipoles are expected to decay at least exponentially in $J$, we argue that this yields a reasonable estimate of the missing strength and thus a conservative uncertainty for the multipole truncation.

Lastly, we turn our attention to the error $\epsilon_\chi$ introduced in truncation of the chiral expansion in the Hamiltonian and in the modelled electroweak currents $\epsilon_{\mathrm{hc}}$. A well motivated approach to the estimation of chiral interaction uncertainties $\epsilon_\chi$ at the many-body level is discussed in Ref. [166] and applied in Ref. [139] within the NCSM formalism. It involves fully consistent calculations at each order in the chiral expansion which, purely as a result of the cost of these calculations, we are sadly not able to perform. Instead, we may still reasonably estimate the effects of the truncation by varying the chiral interaction in use. To this end, we have considered the so-called $E_7$ interaction which includes an additional sub-leading contact interaction in the three-nucleon sector. The final result is taken as the average of those two calculations (at a consistent oscillator frequency) and its dispersion is used as the additional uncertainty $\epsilon_\chi$.

What remains is to estimate the error $\epsilon_{\mathrm{hc}}$ arising from lacking higher-order currents and the approximate SRG

evolution which are most conveniently estimated together. To do so, we rely entirely *ad hoc* on previous literature studies which have systematically explored such effects on the vector electromagnetic current (see Fig. 3 of Ref. [171] for M1 transitions) and the axial part of the axial-vector weak current (see Table IV and Fig. 8 in the Supplemental Material of Ref. [172] for GT transitions, as well as Fig. 2 of Ref. [26] for GT-like transitions) in light nuclei, albeit primarily at zero 3-momentum transfer. While individually significant effects, an important observation made in all of the cited references is the substantial cancellation between the effect of consistent SRG evolution of the operators and the inclusion of higher-order currents. In the end, the combined effect is reduced to the level of a few percent. Detailed in Ref. [172], the total shift was shown to be approximately equivalent to a phenomenological re-scaling of the current coupling constants which, in our case, is equivalent to a re-scaling of the single-nucleon form factors, e.g., $F_1$, $\mu$ and $F_A$. Further noted in such studies is that the effects of higher-order contributions to the vector electromagnetic and axial weak currents are not uncorrelated, i.e., the effects observed in the same system (where the literature studies exist) are similar in magnitude but systematically opposite in sign. Thus, both enhancement of the vector electromagnetic current and quenching of the axial weak current must be considered simultaneously in the amplitudes; we perform a parametric re-scaling of the form factors and extract $\epsilon_{\text{hc}}$ from the variation in $\delta_{\text{NS}}$.

The expected enhancement and quenching of our operator structures is estimated *ad hoc* by considering the percentage change between amplitudes with no SRG evolution and no higher-order current contributions to those with both such treatments, as reported in the aforementioned works. For the exact numbers, see Fig. 3 and Table I of Ref. [171] for M1 transitions, as well as Table IV and Fig. 8 in the Supplemental Material of Ref. [172] for GT transitions. We find that the enhancement in the vector electromagnetic current in M1 transitions is approximately $2-4\%$ and the quenching in the axial weak current for GT transitions is approximately $3-5\%$. As available studies are limited to such operators, these numbers are applied universally regardless of the operator structure at hand. Consequently, we vary the single-nucleon form factors of the vector electromagnetic current according to

$$F_1 \to \tilde{F}_1 = c_V\, F_1 \qquad\qquad \mu \to \tilde{\mu} = c_V\, \mu \quad ,$$

with $c_V \in \left\{\, 1.02,\, 1.04 \,\right\}$, and similarly the single-nucleon form factors of the axial weak current according to

$$F_A \to \tilde{F}_A = c_A\, F_A \quad ,$$

with $c_A \in \left\{\, 0.97,\, 0.95 \,\right\}$. We then extract the uncertainty explicitly as

$$\epsilon_{\text{hc}} = \sup_{c_V,\, c_A} \left| \tilde{\delta}_{\text{NS}}(c_V,\, c_A) - \delta_{\text{NS}} \right| \quad , \tag{4.69}$$

where $\delta_{\text{NS}}$ is the original prediction without re-scaling and $\tilde{\delta}_{\text{NS}}(c_V,\, c_A)$ is a function on the $c_V$-$c_A$ parameter space. We wish to re-emphasize that this *ad hoc* estimate of $\epsilon_{\text{hc}}$ is extracted from the rather limited studies available in literature which, in most cases, consider simplified operator structures at zero 3-momentum transfer in not dissimilar light nuclei. A more rigorous quantification of $\epsilon_{\text{hc}}$ should be based on the explicit inclusion of higher-order corrections to the currents and is deferred to a future study. One possible first step towards this goal would be the approximate inclusion of some higher-order current effects via modifications to the single-nucleon form factors as discussed in Ref. [26].

The above discussion characterizes all truncation uncertainties entering the *ab initio* many-body calculation of $\delta_{\text{NS}}$. The final item to be discussed is the treatment of the 4-momentum dependence of the electroweak multipoles which, as identified in the mutlipole expansion section, are decomposed into an electroweak operator basis under the assumption of vanishing second-class currents [125, 126]. The remaining model dependence consists of the 4-momentum character of the single-nucleon form factors utilized for electromagnetic and weak processes. For a general form factor appearing in the mutlipole amplitudes presented in Sec. 3.1, we use the standard (yet truthfully ill-motivated) dipole form factor approximation

$$F(q^2) = F(0)\left[1 - \frac{q^2}{M^2_{\text{scale}}}\right]^{-2} \quad , \tag{4.70}$$

where in this context $M_{\text{scale}}$ refers to either the vector dipole mass $M_V$ or the axial dipole mass $M_A$. This approximation is uncontrolled in the sense that it is merely recognized as a convenient fitting procedure for a given form factor's momentum distribution. Nevertheless, we can conservatively estimate the error $\epsilon_{M_{\text{scale}}}$ arising from such an approximation by varying the corresponding dipole mass to span the entire range of more sophisticated form factors fitted to reproduce experimental data. Proceeding in this way, the vector dipole mass is varied in a range of 800 – 1000 MeV to cover the range of predictions from the high-quality Padé fits performed in Ref. [167] whereas

the axial dipole mass is varied in a range of 1.09 – 1.270 GeV as recommended in Ref. [14]. The combination of $\epsilon_{N_{\max}}$, $\epsilon_{J_{\max}}$, $\epsilon_{\rm hc}$ and $\epsilon_{M_{\rm scale}}$ make up the partial model error $\epsilon_{\rm PME}$ given in Table 4.3. At the moment, the errors discussed in this section represent the largest contributions to the uncertainty in the $\delta_{\rm NS}$ prediction. Future systematic improvements to the formalism are envisioned, for example, improvements to the theoretical calculation of $\delta_{\rm NS}$ could be achieved by inclusion of higher-body currents and relativistic corrections or simply by using a more precise extractions of form factors. Finally, we note that most of the developments discussed here can be extended to other electroweak radiative corrections.

# Chapter 5

# Summary, Conclusions and Outlook

This dissertation discusses a powerful, generalized methodology for the calculation of electroweak radiative corrections in nuclei and, as a case study, presents a comprehensive investigation into the electroweak radiative corrections relevant to nuclear beta decay with a particular focus on the nuclear $\gamma W$ box diagram. The work demonstrates the manner in which *ab initio* nuclear structure approaches can be adapted and extended to compute radiative effects traditionally approached via phenomenological or shell-model-based techniques. These corrections play a vital role in the extraction of the up-down quark mixing element $V_{ud}$, a cornerstone of precision tests of the Standard Model via the top-row CKM unitarity test, and this dissertation offers an essential step forward in improving the theoretical precision required for robust CKM unitarity tests.

A systematically improvable framework based on *ab initio* nuclear theory is developed to evaluate $\delta_{\rm NS}$ using the formalism of the No-Core Shell Model and Lanczos Strengths Method. The analysis emphasizes the need for a careful treatment of the intermediate nuclear spectrum in order to fully capture the electroweak dynamics of the nucleus. Results are presented for the two lightest superallowed Fermi decays, the $^{10}\mathrm{C} \to {}^{10}\mathrm{B}$ and $^{14}\mathrm{O} \to {}^{14}\mathrm{N}$. The core result is a precision improvement to the prediction for the nuclear-structure-dependent correction in the $^{10}\mathrm{C} \to {}^{10}\mathrm{B}$, as originally quoted in Ref. [1],

$$\delta_{\rm NS}\left[{}^{10}\mathrm{C} \to {}^{10}\mathrm{B}\right] = -0.422\,(14)_{\rm PME}(4)_{\Omega}(9)_{\chi}(24)_{\rm sh}(12)_{n,\rm el}\,\% \quad ,$$

which brings with it a 1.6x reduction in the quoted error despite accounting for a more complete set of nuclear structure uncertainties. We have further presented preliminary results for the $^{14}\mathrm{O} \to {}^{14}\mathrm{N}$ which depict a distinctly different behaviour in the distribution of strength between the residue and Wick contributions to the $\gamma W$ box function; the strong Gamow-Teller suppression in $^{14}\mathrm{O} \to {}^{14}\mathrm{N}$ significantly enhances effects from higher-order multipoles, findings which will have to be taken into account in driving down the uncertainties for $\delta_{\rm NS}$ in this transition. We do not quote a value for the Oxygen transition given the incomplete status of the analysis.

### Impact on Experiment

As the extraction of $V_{ud}$ necessitates a combined effort from both experiment and theory, futures plans to improve the theory precision across the nuclear chart lay the foundation for a revived experimental program on precision $ft$ measurements. Based solely on the work discussed in this dissertation, there is already strong motivation for a new experimental determination of the $^{10}\mathrm{C}$ branching ratio which has historically suffered from a large uncertainty. See Fig. 4.6 for the $^{10}\mathrm{C}$ decay to the first excited state $1^+$ and final state $0^+$ which collectively share the total strength of the Fermi decay. The importance of precision measurements for the $^{10}\mathrm{C} \to {}^{10}\mathrm{B}$ and $^{14}\mathrm{O} \to {}^{14}\mathrm{N}$ transitions lies in the fact that these lightest Fermi decays provide the strongest constraints on scalar currents encoding physics beyond the SM, e.g., see Fig. 7 of Ref. [7]. The reduction in uncertainty we provide purely from this analysis of the radiative corrections thus already impact possible extensions of the SM in this way. In fact, already in contemplation is a new measurement program using superconducting tunnel junctions to detect $^{10}\mathrm{B}$ recoils in analogy with the successful $^{7}\mathrm{Be}$ electron capture measurements [173, 174, 175]. Similar experimental programs with trapped-ion recoil studies have managed to put stringent bounds on BSM currents [176, 177] and will likely contribute future measurements of value to the CKM unitarity puzzle.

Beyond the direct impact of these results, the ever-more-precise electroweak calculations in nuclei encourage continued experimental programs dedicated to the measurment of superallowed and forbidden beta decays, as well

as electromagnetic transitions, to very high precision. Already in pursuit are new measurements of the M1 magnetic dipole transitions at TU Darmstadt [178] which will provide the nuclear physics community with a robust test of the modelling of electroweak currents, e.g., particularly at the level of chiral two-body currents. Akin to this, the precision $\beta$ spectra program in $^{6}$He, $^{14}$O and $^{19}$Ne pursued by the CRES collaboration searches for chirality-flipping beyond SM currents [179]. This program however relies on precision nuclear structure calculations of the $\beta$ spectra for said nuclei, further providing an avenue for testing the uncertainty claims of the present work and works in *ab initio* nuclear theory like it. These combined programs of electroweak theory in nuclei and nuclear experiment will allow for the discrimination between different nuclear models and chiral Hamiltonians, as well as provide avenues for the testing of modern EFTs for beta decay.

## Outlook

There are several improvements to the approach prescribed in this dissertation which may be immediately available to implement. For example, in terms of improving the computational cost of these calculations – which in a naive approach is large – it is possible to exploit analytic properties of the harmonic oscillator basis [180] or to implement analytic continuation in the nuclear amplitudes [181, 182, 183], both approaches which can dramatically reduce the cost of evaluating complicated electroweak processes such as the $\gamma W$ box function described herein. Improvements to the many-body machinery such as those suggested above will allow for the controlled scaling of these computations to larger basis dimensions and higher multipole contributions, further driving down the uncertainty from the many-body aspects of the model.

Beyond improvements to the many-body formalism used to compute the $\gamma W$ box function, pathways to reducing the various uncertainties include a more rigorous treatment of the EFT formalism used (i) in generation of the current amplitudes, e.g., via treatment of higher-order contributions to the current operators consistent with $\chi$EFT and the non-relativistic reduction of the multipoles, (ii) in connecting electroweak, quark-level processes to the nucleon-level processes [184, 185], and (iii) in the proper inclusion of high-energy contributions to the nuclear structure functions, e.g., the aforementioned "nuclear shadowing effects" to be discussed in Ref. [165].

The consistent treatment of hadronic physics over vast energy scales remains an open challenge in nuclear and particle theory which we hope to continue to address in follow-up works on the $\gamma W$ box for precision $\beta$ decay and $V_{ud}$ extractions. Moreover, the methodology explored in this work is readily applicable to the superallowed decays of $^{18}$Ne and $^{22}$Mg, which will be studied in follow-up works, and can be easily generalized to other electroweak processes. To name a few other, very much related projects which are underway (or planned as part of my research program), we seek to compute the $\gamma\gamma$ box (two-photon exchange) for precision measurements of charge-radii, the $\gamma Z$ box for precision weak charge measurements, muon capture processes on light-nuclei for $0\nu\beta\beta$ studies, and neutrino scattering cross sections. With the continued developments and precision gains in non-relativistic many-body methods, the ever-more-formal understanding of low-energy EFTs of QCD, and the increasingly rich domain of SM and beyond SM physics accessible by nuclear experiment, the field of *ab initio* nuclear theory is positioned to be at the forefront of many future developments in modern theoretical physics.

# Bibliography


[1] M. Gennari, M. Drissi, M. Gorchtein, P. Navrátil, and C.-Y. Seng, "Ab Initio Strategy for Taming the Nuclear-Structure Dependence of $V_{ud}$ Extractions: The $^{10}\mathrm{C} \to {}^{10}\mathrm{B}$ Superallowed Transition," *Physical Review Letters*, vol. 134, p. 012501, Jan 2025.

[2] M. Gennari, M. Drissi, M. Gorchtein, P. Navrátil, and C.-Y. Seng, "*On the* $^{14}\mathrm{O} \to {}^{14}\mathrm{N}$ *transition*. In preparation."

[3] M. Drissi, M. Gennari, and P. Navrátil, "*On the* $\gamma\gamma$ *box*. In preparation."

[4] D. A. Najera, M. Gennari, L. Jokiniemi, M. Drissi, and P. Navrátil, "*On muon capture*. In progress."

[5] M. Vorabbi, M. Gennari, P. Finelli, C. Giusti, P. Navrátil, and R. Machleidt, "Elastic proton scattering off nonzero spin nuclei," *Physical Review C*, vol. 105, p. 014621, Jan 2022.

[6] S. Navas *et al.*, "Review of particle physics," *Physical Review D*, vol. 110, no. 3, p. 030001, 2024.

[7] J. C. Hardy and I. S. Towner, "Superallowed $0^+ \to 0^+$ nuclear $\beta$ decays: 2020 critical survey, with implications for $V_{ud}$ and CKM unitarity," *Physical Review C*, vol. 102, p. 045501, Oct 2020.

[8] N. Cabibbo, "Unitary Symmetry and Leptonic Decays," *Physical Review Letters*, vol. 10, pp. 531–533, Jun 1963.

[9] M. Kobayashi and T. Maskawa, "CP-Violation in the Renormalizable Theory of Weak Interaction," *Progress of Theoretical Physics*, vol. 49, pp. 652–657, 02 1973.

[10] V. Cirgiliano, A. Garcia, D. Gazit, O. Naviliat-Cuncic, G. Savard, and A. Young, "Precision Beta Decay as a Probe of New Physics," 2019.

[11] M. Dawid, V. Cirigliano, and W. Dekens, "One-loop analysis of $\beta$ decays in SMEFT," 2024.

[12] B. Belfatto, R. Beradze, and Z. Berezhiani, "The CKM unitarity problem: A trace of new physics at the TeV scale?," *The European Physical Journal C*, vol. 80, no. 2, p. 149, 2020.

[13] C.-Y. Seng, M. Gorchtein, H. H. Patel, and M. J. Ramsey-Musolf, "Reduced Hadronic Uncertainty in the Determination of $V_{ud}$," *Physical Review Letters*, vol. 121, p. 241804, Dec 2018.

[14] C.-Y. Seng, M. Gorchtein, and M. J. Ramsey-Musolf, "Dispersive evaluation of the inner radiative correction in neutron and nuclear $\beta$ decay," *Physical Review D*, vol. 100, p. 013001, Jul 2019.

[15] M. Gorchtein, "$\gamma W$ Box Inside Out: Nuclear Polarizabilities Distort the Beta Decay Spectrum," *Physical Review Letters*, vol. 123, p. 042503, Jul 2019.

[16] V. Cirigliano, A. Crivellin, M. Hoferichter, and M. Moulson, "Scrutinizing CKM unitarity with a new measurement of the $K\mu 3/K\mu 2$ branching fraction," *Physics Letters B*, vol. 838, p. 137748, 2023.

[17] J. C. Hardy and I. S. Towner, "Superallowed $0^+ \to 0^+$ nuclear $\beta$ decays: 2014 critical survey, with precise results for $V_{ud}$ and CKM unitarity," *Physical Review C*, vol. 91, p. 025501, Feb 2015.

[18] M. Gorchtein and C.-Y. Seng, "Superallowed nuclear beta decays and precision tests of the standard model," *Annual Review of Nuclear and Particle Science*, vol. 74, no. Volume 74, 2024, pp. 23–47, 2024.

[19] B. J. P. Jones, "The Physics of Neutrinoless Double Beta Decay: A Primer," 2022.

[20] S. Novario, P. Gysbers, J. Engel, G. Hagen, G. R. Jansen, T. D. Morris, P. Navrátil, T. Papenbrock, and S. Quaglioni, "Coupled-Cluster Calculations of Neutrinoless Double-$\beta$ Decay in $^{48}$Ca," *Physical Review Letters*, vol. 126, p. 182502, May 2021.

[21] A. Belley, C. G. Payne, S. R. Stroberg, T. Miyagi, and J. D. Holt, "Ab Initio Neutrinoless Double-Beta Decay Matrix Elements for $^{48}$Ca, $^{76}$Ge, and $^{82}$Se," *Physical Review Letters*, vol. 126, p. 042502, Jan 2021.

[22] L. Jokiniemi, B. Romeo, P. Soriano, and J. Menéndez, "Neutrinoless $\beta\beta$-decay nuclear matrix elements from two-neutrino $\beta\beta$-decay data," *Physical Review C*, vol. 107, p. 044305, Apr 2023.

[23] A. Belley, J. M. Yao, B. Bally, J. Pitcher, J. Engel, H. Hergert, J. D. Holt, T. Miyagi, T. R. Rodríguez, A. M. Romero, S. R. Stroberg, and X. Zhang, "Ab Initio Uncertainty Quantification of Neutrinoless Double-Beta Decay in $^{76}$Ge," *Physical Review Letters*, vol. 132, p. 182502, Apr 2024.

[24] A. Belley, J. Pitcher, T. Miyagi, S. R. Stroberg, and J. D. Holt, "Correlation of neutrinoless double-beta decay nuclear matrix elements with nucleon-nucleon phase shifts," 2024.

[25] D. Castillo, L. Jokiniemi, P. Soriano, and J. Menéndez, "Neutrinoless $\beta\beta$ decay nuclear matrix elements complete up to N2LO in heavy nuclei," *Physics Letters B*, vol. 860, p. 139181, 2025.

[26] L. Jokiniemi, P. Navrátil, J. Kotila, and K. Kravvaris, "Muon capture on $^{6}$Li, $^{12}$C, and $^{16}$O from ab initio nuclear theory," *Physical Review C*, vol. 109, p. 065501, Jun 2024.

[27] I. Anghel, J. Beacom, M. Bergevin, C. Blanco, E. Catano-Mur, F. Di Lodovico, A. Elagin, H. Frisch, J. Griskevich, R. Hill, *et al.*, "Letter of intent: The accelerator neutrino neutron interaction experiment (ANNIE)," *arXiv preprint arXiv:1504.01480*, 2015.

[28] I. Bernardi, "CEvNS and COHERENT," *PoS*, vol. NOW2022, p. 066, 2023.

[29] A. Aguilar-Arevalo, X. Bertou, C. Bonifazi, G. Cancelo, A. Castañeda, B. Cervantes Vergara, C. Chavez, J. C. D'Olivo, J. a. C. dos Anjos, J. Estrada, A. R. Fernandes Neto, G. Fernandez Moroni, A. Foguel, R. Ford, J. Gonzalez Cuevas, P. Hernández, S. Hernandez, F. Izraelevitch, A. R. Kavner, B. Kilminster, K. Kuk, H. P. Lima, M. Makler, J. Molina, P. Mota, I. Nasteva, E. E. Paolini, C. Romero, Y. Sarkis, M. Sofo Haro, I. a. M. S. Souza, J. Tiffenberg, and S. Wagner, "Exploring low-energy neutrino physics with the Coherent Neutrino Nucleus Interaction Experiment," *Physical Review D*, vol. 100, p. 092005, Nov 2019.

[30] G. Agnolet, W. Baker, D. Barker, R. Beck, T. Carroll, J. Cesar, P. Cushman, J. Dent, S. De Rijck, B. D. tta, W. Flanagan, M. Fritts, Y. Gao, H. Harris, C. Hays, V. Iyer, A. Jastram, F. Kadribasic, A. Kennedy, A. Kubik, K. Lang, R. Mahapatra, V. Mandic, C. Marianno, R. Martin, N. Mast, S. McDeavitt, N. Mirabolfathi, B. Mohanty, K. N. kajima, J. Newhouse, J. Newstead, I. Ogawa, D. Phan, M. Proga, A. Rajput, A. Roberts, G. Rogachev, R. Salazar, J. S. nder, K. Senapati, M. Shimada, B. Soubasis, L. Strigari, Y. Tamagawa, W. Teizer, J. Vermaak, A. Villano, J. Walker, B. Webb, Z. Wetzel, and S. Yadavalli, "Background studies for the MINER Coherent Neutrino Scattering reactor experiment," *Nuclear Instruments and Methods in Physics Research Section A: Accelerators, Spectrometers, Detectors and Associated Equipment*, vol. 853, pp. 53–60, 2017.

[31] J. Billard, J. Johnston, and B. J. Kavanagh, "Prospects for exploring New Physics in Coherent Elastic Neutrino-Nucleus Scattering," *Journal of Cosmology and Astroparticle Physics*, vol. 11, p. 016, nov 2018.

[32] M. Cadeddu, F. Dordei, and C. Giunti, "A view of coherent elastic neutrino-nucleus scattering," *Europhysics Letters*, vol. 143, p. 34001, jul 2023.

[33] V. De Romeri, O. Miranda, D. Papoulias, G. Sanchez Garcia, M. Tórtola, and J. W. Valle, "Physics implications of a combined analysis of COHERENT CsI and LAr data," *Journal of High Energy Physics*, vol. 2023, no. 4, pp. 1–41, 2023.

[34] C. G. Payne, S. Bacca, G. Hagen, W. G. Jiang, and T. Papenbrock, "Coherent elastic neutrino-nucleus scattering on $^{40}$Ar from first principles," *Physical Review C*, vol. 100, p. 061304, Dec 2019.

[35] B. S. Hu, J. Padua-Argüelles, S. Leutheusser, T. Miyagi, S. R. Stroberg, and J. D. Holt, "Ab Initio Structure Factors for Spin-Dependent Dark Matter Direct Detection," *Physical Review Letters*, vol. 128, p. 072502, Feb 2022.

[36] M. Hoferichter, J. Menéndez, and A. Schwenk, "Coherent elastic neutrino-nucleus scattering: EFT analysis and nuclear responses," *Physical Review D*, vol. 102, p. 074018, Oct 2020.

[37] P. Froese and P. Navrátil, "Ab initio calculations of electric dipole moments of light nuclei," *Physical Review C*, vol. 104, p. 025502, Aug 2021.

[38] I. B. Zel'dovich, "Electromagnetic interaction with parity violation," *Soviet Physics JETP*, vol. 6, no. 6, pp. 1184–1186, 1958.

[39] V. V. Flambaum and D. W. Murray, "Anapole moment and nucleon weak interactions," *Physical Review C*, vol. 56, pp. 1641–1644, Sep 1997.

[40] W. C. Haxton and C. E. Wieman, "Atomic Parity Nonconservation and Nuclear Anapole Moments," *Annual Review of Nuclear and Particle Science*, vol. 51, no. 1, pp. 261–293, 2001.

[41] P. Navrátil, S. Quaglioni, G. Hupin, C. Romero-Redondo, and A. Calci, "Unified ab initio approaches to nuclear structure and reactions," *Physica Scripta*, vol. 91, p. 053002, apr 2016.

[42] J. Dohet-Eraly, P. Navrátil, S. Quaglioni, W. Horiuchi, G. Hupin, and F. Raimondi, "$^3$He$(\alpha,\gamma)^7$Be7 and $^3$He$(\alpha,\gamma)^7$Li astrophysical S factors from the no-core shell model with continuum," *Physics Letters B*, vol. 757, pp. 430–436, 2016.

[43] A. Wallner, K. Buczak, I. Dillmann, J. Feige, F. Käppeler, G. Korschinek, C. Lederer, A. Mengoni, U. Ott, M. Paul, and et al., "AMS Applications in Nuclear Astrophysics: New Results for $^{13}$C$(n,\gamma)^{14}$C and $^{14}$N$(n,p)^{14}$C," *Publications of the Astronomical Society of Australia*, vol. 29, no. 2, pp. 115–120, 2012.

[44] M. Wiescher, O. Clarkson, R. J. deBoer, and P. Denisenkov, "Nuclear clusters as the first stepping stones for the chemical evolution of the universe," *The European Physical Journal A*, vol. 57, no. 1, pp. 1–11, 2021.

[45] J. Schwinger, "Chiral dynamics," *Physics Letters B*, vol. 24, no. 9, pp. 473–476, 1967.

[46] S. Weinberg, "Nonlinear Realizations of Chiral Symmetry," *Physical Review Journals Archive*, vol. 166, pp. 1568–1577, Feb 1968.

[47] S. Weinberg, "Effective Field Theory, Past and Future," 2009.

[48] S. Weinberg, "Phenomenological Lagrangians," *Physica A: Statistical Mechanics and its Applications*, vol. 96, no. 1, pp. 327–340, 1979.

[49] J. Gasser and H. Leutwyler, "Chiral perturbation theory to one loop," *Annals of Physics*, vol. 158, no. 1, pp. 142–210, 1984.

[50] J. Gasser and H. Leutwyler, "Chiral perturbation theory: Expansions in the mass of the strange quark," *Nuclear Physics B*, vol. 250, no. 1, pp. 465–516, 1985.

[51] G. Hagen, T. Papenbrock, M. Hjorth-Jensen, and D. J. Dean, "Coupled-cluster computations of atomic nuclei," *Reports on Progress in Physics*, vol. 77, p. 096302, sep 2014.

[52] H. Hergert, "In-medium similarity renormalization group for closed and open-shell nuclei," *Physica Scripta*, vol. 92, p. 023002, dec 2016.

[53] F. A. Evangelista, "A driven similarity renormalization group approach to quantum many-body problems," *The Journal of Chemical Physics*, vol. 141, p. 054109, 08 2014.

[54] V. Somà, "Self-Consistent Green Function Theory for Atomic Nuclei," *Frontiers in Physics*, vol. 8, 2020.

[55] H. Hergert, "A Guided Tour of ab initio Nuclear Many-Body Theory," *Frontiers in Physics*, vol. Volume 8 - 2020, 2020.

[56] E. Epelbaum, H.-W. Hammer, and U.-G. Meißner, "Modern theory of nuclear forces," *Review of Modern Physics*, vol. 81, pp. 1773–1825, Dec 2009.

[57] E. Epelbaum, "Nuclear forces from chiral effective field theory: a primer," *arXiv preprint arXiv:1001.3229*, 2010.

[58] R. Machleidt and D. Entem, "Chiral effective field theory and nuclear forces," *Physics Reports*, vol. 503, no. 1, pp. 1–75, 2011.

[59] R. Machleidt and F. Sammarruca, "Can chiral EFT give us satisfaction?," *The European Physical Journal A*, vol. 56, Mar 2020.

[60] P. Navrátil and B. R. Barrett, "No-core shell-model calculations with starting-energy-independent multivalued effective interactions," *Physical Review C*, vol. 54, pp. 2986–2995, Dec 1996.

[61] D. C. Zheng, J. P. Vary, and B. R. Barrett, "Large-space shell-model calculations for light nuclei," *Physical Review C*, vol. 50, pp. 2841–2849, Dec 1994.

[62] P. Navrátil, J. P. Vary, and B. R. Barrett, "Large-basis ab initio no-core shell model and its application to $^{12}$**C**," *Physical Review C*, vol. 62, p. 054311, Oct 2000.

[63] P. Skands, *Introduction to QCD*, pp. 341–420. 2013.

[64] O. W. Greenberg, "Spin and Unitary-Spin Independence in a Paraquark Model of Baryons and Mesons," *Physical Review Letters*, vol. 13, pp. 598–602, Nov 1964.

[65] M. Y. Han and Y. Nambu, "Three-Triplet Model with Double SU(3) Symmetry," *Physical Review*, vol. 139, pp. B1006–B1010, Aug 1965.

[66] M. Gell-Mann, "Symmetries of Baryons and Mesons," *Physical Review Journals Archive*, vol. 125, pp. 1067–1084, Feb 1962.

[67] K. G. Wilson, "Quantum Field - Theory Models in Less Than 4 Dimensions," *Physical Review D*, vol. 7, pp. 2911–2926, May 1973.

[68] N. Seiberg and E. Witten, "Electric-magnetic duality, monopole condensation, and confinement in N=2 supersymmetric Yang-Mills theory," *Nuclear Physics B*, vol. 426, no. 1, pp. 19–52, 1994.

[69] N. Seiberg and E. Witten, "Monopoles, duality and chiral symmetry breaking in N = 2 supersymmetric QCD," *Nuclear Physics B*, vol. 431, no. 3, pp. 484–550, 1994.

[70] D. Kondo, H. Murayama, and B. Noether, "Near-SUSY to Non-SUSY Crossover," *arXiv preprint arXiv:2505.18138*, 2025.

[71] C. H. de Lima and D. Stolarski, "On s-confining SUSY-QCD with Anomaly Mediation," *arXiv preprint arXiv:2307.13154*, 2024.

[72] E. Noether, "Invariant Variation Problems," *Transport Theory and Statistical Physics*, vol. 1, no. 3, pp. 186–207, 1971.

[73] S. Coleman, J. Wess, and B. Zumino, "Structure of Phenomenological Lagrangians. I," *Physical Review*, vol. 177, pp. 2239–2247, Jan 1969.

[74] C. G. Callan, S. Coleman, J. Wess, and B. Zumino, "Structure of Phenomenological Lagrangians. II," *Physical Review*, vol. 177, pp. 2247–2250, Jan 1969.

[75] A. Bansal, S. Binder, A. Ekström, G. Hagen, G. R. Jansen, and T. Papenbrock, "Pion-less effective field theory for atomic nuclei and lattice nuclei," *Physical Review C*, vol. 98, p. 054301, Nov 2018.

[76] H.-W. Hammer, S. König, and U. van Kolck, "Nuclear effective field theory: Status and perspectives," *Reviews of Modern Physics*, vol. 92, p. 025004, Jun 2020.

[77] A. Ekström and L. Platter, "Quantifying the breakdown scale of pionless effective field theory," *Physics Letters B*, vol. 860, p. 139207, 2025.

[78] C.-J. Yang, "Do we know how to count powers in pionless and pionful effective field theory?," *The European Physical Journal A*, vol. 56, no. 3, p. 96, 2020.

[79] J. M. Bub, M. Piarulli, R. J. Furnstahl, S. Pastore, and D. R. Phillips, "Bayesian analysis of nucleon-nucleon scattering data in pionless effective field theory," *Physical Review C*, vol. 111, p. 034005, Mar 2025.

[80] C.-J. Yang, A. Ekström, C. Forssén, and G. Hagen, "Power counting in chiral effective field theory and nuclear binding," *Physical Review C*, vol. 103, p. 054304, May 2021.

[81] O. Thim, E. May, A. Ekström, and C. Forssén, "Bayesian analysis of chiral effective field theory at leading order in a modified Weinberg power counting approach," *Physical Review C*, vol. 108, p. 054002, Nov 2023.

[82] O. Thim, A. Ekström, and C. Forssén, "Perturbative computations of neutron-proton scattering observables using renormalization-group invariant chiral effective field theory up to N$^3$LO," *Physical Review C*, vol. 109, p. 064001, Jun 2024.

[83] R. Haag, "Quantum Field Theories with Composite Particles and Asymptotic Conditions," *Physical Review Journals Archive*, vol. 112, pp. 669–673, Oct 1958.

[84] B. R. Barrett, P. Navrátil, and J. P. Vary, "Ab initio no core shell model," *Progress in Particle and Nuclear Physics*, vol. 69, pp. 131–181, 2013.

[85] S. Baroni, P. Navrátil, and S. Quaglioni, "Unified ab initio approach to bound and unbound states: No-core shell model with continuum and its application to $^7$He," *Physical Review C*, vol. 87, p. 034326, Mar 2013.

[86] P. Navrátil, S. Quaglioni, I. Stetcu, and B. R. Barrett, "Recent developments in no-core shell-model calculations," *Journal of Physics G: Nuclear and Particle Physics*, vol. 36, p. 083101, may 2009.

[87] P. Navrátil, "Translationally invariant density," *Physical Review C*, vol. 70, p. 014317, Jul 2004.

[88] M. Gennari, M. Vorabbi, A. Calci, and P. Navrátil, "Microscopic optical potentials derived from ab initio translationally invariant nonlocal one-body densities," *Physical Review C*, vol. 97, p. 034619, Mar 2018.

[89] M. Gennari and P. Navrátil, "Nuclear kinetic density from ab initio theory," *Physical Review C*, vol. 99, p. 024305, Feb 2019.

[90] W. Pauli, "The Connection Between Spin and Statistics," *Physical Review Journals Archive*, vol. 58, pp. 716–722, Oct 1940.

[91] J. C. Slater, "The Theory of Complex Spectra," *Physical Review Journals Archive*, vol. 34, pp. 1293–1322, Nov 1929.

[92] T. D. Lee and C. N. Yang, "Question of Parity Conservation in Weak Interactions," *Physical Review Journals Archive*, vol. 104, pp. 254–258, Oct 1956.

[93] C. S. Wu, E. Ambler, R. W. Hayward, D. D. Hoppes, and R. P. Hudson, "Experimental Test of Parity Conservation in Beta Decay," *Physical Review Journals Archive*, vol. 105, pp. 1413–1415, Feb 1957.

[94] J. Zhao and F. Wang, "Experimental searches for the chiral magnetic effect in heavy-ion collisions," *Progress in Particle and Nuclear Physics*, vol. 107, pp. 200–236, 2019.

[95] A. I. Akhiezer, A. G. Sitenko, and V. K. Tartakovskii, *Nuclear Electrodynamics*. Springer, 1994.

[96] J. D. Walecka, *Theoretical Nuclear and Subnuclear Physics*. World Scientific, 2004.

[97] J. Suhonen, "From nucleons to nucleus," *Berlin Heidelberg*, 2007.

[98] D. J. Rowe and J. L. Wood, *Fundamentals of nuclear models: foundational models*. World Scientific, 2010.

[99] D. Varshalovich, A. Moskalev, and V. Khersonskii, *Quantum Theory of Angular Momentum*. World Scientific, 1988.

[100] E. Epelbaum, "Four-nucleon force in chiral effective field theory," *Physics Letters B*, vol. 639, no. 5, pp. 456–461, 2006.

[101] E. Epelbaum, "Four-nucleon force using the method of unitary transformation," *The European Physical Journal A*, vol. 34, no. 2, pp. 197–214, 2007.

[102] S. Binder, J. Langhammer, A. Calci, and R. Roth, "Ab initio path to heavy nuclei," *Physics Letters B*, vol. 736, pp. 119–123, 2014.

[103] T. Miyagi, S. R. Stroberg, P. Navrátil, K. Hebeler, and J. D. Holt, "Converged ab initio calculations of heavy nuclei," *Physical Review C*, vol. 105, p. 014302, Jan 2022.

[104] J. Elliott and T. Skyrme, "Centre-of-mass effects in the nuclear shell-model," *Proceedings of the Royal Society of London. Series A. Mathematical and Physical Sciences*, vol. 232, no. 1191, pp. 561–566, 1955.

[105] P. Navrátil, "Translationally invariant matrix elements of general one-body operators," *Physical Review C*, vol. 104, p. 064322, Dec 2021.

[106] M. Burrows, C. Elster, G. Popa, K. D. Launey, A. Nogga, and P. Maris, "Ab initio translationally invariant nonlocal one-body densities from no-core shell-model theory," *Physical Review C*, vol. 97, p. 024325, Feb 2018.

[107] E. J. Weniger, "Weakly convergent expansions of a plane wave and their use in Fourier integrals," *Journal of Mathematical Physics*, vol. 26, no. 2, pp. 276–291, 1985.

[108] M. Moshinsky and Y. Smirnov, "The harmonic oscillator in modern physics," *The Netherlands*, pp. 289–404, 1996.

[109] D. Gloeckner and R. Lawson, "Spurious center-of-mass motion," *Physics Letters B*, vol. 53, no. 4, pp. 313–318, 1974.

[110] C. Lanczos, "An iteration method for the solution of the eigenvalue problem of linear differential and integral operators," *Journal of Research of the National Bureau of Standards*, vol. 45, pp. 255–282, 1950.

[111] L. Komzsik, *The Lanczos method: evolution and application*. SIAM, 2003.

[112] C. Paige, "Accuracy and effectiveness of the Lanczos algorithm for the symmetric eigenproblem," *Linear Algebra and its Applications*, vol. 34, pp. 235–258, 1980.

[113] B. Parlett, "Do we fully understand the symmetric Lanczos algorithm yet?," 1995.

[114] R. Haydock, "The inverse of a linear operator," *Journal of Physics A: Mathematical, Nuclear and General*, vol. 7, no. 17, p. 2120, 1974.

[115] R. Haydock, "The Recursive Solution of the Schrodinger Equation," vol. 35 of *Solid State Physics*, pp. 215–294, Academic Press, 1980.

[116] V. Heine, "Electronic Structure from the Point of View of the Local Atomic Environment," vol. 35 of *Solid State Physics*, pp. 1–127, Academic Press, 1980.

[117] M. Kelly, "Applications of the Recursion Method to the Electronic Structure from an Atomic Point of View," vol. 35 of *Solid State Physics*, pp. 295–383, Academic Press, 1980.

[118] R. Haydock, V. Heine, and M. J. Kelly, "Electronic structure based on the local atomic environment for tight-binding bands," *Journal of Physics C: Solid State Physics*, vol. 5, p. 2845, oct 1972.

[119] D. G. Pettifor and D. L. Weaire, *The Recursion Method and Its Applications: Proceedings of the Conference, Imperial College, London, England September 13–14, 1984*, vol. 58. Springer Science & Business Media, 2012.

[120] M. Marchisio, N. Barnea, W. Leidemann, and G. Orlandini, "Efficient method for Lorentz integral transforms of reaction cross sections," *Few-Body Systems*, vol. 33, no. 4, pp. 259–276, 2003.

[121] N. Nevo Dinur, N. Barnea, C. Ji, and S. Bacca, "Efficient method for evaluating energy-dependent sum rules," *Physical Review C*, vol. 89, p. 064317, Jun 2014.

[122] Y. Hao, P. Navrátil, E. B. Norrgard, M. Iliaš, E. Eliav, R. G. E. Timmermans, V. V. Flambaum, and A. Borschevsky, "Nuclear spin-dependent parity-violating effects in light polyatomic molecules," *Physical Review A*, vol. 102, p. 052828, Nov 2020.

[123] E. Dagotto, "Correlated electrons in high-temperature superconductors," *Reviews of Modern Physics*, vol. 66, pp. 763–840, Jul 1994.

[124] D. Bessis and M. Villani, "Perturbative-variational approximations to the spectral properties of semibounded Hilbert space operators, based on the moment problem with finite or diverging moments. Application to quantum mechanical systems," *Journal of Mathematical Physics*, vol. 16, no. 3, pp. 462–474, 1975.

[125] T. Donnelly and W. Haxton, "Multipole operators in semileptonic weak and electromagnetic interactions with nuclei: Harmonic oscillator single-particle matrix elements," *Atomic Data and Nuclear Data Tables*, vol. 23, no. 2, pp. 103–176, 1979.

[126] W. Haxton and C. Lunardini, "SevenOperators, a Mathematica script for harmonic oscillator nuclear matrix elements arising in semileptonic electroweak interactions," *Computer Physics Communications*, vol. 179, no. 5, pp. 345–358, 2008.

[127] T. W. Donnelly, J. A. Formaggio, B. R. Holstein, R. G. Milner, and B. Surrow, *Foundations of Nuclear and Particle Physics*. Cambridge University Press, 4 2017.

[128] B. Acharya and S. Bacca, "Neutrino-deuteron scattering: Uncertainty quantification and new $L_{1,A}$ constraints," *Physical Review C*, vol. 101, no. 1, p. 015505, 2020.

[129] A. Glick-Magid, C. Forssén, D. Gazda, D. Gazit, P. Gysbers, and P. Navrátil, "Nuclear ab initio calculations of $^6$He $\beta$-decay for beyond the Standard Model studies," *Physics Letters B*, vol. 832, p. 137259, 2022.

[130] A. Glick-Magid and D. Gazit, "A formalism to assess the accuracy of nuclear-structure weak interaction effects in precision $\beta$-decay studies," *Journal of Physics G: Nuclear and Particle Physics*, vol. 49, no. 10, p. 105105, 2022.

[131] P. Gysbers, P. Navrátil, K. Kravvaris, G. Hupin, and S. Quaglioni, "*Ab initio* investigation of the $^7\mathrm{Li}(p, e^+e^-)^8\mathrm{Be}$ process and the X17 boson," *Physical Review C*, vol. 110, p. 015503, Jul 2024.

[132] D. Morrissey, "Personal Communcation," 2025.

[133] D. Tong, "Lectures on Quantum Field Theory." `https://www.damtp.cam.ac.uk/user/tong/qft.html`, 2006.

[134] J. F. Donoghue, E. Golowich, and B. R. Holstein, *Dynamics of the Standard Model*. Cambridge Monographs on Particle Physics, Nuclear Physics and Cosmology, Cambridge University Press, 2 ed., 2014.

[135] S. Weinberg, *The Quantum Theory of Fields: Foundations*, vol. 1. Cambridge University Press, 1995.

[136] S. Weinberg, "Charge Symmetry of Weak Interactions," *Physical Review*, vol. 112, pp. 1375–1379, Nov 1958.

[137] D. R. Entem, R. Machleidt, and Y. Nosyk, "High-quality two-nucleon potentials up to fifth order of the chiral expansion," *Physical Review C*, vol. 96, no. 2, p. 024004, 2017.

[138] V. Somà, P. Navrátil, F. Raimondi, C. Barbieri, and T. Duguet, "Novel chiral Hamiltonian and observables in light and medium-mass nuclei," *Physical Review C*, vol. 101, p. 014318, Jan 2020.

[139] K. Kravvaris, P. Navrátil, S. Quaglioni, C. Hebborn, and G. Hupin, "Ab initio informed evaluation of the radiative capture of protons on $^7$Be," *Physics Letters B*, vol. 845, p. 138156, 2023.

[140] L. Girlanda, A. Kievsky, and M. Viviani, "Subleading contributions to the three-nucleon contact interaction," *Physical Review C*, vol. 84, no. 1, p. 014001(E), 2011. [Erratum: Physical Review C 102, 019903 (2020)].

[141] S. K. Bogner, R. J. Furnstahl, and R. J. Perry, "Similarity renormalization group for nucleon-nucleon interactions," *Physical Review C*, vol. 75, p. 061001(R), 2007.

[142] A. Sirlin, "Current algebra formulation of radiative corrections in gauge theories and the universality of the weak interactions," *Reviews of Modern Physics*, vol. 50, pp. 573–605, Jul 1978.

[143] C.-Y. Seng, "Radiative Corrections to Semileptonic Beta Decays: Progress and Challenges," *Particles*, vol. 4, no. 4, pp. 397–467, 2021.

[144] C.-Y. Seng, X. Feng, M. Gorchtein, and L.-C. Jin, "Joint lattice QCD–dispersion theory analysis confirms the quark-mixing top-row unitarity deficit," *Physical Review D*, vol. 101, p. 111301, Jun 2020.

[145] K. Shiells, P. G. Blunden, and W. Melnitchouk, "Electroweak axial structure functions and improved extraction of the $V_{ud}$ CKM matrix element," *Physical Review D*, vol. 104, p. 033003, Aug 2021.

[146] A. Czarnecki, W. J. Marciano, and A. Sirlin, "Radiative corrections to neutron and nuclear beta decays revisited," *Physical Review D*, vol. 100, p. 073008, Oct 2019.

[147] A. Sirlin, "General Properties of the Electromagnetic Corrections to the Beta Decay of a Physical Nucleon," *Physical Review*, vol. 164, pp. 1767–1775, Dec 1967.

[148] A. Sirlin and R. Zucchini, "Accurate Verification of the Conserved-Vector-Current and Standard-Model Predictions," *Physical Review Letters*, vol. 57, pp. 1994–1997, Oct 1986.

[149] W. Jaus and G. Rasche, "Radiative corrections to $0^+$-$0^+$ $\beta$ transitions," *Physical Review D*, vol. 35, pp. 3420–3422, Jun 1987.

[150] A. Sirlin, "Remarks concerning the $\mathrm{O}(\mathrm{Z}\alpha^2)$ corrections to Fermi decays, conserved-vector-current predictions, and universality," *Physical Review D*, vol. 35, pp. 3423–3427, Jun 1987.

[151] A. Czarnecki, W. J. Marciano, and A. Sirlin, "Precision measurements and CKM unitarity," *Physical Review D*, vol. 70, p. 093006, Nov 2004.

[152] R. J. Hill and R. Plestid, "Field Theory of the Fermi Function," *Physical Review Letters*, vol. 133, p. 021803, Jul 2024.

[153] R. J. Hill and R. Plestid, "All orders factorization and the Coulomb problem," *Physical Review D*, vol. 109, p. 056006, Mar 2024.

[154] P. V. Griend, Z. Cao, R. Hill, and R. Plestid, "The Fermi function and the neutron's lifetime," 2025.

[155] C.-Y. Seng and M. Gorchtein, "Dispersive formalism for the nuclear structure correction $\delta_{\rm NS}$ to the $\beta$ decay rate," *Physical Review C*, vol. 107, p. 035503, Mar 2023.

[156] W. Satuła, J. Dobaczewski, W. Nazarewicz, and M. Rafalski, "Microscopic Calculations of Isospin-Breaking Corrections to Superallowed Beta Decay," *Physical Review Letters*, vol. 106, p. 132502, Mar 2011.

[157] W. E. Ormand and B. A. Brown, "Corrections to the Fermi Matrix Element for Superallowed $\beta$ Decay," *Physical Review Letters*, vol. 62, pp. 866–869, Feb 1989.

[158] P. Navrátil and B. R. Barrett, "Large-basis shell-model calculations for $p$-shell nuclei," *Physical Review C*, vol. 57, pp. 3119–3128, Jun 1998.

[159] E. Caurier, P. Navrátil, W. Ormand, and J. Vary, "Ab initio shell model for A=10 nuclei," *Physical Review C*, vol. 66, no. 2, p. 024314, 2002.

[160] G. A. Miller and A. Schwenk, "Isospin-symmetry-breaking corrections to superallowed Fermi $\beta$ decay: Formalism and schematic models," *Physical Review C*, vol. 78, p. 035501, Sep 2008.

[161] G. A. Miller and A. Schwenk, "Isospin-symmetry-breaking corrections to superallowed Fermi $\beta$ decay: Radial excitations," *Physical Review C*, vol. 80, p. 064319, Dec 2009.

[162] N. Auerbach and M. L. Bui, "Coulomb corrections to Fermi beta decay in nuclei," *Nuclear Physics A*, vol. 1027, p. 122521, 2022.

[163] TUNL Nuclear Data Evaluation Project, "Energy Level Diagram, $^{10}$B (2004)." `https://nucldata.tunl.duke.edu/nucldata/figures/10figs/10_05_gamma_2004.pdf`.

[164] TUNL Nuclear Data Evaluation Project, "Energy Level Diagram, $^{14}$N (1991)." `https://nucldata.tunl.duke.edu/nucldata/figures/14figs/14_07_1991.pdf`.

[165] C.-Y. Seng and M. Gorchtein, "Personal Communcation," 2023.

[166] E. Epelbaum, H. Krebs, and U. G. Meißner, "Improved chiral nucleon-nucleon potential up to next-to-next-to-next-to-leading order," *The European Physical Journal A*, vol. 51, no. 5, p. 53, 2015.

[167] J. J. Kelly, "Simple parametrization of nucleon form factors," *Physical Review C*, vol. 70, p. 068202, Dec 2004.

[168] M. Gorchtein and C.-Y. Seng, "The Standard Model Theory of Neutron Beta Decay," *Universe*, vol. 9, no. 9, 2023.

[169] P. Maris, J. P. Vary, P. Navrátil, W. E. Ormand, H. Nam, and D. J. Dean, "Origin of the Anomalous Long Lifetime of $^{14}$C," *Physical Review Letters*, vol. 106, p. 202502, May 2011.

[170] O. J. Hernandez, C. Ji, S. Bacca, and N. Barnea, "Probing uncertainties of nuclear structure corrections in light muonic atoms," *Physical Review C*, vol. 100, p. 064315, Dec 2019.

[171] U. Friman-Gayer, C. Romig, T. Hüther, K. Albe, S. Bacca, T. Beck, M. Berger, J. Birkhan, K. Hebeler, O. J. Hernandez, J. Isaak, S. König, N. Pietralla, P. C. Ries, J. Rohrer, R. Roth, D. Savran, M. Scheck, A. Schwenk, R. Seutin, and V. Werner, "Role of Chiral Two-Body Currents in $^{6}$Li Magnetic Properties in Light of a New Precision Measurement with the Relative Self-Absorption Technique," *Physical Review Letters*, vol. 126, p. 102501, Mar 2021.

[172] P. Gysbers, G. Hagen, J. D. Holt, G. R. Jansen, T. D. Morris, P. Navrátil, T. Papenbrock, S. Quaglioni, A. Schwenk, S. R. Stroberg, and K. A. Wendt, "Discrepancy between experimental and theoretical $\beta$-decay rates resolved from first principles," *Nature Physics*, vol. 15, pp. 428–431, 2019.

[173] S. Fretwell, K. G. Leach, C. Bray, G. B. Kim, J. Dilling, A. Lennarz, X. Mougeot, F. Ponce, C. Ruiz, J. Stackhouse, and S. Friedrich, "Direct Measurement of the $^{7}$Be $L/K$ Capture Ratio in Ta-Based Superconducting Tunnel Junctions," *Physical Review Letters*, vol. 125, p. 032701, Jul 2020.

[174] K. G. Leach and S. Friedrich, "The BeEST Experiment: Searching for Beyond Standard Model Neutrinos Using $^{7}$Be Decay in STJs," *J. Low Temp. Phys.*, vol. 209, no. 5-6, pp. 796–803, 2022.

[175] D. Carney, K. G. Leach, and D. C. Moore, "Searches for Massive Neutrinos with Mechanical Quantum Sensors," *PRX Quantum*, vol. 4, no. 1, p. 010315, 2023.

[176] G. Li, R. Segel, N. D. Scielzo, P. F. Bertone, F. Buchinger, S. Caldwell, A. Chaudhuri, J. A. Clark, J. E. Crawford, C. M. Deibel, J. Fallis, S. Gulick, G. Gwinner, D. Lascar, A. F. Levand, M. Pedretti, G. Savard, K. S. Sharma, M. G. Sternberg, T. Sun, J. Van Schelt, R. M. Yee, and B. J. Zabransky, "Tensor Interaction Limit Derived From the $\alpha-\beta-\overline{\nu}$ Correlation in Trapped $^{8}$Li Ions," *Physical Review Letters*, vol. 110, p. 092502, Mar 2013.

[177] G. H. Sargsyan, K. D. Launey, M. T. Burkey, A. T. Gallant, N. D. Scielzo, G. Savard, A. Mercenne, T. Dytrych, D. Langr, L. Varriano, B. Longfellow, T. Y. Hirsh, and J. P. Draayer, "Impact of Clustering on the $^{8}$Li $\beta$ Decay and Recoil Form Factors," *Physical Review Letters*, vol. 128, p. 202503, May 2022.

[178] N. Pietralla, G. Rainovski, M. Reese, C. Stahl, T. Beck, J. Beller, C. Romig, and V. Werner, "Progress on m1 research," *Journal of Physics: Conference Series*, vol. 580, pp. 1–6, April 2024. 11th International Spring Seminar on Nuclear Physics: Shell Model and Nuclear Structure.

[179] W. Byron, H. Harrington, R. J. Taylor, W. DeGraw, N. Buzinsky, B. Dodson, M. Fertl, A. García, G. Garvey, B. Graner, M. Guigue, L. Hayen, X. Huyan, K. S. Khaw, K. Knutsen, D. McClain, D. Melconian, P. Müller, E. Novitski, N. S. Oblath, R. G. H. Robertson, G. Rybka, G. Savard, E. Smith, D. D. Stancil, M. Sternberg, D. W. Storm, H. E. Swanson, J. R. Tedeschi, B. A. VanDevender, F. E. Wietfeldt, A. R. Young, and X. Zhu, "First observation of cyclotron radiation from mev-scale $e^{\pm}$ following nuclear $\beta$ decay," *Phys. Rev. Lett.*, vol. 131, p. 082502, Aug 2023.

[180] W. C. Haxton, K. M. Nollett, and K. M. Zurek, "Piecewise moments method: Generalized Lanczos technique for nuclear response surfaces," *Physical Review C*, vol. 72, p. 065501, Dec 2005.

[181] D. Frame, R. He, I. Ipsen, D. Lee, D. Lee, and E. Rrapaj, "Eigenvector Continuation with Subspace Learning," *Physical Review Letters*, vol. 121, p. 032501, Jul 2018.

[182] X. Zhang, "A non-Hermitian quantum mechanics approach for extracting and emulating continuum physics based on bound-state-like calculations," 2024.

[183] X. Zhang, "A non-Hermitian quantum mechanics approach for extracting and emulating continuum physics based on bound-state-like calculations: technical details," 2024.

[184] V. Cirigliano, W. Dekens, J. de Vries, S. Gandolfi, M. Hoferichter, and E. Mereghetti, "Ab initio electroweak corrections to superallowed $\beta$ decays and their impact on $V_{ud}$," *Physical Review C*, vol. 110, p. 055502, Nov 2024.

[185] V. Cirigliano, W. Dekens, J. de Vries, S. Gandolfi, M. Hoferichter, and E. Mereghetti, "Radiative Corrections to Superallowed $\beta$ Decays in Effective Field Theory," *Physical Review Letters*, vol. 133, p. 211801, Nov 2024.

[186] I. Talmi *Helvetica Physica Acta*, vol. 25, no. 185, 1952.

[187] M. Moshinsky, "Transformation brackets for harmonic oscillator functions," *Nuclear Physics*, vol. 13, no. 1, pp. 104–116, 1959.

[188] Y. Smirnov, "Talmi transformations for particles with different masses," *Nuclear Physics*, vol. 27, no. 2, pp. 177–187, 1961.

[189] Y. Smirnov, "Talmi transformation for particles with different masses (II)," *Nuclear Physics*, vol. 39, pp. 346–352, 1962.

[190] L. Trlifaj, "Simple Formula for the General Oscillator Brackets," *Physical Review C*, vol. 5, pp. 1534–1539, May 1972.

# Appendix A

# Summary of Notation

## A.1 Definition of the Dirac Gamma Matrices and Spinors

Note that we have used the Dirac adjoint notation, $\bar{\psi} = \psi^\dagger \gamma^0$, which guarantees that $\bar{\psi}\psi$ and $\bar{\psi}\gamma^\mu\psi$ transform covariantly. The definitions for the elements of the 4-vector of Dirac gamma matrices $\gamma^\mu = \left(\gamma^0, \gamma^1, \gamma^2, \gamma^3\right)$ utilized in the main text, as well as the definition of the tensor $\sigma^{\mu\nu}$, are provided below.

$$\gamma^0 = \begin{pmatrix} \mathbb{1} & 0 \\ 0 & -\mathbb{1} \end{pmatrix} \qquad \gamma^i = \begin{pmatrix} 0 & \sigma^i \\ -\sigma^i & 0 \end{pmatrix} \qquad \gamma_5 = \begin{pmatrix} 0 & \mathbb{1} \\ \mathbb{1} & 0 \end{pmatrix} \tag{A.1}$$

$$\sigma^{0i} = \begin{pmatrix} 0 & i\sigma^i \\ i\sigma^i & 0 \end{pmatrix} \qquad \sigma^{ij} = \epsilon^{ijk} \begin{pmatrix} \sigma^k & 0 \\ 0 & \sigma^k \end{pmatrix} \tag{A.2}$$

We also provide the definition of the Fermionic spinor which are used for the definition of the relativistic field operators,

$$u_s(p) = \sqrt{m+E} \begin{pmatrix} \chi_s \\ \frac{\vec{\sigma}\cdot\vec{p}}{m+E}\chi_s \end{pmatrix} \quad . \tag{A.3}$$

## A.2 Spin Coupling and Tensors

The total spin momentum of a non-relativistic quantum system is conserved. Let us consider the simplest case of two particles with spin vectors $\vec{J}_1$ and $\vec{J}_2$ corresponding to states $\left|J_1 M_1\right\rangle$ and $\left|J_2 M_2\right\rangle$. Under the standard tensor operation between Hilbert spaces, these states may be combined by the direct tensor product as

$$\left|J_1 M_1 J_2 M_2\right\rangle = \left|J_1 M_1\right\rangle \otimes \left|J_2 M_2\right\rangle \tag{A.4}$$

However, a more convenient prescription exists for multi-particle systems. Since the total spin $\vec{J} = \vec{J}_1 + \vec{J}_2$ is conserved, the allowed values of the total spin coupling $J$ must obey the triangle condition, $\Delta(J_1 J_2 J)$, which constrains $J \in \{|J_1 - J_2|, \ldots, J_1 + J_2\}$. Under the chosen normalization and phase-conventions, we may then write states of total $J$ momentum $\left|J_1 J_2 J M\right\rangle$ as linear combinations of the uncoupled two-particle states via the Clebsch-Gordan coefficients as

$$\left|J_1 J_2 J M\right\rangle = \sum_{M_1 M_2} C^{J_1 J_2\,;\,JM}_{J_1 M_1\,;\,J_2 M_2} \left|J_1 M_1 J_2 M_2\right\rangle \qquad C^{J_1 J_2\,;\,JM}_{J_1 M_1\,;\,J_2 M_2} = \left\langle J_1 M_1 J_2 M_2 | J_1 J_2 J M\right\rangle \tag{A.5}$$

where $M = M_1 + M_2$ and the coefficients are purely real, and consequently, they are guaranteed to be Hermitian. More detailed descriptions of angular momentum coupling, as well as three particle coupling procedures, may be found in Refs. [99]. These procedures can be applied to couple to an arbitrary number of spin momenta.

## A.3 Tensors and Wigner-Eckart Theorem

Here we introduce the basic properties of a rank-$\lambda$ tensor $T^\lambda_\mu$, which is a set of $2\lambda+1$ operators with $\mu \in \{-\lambda, \ldots, \lambda\}$. One may specify the transformation properties of a tensor operator by requiring commutation with the $J_\pm$ and $J_z$

operators, which leads to some remarkable results in quantum theory. In particular, the use of tensors allows for the reduction $M$-state dependence by Wignar-Eckart theorem as

$$\left\langle JM\right| T^{\lambda}_{\mu} \left|J'M'\right\rangle = (-1)^{2\lambda} \frac{(J'M'\lambda\mu|JM)}{\sqrt{2J+1}} \langle J||T^{\lambda}||J'\rangle \ , \tag{A.6}$$

where $\langle J||T^{\lambda}||J'\rangle$ is a $J$-reduced amplitude. Arbitrary tensors $T^{\lambda_1}_{\mu_1}$ and $U^{\lambda_2}_{\mu_2}$ may be combined into the tensor $S^{\lambda}_{\mu}$ with the same angular momentum coupling techniques introduced in the previous appendix section as

$$S^{\lambda}_{\mu} = [T^{\lambda_1} \otimes U^{\lambda_2}]^{\lambda}_{\mu} = \sum_{\mu_1\mu_2} \langle \lambda_1\mu_1\lambda_2\mu_2|\lambda\mu\rangle \, T^{\lambda_1}_{\mu_1} U^{\lambda_2}_{\mu_2} \ . \tag{A.7}$$

One can derive relations for the reduced matrix elements of the tensor product operator; in general one must derive separate results for when $T^{\lambda_1}$ and $U^{\lambda_2}$ act in the same or different vector spaces.

## A.4 Talmi-Moshinsky Transformation

Consider the case of a two-particle system in an external harmonic oscillator potential with mass $m$ and with cartesian vectors $\vec{x}_1$ and $\vec{x}_2$. The Hamiltonian for this system is then written in cartesian form as

$$H = \frac{\vec{p}_1^{\,2} + \vec{p}_2^{\,2}}{2m} + \frac{1}{2} m\Omega^2 (\vec{x}_1^{\,2} + \vec{x}_2^{\,2}) \ . \tag{A.8}$$

We may describe the eigenstates as being two-particle Slater determinant eigenstates by utilizing an expansion in the harmonic oscillator one-particle basis. Yet, the Slater determinant basis contains the unphysical motion of the c.m. and so we must isolate the intrinsic motion of the particles. Let us introduce the same expression in relative coordinates

$$\vec{x} = \frac{1}{\sqrt{2}}(\vec{x}_1 - \vec{x}_2) \qquad\qquad \vec{X} = \frac{1}{\sqrt{2}}(\vec{x}_1 + \vec{x}_2) \quad , \tag{A.9}$$

and in this new coordinate system, the Hamiltonian is then written as

$$H = \frac{\vec{p}_1^{\,2} + \vec{p}_2^{\,2}}{2m} + \frac{1}{2} m\Omega^2 (\vec{x}^{\,2} + \vec{X}^{\,2}) \ , \tag{A.10}$$

which may be similarly described as a product wave function. As these Hamiltonians are equivalent modulo a coordinate change, the eigenenergies are the same, and this hence implies relations between the quantum numbers of the relative and Slater determinant basis states. Further, this means we may express the eigenstates of the respective Hamiltonians in terms of one another,

$$\left|N_1L_1n_1l_1Q\right\rangle = \sum_{nlNL} \langle nlNLQ|N_1L_1n_1l_1Q\rangle \left|nlNLQ\right\rangle \ . \tag{A.11}$$

This expansion may be further generalized to the case of unequal mass particles, for which the product of oscillator functions depending on $\vec{X}$ and $\vec{x}$ transform elegantly as

$$\begin{aligned} &\sum_{M_1m_1} (L_1M_1l_1m_1|Qq) \, \varphi_{N_1L_1M_1}(\vec{R}) \, \varphi_{n_1l_1m_1}(\vec{r}) \\ &\qquad = \sum_{NLMnlm} \langle nlNLQ|N_1L_1n_1l_1Q\rangle_{\frac{1}{A-1}} (lmLM|Qq) \, \varphi_{nlm}(\vec{\xi}_1) \, \varphi_{NLM}(\vec{\xi}_0) \ , \end{aligned} \tag{A.12}$$

where $\langle nlNLQ|N_1L_1n_1l_1Q\rangle_d$ is a generalized Talmi-Moshinsky HO bracket for a two particle system with mass ratio $d = \frac{1}{A-1}$ [186, 187, 188, 189, 190]. Using this transformation, it is possible to express our operators in a translation invariant way by analytically removing c.m. contamination from the ground state harmonic oscillator wave function, as discussed in Sec. 2.3.3.

## A.5 Relative Coordinates

Relative coordinates may be defined in a variety of ways. The particular convention presented here is consistent with the NCSM codes of P. Navrátil at TRIUMF.

Consider a system of $A$ nucleons, each nucleon having the same mass $m$. We neglect the difference between the proton and the neutron masses. We then define

$$\vec{X} = \sqrt{\frac{1}{A}}\vec{\xi}_0 = \sqrt{\frac{1}{A}}\big[\vec{x}_1 + \cdots + \vec{x}_A\big] \quad , \tag{A.13}$$

and so we see $\vec{\xi}_0$ is directly proportional to the c.m. coordinate of the $A$-nucleon system, $\vec{X}$. We further define the remaining $A-1$ coordinates, denoted with the index $i$ as $\vec{\xi}_i$, as being relative coordinates between the $(i+1)$-th nucleon with respect to the c.m. position of the $i$-nucleon system. We may write these coordinates as

$$\begin{aligned}
\vec{\xi}_1 &= \sqrt{\frac{1}{2}}\big[\vec{x}_1 - \vec{x}_2\big] \\
\vec{\xi}_2 &= \sqrt{\frac{2}{3}}\left[\frac{1}{2}\big(\vec{x}_1 + \vec{x}_2\big) - \vec{x}_3\right] \\
&\vdots \\
\vec{\xi}_{A-2} &= \sqrt{\frac{A-2}{A-1}}\left[\frac{1}{A-2}\big(\vec{x}_1 + \cdots + \vec{x}_{A-2}\big) - \vec{x}_{A-1}\right] \\
\vec{\xi}_{A-1} &= \sqrt{\frac{A-1}{A}}\left[\frac{1}{A-1}\big(\vec{x}_1 + \cdots + \vec{x}_{A-1}\big) - \vec{x}_A\right] \quad .
\end{aligned} \tag{A.14}$$

Using the definition $\vec{X}_{c.m.}^{(A-1)} = \sqrt{\frac{1}{A-1}}\big[\vec{x}_1 + \cdots + \vec{x}_{A-1}\big]$, it is possible to write $\vec{\xi}_0$ and $\vec{\xi}_{A-1}$ respectively as

$$\begin{aligned}
\vec{\xi}_0 &= \sqrt{\frac{A-1}{A}}\vec{X}_{c.m.}^{A-1} + \sqrt{\frac{1}{A}}\vec{x}_A \\
\vec{\xi}_{A-1} &= \sqrt{\frac{1}{A}}\vec{X}_{c.m.}^{A-1} - \sqrt{\frac{A-1}{A}}\vec{x}_A \quad .
\end{aligned} \tag{A.15}$$